

Pre-Combustion CO_2 Capture by Hydrate Formation Using Silica as a Promoter

Mohd Hafiz bin Abu Hassan, MEng.

Thesis submitted to the University of Nottingham for the degree of Doctor of Philosophy

January 2017

Cleaner Fossil Energy and Carbon Capture Technologies Research Group

Faculty of Engineering

ABSTRACT

A rise of 2 ^{o}C in the Earth's temperature is likely to occur when the concentration of CO_2 in the atmosphere reaches approximately 450 ppm. CO_2 emissions are closely related to the continual use of fossil fuels. In order to make fossil fuels sustainable, carbon capture & storage (CCS) is required to reduce CO_2 emissions. There are three leading CO_2 capture methods, namely post-combustion capture, oxy-fuel combustion and integrated gasification combined cycle (IGCC) pre-combustion capture. CO_2 hydrate (CO_2:$6H_2O$) formation has been investigated as a way to capture CO_2 in the IGCC conditions.

The formation of hydrate in this work was experimentally investigated in an isochoric system (batch mode) inside a vertical fixed bed reactor (FBR), also known as high pressure volumetric analyser (HPVA). Standard silica gel with an average particle size of 200-500 µm, mean pore size of 5.14 nm, a pore volume of 0.64 cm^3/g and a surface area of 499 m^2/g was used as a porous medium. The presence of hydrate in FBR was justified by using graphic methods. The solubility of CO_2 in water using Henry's Law and the experimental pressure–time (P-t) curve were analysed to determine the formation of hydrate. Hydrate formation was confirmed when the mole fraction of CO_2 dissolved in water exceeded the Henry's Law value as well as a two-stage pressure drop in the experimental P-t curve.

Initially, various sample preparation methods (methods 1, 2, 3 and 4) were studied leading to the selection of method 4 (the use of vigorous stirring) which had the highest moisture content (14.8 wt%) and the greatest water conversion to hydrate (40.5 mol%) at 275 K and 36 bar in a pure CO_2 gas system. Also, high regeneration and repeatability of the results for all samples prepared by method 4 were expected as less water was occluded inside silica gel pores. Further investigations in pure CO_2 gas

systems highlighted the effect of type of silicas used, the importance of the type of promoters used, the concentration of promoters, experimental driving force, silica pore size, bed height and the amount of moisture content for formation of hydrate.

Standard silica gel was the only silica found to show hydrate formation due to the best distribution of pore size. The high amount of bulk water inside zeolites 13X and spherical MCF-17 (21.3 and 50.8 wt% respectively) was the main reason of no hydrate formation observed. Additionally, the combined-promoters designated type T1-5 (0.01 mol% sodium dodecyl sulphate (SDS) + 5.6 mol% tetrahydrofuran (THF)) and type T3-2 (0.01 mol% SDS + 0.1 mol% tetra-butyl ammonium bromide (TBAB)) were the two best obtaining a CO_2 uptake of 5.95 and 5.57 mmol of CO_2 per g of H_2O respectively. Ethylene glycol mono-ethyl ether (EGME; 0.1 mol%) was a good alternative to THF when combined with SDS (0.01 mol%) with a CO_2 uptake of 5.45 mmol of CO_2 per g of H_2O for this combined-promoter designated type T1A-2. In addition, the CO_2 uptake increased as ΔP increased or ΔT decreased. Moreover, mesoporous silica (silica gel) performed better than microporous silica (zeolite 13X) where the formation of hydrate by zeolite 13X was observed with minimal CO_2 uptake (0.58 mmol of CO_2 per g of H_2O) when the bed height was reduced. Additionally, the total amount of CO_2 consumed through hydrate formation increased as the amount of water inside mesoporous silica increased which was not the case for microporous silica.

Furthermore, the experiments performed in the IGCC conditions (283 K and 70 bar) by employing T1-5 and T3-2 in a fuel gas mixture demonstrated low hydrate formation with a CO_2 uptake of 1.5 and 1.1 mmol of CO_2 per g of H_2O respectively. This was expected due to the slow kinetics since CO_2 molecules were competing with H_2 molecules which also reduced the selectivity of CO_2 molecules during hydrate

formation. Hence, in reality, pure CO_2 system is the best option for CCS through hydrate formation at the right operating conditions as compared to fuel gas mixture.

ACKNOWLEDGEMENTS

The work presented in this thesis might not have been completed without the involvements and support of the people that I have owed my gratitude to.

First & foremost, I would like to thank my supervisor Prof. Colin E. Snape for all the guidance, encouragement and support in both academic and personal level.

I would also like to thank Dr. Lee Stevens and Dr. Nannan Sun for their guidance on the lab works and not to forget, all the members of the University of Nottingham's technical staff who gave me their support in the laboratory.

A thousand thank you to Dr. Cheng-Gong Sun and Prof. Hao Liu for their kind advices related throughout my Ph.D journey.

A big appreciation to the Ministry of Higher Education and Islamic Science University of Malaysia (USIM) for their benevolence in supporting my Ph.D program financially for the last three and half years. Also, thank you to Education Malaysia for their support in assisting me during my wonderful stay in the UK.

Also, I would like to thank all of my officemates, labmates, Nottingham Malaysian Community (NMC) members and friends for their encouragements and support in making my journey smooth, meaningful and memorable.

Last but not least, I would like to thank my adored family: my wife Nurain Saiful Ahmad, my daughters Dhia Insyirah and Damia Irdina, my father Abu Hassan, my mother Kelthom, my parents-in-law, Saiful Ahmad and Maslina and my sister-in-law Nur Alyah, for their continuous support, patience and love.

Table of Contents

ABSTRACT i
ACKNOWLEDGEMENTS iv
List of figures ix
List of tables xv
ABBREVIATIONS xviii
CHAPTER 1: RESEARCH BACKGROUND 1
1.1. Introduction 1
1.2. CO_2 emissions and CCS 1
1.3. CO_2 capture leading technologies 6
1.3.1. Post-combustion capture 7
1.3.2. Oxy-fuel combustion 8
1.3.3. Pre-combustion capture in IGCC plant 10
1.3.4. Existing technologies for CO_2 capture 11
1.3.5. Emerging technologies for CO_2 capture 15
1.4. Advantages of pre-combustion CO_2 capture by HBGS 17
1.5. Clathrate hydrate 20
1.5.1. Definition 20
1.5.2. Structures 21
1.5.3. Mechanism of hydrate formation 23
1.5.4. Hydrate forming conditions 26
1.6. Previous works on HBGS for pre-combustion CO_2 capture 28
1.6.1. Bulk water 28
1.6.2. Solid adsorbent 28
1.6.3. Oxygenated solvent as a promoter 30
1.6.4. Surfactant as a promoter 32
1.6.5. Semi-clathrate hydrate former as a promoter 33
1.6.6. Hydrophobic former as a promoter 36
1.6.7. Synergic effect of combined-promoter 37
1.7. Reactor configuration highlights in HBGS 42
1.8. Variation in experimental parameters in HBGS 43
1.8.1. Sample preparation of solid adsorbent 44
1.8.2. Driving force 45
1.8.3. Promoter concentration 46
1.8.4. Characteristics of solid adsorbent 48

1.8.5. Fixed bed height 50
1.9. The principle conclusions from background works 51
1.10. Research objectives 56
1.11. Thesis structure 57
CHAPTER 2: EXPERIMENTAL METHODS 58
2.1. Introduction 58
2.2. Characterisation of silicas 58
2.2.1. Type of silica 58
2.2.2. Principle of the Brunauer, Emmett and Teller (BET) surface area and porosity analyser… 59
2.2.3. Surface area and pore size analysis 60
2.3. Various sample preparation methods 62
2.3.1. Method 1 65
2.3.2. Method 2 65
2.3.3. Method 3 65
2.3.4. Method 4 65
2.4. Sample preparation procedure for promoters' contact with silica gel 66
2.4.1. Calculation for the amount of promoter used 67
2.5. Equilibrium moisture content measurement 67
2.5.1. Experimental procedure 68
2.5.2. Calculation of the amount of equilibrium moisture content 69
2.6. CO_2 hydrate formation 70
2.6.1. Principles of the HPVA 72
2.6.2. Experimental procedure 73
2.6.3. Calculation of the amount of CO2 consumed (mol) 76
2.6.4. Calculation of the amount of CO2 involved in hydrate formation 76
2.6.5. Conversion of water to hydrate (mol%) 77
2.6.6. CO_2 uptake (mmol of CO_2/g of H_2O) 78
2.6.7. Rate of hydrate formation (mmol CO_2 per g H_2O per min) 78
CHAPTER 3: THE EFFECT OF VARIOUS SAMPLE PREPARATION METHODS 79
3.1. Introduction 79
3.2. Analysis of various sample preparation methods 79
3.2.1. The effect on the amount of equilibrium moisture content 80
3.2.2. Hydrate formation 81

3.3. Control experiments 89
3.3.1. CO_2 adsorption profile for dry and wet silica gel 89
3.3.2. Various operating conditions 90
3.4. Effect of single promoter on gas uptake and hydrate formation kinetics 97
3.4.1. CO_2 solubility in water in the presence of promoter 98
3.4.2. Water conversion to hydrate and CO_2 uptake 99
3.5. Hydrate formation comparison between three silicas 102
3.6. Summary 104
CHAPTER 4: THE EFFECT OF COMBINING PROMOTERS 106
4.1. Introduction 106
4.2. Various combinations of promoters 106
4.2.1. Hydrate formation 107
4.2.2. Optimum combined-concentrations 124
4.3. Enhancing hydrate formation in microporous silica 127
4.3.1. CO_2 solubility in water 127
4.3.2. Water conversion and maximum gas uptake 128
4.3.3. Rate of hydrate formation 131
4.4. Summary 132
CHAPTER 5: IGCC PLANT CONDITIONS 134
5.1. Introduction 134
5.2. Various driving forces in hydrate forming region 134
5.2.1. Water conversion and maximum gas uptake 135
5.2.2. Rate of hydrate formation 138
5.3. Enhanced hydrate formation in non-hydrate forming region 139
5.3.1. Pure CO_2 gas investigation 140
5.3.2. IGCC operating conditions and the effect of bed height on hydrate formation 146
5.3.2.1. CO_2 solubility in water 146
5.3.2.2. Water conversion and maximum gas uptake 148
5.4. Long experiments 150
5.4.1. CO_2 solubility in water 151
5.4.2. Water conversion to hydrate 153
5.5. Comparison with previous works 154
5.5.1. Experiments on fuel gas mixture in the non-IGCC operating conditions 155
5.5.2. Experiments on fuel gas mixture for the IGCC operating conditions 157

5.5.3. Comparison between pure CO_2 gas and fuel gas mixture systems 158
5.6. Summary 161
CHAPTER 6: DISCUSSION OF RESULTS 163
6.1. Introduction 163
6.2. Vigorous stirring increased the amount of equilibrium moisture content inside silica gel pores as well as gas uptake with minimum error bars 163
6.3. Hydrate formation mechanism in the HPVA 166
6.4. Various factors that affected hydrate formation 168
6.4.1. Synergic effect of combined-promoters 168
6.4.2. Improving driving force 181
6.4.3. Mesoporous silica and batch FBR concurrently reduced hydrate formation in fuel gas mixture 184
6.4.5. Bed height roles in enhancing hydrate formation 190
6.4.6. Equilibrium moisture content affected total CO_2 consumed 191
6.5. Summary of the factors improving hydrate formation 194
CHAPTER 7: CONCLUSIONS AND RECOMMENDATIONS FOR FUTURE WORK 198
7.1. Conclusions 198
7.1.1. Vigorous stirring during sample preparation enhanced hydrate formation 198
7.1.2. Synergic effect of combined-promoters 199
7.1.3. Other factors that affected hydrate formation 201
7.1.4. The feasibility of CO2 capture through hydrate formation in the IGCC conditions 202
7.2. Recommendations for future work 203
7.2.1. GC analysis on the selectivity of CO_2 hydrate from fuel gas mixture 203
7.2.2. FBR configurations involving macroporous/mesoporous silicas for HBGS improvement in the IGCC 204
REFERENCES 206
APPENDIX 219
Appendix 1. BET sample calculation 219
Appendix 2. Promoter concentration 219
Appendix 3. Combined gas law 222
Appendix 4. Summary of calculated data 222
Appendix 5. Solubility of CO_2 in H_2O 225
Appendix 6. Solubility of H_2 in H_2O 230

Appendix 7. Hydrate phase equilibrium for H_2+THF and H_2+TBAB 231
Appendix 8. Hydrate phase equlibrium in this work 232
Appendix 9. Effect of THF on hydrates cage occupancy 233
Appendix 10. Water saturation inside silica pores 233
Appendix 11. Changing the process from batch to continuous process 234

List of figures

Figure 1- 1: Carbon dioxide concentration in the atmosphere from 1960 – 2013 (Biello, 2013) 2

Figure 1- 2: Global year to date temperature variances (NOAA, 2015) 3

Figure 1- 3: CO_2 emissions from fossil fuel combustion (IEA, 2015) 4

Figure 1- 4: Fuel shares in global CO_2 emissions (IEA, 2015) 4

Figure 1- 5: Overview of CO_2 capture approaches (Hu, 2011) 6

Figure 1- 6: Combined SO_2 and CO_2 capture process (IEAGHG, 2015) 8

Figure 1- 7: The process flow of the 100 MWth Callide oxy-fuel pilot in Australia (PAH, primary air heater; SAH, secondary air heater; FF, fabric filters; IDF, induction draught fan; GRF, gas recirculation fan) (IEA, 2014) 9

Figure 1- 8: Pre-combustion capture IGCC process schematic (Rackley, 2010) 11

Figure 1- 9: Materials for CO_2 capture in the context of post-combustion, pre-combustion and oxy-fuel processes (D'Alessandro et al., 2010) 11

Figure 1- 10: Simplified schematic of HBGS 16

Figure 1- 11: Chemical looping combustion (Me: metal; MeO: metal oxide as oxygen carrier (Yang et al., 2008)) 17

Figure 1- 12: HBGS process for CO_2 pre-combustion capture (Babu et al., 2015) 19

Figure 1- 13: CO_2 hydrate structure (Rackley, 2010) 22

Figure 1- 14: Pressure change during the hydrate formation process (Tang et al., 2013) 25

Figure 1- 15: Labile cluster growth (Sloan et al., 2008) 25

Figure 1- 16: Pressure variations with different SDS concentrations (Tang et al., 2013) 26

Figure 1- 17: Hydrate phase equilibrium of CO_2, H_2 and fuel gas mixture (Babu et al., 2015) 27

Figure 1- 18: CO_2-H_2 (40:60) mixture and H_2 pure gases hydrate phase equilibrium with additive of TBAB (Kim et al., 2011) 35

Figure 1- 19: Hydrate phase equilibrium for the fuel gas mixture with or without promoter (Babu et al., 2015) 37

Figure 1- 20: Hydrate forming conditions for experiments using 99.9% CO_2 gas supply (Yang et al., 2013) 39

Figure 1- 21: Induction time relative to that of 1000 mg/L SDS (Yang et al., 2013) .. 40

Figure 1- 22: Path to commercialisation for the HBGS process (Babu et al., 2015) ... 43

Figure 1- 23: Hydrate phase equilibria for fuel gas mixture + THF + water mixtures (Park et al., 2013) 47

Figure 1- 24: Hydrate phase equilibria for the H_2 (60%) + CO_2 (40%) + water mixtures in silica gel pores (Park et al., 2013) 49

Figure 1- 25: Historical perspective of gas hydrates research (Babu et al., 2015) 51

Figure 1- 26: Summary of highest normalised gas uptake for 120 min from IP reported so far in the literature at different experimental conditions (Babu et al., 2015) 55

Figure 2- 1: BET surface analyser 60

Figure 2- 2: N_2 adsorption/desorption isotherms for each silica; (a) standard silica gel, (b) zeolite 13X and (c) spherical MCF-17 61

Figure 2- 3: Methods 1 and 3 for sample preparations without agitation 63

Figure 2- 4: Methods 2 and 4 for sample preparations with agitation 64

Figure 2- 5: Degassing unit 68

Figure 2- 6: Work station 71

Figure 2- 7: High pressure volumetric analyser (HPVA) 73

Figure 2- 8: Manual control window during purging process 75

Figure 2- 9: Define run experiment window to insert operating conditions 75

Figure 3- 1: The equilibrium moisture content in wet silica gel for methods 1 – 4 81

Figure 3- 2: P-t curves that show 2-stage pressure drop in 1200 minutes and the first 100 minutes respectively for methods 1 – 4 83

Figure 3- 3: Mole fraction of CO_2 in water inside silica gel pores for methods 1 – 4 at experimental conditions of 275 K and 35 bar in 1200 minutes; (a) total mole fraction of CO_2, (b) mole fraction of CO_2 during hydrate growth 85

Figure 3- 4: Comparison of (a) water conversion to hydrate and (b) gas uptake for methods 1 - 4 at the operating conditions of 275 K and 35 bar in 1200 minutes 87

Figure 3- 5: Rate of hydrate formation for 1200 minutes and inset for the first 150 minutes (methods 1 - 4) 88

Figure 3- 6: P-t curves for dry and wet silica gels at the operating pressure of 36 bar and temperatures of 275 K and 298 K in 600 minutes 90

Figure 3- 7: Mole fraction of CO_2 consumed at the operating temperature of 275 K and various operating pressures in 600 minutes 93

Figure 3- 8: Mole fraction of CO_2 consumed at the operating conditions of 280 K and 36 bar in 600 minutes 93

Figure 3- 9: Mole fraction of CO_2 consumed at the non-hydrate forming conditions (experiments 5 – 8) in 600 minutes 94

Figure 3- 10: Comparison of (a) water conversion to hydrate and (b) CO_2 uptake at the hydrate forming conditions in 600 minutes 96

Figure 3- 11: Rate of hydrate formation for 600 minutes and inset for the first 150 minutes (experiments 1 - 4) 97

Figure 3- 12: CO_2 solubility in water in the presence of promoter at operating conditions of 275 K and 36 bar in 600 minutes 99

Figure 3- 13: CO_2 solubility in water in the presence of promoter at operating conditions of 288 K and 36 bar in 600 minutes 99

Figure 3- 14: Comparison of water conversion to hydrate by employing promoters in 600 minutes 101

Figure 3- 15: Comparison of CO_2 uptake by employing promoters in 600 minutes at 36 bar and various operating temperatures (275 K & 288 K) 101

Figure 3- 16: Rate of hydrate formation at 36 bar for 600 minutes and inset for the first 150 minutes (various promoters) 102

Figure 3- 17: Comparison of (a) CO_2 dissolved in water and (b) P-t curve for various silicas at the operating conditions of 275 K and 35 bar in 1200 minutes 104

Figure 4- 1: Summary of results for equilibrium moisture content at various T1 samples.....109

Figure 4- 2: Comparison of (a) water conversion to hydrate and (b) gas uptake for various T1 samples and baseline experiments at the operating conditions of 275 K and 36 bar in 1200 minutes.....111

Figure 4- 3: Rate of hydrate formation at 275 K and 36 bar for 1200 minutes and inset for the first 150 minutes (various T1 concentrations and baseline experiments).....113

Figure 4- 4: Summary of results for equilibrium moisture content at various T2 and T3 samples.....115

Figure 4- 5: Comparison of (a) water conversion to hydrate and (b) maximum CO_2 uptake for various T2 and T3 samples and baseline experiments at the operating conditions of 275 K and 36 bar in 1200 minutes.....117

Figure 4- 6: Rate of hydrate formation at 275 K and 36 bar for 1200 minutes and inset for the first 150 minutes (various T2 and T3 concentrations and baseline experiments).....119

Figure 4- 7: Summary of results for equilibrium moisture content at various T1A samples.....121

Figure 4- 8: Comparison of (a) water conversion to hydrate and (b) maximum CO_2 uptake for various T1A samples and baseline experiment at the operating conditions of 275 K and 36 bar in 1200 minutes.....122

Figure 4- 9: Rate of hydrate formation at 275 K and 36 bar for 1200 minutes and inset for the first 150 minutes (various T1A concentrations and baseline experiment).....124

Figure 4- 10: Comparison of (a) maximum CO_2 uptake and (b) rate of hydrate formation for the optimum concentration of each combined-promoter and baseline experiment at the operating conditions of 275 K and 36 bar.....126

Figure 4- 11: Mole fraction of CO_2 consumed at the operating conditions of 275 K and 36 bar in 1200 minutes (*13X-5 = zeolite contacted with 5.6 mol% THF and 0.01 mol% SDS).....128

Figure 4- 12: Comparison of (a) equilibrium moisture content at 3cm bed height, (b) maximum gas uptake and (c) water conversion to hydrate for 13X-5_2cm, T1-5_3cm and baseline experiment at 275 K and 36 bar in 1200 minutes.....130

Figure 4- 13: Rate of hydrate formation at 275 K and 36 bar for 1200 minutes and inset for the first 400 minutes (13X-5_2cm, T1-5_3cm and baseline experiment)...131

Figure 5- 1: Comparison of (a) water conversion to hydrate and (b) gas uptake for T1-5, T3-2 and baseline experiment at 275 K and 30 bar in 1200 minutes.....136

Figure 5- 2: Comparison of (a) water conversion to hydrate and (b) gas uptake for T1-5, T3-2 and baseline experiment at 275 K and 22 bar in 1200 minutes 137

Figure 5- 3: Rate of hydrate formation at 275 K and 30 bar for 1200 minutes and inset for the first 150 minutes (T1-5, T3-2 and baseline experiment)..... 139

Figure 5- 4: Rate of hydrate formation at 275 K and 22 bar for 1200 minutes and inset for the first 150 minutes (T1-5, T3-2 and baseline experiment)..... 139

Figure 5- 5: The comparison of (a) water conversion to hydrate and (b) gas uptake for T1-5, T3-2, T1-A and baseline experiments at 288 K and 36 bar in 1200 minutes .. 142

Figure 5- 6: The comparison of (a) water conversion to hydrate and (b) gas uptake for T1-5 and T3-2 at 293 K and 36 bar in 1200 minutes..... 143

Figure 5- 7: Rate of hydrate formation at 288 K and 36 bar for 1200 minutes and inset for the first 150 minutes (T1-5, T3-2, T1A-2 and baseline experiments)..... 145

Figure 5- 8: Rate of hydrate formation at 293 K and 36 bar for 1200 minutes and inset for the first 500 minutes (T1-5 and T3-2)..... 145

Figure 5- 9: CO_2 solubility in water for T1-5_2cm, T1-5_3cm and T3-2_3cm at the operating conditions of 283 K and 58 bar by employing fuel gas mixture..... 147

Figure 5- 10: CO_2 solubility in water for T1-5_2cm, T3-2_2cm and T3-2_3cm at the operating conditions of 283 K and 70 bar by employing fuel gas mixture..... 148

Figure 5- 11: Comparison of (a) water conversion to hydrate and (b) gas uptake for T1-5_2cm and T3-2_2cm at 283 K and various IGCC operating pressures..... 150

Figure 5- 12: CO_2 solubility in water for long experiments; (a) pure CO_2 gas system at 275 K and various driving forces, (b) pure CO_2 gas system at 280 K and 36 bar and (c) fuel gas system at 283 K and 28 bar 152

Figure 5- 13: Comparison of water conversion to hydrate at various experimental conditions; non-filled box indicates long experiments and filled-box indicates short experiments..... 153

Figure 5- 14: CO_2 uptake at various non-IGCC operating conditions by employing fuel gas mixture (thick border – literature results; dotted – batch FBR, crossed – semi-batch FBR, unfilled – semi-batch STR)..... 156

Figure 5- 15: CO_2 uptake at various IGCC operating conditions by employing fuel gas mixture (thick border – literature results; dotted – vertical batch FBR, grid – horizontal batch FBR, slanted – batch STR) 158

Figure 5- 16: Comparison of gas uptake between pure CO_2 gas and fuel gas mixture systems after 120 min by employing silica in non-IGCC conditions (thick border –

literature results; dotted – batch FBR, crossed – semi-batch FBR; P-pure CO_2 gas, F-fuel gas mixture) 160

Figure 6- 1: P-t curve for T3-2 at 283 K and 70 bar in fuel gas mixture system after 1200 minutes inside batch FBR (insert is the P-t curve for the first 100 minutes; points D & H are the process repetition of point b-c and e-g respectively) 166

Figure 6- 2: Hydrate phase equilibrium of pure CO_2 gas (comparison with the literature) 171

Figure 6- 3: Hydrate phase equilibrium of fuel gas (comparison with the literature); black-dotted region represents the IGCC operating conditions 173

Figure 6- 4: Factors that improved CO_2 capture through formation of hydrate 197

Figure A- 1: Plot of $\frac{p/p_0}{(1-p/p_0)n_a}$ vs $\frac{p}{p_0}$ for BET calculation 225

Figure A- 2: Plot of the equilibrium mole fraction of CO_2 in water vs. temperature at given pressures (Servio et al., 2001) 225

Figure A- 3: P-T diagram showing solubility of CO_2 in water (Diamond et al., 2003) 225

Figure A- 4: CO_2 solubility in water for type 1 combined-promoters at the operating conditions of 275 K and 36 bar by employing pure CO_2 gas 226

Figure A- 5: CO_2 solubility in water for type 2 & 3 combined-promoters at the operating conditions of 275 K and 36 bar by employing pure CO_2 gas 226

Figure A- 6: CO_2 solubility in water for type 1A combined-promoters at the operating conditions of 275 K and 36 bar by employing pure CO_2 gas 227

Figure A- 7: CO_2 solubility in water for T1-5 & T3-2 combined-promoters at the operating conditions of 275 K and 30 bar by employing pure CO_2 gas 227

Figure A- 8: CO_2 solubility in water for T1-5 & T3-2 combined-promoters at the operating conditions of 275 K and 22 bar by employing pure CO_2 gas 228

Figure A- 9: CO_2 solubility in water for T1-5, T3-2 & T1A-2 combined-promoters at the operating conditions of 288 K and 36 bar by employing pure CO_2 gas 228

Figure A- 10: CO_2 solubility in water for T1-5 & T3-2 combined-promoters at the operating conditions of 293 K and 36 bar by employing pure CO_2 gas 229

Figure A- 11: CO_2 solubility in water for T1-5_3cm at the operating conditions of 275 K and 58 bar (P_{CO2}=23 bar) by employing fuel gas mixture 229

Figure A- 12: Hydrate phase equilibrium for H_2+THF and H_2+TBAB (Hashimoto et al., 2006) 231

Figure A- 13: Some of pressure profiles used to determine hydrates phase equilibria in this work; (a) 275 K & 22 bar, (b) 288 K & 35 bar, (c) 293 K & 36 bar.....232

Figure A- 14: Schematic diagram of modified HPVA (dotted region) 234

Figure A- 15: Schematic diagram of semi-batch horizontal FBR 234

Figure A- 16: Schematic design of dual-batch horizontal FBRs and valve sequencing for four steps in the cycle.....235

List of tables

Table 1- 1: Pre and post CCS design performance (IEAGHG, 2015) 8

Table 1- 2: Geometry of cages (Sloan et al., 2008) 23

Table 1- 3: Hydrate forming conditions for CO_2 (Carrol, 2009) 27

Table 1- 4: Silica gel properties (Adeyemo et al., 2010) 48

Table 1- 5: Possible promoter combinations 54

Table 2- 1: The properties of each silica.....62

Table 2- 2: The amount of each promoter used to prepare sample at the required concentration.....67

Table 3- 1: Brief description of the type of methods that were investigated.....80

Table 3- 2: The equilibrium moisture content in wet silica gel for different types of sample preparation methods 81

Table 3- 3: Summary of results for hydrate formation experiments performed at 275 K and 35 bar in 1200 minutes (samples prepared by Methods 1 – 4) 86

Table 3- 4: Experimental operating conditions with their respective calculated driving force 90

Table 3- 5: Summary of results for hydrate formation experiments performed at various hydrate forming conditions in 600 minutes (experiments 1 – 4) 96

Table 3- 6: Type of promoters employed in this work based on the optimum concentration obtained by previous researchers 98

Table 3- 7: Summary of results for hydrate formation experiments performed by employing promoter at 36 bar and various operating temperatures (275 K and 288 K) in 600 minutes.....101

Table 4- 1: Combinations of promoters investigated in this particular study.....107

Table 4- 2: The summary of results for equilibrium moisture content at various concentrations of T1 combined-promoter.....108

Table 4- 3: Maximum CO_2 uptake in 1200 minutes at 275 K and 36 bar for various concentrations of T1 combined-promoter and baseline experiments 112

Table 4- 4: Summary of results for equilibrium moisture content at various concentrations of T2 and T3 combined-promoters.....115

Table 4- 5: Maximum CO_2 uptake in 1200 minutes at 275 K and 36 bar for various concentrations of T2 and T3 combined-promoters and baseline experiments 118

Table 4- 6: Summary of results for equilibrium moisture content at various concentrations of type T1A combined-promoters 120

Table 4- 7: Maximum CO_2 uptake in 1200 minutes at 275 K and 36 bar for various concentrations of T1A combined-promoters and baseline experiment 123

Table 4- 8: The optimum results observed for each type of combined-promoter and baseline experiment at 275 K and 36 bar.....125

Table 4- 9: The comparison of gas uptake of 13X-5_2cm, 13X-5_3cm, 13X-H_2O_3cm, T1-5_3cm and baseline experiment at 36 bar and 275 K in 1200 minutes 129

Table 5- 1: Comparison of gas uptake for T1-5, T3-2 and baseline experiment at 275 K and the operating pressures of 36, 30 and 22 bar in 1200 minutes.....138

Table 5- 2: The comparison of gas uptake at 36 bar and operating temperatures of 288 K & 293 K in 1200 minutes.....144

Table 5- 3: Comparison of gas uptake at various IGCC operating conditions and bed heights of T1-5 and T3-2 149

Table 5- 4: Comparison of water conversion to hydrate for long and short experiments at various experimental conditions 154

Table 5- 5: CO_2 uptake for silica contacted with promoters at various non-IGCC operating conditions by employing fuel gas mixture in this work.....156

Table A- 1: The calculated experimental values to plot $\frac{p/p_0}{(1-p/p_0)V_a}$ vs $\frac{p}{p_0}$ 22119

Table A- 2: The amount of each promoter used to prepare each combined-promoter 221

Table A- 3: The summary of equilibrium moisture content (wt%) for method 1, 2, 3 and 4 (baseline experiment) 222

Table A- 4: The summary of equilibrium moisture content (wt%) for T1, T2, T3, T1A and baseline experiments 223

Table A- 5: The summary of hydrates formation results for T1, T2, T3, T1A and baseline experiments 224

Table A- 6: Experimental values of the solubility of H_2 gas in water at different partial pressures (Young, 1981) 230

Table A- 7: Interpolated values of the solubility of H_2 gas in water at the IGCC and non-IGCC conditions 230

Table A- 8: Ratio of molecular diameter to cage diameter for the guest molecules of sI and sII hydrates (Sowjanya et al., 2014) 233

Table A- 9: Valve sequencing for four steps in the cycle 235

ABBREVIATIONS

AMP – 2-Amino-2-Methyl-Propanol

BET - Brunauer, Emmett and Teller

BJH - Barret-Joyner-Halenda

CCS – CO_2 Capture & Storage

CMC - Critical Micelle Concentration

CO – Carbon Monoxide

CO_2 – Carbon Dioxide

CI – Confidence Interval

CP - Cyclopentane

DEA – Diethanolamine

DTAB – Dodecyl Tri-methyl-Ammonium Bromide

DTACl – Dodecyl Tri-methyl-Ammonium Chloride

EGME – Ethylene Glycol Mono-ethyl Ether

EGR – Enhanced Gas Recovery

EOR – Enhanced Oil Recovery

FBR - Fixed Bed Reactor

He - Helium

H_2 - Hydrogen

H_2O – Water

HBGS – Hydrate Based Gas Separation

HPVA – High Pressure Volumetric Analyser

IEA – International Energy Agency

IGCC – Integrated Gasification Combined Cycle

MDEA – Methyldiethanolamine

MEA – Monoethanolamine

MOF – Metal-Organic Frameworks

N_2 – Nitrogen

NGHD - Natural Gas Hydrate Deposits

O_2 - Oxygen

ppm – Parts-Per-Million

PSA – Pressure Swing Adsorption

P-t curve - Pressure–time curve

SDS – Sodium Dodecyl Sulphate

SHS – Sodium Hexadecyl Sulphate

STR – Stirred Tank Reactor

STS – Sodium Tetradecyl Sulphate

T1 – Type 1

T1-1 – 3.000 mol% THF & 0.010 mol% SDS

T1-2 – 3.000 mol% THF & 0.020 mol% SDS

T1-3 – 3.000 mol% THF & 0.100 mol% SDS

T1-4 – 1.000 mol% THF & 0.010 mol% SDS

T1-5 – 5.600 mol% THF & 0.010 mol% SDS

T1-6 – 3.000 mol% THF & 0.005 mol% SDS

T1-7 – 7.000 mol% THF & 0.010 mol% SDS

T2 – Type 2

T2-1 – 3.000 mol% THF & 0.290 mol% TBAB

T3 – Type 3

T3-1 – 0.010 mol% SDS & 0.290 mol% TBAB

T3-2 – 0.010 mol% SDS & 0.100 mol% TBAB

T1A – Type 1(Alternative)

T1A-1 – 0.010 mol% EGME & 0.010 mol% SDS

T1A-2 – 0.100 mol% EGME & 0.010 mol% SDS

T1A-3 – 1.000 mol% EGME & 0.010 mol% SDS

TBAB – Tetra-n-butyl Ammonium Bromide (TBAB)

THF – Tetrahydrofuran

UTR – Unstirred Tank Reactor

WGS – Water-Gas Shift

Zeolite 13X-5 - Zeolite 13X contacted with T1-5 combined-promoter

Θ/β – Type of Guest Molecules

CHAPTER 1: RESEARCH BACKGROUND

1.1.Introduction

This chapter summarises the current research on global CO_2 emissions and also the need and challenge faced by carbon capture & storage (CCS) to reduce emissions from fossil fuel combustion. The current CO_2 capture technologies are then introduced to address this issue. Pre-combustion capture in integrated gasification combined cycle (IGCC) plants is then described in more detail as CO_2 is at high partial pressure and hydrate based gas separation (HBGS) can be considered for CO_2 capture. The perspective on CO_2 hydrate and previous works conducted by researchers are then further explained. Finally, the aim and objectives for this study are described.

1.2.CO_2 emissions and CCS

CO_2 belongs to a category of gases known as 'greenhouse gases (GHG)' which absorb warmth from the surroundings and re-radiate some of it back toward Earth's surface. This process is necessary for slowing the rate at which the planet loses heat and the Earth's average temperature would fall below freezing without it. However, human activities since the Industrial Revolution such as burning coal, natural gas and oil to power machines for manufacturing and transportation have now increased the concentration of CO_2 in the atmosphere, intensifying the natural warming caused by the greenhouse effect (Caitlyn, 2014).

CO_2 emissions from the use of fossil fuels have increased over the past century; according to the International Energy Agency (IEA, 2013), climate scientists have observed that CO_2 concentrations in the atmosphere in 2012 were about 397 ppm, with an average growth of 2 ppm/year in the last ten years. In addition, Biello (2013) reported that CO_2 levels in the atmosphere have reached 400 ppm for the first time in at least 800,000 years on May 7,

2013 (Figure 1- 1). This value is far above the value recorded before the Industrial Revolution: 280 ppm (Caitlyn, 2014).

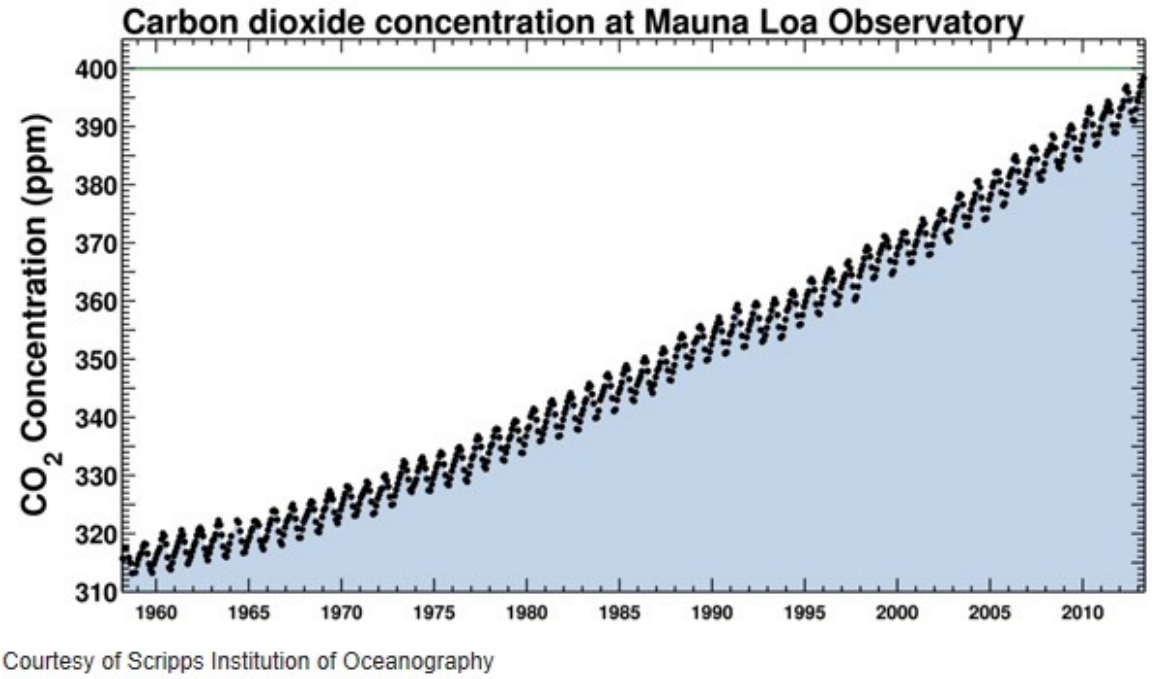


Figure 1- 1: Carbon dioxide concentration in the atmosphere from 1960 – 2013 (Biello, 2013)

Figure 1- 2 compares the year-to-date temperature variances for 2015 (black line) to the six warmest years on record: 2014, 2010, 2013, 2005, 2009 and 1998 in which the January value is the January average temperature, the February value is the average of both January and February, and so on. Climate change has resulted in all-time global average temperature records for all months since 1880 differing from the 20th century average by 1.11 ^{o}C; this is the first time the deviation exceeded 1 ^{o}C (NOAA, 2015). Biello (2013) stated that global temperatures are estimated to rise by 2 ^{o}C if the concentration of CO_2 in the atmosphere reaches 450 ppm.

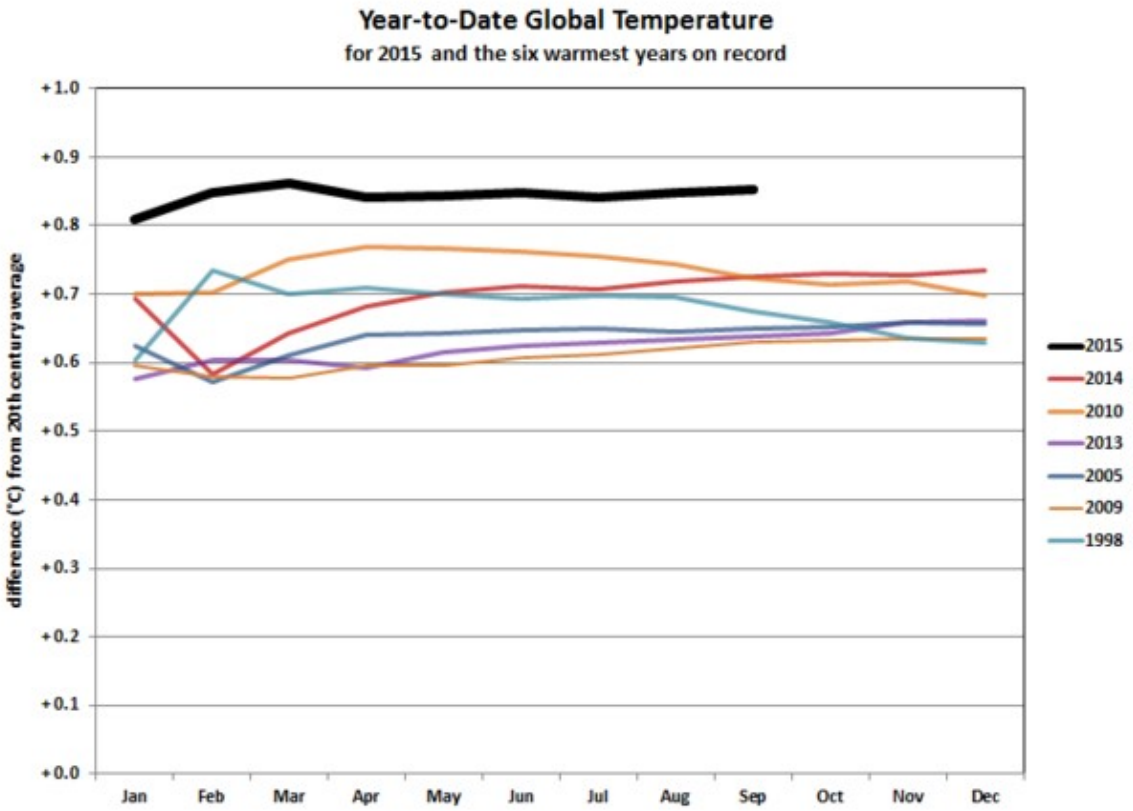
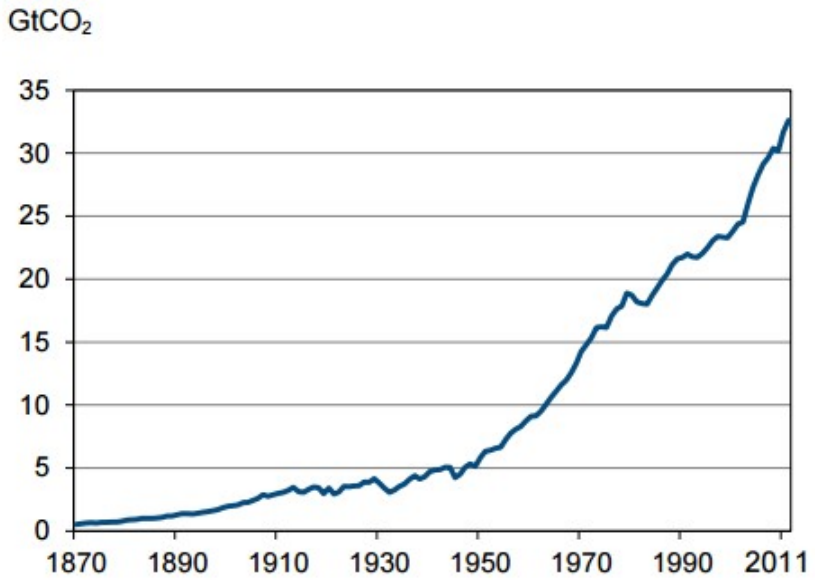


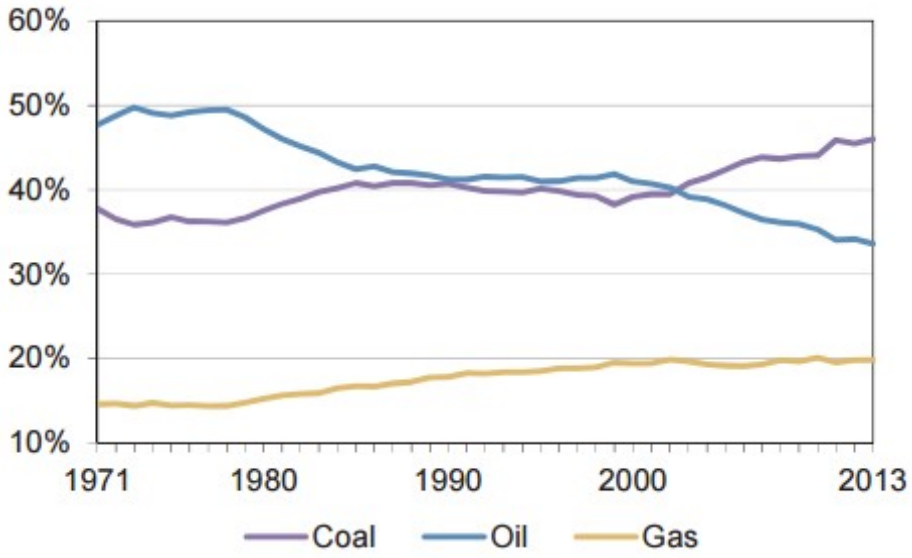
Figure 1- 2: Global year to date temperature variances (NOAA, 2015)

As mentioned, the reason for such an extreme rise in CO_2 concentrations in the atmosphere is due to the continual use of fossil fuels (Figure 1- 3), especially with a rapid growth of coal combustion (Figure 1- 4) in developing countries (such as China and India) accounting for almost 46% of total fossil fuel combustion in 2013 (IEA, 2015). Even though the share from oil has decreased from 40% to 33% and the share of emissions from natural gas staying approximately stable at 20% within a 13 year period (Figure 1- 4), the rise of CO_2 emissions in the atmosphere remains a big problem that needs to be seriously resolved.



Source: Carbon Dioxide Information Analysis Center, Oak Ridge National Laboratory, US Department of Energy, Oak Ridge, Tenn., United States.

Figure 1- 3: CO_2 emissions from fossil fuel combustion (IEA, 2015)



Key point: The global fossil fuel mix changed significantly in recent years, with coal replacing oil as the largest source of CO_2 emissions.

Figure 1- 4: Fuel shares in global CO_2 emissions (IEA, 2015)

With the persistent use of fossil fuels, the capture of CO_2 needs to be considered (Kunze et al., 2012). According to IEA (2008), CCS has been a favourable mitigation against climate change where it will be 70% more costly without CCS than with it by 2050. CCS is a 3-step process including CO_2 capture from power plants, industrial sources, and natural gas wells with high CO_2 content, transportation (usually via pipelines) to the storage site, and geological storage in deep saline formations, depleted oil/gas fields, unmineable coal seams, and enhanced oil or gas recovery (EOR or EGR) sites (IEA, 2006).

In addition, Alphen et al. (2010) mentioned that CCS is an important solution to solve the dual-challenge of reducing GHG emissions, while utilising fossil fuel reserves to meet future energy requirements. Their study on the development of CCS technologies in the United States highlighted that a policy strategy is important to (1) stimulate technology learning, (2) facilitate collaboration and coordination in CCS actor networks, (3) create financial and market incentives for the technology, and (4) provide supportive regulation and sound communication on CCS.

In 2012, IEA introduced a policy strategy to assist those involved in designing national and international policies related to CCS. This policy covers both conventional fossil-fuel CCS and bioenergy with CCS (BECCS) by exploring development of CCS from its early pilot and demonstration project stages to wide-scale operation of the technology. The policy instruments were introduced focussing on controlling carbon emissions, promoting learning especially for those who are not directly involved, explaining the possible return on investment (ROI) on capital and financial markets to investors and also encouraging CCS development for infrastructure related to transport and storage.

Recently, the UK government shocked the industry and investors when they unexpectedly announced withdrawing the allocated budget of £1 billion for UK's future CCS projects (Angus MacNeil's committee, 2016). The UK's CO_2 emissions are expected to reduce the

government's intention to focus on gas-fired power stations. However, Angus MacNeil's committee mentioned that there is a need for CCS to ensure that the decarbonisation targets in 2030 and 2050 can be achieved. Thus, the committee pointed out how CCS infrastructure and the UK's geological capital could be combined to provide storage capacity that can be turned into new revenue streams as a possible way to ensure the feasibility of CCS. In summary, CCS remains the best option to achieve mid- to long-term reduction of CO_2 emissions in light of the world's dependence on fossil fuel for growing energy demand.

1.3.CO_2 capture leading technologies

The three leading technologies for CO_2 capture are post-combustion capture, pre-combustion capture at IGCC plants and oxy-fuel combustion Figure 1- 5 shows a schematic of these CO_2 capture approaches (Hu, 2011).

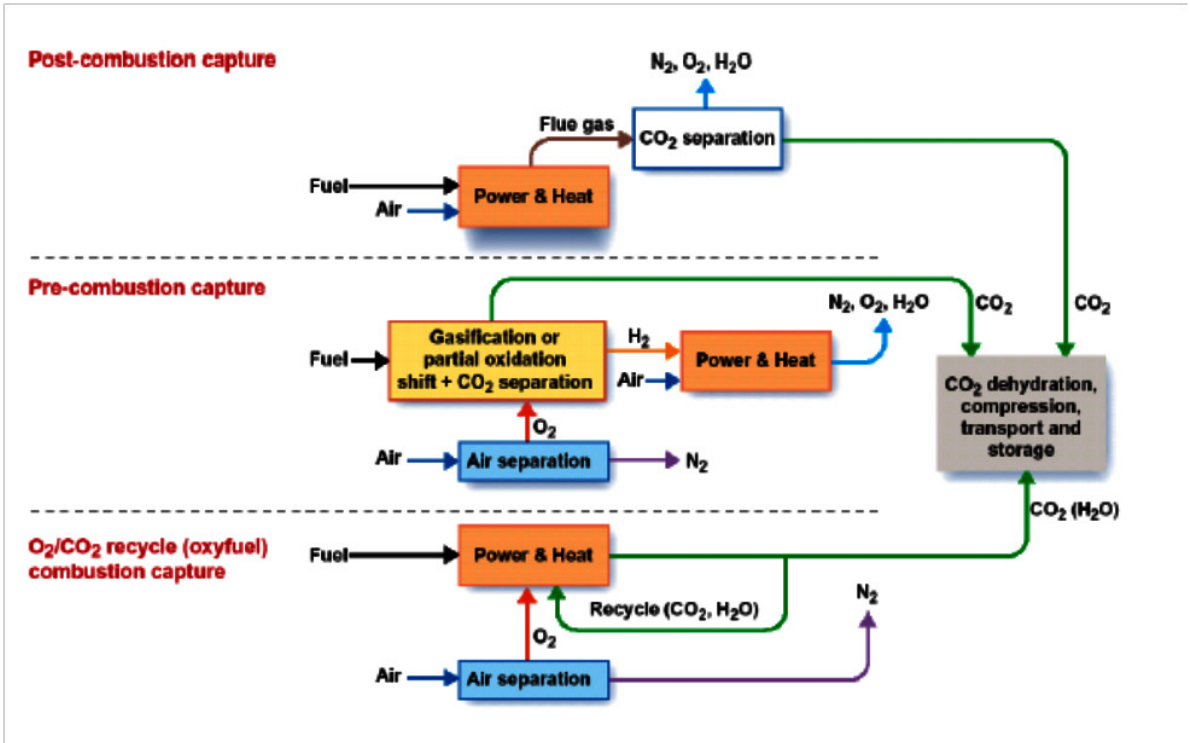


Figure 1- 5: Overview of CO_2 capture approaches (Hu, 2011)

1.3.1. Post-combustion capture

Post-combustion capture can be attained in the flue gas stream emitted from conventional steam power plants entailing the separation of CO_2 from the flue gas mixture (Figure 1- 5). Typical CO_2 concentration in flue gas is 10-15%. The existing power plants can be revamped with post-combustion capture technology and thus it has the greatest imminent potential for reducing CO_2 emission. However, this post-combustion capture is said to only have a minor impact on the power conversion process and due to the low concentration of CO_2 in the flue gas, the capture process is less efficient (because of high energy penalty) and the solvent regeneration energy is rigorous (Kunze et al., 2012).

The IEAGHG (2015) explained the success of the first-ever, commercial-scale, coal-fired power plant incorporating amine solvent absorption carbon capture (Figure 1- 6) which began operation in October 2014 in Canada known as the 'Boundary Dam Integrated CCS Project'. Combined with the pre-conditioning of the flue gas before entry to the capture plant, the new flue gas emitted from the stack has made significant improvements on all air emissions compared to its pre-retrofit emission performance (Table 1- 1) with a calculated 90% reduction in CO_2 emissions. Furthermore, the emissions of SO_2 improved by 100%, PM_{10} by 92%, $PM_{2.5}$ by 70% and NO_x by 56%. This project has shown a bright future in post-combustion CO_2 capture and can absolutely provide insight to other clean-coal initiatives.

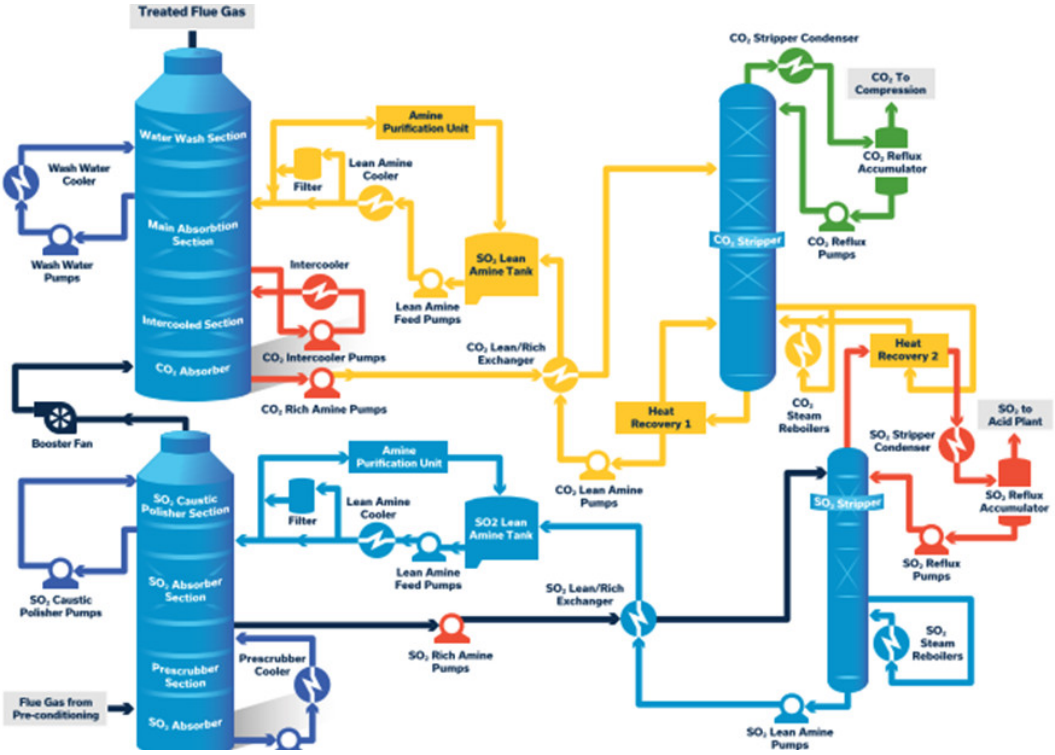


Figure 1- 6: Combined SO_2 and CO_2 capture process (IEAGHG, 2015)

Table 1- 1: Pre and post CCS design performance (IEAGHG, 2015)

Constituent	Pre-CCS	Post-CCS*	Change (%)
Power	139 MW	120 MW	13.6
CO_2	3604 tonnes/day	354 tonnes/day	90
SO_2	7 tonnes/day	0 tonnes/day	100
NO_X	2.4 tonnes/day	1.05 tonnes/day	56
PM_{10}	190 kg/day	15 kg/day	92
PM_{25}	65 kg/day	7 kg/day	70

* Design values

1.3.2. Oxy-fuel combustion

Oxy-fuel combustion is a process where a fuel is combusted with oxygen (O_2) in a nitrogen (N_2) free environment to produce a flue/exhaust gas consisting of CO_2 and water (H_2O) (Figure 1- 5). CO_2 can be recovered with values up to 90% by condensing the water proportion due to the fact that the proportion of other gas species in the flue gas is low.

Therefore, the energy penalty for this method will be lower than post-combustion capture. This has led to the world's first '30 MWth' full chain demonstration at Schwarze Pumpe Pilot Plant in 2009, followed by Callide with the world's first '100 MWth' retrofitted oxy-fuel power plant in 2012 (IEA, 2014).

However, further scale-up to a demonstration plant of over 100MW, integrated with CO_2 transport and storage is required before oxy-fuel combustion can be considered technologically ready for commercialisation. Additionally, in order to carry coal moisture as vapour at relatively low temperature and avoid the risk of explosion as well as the problem of corrosion, the primary recycle stream (Figure 1- 7) must be dried and recycled after all flue gas cleaning units (Hu, 2011). Therefore, this method has a higher impact on the power plant process, where it complicates the operation and requires retrofitting existing plants because of the need for cold flue gas recycling which limits the combustion temperature (Kunze et al., 2012).

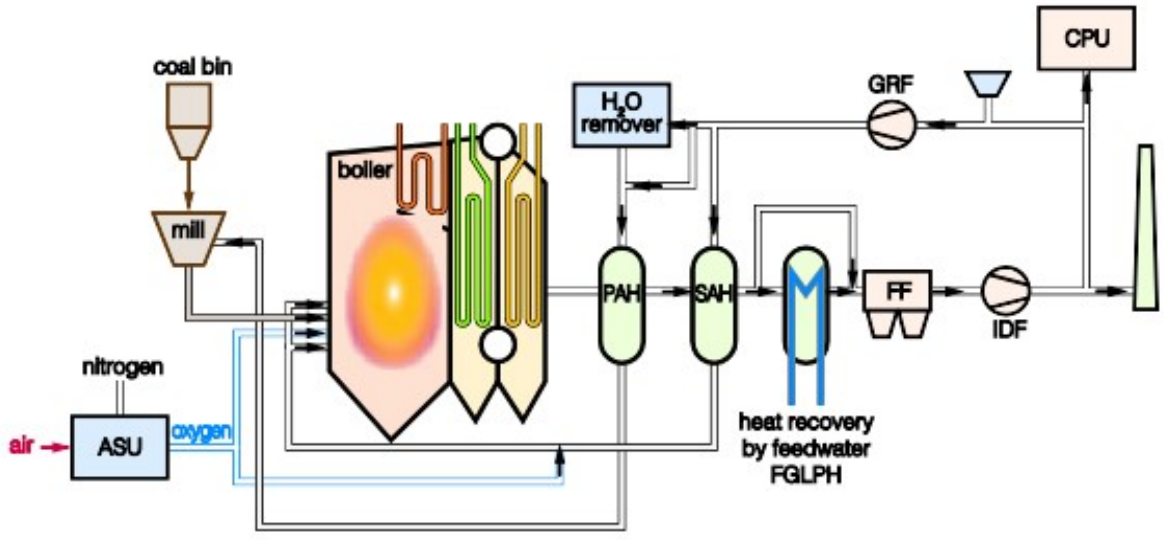


Figure 1- 7: The process flow of the 100 MWth Callide oxy-fuel pilot in Australia (PAH, primary air heater; SAH, secondary air heater; FF, fabric filters; IDF, induction draught fan; GRF, gas recirculation fan) (IEA, 2014)

1.3.3. Pre-combustion capture in IGCC plant

The main concept of pre-combustion is to produce fuel gas containing mostly CO_2 and H_2 (an attractive future clean energy source) emitted in the range between 283-290 K at a pressure range of 20-70 bar (Metz et al., 2005). Thus, pre-combustion CO_2 capture involves the removal of CO_2 from a fuel gas mixture and simultaneous H_2 production in which the technologies involved are IGCC, coal or biomass gasification and methane reforming processes. IGCC involves reacting a fuel with oxygen or air and/or steam to produce mainly a synthesis gas (syngas) or fuel gas composed of carbon monoxide (CO) and H_2 (IEA, 2011 and Rackley, 2010). Figure 1- 8 shows that the syngas is further converted to CO_2 and hydrogen (H_2) through the water gas shift (WGS) reaction: $CO + H_2O \leftrightarrow CO_2 + H_2$. Then, carbon capture is completed by separating H_2 from the gaseous mixture, usually by a physical or chemical absorption process, resulting in a H_2-rich fuel which later can be used as energy sources for many applications such as boilers and gas turbines.

This approach is not feasible in conventional steam power plants, but is used in IGCC plants due to the high concentration of gas in the gasification which allows efficient de-carbonisation of the fuel (Kunze et al., 2012). In addition, CO_2:H_2 separation is somewhat easier than the post-combustion separation of CO_2 and N_2 due to the greater difference in molecular weights and molecular kinetic diameters for CO_2 versus H_2 than for CO_2 versus N_2. Moreover, the Global CCS Institute (2013) listed almost all projects related to CCS and the pre-combustion capture method is the preferred method in which the 'Century Plant Project' in the United States has the highest capture capacity of 8.4 Mtpa, and has been in operation since 2010.

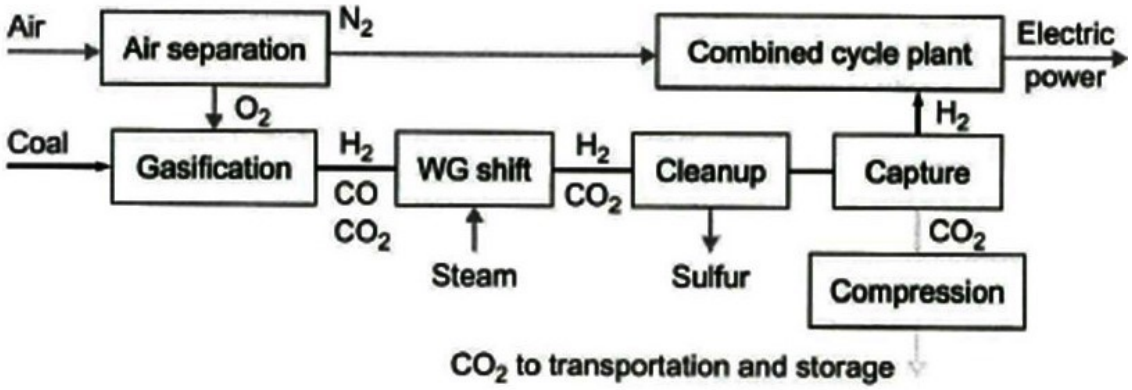


Figure 1- 8: Pre-combustion capture IGCC process schematic (Rackley, 2010)

1.3.4. Existing technologies for CO_2 capture

Figure 1- 9 shows examples of promising new materials for CO_2 capture methods such as physical or chemical absorbents, adsorption of solids, cryogenic systems, membranes, gas hydrate formation and chemical looping combustion by metal oxides.

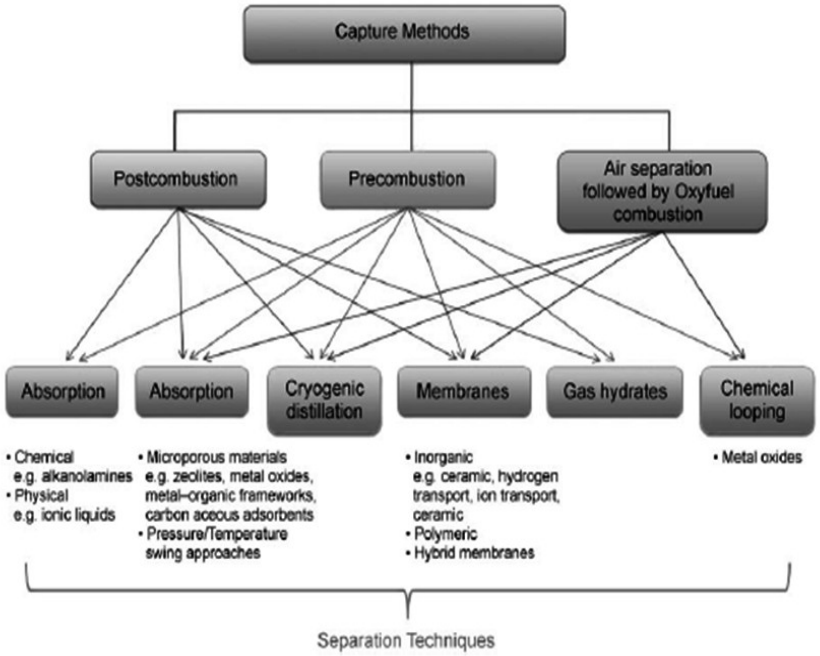


Figure 1- 9: Materials for CO_2 capture in the context of post-combustion, pre-combustion and oxy-fuel processes (D'Alessandro et al., 2010)

1.3.4.1. Absorption

Physical absorption is the most common pre-combustion CO_2 capture. Basically, CO_2 separation from syngas is often commenced using physical absorption solvents such as Selexol where it exploits the high pressures of the fuel gas to achieve strong absorption into solvents that have a high solubility for CO_2. The Selexol process can be operated in the pressure range of 20-130 bar and temperature range of 255-448 K. Nevertheless, the vented gas from this process often does not have the CO_2 purity required for CCS purpose due to the absorption of other syngas components such as H_2, CO and N_2 in the solvent and generally the focus of this technique is on recovery and recycling valuable fuel gas components, such as H_2 (Scholes, 2013). Moreover, the main obstacle of using physical absorption is probably the need to cool the gas to allow CO_2 capture followed by heating it up again for firing the IGCC gas turbine which decreases the plant's thermal efficiency and thus increases the overall costs (IEA, 2011).

Monoethanolamine (MEA) is a chemical absorption solvent that is most commonly used for post-combustion CO_2 capture operating in the pressure range of 10-80 bar and temperature range of 303-343 K. This method can be accomplished due to the fact that CO_2 is acidic and it can be bound to a basic solvent. This CO_2 rich solvent is then regenerated to strip off the CO_2 to recover in high concentrations and the solvent is then recycled. CO_2 recovery rates of 98% and product purity of 99% can be accomplished. MEA is the industrial standard alkanolamine for CO_2 absorption because of its fast kinetics, low density and viscosity but it has some drawbacks such as high oxidative degradation, high corrosion rate, high absorption enthalpy, high energy penalty due to solvent regeneration and high capital cost (Adeosun et al., 2013). Therefore, alternative options have been investigated to overcome the drawbacks of MEA by considering mixed amines, such as monoethanolamine/methyldiethanolamine (MEA/MDEA),

diethanolamine/methyldiethanolamine (DEA/MDEA) and monoethanolamine/2-amino-2-methyl-propanol (MEA/AMP) systems.

1.3.4.2. Solid physical adsorption

Microporous and mesoporous materials such as zeolites, metal oxides, metal-organic frameworks (MOF) and carbonaceous adsorbents can be used for solid physical adsorption. Zeolites 13X and MOF have been used for pre-combustion CO_2 capture from fuel gas by using pressure swing adsorption (PSA). The process and boundary conditions of this separation step, especially a high feed pressure between 30 and 50 bar and a CO_2 mole fraction of about 40% (dry basis), makes PSA a promising process since no further compression energy is needed. In this process, the gas mixture flows through a packed bed of solid adsorbent at elevated pressure until the concentration of desired gas reaches equilibrium. The bed can be regenerated by reducing the pressure. However, the high energy loss due to the transportation and storage that follows the capture where it requires CO_2 compression to about 110 bar is the drawback of this method. Furthermore, the energy penalty of this step depends mainly on the pressure level of the CO_2 before compression and on its purity, i.e. on the fraction of non-condensable gases present (Schell, 2013).

This CO_2 capture method can also be applied by using temperature swing adsorption (TSA) wherein the bed can be regenerated by raising the temperature. In pre-combustion capture, PSA is more favourable since the TSA system involves massive heating of the adsorbent during regeneration and the physical size of the TSA plant is much larger. Yang et al. (2014) used TSA for post-combustion CO_2 capture using polyaniline solid sorbent and the results with optimal operation conditions were 92.5% recovery and 47.7% CO_2 purity which is lower than the previously mentioned method, chemical absorption by MEA (CO_2 recovery rates were 98% and CO_2 purity was 99%).

1.3.4.3. Cryogenic systems

Atsonios et al. (2013) investigated the CO_2 separation process with two proposed cryogenic systems: flash separation with internal cooling and separation with distillation column. Cryogenic separation allows for direct production of liquid CO_2 needed for transport. Cryogenic distillation is extensively used commercially for streams that already have high CO_2 concentrations and can be used in oxy-fuel combustion or pre-combustion capture. As for flash separation with internal cooling, electrical power is produced while the separation efficiency is reasonable, as 62.6% of the heat input from combustibles is recovered. Instead, separation by a distillation column may result in the complete separation of combustibles providing high purity in the final CO_2 stream (>99%). As a major drawback of cryogenic separation, more energy duty is required due to the external cooling system (Atsonios et al., 2013). Another drawback is that some components such as water, NOx and SOx can cause blockage, fouling and corrosion if they are not removed before the gas stream is cooled.

1.3.4.4. Membrane separation

Membrane separation technologies have some advantages such as low energy requirements, selective extraction of CO_2 from mixed gas streams and flexibility in their possible configurations in industrial plants relative to conventional amine absorber/desorber columns (D'Alessandro et al., 2010). These consist of semi-selective films that allow one or more gases to pass at the expense of other gases which enable CO_2 to be concentrated on one side of the membrane (Scholes et al., 2013). This method depends on the driving force pressure across the membrane to achieve separation, which is beneficial for syngas based processes. Nonetheless, much membrane research has been directed at H_2 purification resulting in a need to develop membrane systems that have high selectivity for CO_2 over H_2 (IEA, 2011).

Gas absorption membranes are hybrid systems that engage gas-liquid interaction in which CO_2 is removed by absorption liquids such as amine after it diffuses through a membrane. This method can avoid operational problems such as flooding, entrainment, foaming and channelling and the process selectivity is establish by the absorption liquid. The disadvantages of this method include the massive increase in cost, complexity and energy consumption due to the requirement of multiple stages in order to attain high degrees of separation.

1.3.5. Emerging technologies for CO_2 capture

This section discusses carbon capture technologies which include novel concepts based on techniques at the pilot or laboratory stages of development such as separation of CO_2 by hydrate formation and chemical looping.

1.3.5.1. Hydrate based gas separation (HBGS)

HBGS is one of the most promising approaches in CO_2 capture field (Zheng et al., 2016; Babu et al., 2014; Linga et al., 2007, McCallum et al., 2005). This CO_2 capture method involves clathrate or gas hydrate crystallisation and can be applied to both post- (from flue gas) and pre-combustion (from fuel gas) capture respectively. The process relies on the ability of water to form non-stoichiometric crystalline compounds in the presence of CO_2, N_2, O_2 and H_2, as well as natural gas components at high pressures (10-70 bar) and low temperatures (near 273 K) (D'Alessandro et al., 2010). This separation method is believed to be energy efficient where the energy penalty imposed by HBGS in the IGCC is only 4.4 - 8% (Elwell et al., 2006; Aaron et al., 2005) and the energy consumption could be as low as 2.05 MJ/kg-CO_2 (Fan et al., 2011).

The HBGS process is more suitable for pre-combustion CO_2 capture from a fuel gas mixture than a flue gas mixture because the partial pressure of the shifted fuel gas (40% CO_2& 60% H_2) is up to 1000 times higher than that of the flue gas (17% CO_2& 83% N_2) in post-combustion capture (IEA, 2011). Thus, the limitation of implementing the HBGS process in post-combustion capture will be the compression costs and the requirement to build huge CO_2 capture equipment. Figure 1- 10 shows the simplified schematic of the HBGS process.

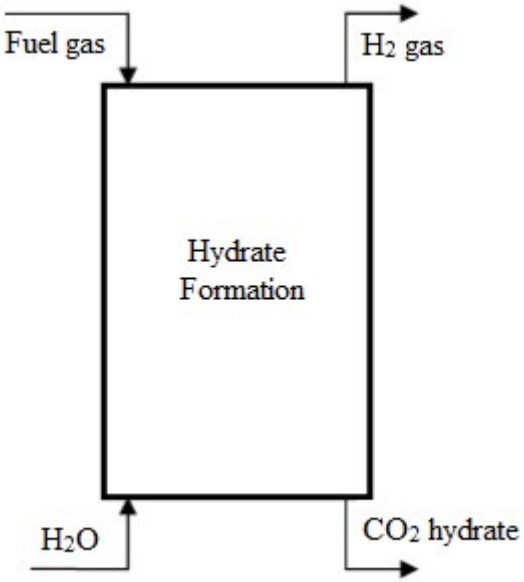


Figure 1- 10: Simplified schematic of HBGS

1.3.5.2. Chemical looping combustion (CLC)

D'Alessandro et al. (2010) explained that in CLC, the combustion step is separated into oxidation and reduction reactions, and a transition metal oxide (e.g., of Mn, Fe, Co or Ni) is employed as an oxygen carrier to circulate between the two reactors. This process has been called unmixed combustion since direct contact between fuel and combustion air is avoided. Figure 1- 11 shows a basic CLC system. In the air reactor, the carrier is oxidised by oxygen where the reaction involved is $O_2 + 2Me \rightarrow 2MeO$ (strongly exothermic). In the fuel reactor, the metal oxide is reduced by fuel, which is oxidised to CO_2 and H_2O with the following reaction: $C_nH_m + (2n + 0.5m)MeO \rightarrow nCO_2 + 0.5mH_2O + (2n + 0.5m)Me$ (endothermic or

slightly exothermic for some combinations of fuel and oxygen carrier). Separation of CO_2 can be done by a condenser comprising a major advantage for CLC by avoiding the huge energy penalty necessary in traditional amine scrubbing. In addition, the exhaust gas stream from the air reactor is harmless (mainly N_2) and no thermal formation of NOx occurs since the regeneration of the oxygen carrier takes place without a flame and at moderate temperatures (Yang et al., 2008).

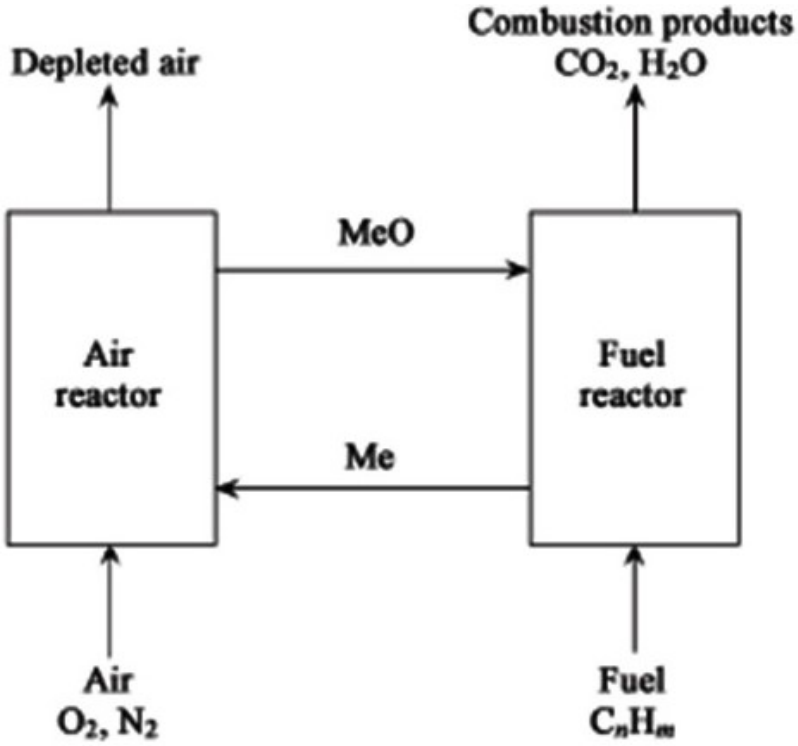


Figure 1- 11: Chemical looping combustion (Me: metal; MeO: metal oxide as oxygen carrier (Yang et al., 2008))

1.4.Advantages of pre-combustion CO_2 capture by HBGS

Pre-combustion capture has been chosen in this study rather than post-combustion and oxy-fuel combustion due to its high shifted gas pressure where the partial pressure of CO_2 is in the range of 8 to 28 bar (Metz et al., 2005) and the fact that it can separate H_2 gas from fuel gas which can produce future clean energy. Moreover, due to the high CO_2 concentration and high pressure in the output stream, the size of CO_2 capture equipment is expected to be

much smaller and different solvents with low energy penalties for regeneration can also be used. Currently, there are various methods for pre-combustion CO_2 capture such as chemical or physical absorption, solid physical adsorption, cryogenic distillation and membrane separation. These techniques have respective advantages, but they also have individual issues that should be resolved, including cost, capacity, corrosion and energy consumption (Kang et al., 2013). The main reason CO_2 capture through solid physical adsorption is not being considered for this particular study is because the H_2 recovery is not really critical whereas for pre-combustion capture in IGCC plants, both H_2 recovery rate and CO_2 purity are important (IEA, 2011). In addition, CO_2 selectivity and capacity are the major drawbacks of adsorption and therefore it is not yet considered attractive for large-scale separation of CO_2 (Aaron et al., 2005).

Recently there have been two developing technologies for pre-combustion CO_2 capture: HBGS and CLC. HBGS has been chosen in this study because the CO_2 hydrate formation conditions fall within the range of operating conditions for pre-combustion in IGCC: shifted gas pressure range of 20-70 bar and temperature between 283-290 K. Therefore, this method can be immediately applied to IGCC plants with no major retrofitting. Furthermore, it is a continuous operation, thus making it possible to treat a large amount of gaseous stream, recovering more than 99 mol% of CO_2 from the fuel gas (Babu et al., 2013). Figure 1- 12 shows the HBGS process for pre-combustion CO_2 capture in IGCC.

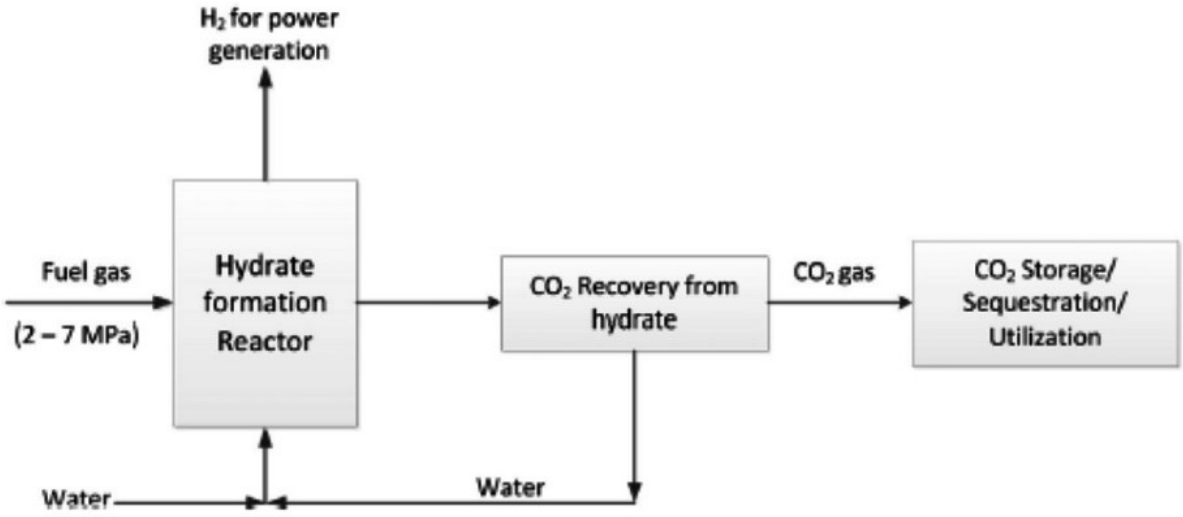


Figure 1- 12: HBGS process for CO_2 pre-combustion capture (Babu et al., 2015)

Moreover, the development of hydrate-based technologies including CO_2 sequestration by forming hydrate, gas separation as well as gas storage are progressing optimistically (Changyu et al., 2011). Chatti et al. (2005) reviewed several studies on clathrate hydrate application and the benefits that can be achieved. Marine CO_2 sequestration is beneficial where the idea is to release CO_2 in water using a process adapted to the injection depth. The application of natural gas storage and transportation which involves gas hydrate production, transportation to the place of use and gas recovery by dissociation of the hydrate structure are also advantageous. Clathrate hydrate is also being associated with cool storage application where the use of hydrate energy is clearly relevant for the field of air conditioning.

Further explanations on the basic theory, properties of CO_2 hydrate and also previous works related to HBGS technology for pre-combustion CO_2 capture are presented in the next section. Then, the challenges of the HBGS process for pre-combustion capture of CO_2 are explained and the objectives of the study are presented, followed by the organisation of this thesis.

1.5.Clathrate hydrate

1.5.1. Definition

The concept of clathrate or gas hydrate formation was initially proposed in the 1930s wherein Hammerschmidt clearly demonstrated that the 'ice' plugged inside gas pipelines and processing equipment was actually gas hydrate (Carrol, 2009). Before that time in the natural gas business, there was no problem related to gas hydrate because the gas was produced and delivered at relatively low pressure. In the twentieth century, the problem of gas hydrate became a major dilemma for the oil and gas industry because of the production, processing and distribution of gas at the time with high-pressure operations with expansion of the industry. After much research, it was established that in seawater, gas hydrate can form naturally. Since natural gas hydrate is widely distributed in permafrost regions and offshore, it is estimated that the global hydrate-bound gas is about $2.5x10^{15}$ m^3 of methane with 230 natural gas hydrate deposits (NGHD) being discovered in deep water across 79 countries (Changyu et al., 2011).

The simplest definition of gas hydrate given by Sloan (2011) is inclusion compounds. This means that there is a network of cages of water molecules that can trap small guest molecules, including CO_2, methane, ethane and propane (Sloan et al., 2008). Additionally, Rackley (2010) said hydrates are a weakly bound molecular complex in which a guest molecule is trapped within a cage of water molecules. Furthermore, Carrol (2009) mentioned that the presence of certain compounds causes the aligned water molecules with hydrogen bonds to stabilise and a solid mixture precipitates. Meanwhile, Demirbas (2010) defined gas hydrate as crystalline solids formed by the combination of gas and water at low temperatures and high pressures. In the context of CO_2 capture, CO_2 hydrate is often referred to as non-stoichiometric solid inclusion bodies, where water (host) forms a lattice

with hydrogen bonding and generates a number of empty cavities, in which CO_2 may be captured (Herslund et al., 2013).

1.5.2. Structures

There are several known structures of hydrate in which the most common are sI, sII and sH. Type sI is the simplest of the clathrate hydrate structures made from two types of cages which are dodecahedron (small cages) and tetrakaidecahedron (large cages). Dodecahedron is a twelve-sided polyhedron wherein each face is a regular pentagon and tetrakaidecahedron is a fourteen-sided polyhedron with twelve pentagonal faces and two hexagonal faces. This type of hydrate consists of 46 water molecules and if a guest molecule occupies each of the cages, the theoretical formula for the hydrate is Θ.5 3/4 H_2O, where Θ is the guest molecule. Some of the type sI guest molecules include methane, hydrogen sulfide, carbon dioxide and ethane where the first three mentioned guest molecules can occupy both the small and the large cages whereas the ethane molecule can only occupy the large cages. Rackley (2010) mentioned that the stoichiometry of CO_2 hydrate is approximately (CO_2:6H_2O) where six molecules of H_2O are needed to trap one molecule of CO_2 (Figure 1- 13). The maximum (theoretical) gas uptake for the CO_2 capacity in sI hydrate will be 0.174 mol of CO_2/mol of H_2O calculated based on the theoretical hydration number of 5.75 for ideal occupancy (Babu et al., 2015).

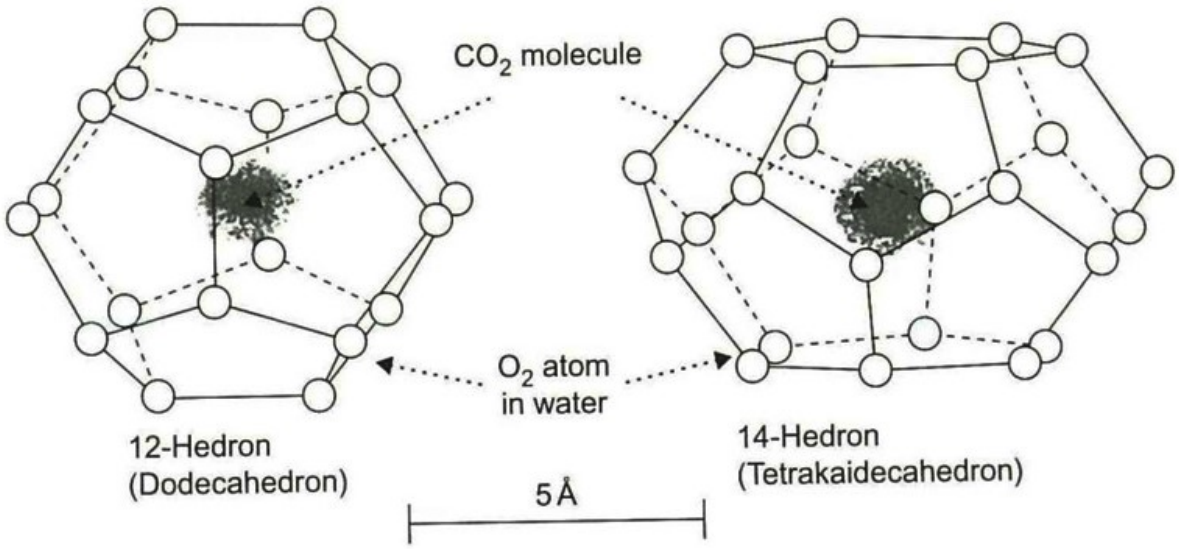


Figure 1- 13: CO_2 hydrate structure (Rackley, 2010)

The structure of type sII hydrate is more complicated than that of sI and it is also constructed from two cages. The first one is still a dodecahedron (small cages) while the other one is hexakaidecahedron (large cages), a sixteen-sided polyhedron with twelve pentagonal faces and four hexagonal faces. The sII type clathrate hydrate consists of 136 water molecules with the theoretical composition of Θ.5 2/3 H_2O for fully occupied cages and Θ.17 H_2O if the guest occupies only the large cages (more common case). N_2 occupies both the large and small cages of type sII hydrate whilst propane and isobutene only occupy the large cages. The maximum (theoretical) gas uptake for the CO_2 capacity in sII hydrate will be 0.176 mol of CO_2/mol of H_2O. The final structure is type sH hydrate consisting of three cages known as dodecahedron (3 cages), an irregular dodecahedron (2 cages) and an irregular icosahedron (1 cage). Type sH hydrate is always double hydrates. Small guest molecules such as methane, occupy the small and medium cages of the structure while a larger molecule such as 2-methylbutane or cyclopentane occupies the large cage. The theoretical formula of type sH hydrate is quite complicated but for the ideal case the formula

should be $\beta.5\Theta.34H_2O$ in which β is the large cage and Θ are the small and medium cages. Table 1- 2 summarises the geometry of these structures.

Table 1- 2: Geometry of cages (Sloan et al., 2008)

Hydrate crystal structure	I		II		H		
Cavity	Small	Large	Small	Large	Small	Medium	Large
Description	5^{12}	$5^{12}6^2$	5^{12}	$5^{12}6^4$	5^{12}	$4^35^66^3$	$5^{12}6^8$
Number of cavities/unit cell	2	6	16	8	3	2	1
Average cavity radius[a] (Å)	3.95	4.33	3.91	4.73	3.94[b]	4.04[b]	5.79[b]
Variation in radius[c] (%)	3.4	14.4	5.5	1.73	4.0*	8.5*	15.1*
No. of water molecules/cavity[d]	20	24	20	28	20	20	36

[a] The average cavity radius will vary with temperature, pressure and guest composition
[b] From the atomic coordinates measured using single crystal x-ray diffraction on 2,2-dimethylpentane-5 (Xe,H_2S)-$34H_2O$ at 173 K (from Udachin et al., 1997b). The Rietveld refinement package, GSAS was used to determine the atomic distances for each cage oxygen to the cage centre.
[c] Variation in distance of oxygen atoms from the centre of a cage. A similar variation in radius reflects a more symmetric cage.
[d] Number of oxygen atoms at the periphery of each cavity.
* represent the variation in radius taken by dividing the difference between the largest and smallest distances by the largest distance.

In the context of pre-combustion CO_2 capture, **w**hen a gas mixture of CO_2 and H_2 forms gas hydrates at moderate pressure, the CO_2 (sI hydrate) is more likely to be in the hydrate phase. As for H_2, it forms sII hydrate at a high pressure of 2000 bar or at a low temperature of about 80 K. This provides the basis for the separation of CO_2 from the fuel gas mixture (Linga et al., 2007).

1.5.3. Mechanism of hydrate formation

Theoretically, the mechanism of hydrate formation can be described through a P-t curve such as in Figure 1- 14 with three phases: dissolution, nucleation and hydrate growth phase. The decrease in the initial pressure of the system, P_o at time t_o to time t_s indicates the

dissolution phase of hydrate formation. Figure 1- 15 shows labile cluster growth during hydrate formation wherein the labile cluster will form immediately upon dissolution of gas in water and according to Sloan et al. (2008) there are several types of clusters such as $CO_2[(H_2O)_{20}]$,$CO_2[(H_2O)_{24}]$and $CO_2[(H_2O)_{28}]$ (Table 1- 2). Later, the pressure will become constant from time t_s to time t_r indicating the nucleation phase of hydrate formation with the total time from t_0 to t_r known as the induction time. At this stage, labile clusters will agglomerate to form dodecahedral, tetrakaidecahedral or hexakaidecahedral clusters. Induction time usually refers to the time required to form the first clathrate hydrate cluster on which the microscopic hydrate grow (Tang et al., 2013). Finally, when the size reaches a critical value, growth begins. The hydrate growth phase is represented by the curve from time t_r until time t_d where the total time to achieve equilibrium can be obtained accordingly. Figure 1- 16 shows the experimental P-t curve obtained by Tang et al. (2013) with different SDS concentrations where several stages of pressure drop can be observed for each SDS concentration. Thus, this will be a basic guideline to determine the formation of CO_2 hydrate in this work together with the study on CO_2 dissolution in water wherein Servio et al. (2001) plotted the equilibrium mole fraction of CO_2 in water in the presence of hydrate at various operating temperatures and pressures.

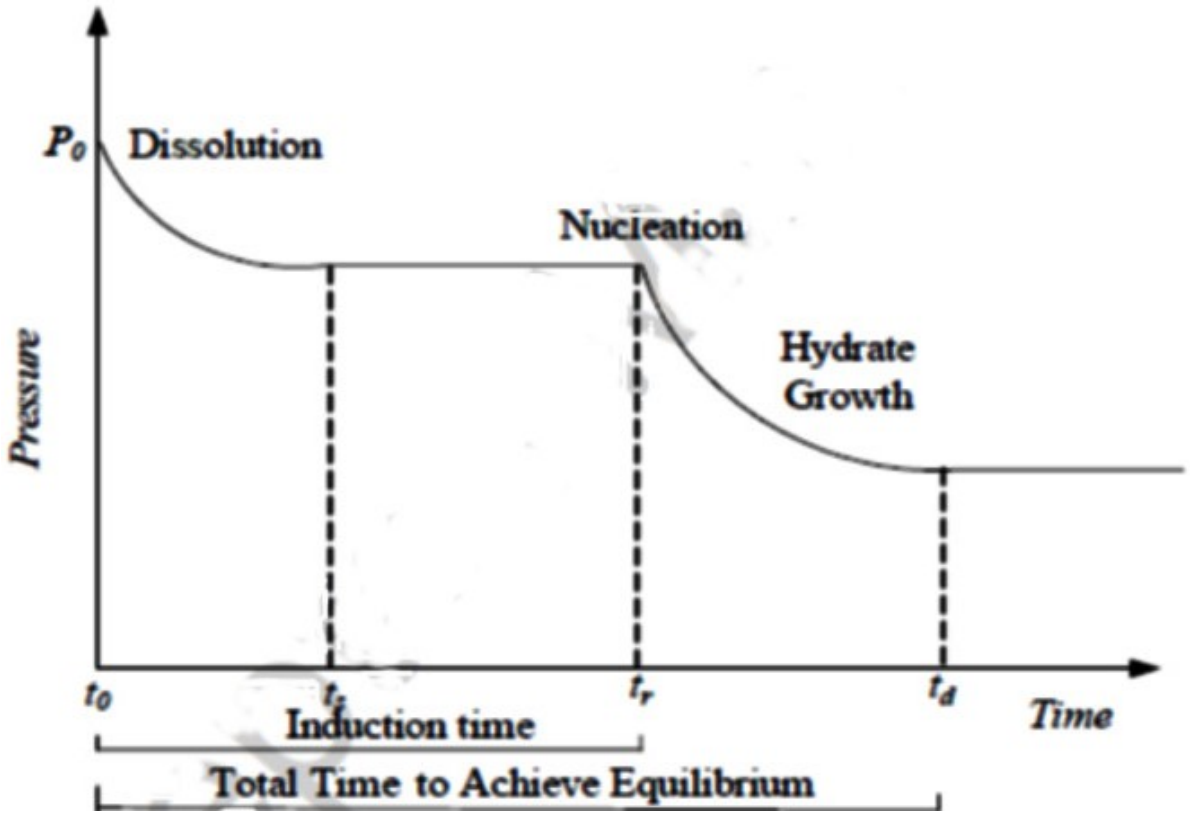


Figure 1- 14: Pressure change during the hydrate formation process (Tang et al., 2013)

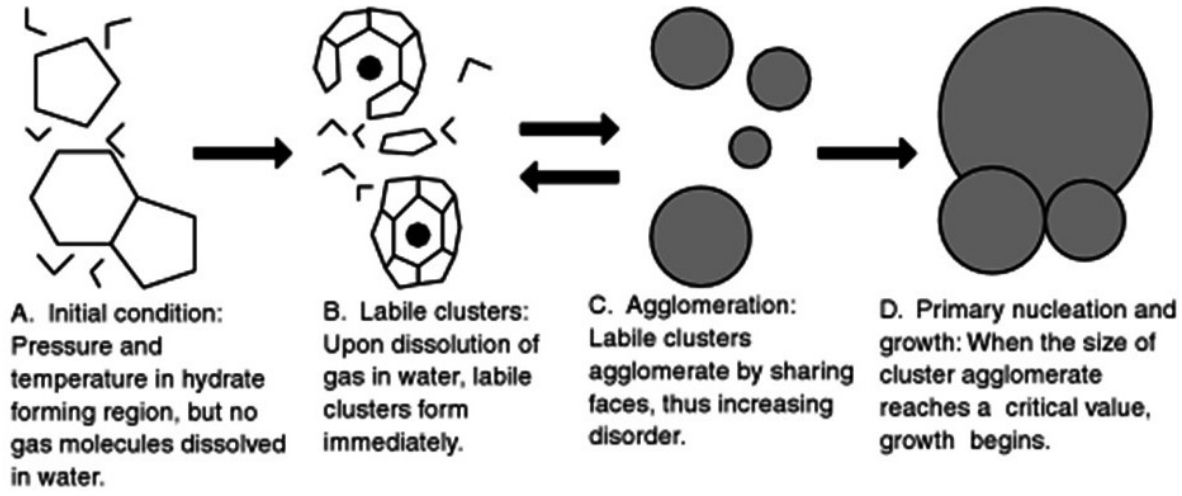


Figure 1- 15: Labile cluster growth (Sloan et al., 2008)

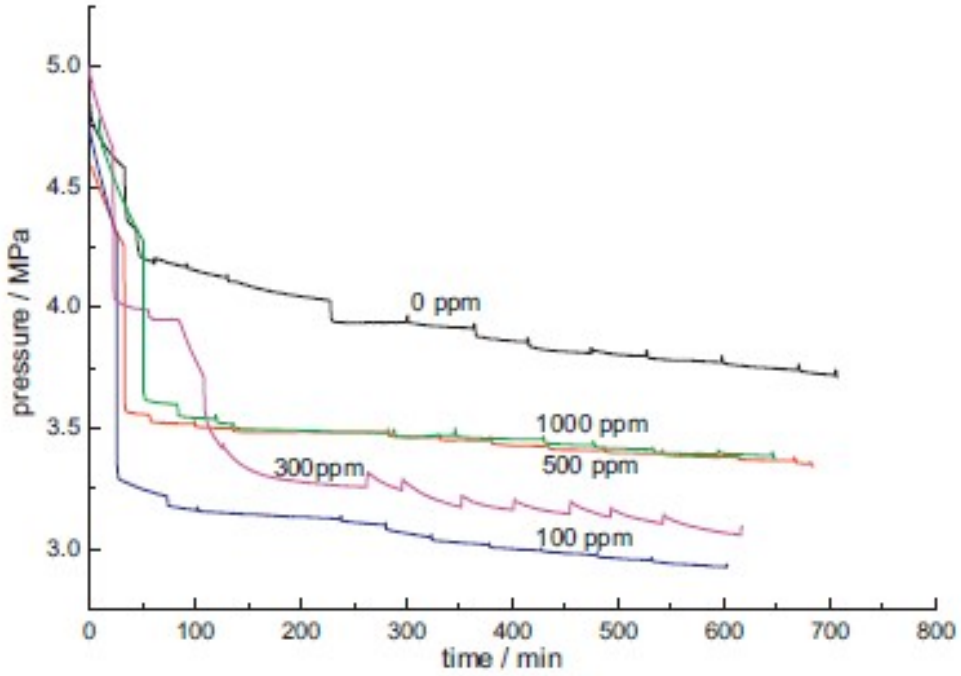


Figure 1- 16: Pressure variations with different SDS concentrations (Tang et al., 2013)

1.5.4. Hydrate forming conditions

Mainly, there are three conditions necessary for hydrate formation to occur: (i) Low temperature and high pressure are needed for these solid compounds to form from pure water depending on the physical and chemical properties of the guest molecule; (ii) guest molecules must be present such as methane, ethane or carbon dioxide; (iii) a sufficient amount of water, not too much and not too little (Carrol, 2009). Table 1- 3 shows that the CO_2 hydrate formation conditions are in the range of 273.15-283 K at the pressure range of 12.7-45 bar. This is the case for a pure CO_2 system. For pre-combustion CO_2 capture, the separation of CO_2 from fuel gas mixture can be achieved due to a massive discrepancy in hydrate phase equilibrium of CO_2 and H_2. Figure 1- 17 shows that at 274 K, the minimum pressure required to form pure CO_2 and pure H_2 hydrates were around 20 bar and 5000 bar respectively. At this temperature, the minimum pressure required for fuel gas mixture to

form CO_2 hydrate is 70 bar which is in the range of shifted gas pressure in the IGCC as previously mentioned.

Table 1- 3: Hydrate forming conditions for CO_2 (Carrol, 2009)

Temp. (K)	Press. (bar)	Phases	Composition (mol%)		
			Aqueous	Non-Aqu.	Hydrate
273.15	12.7	L_A-H-V	1.46	0.058	13.8
275.15	15.2	L_A-H-V	1.67	0.056	13.9
277.15	19.4	L_A-H-V	1.92	0.053	13.9
279.15	25.1	L_A-H-V	2.21	0.051	14.1
281.15	33.0	L_A-H-V	2.54	0.049	14.2
282.95	45.0	L_A- L_C H-V	2.93	0.051 - V 0.021 - L_C	14.2

Notes: Composition for aqueous phase and for the hydrate is the mole percent of the hydrate former (CO_2). For the non-aqueous phase (either the vapour or a second liquid), the composition is the mole percent water. The phase designated L_C is a CO_2-rich liquid.

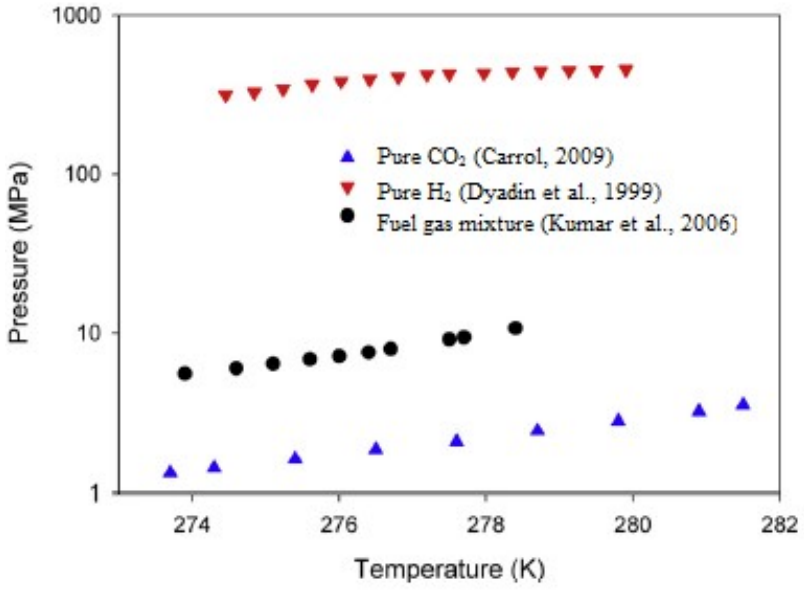


Figure 1- 17: Hydrate phase equilibrium of CO_2, H_2 and fuel gas mixture (Babu et al., 2015)

1.6. Previous works on HBGS for pre-combustion CO_2 capture

There are a number of techniques which have been investigated by researchers to capture CO_2 with gas hydrate formation. In this section, these techniques are described with the application of the most traditional way (bulk water), solid adsorbent and promoters (oxygenated solvents, surfactants, semi-clathrate hydrate and hydrophobic former) to facilitate CO_2 hydrate formation.

1.6.1. Bulk water

Linga et al. (2007)investigated hydrate formation from CO_2/H_2 mixtures in which semi-batch stirred vessel with a magnetic stirrer was used to ensure the pressure was always constant inside the reactor. CO_2 was found to prefer the hydrate phase while very small amounts of H_2 were found in the hydrates. The CO_2 uptake was 0.9 mmol of CO_2/g of H_2O only at the operating conditions of 273.75 K and 85 bar respectively. Park et al. (2013) managed to enhance CO_2 uptake in fuel gas mixture to 1.3 mmol of CO_2/g of H_2O by implementing a mechanical agitator at the operating conditions of 275.5 K and 80 bar. Both researchers have suggested that promoters must be used in order to improve the economics of the process because the traditional hydrate formation from fuel gas requires high pressure at low temperature conditions.

1.6.2. Solid adsorbent

A few investigations have examined the capture of CO_2 using FBR in which solid adsorbent has been used to omit the stirring process inside the reactor. Adeyemo et al. (2010) investigated clathrate crystallisation in a silica gel column from fuel gas mixture at the operating conditions of 272.15 K and 70 bar respectively. Three different silica gels were used (gel 1 with a pore size of 30 nm and particle size of 40-75 μm; gel 2 with a pore size of

100 nm and particle size of 40-75 μm; gel 3 with a pore size of 100 nm and particle size of 75-200 μm) and the highest CO_2 composition in hydrate was observed for gel 3 around 92 mol%. Kang et al. (2013)managed to improve CO_2 in the hydrate phase to 96.5 mol% at the operating conditions of 274.15 K and 60 bar. Babu et al. (2013) employed silica sand and silica gel as solid beds in the reactor at the operating temperature of 274.15 K and three different pressures (75, 85, 90 bar). The results showed the silica sand bed provided better CO_2 capture capability with water conversion up to 36 mol% compared to 13 mol% for silica gel bed.

Most of the experiments that used silica saturated with water inside FBR have shown greater CO_2 uptake as compared to bulk water in a stirred tank reactor (STR) where the highest value obtained in a fuel gas mixture was 2 mmol of CO_2/g of H_2O (Adeyemo et al., 2010). For gas hydrate formation in silica gel pores, there is an inhibition effect from the capillary effect, but pores can supply a large amount of contact area between water and gas molecules in a short amount of time. Thus, it increases the rate of hydrate formation and enhances the conversion rate of water to hydrate compared to those of bulk water (Adeyemo et al., 2010; Kang et al., 2013). In addition, solid adsorbent can overcome the gas/water contact limitation wherein the gas phase will have better contact with water dispersed in the pores of silica gel (Kumar et al., 2013). Even though the adsorbent application for clathrate hydrate process can eliminate the need for stirring which is economical, the operating conditions for both cases show that high pressure needs to be used approximately between 60 bar and 90 bar for an effective CO_2 capture process. Hence, the use of solid adsorbent together with a promoter needs to be applied to improve the driving force of the system.

1.6.3. Oxygenated solvent as a promoter

Currently there is a continuous interest in using oxygenated solvents to reduce the operating pressure, shorten the induction time and accelerate the formation rate. Oxygenated solvent is define as an organic solvent containing oxygen as part of the molecular structure such as alcohols and ketones (EPA, 1970). The most common oxygenated solvent used in HBGS technology is tetrahydrofuran (THF). This work will investigate an alternative oxygenated solvent that can be used to enhance CO_2 hydrate formation; specifically ethylene glycol mono-ethyl ether (EGME) was identified as a possible substitute for THF.

1.6.3.1. THF

THF is water-miscible which means it has the advantage of mixing with water in all proportions to form a homogeneous solution. Lee et al. (2010) found that the addition of THF as an additive can reduce the operating pressure from 110 bar to 18.7 bar at 278.7 K. This experiment demonstrated that the concentration of THF addition and the hydrate formation driving force greatly influence the occupation rates of the cavities by the individual CO_2 and H_2 gases; results showed that the gas uptake obtained was 0.5 mmol of CO_2/g of H_2O which was slightly lower than the traditional method. They stated that the decreased CO_2 composition in hydrate was probably due to the decreased available cavities for the individual CO_2 and H_2 gases which resulted from the pre-occupation of large $5^{12}6^4$ cavities by THF. In other words, CO_2 acted as an inhibitor to sII hydrate formation due to the competition with THF (Yang et al., 2013). Park et al. (2013) recently discovered that with the addition of THF, the fuel gas mixture from the IGCC plants can form mixed gas hydrate at the range of operating conditions of 282-293 K and 10-90 bar. The stabilisation effect of THF appeared to be the highest at THF 5.6 mol%, which is the stoichiometric concentration of the THF hydrate ($THF.17H_2O$). At THF 5.6 mol% solution, the gas uptake

in STR was relatively high (1.2 mmol of CO_2/g of H_2O) comparable to pure bulk water in their work but the gas consumption plateaued after 60 minutes of hydrate formation due to crystal agglomeration and limited surface area at the gas/water interface. Recently, Babu et al. (2016) studied the effect of THF on hydrate formation for pre-combustion capture of CO_2 by employing various concentrations of THF (0.5, 1.0, 3.0 and 5.56 mol%) in STR (batch mode). They observed 5.56 mol% was the optimum concentration of THF to be implemented immediately in the IGCC (287 K and 60 bar) with a CO_2 uptake of 0.9 mmol of CO_2 per g of H_2O.

Furthermore, Adeyemo et al. (2010) discovered that the addition of 1 mol% of THF in FBR reduced the operating pressure of the fuel gas mixture system from 70 bar to 50 bar at 274.15 K with a gas uptake of 0.5 mmol of CO_2/g of H_2O. Additionally, Babu et al. (2014) managed to obtain gas uptake at 2.5 mmol of CO_2/g of H_2O in FBR by employing 5.53 mol% THF at the operating conditions of 279 K and 60 bar. According to Tang et al. (2013), the capability of THF to be easily encaged in clathrate hydrate cavities means the hydrate formation condition can be mitigated greatly with its existence. In addition, THF can also strengthen hydrate formation wherein the THF effect on separation performance is related to the feed gas components.

1.6.3.2. EGME

Presently, no research has focussed on the implementation of EGME for CO_2 capture with the HBGS process. Recently, Zare et al. (2015) investigated the effect of EGME solutions on the kinetics of methane hydrate formation. The results indicated that using 0.75 wt% EGME in the presence of ionic liquids led to the promotion of methane hydrate formation. However, the system showed an inhibition effect when 10 wt% of EGME was used. Thus,

the investigation of using EGME for CO_2 hydrate formation will be presented in the next chapter.

1.6.4. Surfactant as a promoter

Surfactant is a chemical species that acts as a wetting agent to lower the surface tension of a liquid-liquid or liquid-gas interface and allow for increased spreadability (Helmenstine, 2014). There are several types of well-known surfactants such as non-ionic (poly-oxy-ethylene, nonyl-phenyl-ether and Tween-40), cationic (dodecyl tri-methyl-ammonium chloride (DTACl) and dodecyl tri-methyl-ammonium bromide (DTAB)) and anionic (sodium dodecyl sulphate (SDS), sodium tetradecyl sulphate (STS) and sodium hexadecyl sulphate (SHS)) surfactants. Kumar et al. (2015) reviewed the role of surfactants in promoting gas hydrate formation mentioning that surfactants act as surface active agents which promote kinetic hydrate formation. They also explained the relation between surfactants with critical micelle concentration (CMC), hydrate interface (contact angle) and morphology of gas hydrate formation that enhance the formation of hydrate. SDS is the most common surfactant used in HBGS technology and further explanation about this anionic surfactant is presented.

1.6.4.1. Sodium Dodecyl Sulphate (SDS)

Recently, Kumar et al. (2013) investigated the effect of surfactant on hydrate formation behaviour by using CO_2 gas supply with a purity of more than 99%. They prepared SDS-water solution at different concentrations (500 ppm, 2000 ppm and 4000 ppm). Each solution equal to the pore volume of silica gel was added to obtain pore saturated silica. Experiments were conducted at 274 K and 36 bar and the solution with a concentration of 4000 ppm showed the highest water to hydrate conversion (52 mol%) which was 2 mol%

higher than pore saturated silica with water (control experiment). Also, the rate of gas uptake was greater than the control experiment. Hence, they suggested that SDS had little effect on the total amount of CO_2 enclatharation but it could give higher hydrate formation rates.

As for the role of surfactants, Kumar et al. (2013)stated that obstructing hydrate film did not develop if a surfactant was added to the aqueous phase at certain concentrations to enhance water to hydrate conversion. Furthermore, surfactant addition in the presence of water allows the association of surfactant molecules in the form of micelles at concentrations above the CMC. Thus, it has been proposed that the formation of micelles increases the solubility of gas in the aqueous phase and also enhances hydrate growth by inducing the formation of clathrate hydrate crystals around the micelle in the bulk water phase. They reported that anionic surfactants such as SDS fare better in improving the water to hydrate conversion rate compared to cationic and non-ionic surfactants. Thus, SDS has been used in this study and the ideal combination of this surfactant with other promoters is reported in the next chapter.

1.6.5. Semi-clathrate hydrate former as a promoter

Semi-clathrate hydrate is a type of hydrate where some cages are broken to encage big guest species and water molecules of the structure are partially replaced by the atoms of guest species (Davidson, 1973). Babu et al. (2015) mentioned that this type of hydrate can form hydrate at milder experimental conditions compared to the gas hydrate in which small gas molecules like CH_4, H_2 and CO_2 can occupy the small cages.

1.6.5.1. Tetra-n-butyl ammonium bromide (TBAB)

In TBAB hydrate, bromine is part of the cage structure and the tetra-n-butyl ammonium located on the centre of four cages as a guest makes this semi-clathrate hydrate stable even at atmospheric pressure and also easy to handle (Shimada et al., 2005). Li et al. (2010) employed 0.3 mol% TBAB in STR and a 20% improvement in gas uptake was observed compared to the most traditional method. They found that the addition of TBAB enhanced CO_2 encaged in the hydrate and the driving force of the process also increased where the operating conditions were shifted to 50 bar and 278 K. However, the number of moles of CO_2 transferred into the hydrate slurry phase decreased with the increase of TBAB concentration above 0.3 mol%. Kim et al. (2011) studied the phase equilibrium of hydrate in fuel gas mixture with TBAB additive located in the range of 283-290 K in a IGCC process with a pressure range of 25-50 bar (Figure 1- 18). They also revealed (through Raman analyses) that only CO_2 molecules enclathrated under these experimental conditions which served as the basis for CO_2 capture from fuel gas mixture. Even though it showed the potential for the hydrate process to be applied in the IGCC process without significantly lowering the processing temperature, the drawback of using this method was the need for mechanical force to agitate the water-additives mixture. Therefore, Babu et al. (2014) investigated the performance of employing 0.3 mol% TBAB in FBR and the results showed a slight increase in gas uptake to 1.2 mmol of CO_2/g of H_2O at the operating conditions of 279 K and 60 bar.

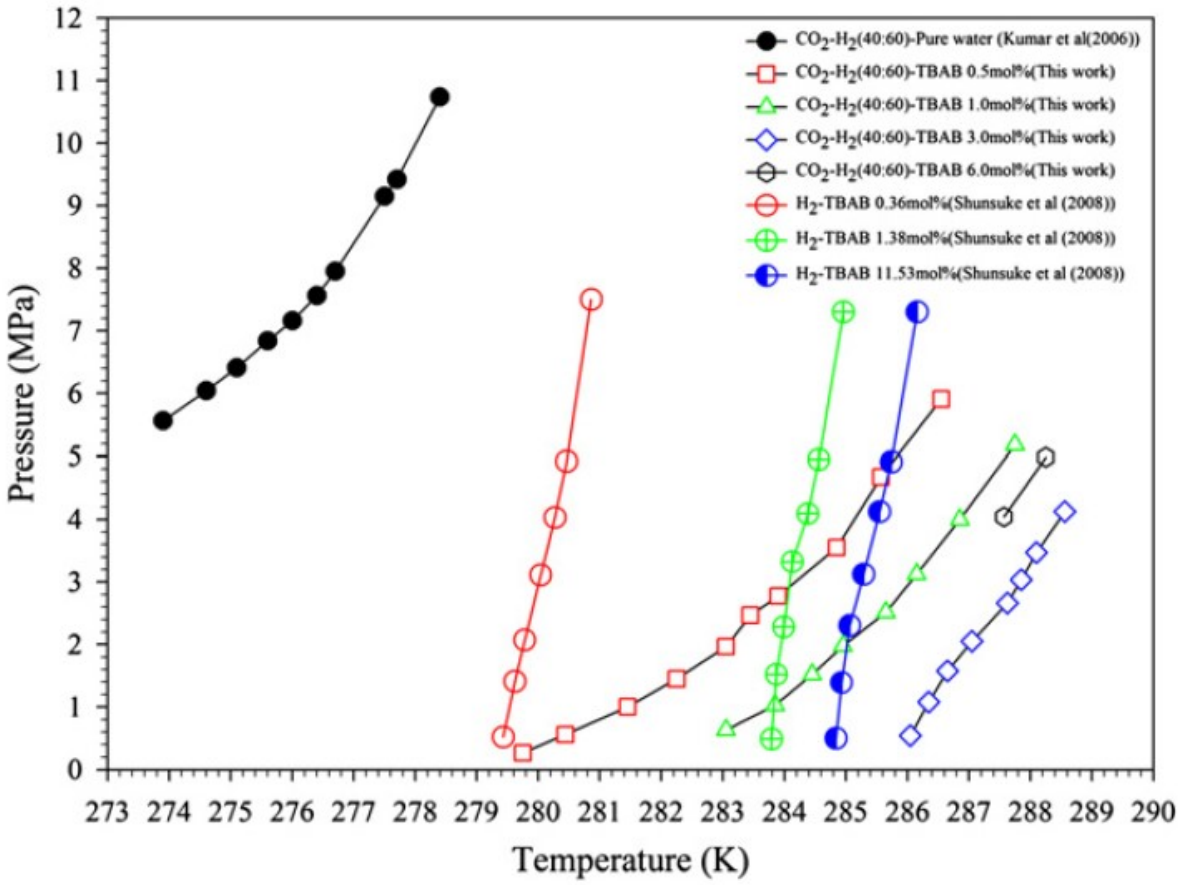


Figure 1- 18: CO_2-H_2 (40:60) mixture and H_2 pure gases hydrate phase equilibrium with additive of TBAB (Kim et al., 2011)

1.6.5.2. Tetra-n-butyl ammonium fluoride (TBAF)

Park(b) et al. (2013) employed 3.3 mol% TBAF in STR at fuel gas mixture composition and hydrate formation was observed at room temperature. However, the operating pressure required was too high which was 80 bar and the gas uptake obtained was too low (0.3 mmol of CO_2/g of H_2O) which was 60% lower than the TBAB system. They concluded that the addition of TBAF did not increase the gas uptake but instead significantly reduced the kinetics for hydrate formation.

1.6.5.3. Tetra-n-butyl ammonium nitrate ($TBANO_3$)

Recently, Babu(b) et al. (2014) applied $TBANO_3$ in STR in the presence of fuel gas mixture and the gas uptake attained (0.8 mmol of CO_2/g of H_2O) at 1.0 mol% $TBANO_3$ was higher than the TBAF system by 40% but still lower than the TBAB system by 30%. However, an improvement in operating conditions was observed at 3.7 mol%, within the range of IGCC conditions.

1.6.6. Hydrophobic former as a promoter

1.6.6.1. Cyclopentane (CP)

CP is known as hydrophobic former (Lo et al., 2008); Li et al. (2011) investigated that the addition of CP in STR containing fuel gas mixture massively enhanced the driving force by almost half as compared to the most traditional way while the operating pressure was 45 bar at 274.2 K and the gas uptake was 0.2 mmol of CO_2/g of H_2O. Then, Ho et al. (2013) managed to obtain 0.8 mmol of CO_2/g of H_2O gas uptake with an increase in driving force to 60 bar. Additionally, they managed to improve the gas uptake to 1.5 mmol of CO_2/g of H_2O gas by employing CP in an unstirred tank reactor (UTR). The presence of an immiscible CP layer above water aids in diffusion of guest gas to the bulk phase in UTR while in a STR, CP is diffused in the bulk phase due to agitation. They concluded that CP can enhance the HBGS process by reducing the operating pressure and providing effective gas-liquid contact with no stirring needed. Finally, Figure 1- 19 summarises the hydrate phase equilibrium for the fuel gas mixture in the presence of thermodynamic promoters (THF, CP, TBAB, TBAF and $TBANO_3$) wherein all promoters shifted the phase equilibrium of bulk water to the higher temperature region.

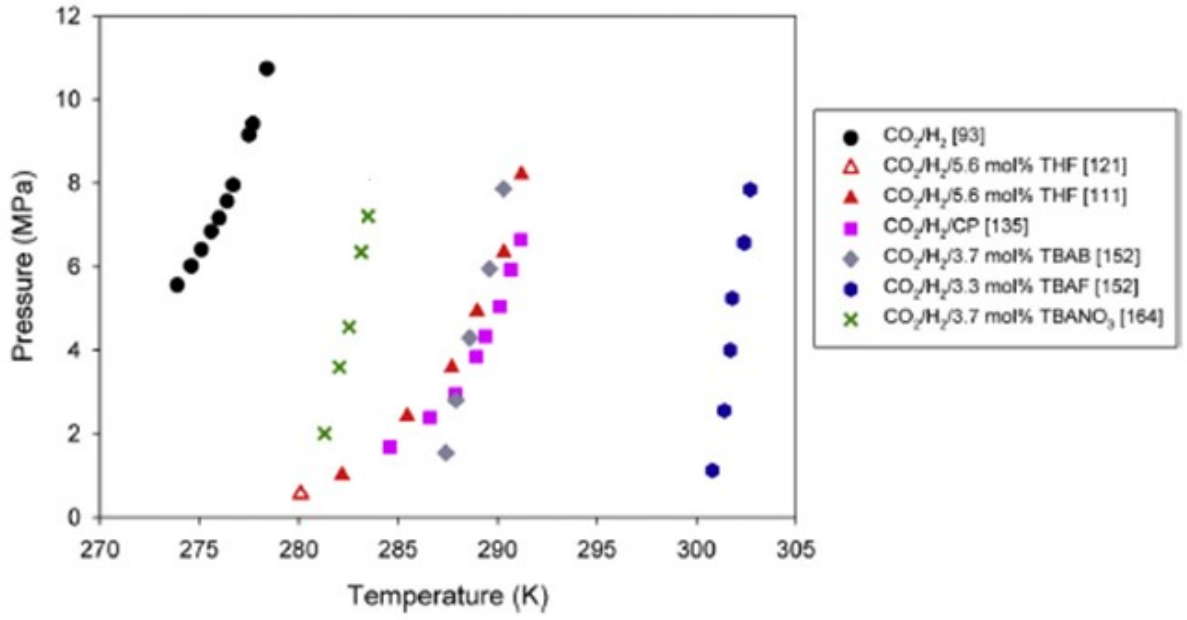


Figure 1- 19: Hydrate phase equilibrium for the fuel gas mixture with or without promoter (Babu et al., 2015)

1.6.7. Synergic effect of combined-promoter

As mentioned in previous sections, massive efforts have been done to enhance the driving forces and gas uptake of CO_2 hydrate formation by adding promoters such as THF, SDS, tetra-butyl ammonium salts and CP so that it can readily be applied for pre-combustion capture in the IGCC. The addition of THF (oxygenated solvent) shifted the phase equilibrium to a much lower pressure and higher temperature. The same happened for tetra-butyl ammonium salts, also known as semi-clathrate hydrate promoter. However, both types of promoters have shown a decreased gas uptake with TBAB and decreased hydrate formation rate. In contrast, SDS (surfactant) improved the hydrate formation rate and the gas uptake was comparable to the system without a promoter. Yet, the phase equilibrium did not shift to the IGCC conditions. CP, also known as hydrophobic former, could increase the gas uptake and lower the operating pressure. However, the investigations are limited to the application inside STR and UTR only. Therefore, some works have been done to investigate the synergic effect of a combined-promoter so that the system can readily be applied in the

IGCC conditions. Herslund et al. (2013) mentioned that the synergic effect is the result of different formation mechanisms for the polar and the non-polar hydrates, with the former resulting in an overall reduction in formation pressure.

1.6.7.1. THF and SDS

Based on the previous explanation, gas hydrate additives such as THF and SDS can be used to mitigate hydrate formation conditions, promote hydrate growth rate and improve separation efficiency. Silva et al. (2013) studied the formation of hydrate in pure CO_2 by using STR with SDS and THF as promoters. They concluded that if only SDS was used, clathrate hydrate was formed in a traditional way but when THF was mixed with SDS in an ideal proportion, it was possible to observe crystals of THF hydrate which stabilised the system and acted as promoters of CO_2 hydrate. Yang et al. (2013) performed a study on the effect of using a combined-promoter in FBR. Dry glass beads were tightly packed into a vessel containing different concentrations of SDS solution (0, 500, 1000, 1500 and 2000 ppm) coupled with 3 mol% THF and the experiments were conducted in batch mode by using 99.9% purity of CO_2 gas supply. The study on phase equilibrium for the THF-CO_2-H_2O system showed a drastic decrease in pressure in the presence of 3.0 mol% THF and SDS (at all concentrations) respectively (Figure 1- 20) and the induction time obtained was very low, approximately 1 minute (Figure 1- 21). Also, the highest equilibrium temperature obtained was 291.55 K at 30 bar in the presence of 3.0 mol% THF and 0 mg/L SDS respectively. The experiments on hydrate formation have indicated that CO_2 hydrate forms rapidly at all experimental pressures when the SDS concentration is 1000 ppm which indicates that SDS enhances the hydrate formation rate.

Moreover, Ricaurte et al. (2014) studied the effect of several combined-promoters on CO_2 hydrate formation in which SDS was paired with one of the thermodynamic promoters

(THF, 1,3-dioxolane, 2-methyl-THF and CP) and THF was paired with one of the kinetic promoters (SDS, SDBS and DATCI). They highlighted that the combination of SDS and THF was the best for the formation of CO_2 hydrate from natural gas. Recently, Torre et al. (2015) mentioned that the combination of THF and SDS was very advantageous in accelerating hydrate formation where they found that the CO_2 consumed was increased dramatically when compared to the single promoter.

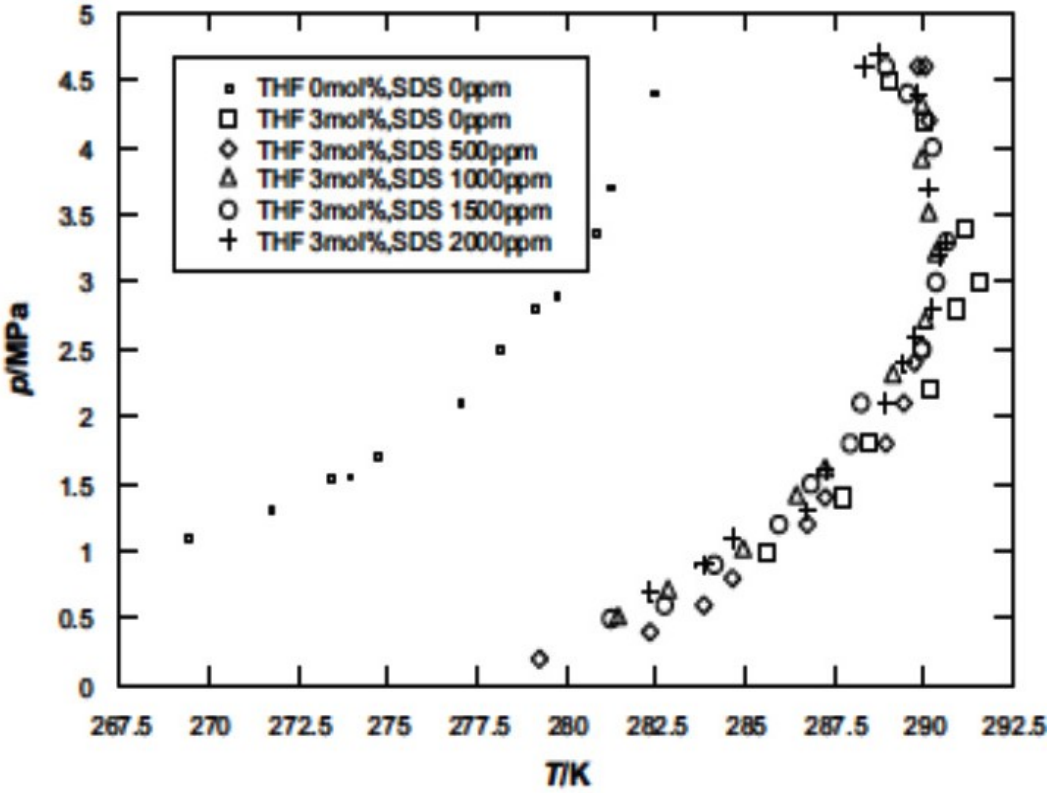


Figure 1- 20: Hydrate forming conditions for experiments using 99.9% CO_2 gas supply (Yang et al., 2013)

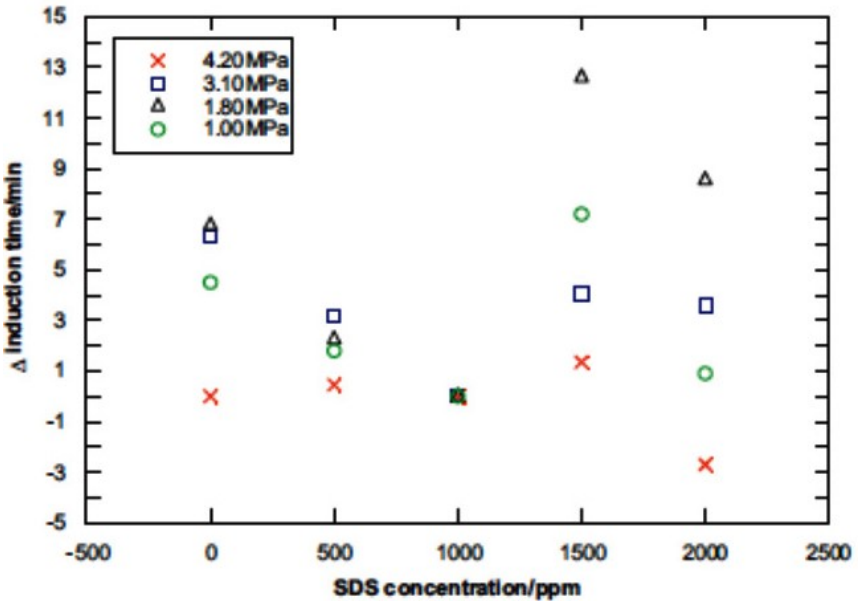


Figure 1- 21: Induction time relative to that of 1000 mg/L SDS (Yang et al., 2013)

1.6.7.2. THF and CP

Herslund et al. (2013) presented new equilibrium data for the quaternary system H_2O-THF-CP-CO_2 in the temperature range from 275.1 K to 286.6 K. Adding THF to the system of H_2O-CP-CO_2 lowered the equilibrium pressure of this ternary system by 25-30% due to the formation of CP and THF hydrates simultaneously.

1.6.7.3. TBAB and CP

Li et al. (2012 & 2011) discovered that the addition of CP into a TBAB solution remarkably enhanced the CO_2 separation and sped up the hydrate nucleation rate in STR. The main improvement for this type of system was the induction time which was ten times better compared to other systems and more than 80% of the total gas uptake could be obtained after 400 seconds in the process of separation. The biggest gas uptake and the highest CO_2 separation efficiency were obtained at 274.65 K and 40 bar when the CP/TBAB ratio was 5 vol % and the volume ratio of the TBAB solution/CP was 0.54. Li et al. (2012) mentioned

that two aspects of a synergic effect were involved in this system: 1) the CP molecules housed in the hollow centres of the large cavities together with TBAB cations (TBA^+) made the semi-clathrate hydrate more stable and 2) the TBA^+ displaced out of the large cavities by the CP molecules made the ionisation reaction of TBAB in the solution head in the reverse direction which made more TBAB molecules available to form semi-clathrate hydrate, resulting in more CO_2 uptake. Among all works that implemented STR for hydrate formation, Li et al. (2011) managed to achieve the highest gas uptake of 1.4 mmol of CO_2/g of H_2O.

1.6.7.4. SDS and CP

Ho et al. (2013) reported that the addition of SDS to CP did not show a synergic effect in which no further improvement in gas uptake was observed in UTR; instead the gas uptake was reduced by 15% as compared to the CP system. SDS is said to have an inhibitory effect for this combined system indicating that a proper combination of promoters is necessary to enhance hydrate formation. In addition, Lim et al. (2013) discovered that by adding SDS to CP, the morphology of hydrate crystal just below the CP-water interface changed from mushy & cloud-like hydrate to fibre-like crystals. Furthermore, rapid hydrate formation observed for the experiments with 0.9 mL CP with or without the presence of SDS justified the result obtained by Ho et al. (2013).

1.6.7.5. THF and TBAB

Yang et al. (2015) performed a hydrate phase equilibrium investigation on various combinations of THF and TBAB concentrations in the pure CO_2 gas system by employing glass beads as the porous medium in the range of 276-291 K and 9-44 bar. They found that the addition of 5 mol% THF and 5 mol% TBAB greatly shifted the hydrate phase

equilibrium to the higher temperature region around 291 K at the operating pressure of 42 bar. They mentioned that the observed results were due to the formation of THF sII hydrate and TBAB semi-clathrate hydrate wherein CO_2 molecules had occupied the small cages of this sII hydrate and also filled the cavities of TBAB semi-clathrate hydrate respectively.

1.7. Reactor configuration highlights in HBGS

Figure 1- 22 shows the configurations of reactors in HBGS technology which consist of continuous process (CPR) (Tam et al., 2013; Currier et al., 2006), STR (Babu(b) et al., 2014; Park et al., 2013b; Li et al., 2011; Lee et al., 2010; Li et al., 2010; Linga et al., 2007), FBR (Zheng et al. 2016; Babu et al., 2014; Babu et al., 2013; Adeyemo et al., 2010) and UTR (Ho et al., 2013).

Some of these configurations have several issues related to hydrate formation which are not good for the future of HBGS technology. CPR is associated with the formation of a hydrate plug which can block the flow lines such as in oil and gas flow lines. Meanwhile, STR is normally used in laboratories to study the phase equilibrium measurements and fundamental kinetics of hydrate formation. Both CPR and STR require considerable energy for stirring to ensure gas/liquid agitation which can increase the operational costs. Furthermore, both configurations also have an issue with attaining higher water conversions due to the insufficient residence time and agglomeration of gas hydrate crystals at the gas-liquid interface respectively. As mentioned previously, Ho et al. (2013) reported that UTR showed superior performance compared to STR in the presence of CP. However, the main drawback of this configuration is the requirement of an immiscible promoter. Recently, FBR has been used extensively due to the fact that a solid adsorbent bed can provide large gas-liquid contact area and also enhance kinetics. Also, Zheng et al. (2016) just discovered that the gas uptake of horizontal FBR is 1.5 times higher than the vertical with the same operating

conditions. Moreover, the costs of some solid adsorbents that can be employed in this reactor are not that expensive such as PU foam and silica sand. Both UTR and FBR do not require stirring which can reduce the operational costs. The use of high pressure volumetric analyser (HPVA) in this work can be associated with the FBR vertical configuration and is further explained in the next chapter.

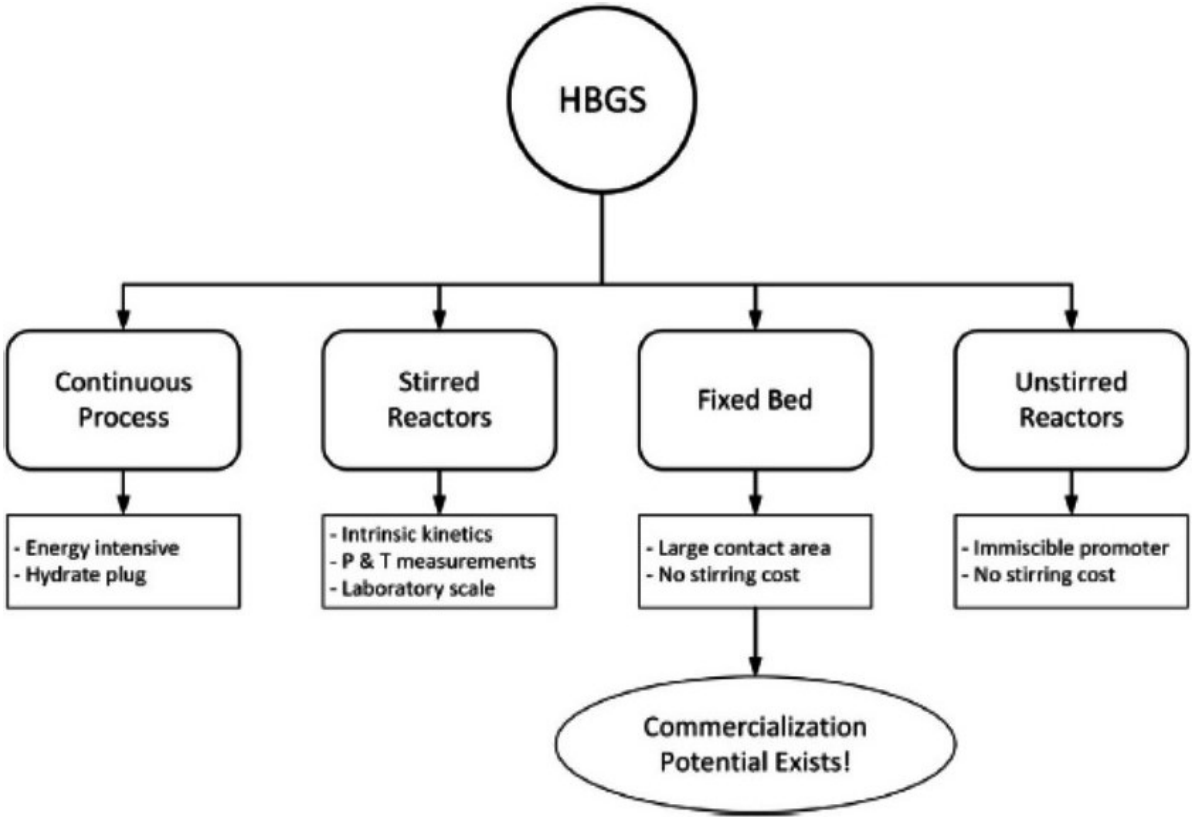


Figure 1- 22: Path to commercialisation for the HBGS process (Babu et al., 2015)

1.8. Variation in experimental parameters in HBGS

A number of works have examined pre-combustion CO_2 capture by HBGS starting with the most traditional up to the most conventional approaches. Throughout this period, numerous parameters have been investigated to improve CO_2 uptake, ease of hydrate formation and operational costs so that HBGS will become the most preferred method in the CCS industry. Several parameters such as sample preparation methods, promoter concentrations, driving forces, fixed bed heights and pore sizes of solid adsorbents were selected in this study so

that the best approaches can be proposed for the commercialisation of HBGS in CO_2 capture. The previous investigations regarding these parameters were briefly explained in this section and the results obtained in this study are presented in the next chapter.

1.8.1. Sample preparation of solid adsorbent

Babu et al. (2015) mentioned that in general, silica gel has an issue with kinetics as compared to silica sand. They said that for silica gel, the water is dispersed inside the gel pores which causes the kinetics to slow down and reach a plateau which is much lower than the silica sand due to the considerable amount of water that gets occluded inside silica gel pores and does not participate in hydrate formation. As for silica sand, they said enhanced kinetics can be observed because the water is dispersed inside the inter-particle pore space. Moreover, Babu et al. (2013) found the same result as silica sand by employing polyurethane (PU) foam where they said interstitial pore space is dominant and well interconnected in FBR. Babu et al. (2015) also said that for these two porous mediums, dispersion of water into the pore space is a simple procedure and consistent results have been reported in the literature (Babu et al., 2014; Babu(c) et al., 2014; Mekala et al., 2014). However, some investigations in the literature have reported enhanced kinetics in the presence of silica gel (Kang et al., 2013; Park et al., 2013; Adeyemo et al., 2010; Wang et al., 2008) due to the procedure of dispersing water into silica gel pores or type of gel used. Consequently, several available options for sample preparation methods by using solid adsorbent in gas capture field were studied. Basically each method has the same objective which is to completely fill the pores with water. Babu et al. (2013) used silica sand and silica gel as the solid beds in the reactor wherein they used a stirrer (3000 rpm) for 3 minutes to aid the dispersion of water into pore saturated silicas. This method was adopted from Adeyemo et al. (2010). Park et al. (2013) mixed an amount of water identical to the

pore volume of silica gel inside the bottle consisting of dry silica gel and an ultrasonic wave was used to blend them. Wang et al. (2008) prepared numerous samples wherein the mixture of hydrophobic silica and water were stirred at three different speeds (16450, 17500 and 19000 rpm) for 90 seconds and they discovered that the formation of methane hydrate for the sample stirred at the highest speed gave the highest gas uptake. In other work, Dawson et al. (2014) mixed hydrophobic silica and alkaline solution and this mixture was stirred at 37000 rpm for 30 seconds to prepare a porous sample for CO_2 capture investigation at low pressure (2-3 bar).

The sample preparation method employed by Wang et al. (2008) and Dawson et al. (2014) is beneficial because a water-in-air inverse foam consisting of water droplets is surrounded by a network of hydrophobic fumed silica which prevents coalescence of the droplets. In other words, it can increase the amount of water inside silica pores which is essential for hydrate formation. Thus, in this work the investigation of vigorous stirring was performed together with other possible sample preparation methods; by using vigorous stirring, the amount of water that gets occluded inside silica gel pores can be overcome.

1.8.2. Driving force

There are two common types of driving force in the HBGS field which are known as pressure driving force (ΔP) and temperature driving force (ΔT). Babu et al. (2015) stated that the deviation of the experimental and corresponding equilibrium pressure for hydrate formation at a given temperature is known as ΔP. In contrast, ΔT is the difference between experimental and corresponding equilibrium temperature for hydrate formation at a given pressure. Alternatively, Lee et al. (2010) mentioned that anything that enhance the occupation rates of the cavities by the individual CO_2 and H_2 gases for the formation of hydrates in fuel gas indicates good driving force is available in the system. From another

perspective, Kobayashi et al. (2007) said a batch system is assumed to instantaneously keep itself in thermodynamic equilibrium which can be associated with change in driving force upon hydrate growth. Generally, an increase in the driving force increases the gas uptake and rate of hydrate formation.

Adeyemo et al. (2010) performed an investigation on the HBGS process from flue gas mixture in FBR consisting of silica gel bed at constant temperature (272.15 K) and two different pressures (80 and 90 bar). The highest water conversion to hydrate observed was at 90 bar with a value of 15 mol% which was almost two-thirds higher than the other one. Babu et al. (2013) used three different pressures (75, 85 and 90 bar) at 274.15 K to investigate hydrate formation in fuel gas mixture and the highest water conversion to hydrate obtained was 13 mol% at 90 bar. Kang et al. (2013) investigated formation of hydrate in bulk water at 60, 64, 70, 81 and 92 bar and the CO_2 uptakes from fuel gas mixture were found to increase as the operating pressure increased. In contrast, Zheng et al. (2016) studied CO_2 hydrate formation in FBR at 279.2, 282.2 and 285.2 K (at 60 bar) and reported the CO_2 uptakes from fuel gas mixture were found to increase as the operating temperature decreased. Thus, as ΔP increases or as ΔT decreases, the driving force also increases.

1.8.3. Promoter concentration

Some works have investigated various concentrations of the promoter to find the optimum concentration that can enhance the driving force, gas uptake and also rate of hydrate formation. Essentially, the investigations were conducted at the same operating conditions by varying the concentration of the promoter. Lee et al. (2010) investigated the formation of hydrate in STR with different concentrations of THF (0.5, 1.0, 3.0 mol%). They reported that THF at 3 mol% gave the highest driving force, however the highest CO_2 uptake was observed at 1mol% THF. Furthermore, for all THF concentrations, the CO_2 uptake obtained

was lower than the bulk water due to the competition from THF and CO2 hydrate to fill in the available cavities during hydrate formation. In contrast, Park et al. (2013) managed to improve the gas uptake by employing 5.6 mol% THF in which CO_2 uptake was comparable to bulk water and the driving force was further improved. However, they reported that the use of 10 mol% THF did not further increase the driving force of hydrate formation.

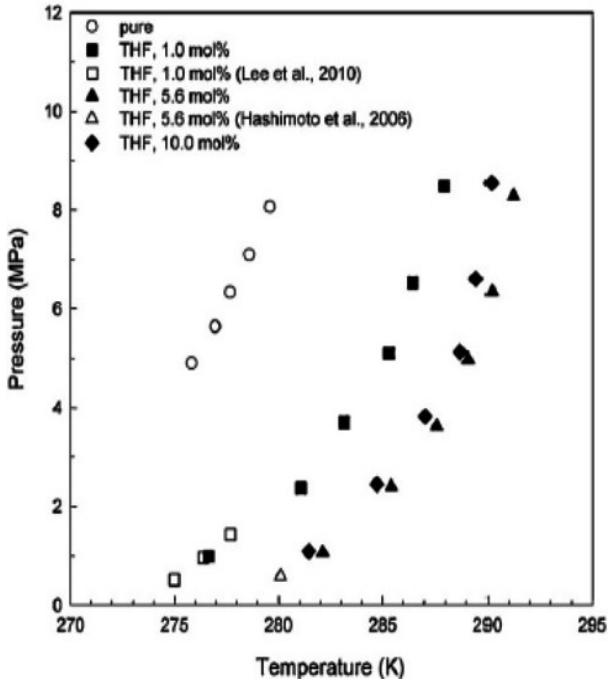


Figure 1- 23: Hydrate phase equilibria for fuel gas mixture + THF + water mixtures (Park et al., 2013)

Figure 1- 23 shows that by increasing the amount of THF, the equilibrium pressure of the fuel gas mixture shifts to low pressures as well as increasing the hydrate formation driving force. The study on varying SDS concentrations (0, 500, 1000, 1500 and 2000 ppm) coupled with THF (3 mol% THF) in FBR by Yang et al. (2013) demonstrated a drastic decrease in pressure as previously mentioned. CO_2 hydrate formed rapidly at all experimental pressures when the SDS concentration was 1000 ppm which indicates the optimum concentration of SDS in the system. Park(b) et al. (2013) studied the effect of TBAF on the thermodynamics of hydrate formation at different concentrations (0.8, 3.3 and 5.3 mol%) in which the

maximum shift was achieved at the concentration of 3.3 mol%. Also, Babu(b) et al. (2014) presented phase equilibrium data in the presence of 0.5, 1.0, 1.5, 2.0, 3.0 and 3.7 mol% $TBANO_3$ which reduced the phase equilibrium considerably. The optimum concentration was found at 1.0 mol% TBAF for hydrate formation at 274.2 K and 60 bar.

1.8.4. Characteristics of solid adsorbent

The variation of pore size, pore volume, surface area and particle size of solid adsorbent can affect the driving force, gas uptake and rate of hydrate formation. Adeyemo et al. (2010) used three types of silica gel as shown in Table 1- 4 to investigate CO_2 hydrate formation in FBR and type #3 silica gel with a larger particle size and pore diameter was found to enhance CO_2 consumption.

Table 1- 4: Silica gel properties (Adeyemo et al., 2010)

Silica gel type	Particle size distribution (μm)	Pore diameter (nm)	Pore volume (ml/g)	Surface area (m^2/g)
#1	45-75	30.0	0.81	100
#2	45-75	100.0	0.81	50
#3	75-200	100.0	0.83	50

Kumar et al. (2013) employed three types of silica gel (mesh size of 60-120 (type A), 100-200 (type B) and 230-400 (type C)) which had almost similar pore diameters and different surface areas with type C having the highest surface area and type A the lowest. The CO_2 uptake obtained at 274 K and 36 bar in pure CO_2 indicated silica gel with larger surface area (type C) led to the higher gas consumption as well as reduced the induction time. The conversion of water to hydrate for type C was 50 mol% which was 20% higher than type B and almost 50% higher than type A. Figure 1- 24 shows the hydrate phase equilibria for the fuel gas and water mixtures inside various sizes of silica gel pores by Park et al. (2013) in

which silica gel with the highest pore diameter exhibited the best driving force for hydrate formation which was close to the bulk water. They mentioned that the capillary effect due to the presence of geometrical constraints caused the equilibrium lines to be shifted to the inhibition region which was to the left hand side of the bulk water system. They added that this effect was more significant at smaller pore sizes (6.0 nm) due to the decreased activity of water caused by the partial ordering and bonding of water molecules with hydrophilic surfaces of pores.

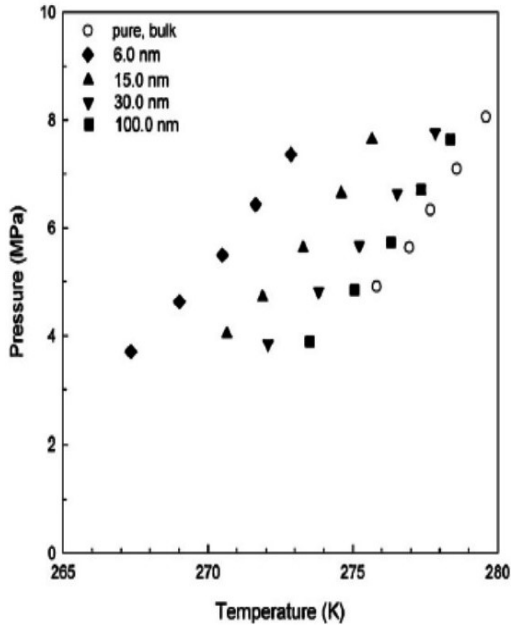


Figure 1- 24: Hydrate phase equilibria for the H_2 (60%) + CO_2 (40%) + water mixtures in silica gel pores (Park et al., 2013)

Kang et al. (2013) conducted an investigation on three different silica gel pores (25, 100 and 250 nm) and the observed phase equilibria justified the statement made by Park et al. (2013) in which silica gel with pore size of 25 nm demonstrated the highest inhibition effect. Babu et al. (2013) used silica sand (average pore diameter of 329 μm and pore volume of 0.22 cm^3/g) and silica gel (average pore diameter of 100 nm and pore volume of 0.83 cm^3/g) as the solid beds in the reactor to explore the formation of hydrate from fuel gas mixture. Silica sand demonstrated better CO_2 capture capability with a 36 mol% conversion of water to

hydrate which was almost two-thirds higher than silica gel. Further work on silica sand was performed by Mekala et al. (2014) at different particle sizes (0.16, 0.46 and 0.92 mm) wherein 0.46 mm silica sand was found to have the optimum CO_2 uptake and rate of hydrate formation.

Other than silicas, there are two more solid adsorbents being investigated by the researchers in the HBGS field which are zeolites (Zhong et al., 2015; Xiaoya et al., 2009) and glass beads (Yang, 2013). Xiaoya et al. (2009) proved that the formation of CH_4 hydrate inside zeolite A-type pores is possible. Zhong et al. (2015) conducted an investigation using zeolite 13X in FBR for the HBGS process from a CO_2/CH_4 gas mixture (40 mol% CO_2 and 60 mol% CH_4) at 277.15 K and in the pressure range of between 52-67 bar. They found that hydrate growth in the fixed bed zeolite 13X was improved as the driving force increased from 25 to 40 bar. However, the comparison with STRs showed that the selectivity towards hydrate formation was lower for the fixed bed of zeolite 13X due to the massive moisture content available inside the pores which increased the geometrical constraint or capillary effect (Park et al., 2013). Hence, they concluded that zeolite 13X can be used to enhance hydrate formation but may not be a proper candidate for CO_2 capture from the CO_2/CH_4 gas mixture. Thus, the investigation on CO_2 hydrate formation from pure CO_2 gas by employing zeolite 13X with improved parameters will be presented later in chapter 4.

1.8.5. Fixed bed height

Linga et al. (2009) suggested that the dependency of hydrate formation rate on the size of the fixed bed should be taken into account for the HBGS process. Babu(c) et al. (2014) managed to double the CO_2 uptake in FBR with the presence of silica sand as porous medium with a 1.5 cm bed height as compared to a 5 cm bed height employed by Babu(c) et

al. (2013). Since the operating conditions were the same, the effect of bed height on hydrate formation was demonstrated.

1.9. The principle conclusions from background works

Currently, HBGS technology is being investigated extensively. Figure 1- 25 shows a historical perspective of 'gas hydrates' or 'clathrate hydrates' research presented by Babu et al. (2015) in which there has been an exceptional increase in research activity in the last 20 years.

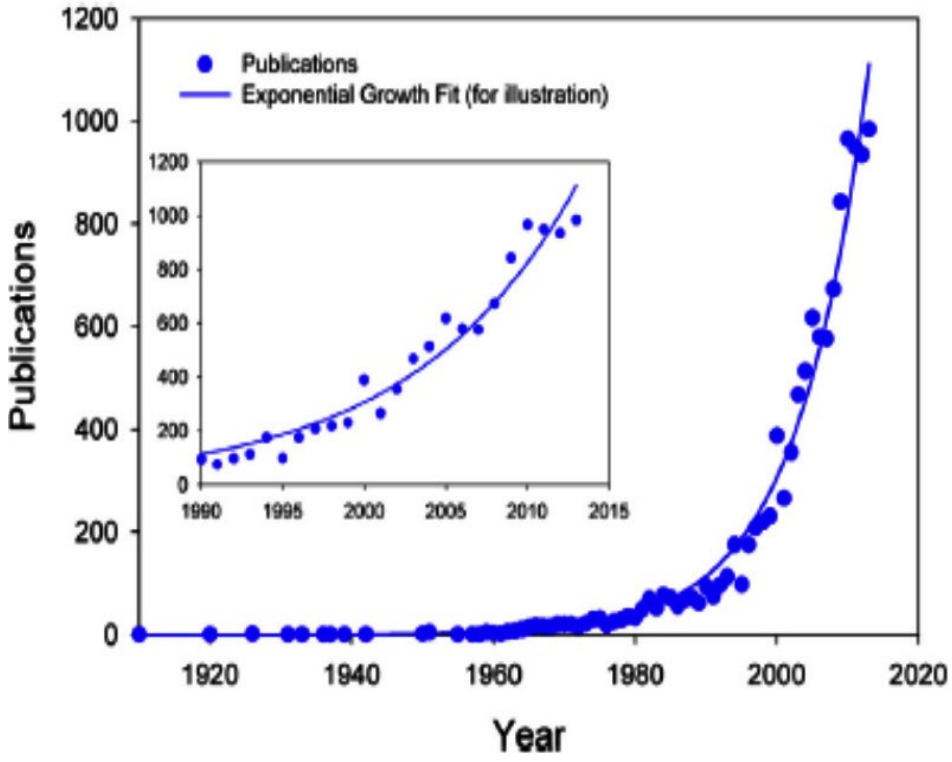


Figure 1- 25: Historical perspective of gas hydrates research (Babu et al., 2015)

Next, the summary of some results obtained in previous works related to pre-combustion CO_2 capture by HBGS is presented in Figure 1- 26. A number of parameters have been investigated to improve the gas uptake of hydrate formation in fuel gas mixture such as

employing different types of reactor configurations, altering porous medium parameters used inside the reactor, varying the concentration of promoters and combining promoters.

As for the use of FBR, Babu et al. (2014) managed to observe hydrate formation by employing 5.53 mol% THF and 0.3 mol% TBAB in batch mode (1.5 cm bed height of silica sand) respectively at 279 K and 60 bar. Then, Babu(c) et al. (2014) managed to achieve very high gas uptake (around 4 mmol of CO_2 per g of H_2O) in fuel gas mixture (at 274 K and 60 bar) with the use of propane and silica sand in batch mode at a bed height of 1.5 cm too. Yet, the optimum operating conditions for CO_2 hydrate formation by using porous medium such as silicas in FBR are still outside the range of IGCC plant operating conditions. Recently, Zheng et al. (2016) managed to obtain CO_2 uptake of 2.4 mmol of CO_2 per g of H_2O at 283 K and 60 bar by employing 5.56 mol% THF inside a horizontal batch FBR (100 nm silica sand was used as porous media). They also discovered that this horizontal orientation had 1.5 times higher gas uptake as compared to the common (vertical) orientation. This new finding demonstrates the continuous interest by researchers to ensure that CO2 hydrate can be immediately applied in the IGCC especially by exploiting the advantages of porous medium in FBR such as those examined in this work.

As for the other types of reactor configurations, Kim et al. (2011) managed to demonstrate hydrate formation in STR (batch mode) where the hydrate phase equilibrium was observed between 283-290 K and 25-50 bar in the presence of 3 mol% TBAB. Park et al. (2013) also demonstrated hydrate formation in IGCC conditions by using STR in a semi-batch manner in the presence of 5.6 mol% THF with the observation at 286-290 K and 30-50 bar. Recently, Babu et al. (2016) reported that 5.56 mol% was the optimum concentration of THF to be implemented immediately in the IGCC (287 K and 60 bar) with a CO_2 uptake of 0.9 mmol of CO_2 per g of H_2O in batch STR. However, the use of STR in their work required stirring during hydrate formation which is not an option in this work.

Lately, most of the researchers have used batch mode to investigate hydrate formation in fuel gas mixture as an alternative to semi-batch mode. Additionally, Babu et al. (2015) said that for the commercialisation of HBGS, the use of FBR in batch mode was proposed by Babu(b) et al. (2013) which is similar to an industrial process: Skarstrom cycle (Skarstrom, 1960). Also, they said this HBGS cycle can be conducted in a four step batch process namely pressurisation, hydrate formation, depressurisation or thermal stimulation (H_2 rich) and hydrate decomposition (CO_2 rich). Moreover, Babu(b) et al. (2013) said the proposed cycle involves two fixed bed columns and enables a continuous operation similar to how a pressure swing adsorption cycle would operate (Grande, 2012).

Furthermore, most of the researchers preferred using macroporous (pore diameter more than 50 nm) adsorbents due to the experimental results with the highest pore diameter exhibiting the highest CO_2 uptake (Adeyemo et al., 2010) and also the best driving force for hydrate formation which is close to bulk water (Park et al., 2013). Recently, Babu(c) et al. (2014) investigated the formation of hydrate from propane-fuel gas mixture-silica sand-water in batch FBR where the pore size of silica sand used was 100 nm. Then, the same silica pore size was used by Zheng et al. (2016) in batch FBR in the presence of 5.56 mol% THF and fuel gas mixture. Both Zheng et al. (2016) and Babu(c) et al. (2014) managed to achieve massive CO_2 uptake in this macroporous silica which explained less research examining mesoporous (pore diameter between 2-50 nm) or microporous (pore diameter less than 2 nm) adsorbents. However, it is believed that the investigation of microporous and mesoporous silicas in this work will provide further options for the application of porous medium in hydrate formation in the IGCC. Additionally, no research has been done yet on the system where the combined-promoter is saturated into adsorbent pores to promote CO_2 hydrate formation in FBR in the presence of fuel gas mixture.

Table 1- 5 shows that there are a lot of possible promoter combinations possible that can be applied in the HBGS process especially in combination with adsorbent. Some of the possible combinations have been explored by researchers such as type 1 (THF+SDS), type 2 (THF+TBAB), type 4 (THF+CP), type 5 (SDS+CP) and type 6 (TBAB+CP) in which only type 5 did not exhibit a synergic effect for hydrate formation. Park et al. (2013) mentioned that there are much more stabilised hydrate formation conditions, especially those represented by higher temperature regions at the available pressure conditions of the fuel gas mixture (20-70 bar). Hence, there is still room for improvement in order to create a similar condition to the IGCC plant which can be applied readily without any significant plant modifications by exploring possible promoter combinations to give a synergic effect to the system. The investigation of these combined-promoters especially on types 1 (THF+SDS), 2 (THF+TBAB) and 3 (SDS+TBAB) are presented in the next chapter. Also, the investigation on alternatives to THF by employing EGME combined with SDS (type 1A) is reported. Moreover, the investigation on new combined-promoters (types 3 and 1A) in this work will provide further options for promoters in hydrate formation. Thus, the use of batch FBR by employing combined-promoter contacted with silicas for the formation of CO_2 hydrate in fuel gas mixture (at the IGCC conditions) in this work is considered unique with implications for future research.

Table 1- 5: Possible promoter combinations

Promoters	OS	S	SC	HF
OS		OS+S (Type 1)	OS+SC (Type 2)	OS+HF (Type 4)
S			S+SC (Type 3)	S+HF (Type 5)
SC				SC+HF (Type 6)
HF				

where, OS: oxygenated solvent; S: surfactant; SC: semi-clathrate; HF: hydrophobic former

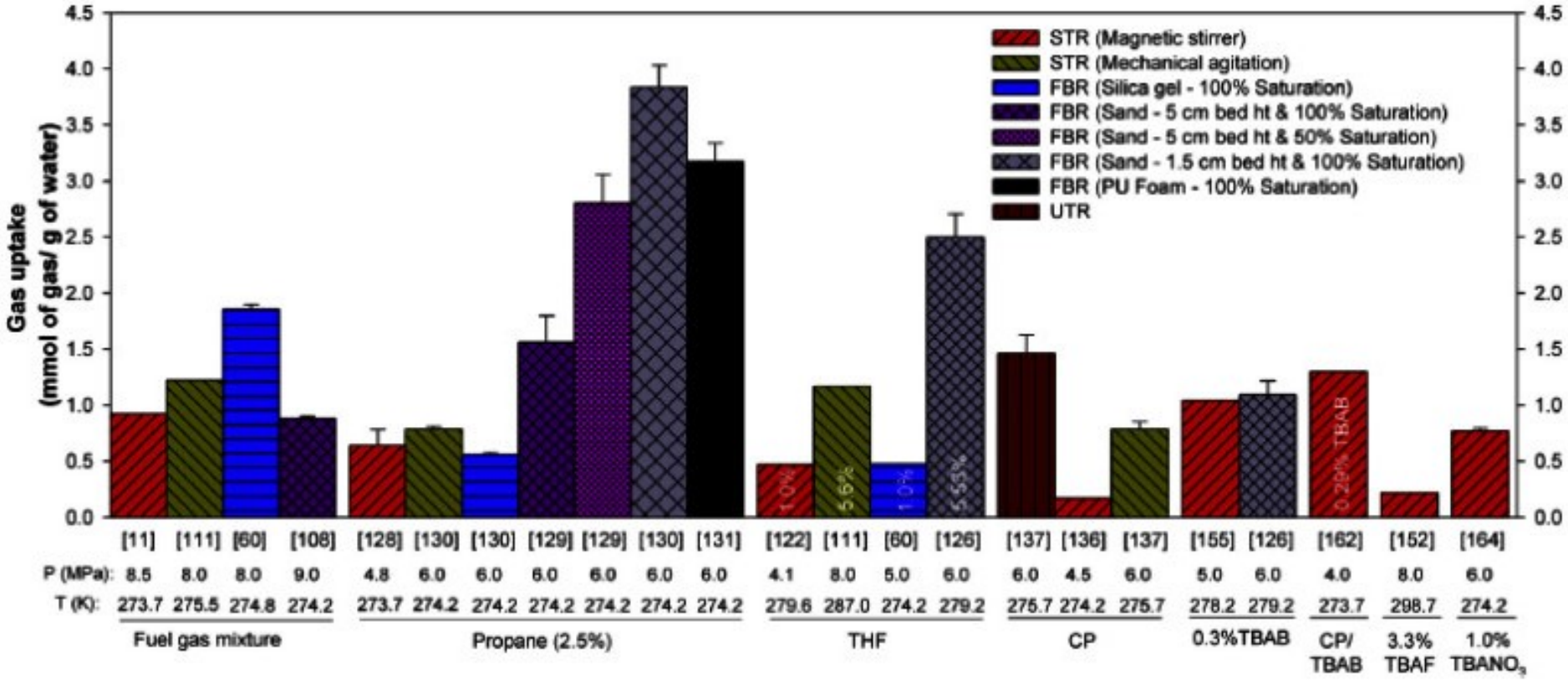


Figure 1- 26: Summary of highest normalised gas uptake for 120 min from IP reported so far in the literature at different experimental conditions (Babu et al., 2015)

1.10. Research objectives

Reviewing previous works has led to the aim and objectives of this particular study, where the formation of CO_2 hydrate was investigated by using a combination of silica gel with combined-promoters in the HPVA (vertical batch mode). There are plenty of developments that can be done in order to improve pre-combustion CO_2 capture capability at IGCC plant conditions. Different parameters (sample preparation method, driving force, promoter concentration, promoter combination, silica pore diameter and fixed bed height) were investigated in this work. Thus, the aim and objectives for this specific study are listed below.

The overall aim of this study was to investigate ways to improve CO_2 hydrate formation in the IGCC conditions by using batch FBR in the presence of mesoporous silica contacted with combined-promoters and focusing on alternative sample preparation methods as well as improving hydrate formation with several parameters.

The specific objectives are:

1) To study the formation of CO_2 hydrate in batch operation by using the high pressure volumetric analyser (HPVA) at various operating conditions;
2) To study the effect of various sample preparation methods especially with vigorous stirring on moisture content inside silica gel pores as well as CO_2 uptake upon hydrate formation;
3) To study the synergic effect on CO_2 hydrate formation especially when applying new combined-promoters (SDS+TBAB and SDS+EGME) inside mesoporous silica gel and discover the alternative oxygenated solvent to THF for CO_2 hydrate formation;

4) To propose the optimum parameters that can be applied immediately in the IGCC conditions by using mesoporous silica as an alternative to macroporous silica in batch FBR;
5) To improve the rate of hydrate formation for silica that have microporous characteristics such as zeolite 13X.

1.11. Thesis structure

The review of research on pre-combustion capture using the HBGS technique which led to the aim and objectives of this work were presented in chapter 1. Then, the methodology and formulae used to investigate rate of hydrate formation at specific parameters are described in chapter 2. Chapter 3 reports the effect of sample preparation methods on final equilibrium moisture content available for hydrate formation. Inevitably, this leads to the selection of the best sample preparation method that was implemented throughout this work. The introduction on promoters that were used in this study are also highlighted. Next, the synergic effect of combined-promoter on hydrate formation is presented in chapter 4 in which the optimum combined-concentrations of each promoter is discovered and an alternative oxygenated solvent to THF is recommended. Also, the improvements that were done to make hydrate formation feasible when employing microporous silica (zeolite 13X) is reported in this chapter. Subsequently, the optimum operating conditions that can be immediately applied in IGCC plant are identified and presented in chapter 5. Chapter 6 discusses the results to provide better understanding of HBGS technology so that it can be commercialised in the carbon capture industry. Finally, chapter 7 concludes the thesis and suggestions for future research are proposed.

CHAPTER 2: EXPERIMENTAL METHODS

2.1.Introduction

As mentioned in the previous chapter, STR is the traditional way of performing hydrate formation. This can cause agglomeration of hydrate crystals at the gas/liquid interface and as a result the conversion of water and gas to hydrate are restricted. Hence, silica gel in this work is used to avoid these disadvantages.

This chapter was structured so as to generally reflect the sequence in which the samples were prepared and analysed. Hence, the following sub-section explains the characterisation of silicas investigated in this work. Then, how the samples were prepared by using various techniques was described. Next, the effect of various sample preparation methods on equilibrium moisture content was studied. Finally, the experiments on CO_2 hydrate formation by employing each prepared sample were performed and analysed.

2.2.Characterisation of silicas

2.2.1. Type of silica

Three adsorbents employed were standard silica gel, purchased from Fisher Scientific; zeolite 13X, purchased from Sigma-Aldrich; and spherical MCF-17*, obtained from Han et al. (2007).

***Synthesis of Spherical MCF-17**

The process was as follows: 4 g of triblock copolymer Pluronic P123 were dissolved in an acidic solution (10 mL of Hydrochloric acid (HCl, 37%) and 65 mL of H_2O). A total of 4 g of 1,3,5-trimethylbenzene (TMB) were then added, and the resulting solution was heated to 37 – 40^oC with vigorous stirring for 2 h. A total of 9.2 mL of tetraethoxysilane (TEOS) was then added and stirred for 5 min. The solution was transferred to an autoclave and aged at 40^oC for 20 h under a

quiescent condition. A total of 46 mg of Ammonium Fluoride (NH_4F) was added, and the mixture was aged at 100°C for another 24 h. The resulting precipitate was filtered, washed with water and ethanol, and dried. The white powder obtained was calcined in air at 900°C for 6 h.

2.2.2. Principle of the Brunauer, Emmett and Teller (BET) surface area and porosity analyser

The analysis on the sample was conducted using the BET surface area and porosity analyser (Micromeritics-ASAP 2420; Figure 2- 1). The principle of BET method was referred to ISO 9277 (2010). The method specified involves the determination of the amount of adsorbate or adsorptive gas required to cover the external and the accessible internal pore surfaces of a solid with a complete monolayer of adsorbate. This monolayer amount can be calculated from the adsorption isotherm using the BET equation:

$$\frac{p/p_0}{(1-p/p_0)V_a} = \frac{1}{CV_m} + \frac{C-1}{CV_m}\frac{p}{p_0} \qquad (2-1)$$

where, V_a is the amount of gas adsorbed; V_m is the monolayer amount; C is the BET parameter.

N_2 at its boiling point (about 77.3 K) is usually the most suitable adsorptive. This gas is admitted to the sample container which is held at a constant temperature. The amounts adsorbed are measured in equilibrium with the adsorptive gas pressure, p and plotted against relative pressure, p/p_0, to give an adsorption isotherm. Adsorption isotherms may be obtained by volumetric, gravimetric, calorimetric or spectroscopic measurement or by the carrier gas method using continuous or discontinuous operation.

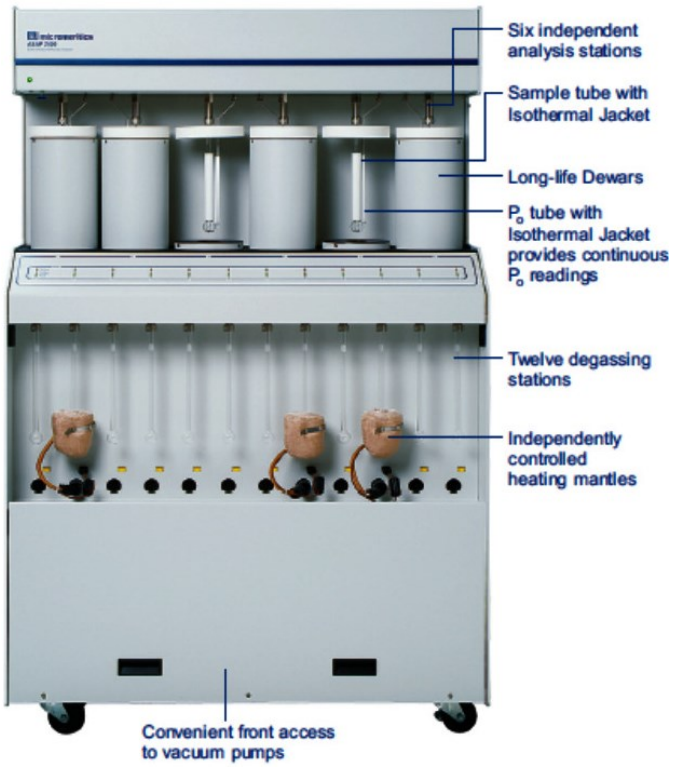


Figure 2- 1: BET surface analyser

2.2.3. Surface area and pore size analysis

Textural characterization was carried out by using N_2 as the adsorbate. The analyses were done based on the method employed by Stevens et al. (2013). Approximately 0.20 g of sample was accurately weighed into a glass sample tube, with filler rod and sealed frit. The samples were degassed under vacuum at 383 K for 48 hr to remove moisture and other adsorbed gases. N_2 isotherms were acquired from 1.00 X 10^{-7} to 0.99 relative pressure (p/p_0) at 77 K in liquid N_2. Helium (He) was used to measure the free space prior to analysis. Figure 2- 2 illustrates the adsorption/desorption isotherms for each silica. The BET surface area (S_{BET}), total pore volume (V_{tot}) at 0.99 p/p_0 and pore size (D) obtained from N_2 adsorption/desorption isotherms for each silica are summarised in Table 2- 1.

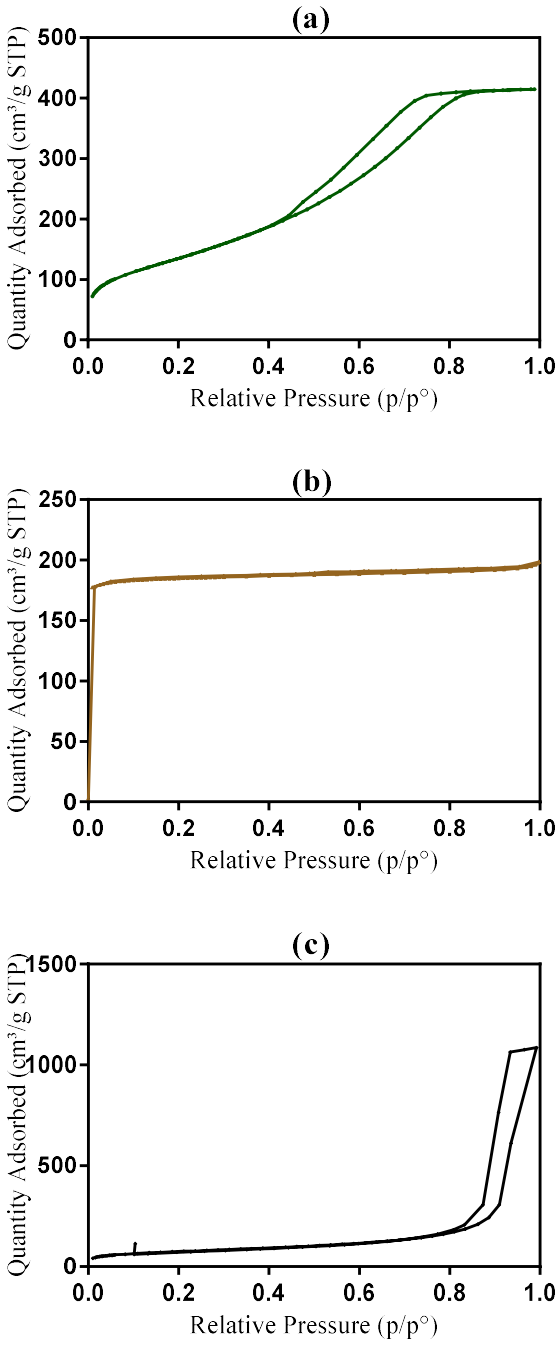


Figure 2- 2: N_2 adsorption/desorption isotherms for each silica; (a) standard silica gel, (b) zeolite 13X and (c) spherical MCF-17

Table 2- 1: The properties of each silica (BET sample calculation – Appendix 1)

Type of silica	Particle size distribution (μm)	S_{BET} (m^2/g)	V_{micro} (cm^3/g)	V_{meso} (cm^3/g)	V_{tot}* (cm^3/g)	D ($4V_{tot}/S_{BET}$) (nm)
Standard silica gel	200-500	499	0.17	0.44	0.64	5.14
Zeolite 13X	2	819	0.29	0.02	0.31	1.50
Spherical MCF-17	1-20	268	0.10	1.49	1.68	25.05

* V_{micro} was determined by Dubinin-Raduskevich model; V_{meso} was determined by Barret-Joyner-Halenda (BJH) model (Harkins Jura correction) for D between 2-50 nm

2.3.Various sample preparation methods

The adsorbent employed was standard silica gel and it was noted that the particle size was almost similar to the one used by Kumar et al. (2013; 0.13-0.25 mm). Four methods were used for the preparation of wet silica gel, namely methods 1 (silica was left to naturally adsorbed moisture), 2 (the lowest rates of stirring of silica), 3 (silica was submerged in excess water) and 4 (the highest rates of stirring of silica) (Figure 2- 3 and Figure 2- 4). For all methods, silica gel was initially dried inside the oven for one night at 200^{o}C before the commencement of each experiment. The oven used (Model AX30) was manufactured by Carbolite and has a maximum temperature of 250 ^{o}C and a minimum temperature of 40 ^{o}C. For all methods, each final equilibrium mass of wet silica gel was deducted with dry silica gel mass to obtain the final moisture content respectively. The weighing balance (Model: AEA – 220A) used was manufactured by AE Adam and it can measure a maximum mass up to 220g and a minimum mass of 10mg.

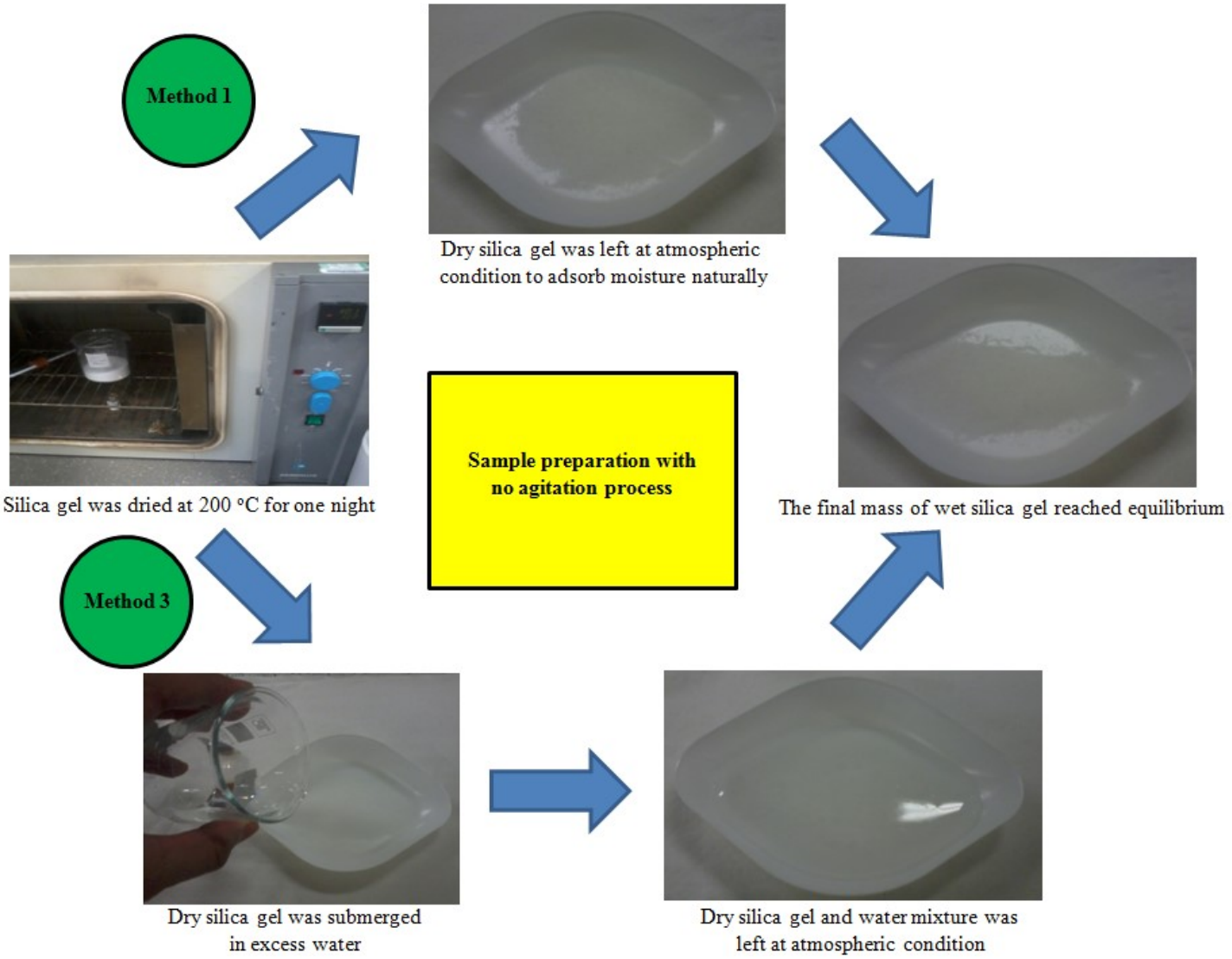


Figure 2- 3: Methods 1 and 3 for sample preparations without agitation

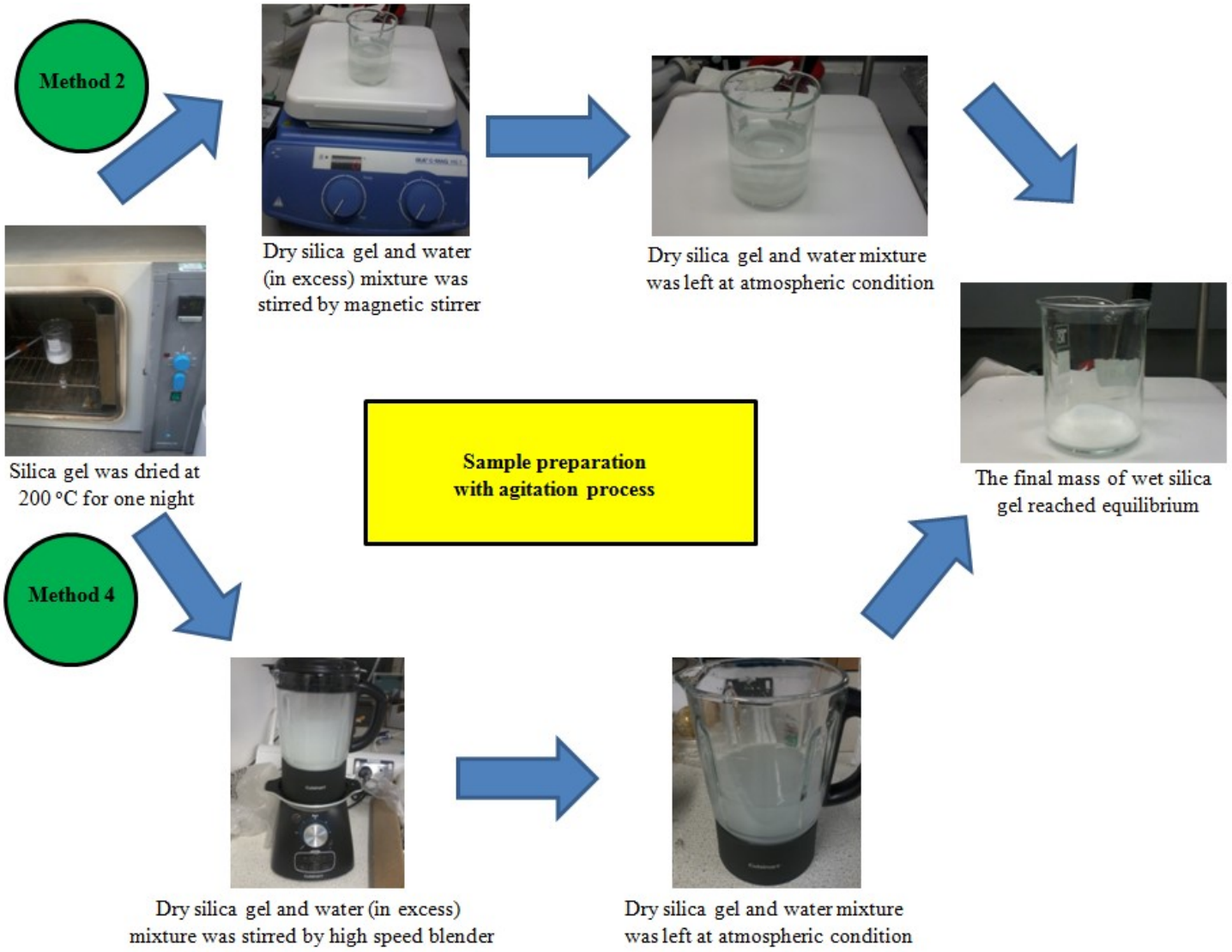


Figure 2- 4: Methods 2 and 4 for sample preparations with agitation

2.3.1. Method 1

i. Dry silica gel (2.5g) was placed inside weighing boat and left at atmospheric condition.

ii. The silica gel naturally adsorbed water until the final mass reached equilibrium.

2.3.2. Method 2

i. Dry silica gel (2.5g) was placed inside beaker and water was added in excess (19 times the mass of dry silica gel) so that the total mass of the mixture was 50g.

ii. The silica gel and water mixture were slowly stirred by using a magnetic stirrer for one night.

iii. Then, the beaker was left at atmospheric condition until the final mass of the mixture reached equilibrium.

2.3.3. Method 3

i. Dry silica gel (0.5g) was placed inside weighing boat and water was added in excess (19 times the mass of dry silica gel) so that the total mass of the mixture was 50g.

ii. Then, it was left at atmospheric condition until the final mass reached equilibrium.

2.3.4. Method 4

i. Dry silica gel (0.5g) was placed inside blender and water was added in excess (19 times the mass of dry silica gel) so that the total mass of the mixture was 50g.

ii. The silica gel and water mixture were vigorously stirred at the speed of 37,000 rpm (Dawson et al., 2014) by using a high speed blender for 90 seconds.

iii. Then, the mixture was left at atmospheric condition until the final mass reached equilibrium.

2.4.Sample preparation procedure for promoters' contact with silica gel

The promoters (supplied by Fisher Scientific) used were THF (99.9% purity), TBAB (98% purity) and SDS (97.5% purity). Each promoter was diluted in water to obtain SDS with a concentration of 0.01 mol% (Yang et al., 2013), THF with a concentration of 3 mol% (Yang et al., 2013) and TBAB with a concentration of 0.29 mol% (Li et al., 2011). These were the optimum concentrations obtained by both researchers in their works.

Table 2- 2 summarises the amount of each promoter used to prepare the sample at the required concentration. The amount of dry silica gel used to prepare each sample was 2.5 g. Then, promoter-water solution equal to 47.5 g was added to make the total mass of dry silica gel-promoter-water mixture equal to 50.0 g. In order to prepare 3 mol% of THF, 5.229 g of THF was diluted into 42.271 g of H_2O. Next, 0.076 g of SDS was mixed with 47.424 g of H_2O to prepare 0.01 mol% of SDS and 2.348 g of TBAB was added with 45.152 g of H_2O to prepare 0.29 mol% of TBAB. These samples were prepared by implementing the highest rates of stirring (method 4) (Figure 2- 4). Also, the concentration required for each combined-promoter employed in this work is presented in Table A- 2 (Appendix 2).

Table 2- 2: The amount of each promoter used to prepare sample at the required concentration

No.	Type of promoter	Concentration of promoter (mol%)	Mass of promoter (g)	Mass of dry silica gel (g)	Mass of water (g)
1	THF	3.000	5.229	2.500	42.271
2	SDS	0.010	0.076	2.500	47.424
3	TBAB	0.290	2.348	2.500	45.152

2.4.1. Calculation for the amount of promoter used

Equation 2-2 was used to calculate the amount of promoter used.

$$concentration\ of\ promoter\ (mol\%) = \frac{mol\ of\ promoter\ (mol)}{mol\ of\ promoter\ (mol) + mol\ of\ water\ (mol)} X\ 100\% \qquad (2-2)$$

where, equation 2-3 was used to calculate the number of moles of promoter required.

$$number of moles(mol) = \frac{mass(g)}{MR\left({}^{g}/_{mol}\right)} \qquad (2-3)$$

where, MR is the molecular weight of promoter.

2.5.Equilibrium moisture content measurement

The amount of equilibrium moisture content inside silica gel pores was measured by using a degassing unit (Figure 2- 5 and Figure 2- 7). The amount of water content was necessary to calculate the final conversion of water to CO_2 hydrate.

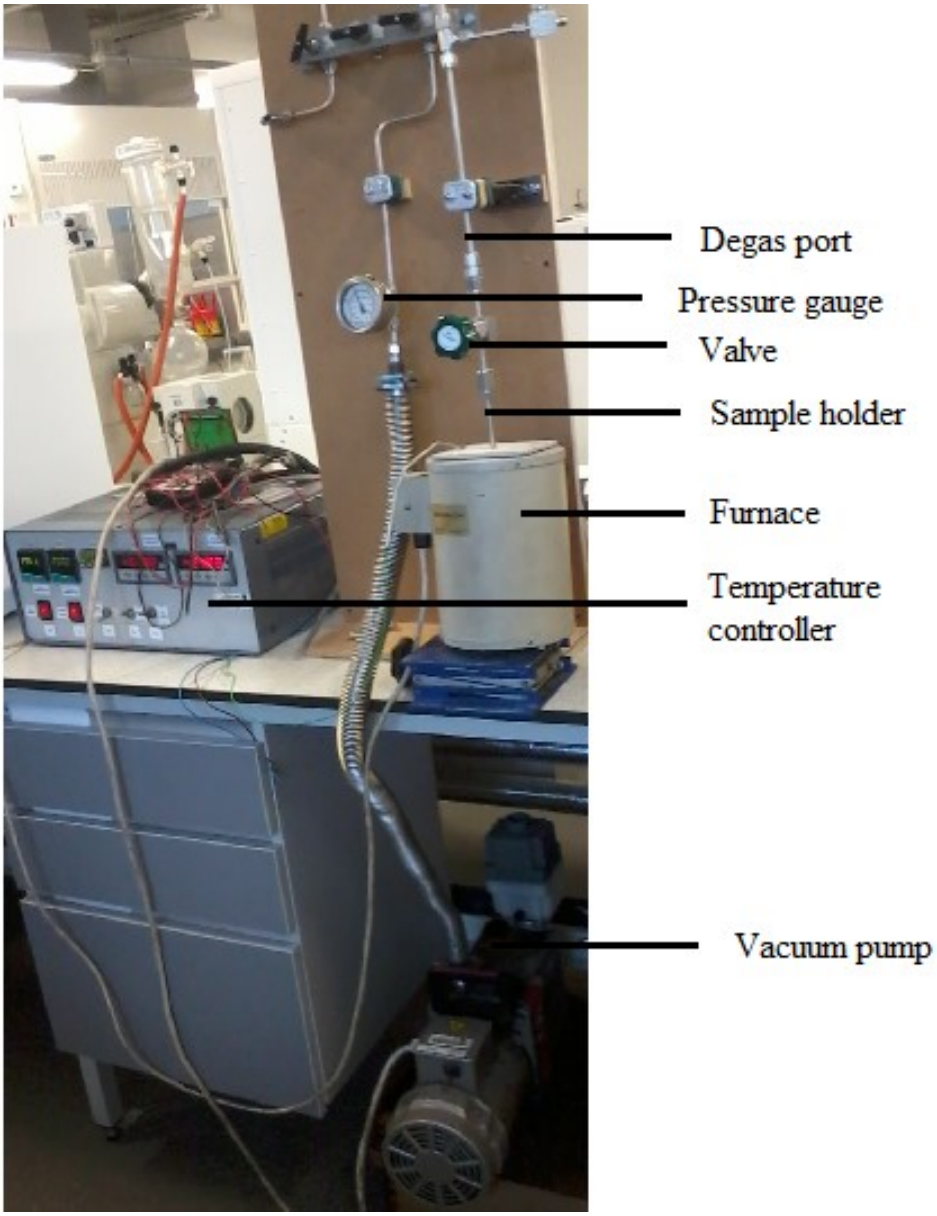


Figure 2- 5: Degassing unit

2.5.1. Experimental procedure

i. The sample cell was charged with wet silica gel and was placed inside furnace and the cell's valve was initially closed.

ii. Then, the furnace was heated to 200 ^{o}C by temperature controller and at the same time the vacuum pump was switched on to vent out any gas and moisture presence in the system.

iii. After the operating temperature was achieved, then the cell's valve was slowly opened until maximum opening.

iv. The experiment was left running for one night.

v. Finally, the amount of equilibrium moisture content was calculated.

2.5.2. Calculation of the amount of equilibrium moisture content

2.5.2.1. Moisture content inside silica gel pores (g)

The weight of wet silica gel was measured before the experiment and the weight of dry silica gel was measured immediately after the completion of experiment.

Equation 2-4 was used to calculate the amount of moisture content.

$$moisturecontent(g) = wetsilicagel(g) - drysilicagel(g) \qquad (2-4)$$

2.5.2.2. Equilibrium moisture content with respect to wet silica gel (wt%)

The amount of equilibrium moisture content was presented in weight percent of wet silica gel.

Equation 2-5 was used to calculate weight percent of moisture content available inside wet silica gel pores.

$$equilibriummoisturecontent(wt\%) = \frac{moisturecontent(g)}{wetsilicagel(g)} X\ 100\% \qquad (2-5)$$

2.6.CO_2 hydrate formation

Figure 2- 6 shows the work station for hydrate formation experiments consisting of the high pressure volumetric analyser (model HPVA-100, manufactured by Micromeritics), a computer unit, a constant temperature bath, gas cylinders and a vacuum pump. The description of each piece of equipment is explained.

i) The HPVA (with a 100 bar pressure range from vacuum) was used to investigate hydrate formation in batch operation at desired operating pressure and temperature. The analysed sample was placed inside sample chamber and the analysed gas was supplied to the sample cell through analysis port. The operating pressure and temperature were displayed on the HPVA front panel.

ii) A computer unit was required in which the analysis results were presented in real-time on the computer screen during an experiment and the details were observed and printed via a Microsoft Excel macro provided with the application software. The minimum requirements were Intel Core 2 Duo processor (2.0 GHz or faster), 1 gigabyte of RAM, 20-gigabyte hard disk space and Windows 7 with Microsoft Excel 2002 or higher.

iii) A constant temperature bath was used to control the operating temperature inside the temperature control vessel. The mixture of 70 vol% water + 30 vol% antifreeze was used to avoid the formation of ice inside temperature control vessel and to make sure that the water mixture was consistently circulated throughout the process.

iv) Gas cylinders were necessary to provide analysis gas with purity of 99.99% (maximum 103 bar), He gas with purity of 99.99% (34.4 bar) for venting or cleaning purposes and N_2 gas/compressed air (5.2 to 5.5 bar) to control the pneumatic valves of the HPVA.

v) A vacuum pump was needed to ensure the system reached full vacuum during the purging process before the commencement of each experiment.



Figure 2- 6: Work station

2.6.1. Principles of the HPVA

The HPVA-100 (Figure 2- 7) was designed to obtain high-pressure adsorption isotherms by employing the static volumetric method where it consists of introducing (dosing) a known amount of gas (adsorptive) into the chamber containing the sample to be analysed. It is capable of achieving pressures up to 100 bar. When the sample reaches equilibrium with the adsorbate gas, the final equilibrium pressure is recorded and this process is repeated at given pressure intervals until the maximum pre-selected pressure is reached. These data are then used to calculate the quantity of gas adsorbed by the sample and resulting equilibrium points (volume adsorbed and equilibrium pressure) are then plotted to provide an isotherm. Excellent reproducibility and accuracy are obtained by using separate transducers for dosing the sample and for monitoring the pressure in the sample chamber.

2.6.1.1. Description of the HPVA

The HPVA-100 includes a safety feature whereby if tripped, the safety circuit places the unit in a safe condition by eradicating power to the unit and closing all valves. The standard system consists of a system schematic, a gas manifold maintained at a constant temperature (40 ^{o}C) with two pressure transducers (reading accuracy is $\pm$0.04% full scale with a stability of $\pm$0.1%), two stainless steel sample holders with diaphragm shut-off valves, an analysis port, a degas port, thermocouple connectors, pressure and temperature control displays, vent valve and vacuum valve controls, a sample chamber, a furnace and a temperature control vessel that can be connected to a constant temperature bath (Figure 2- 6).

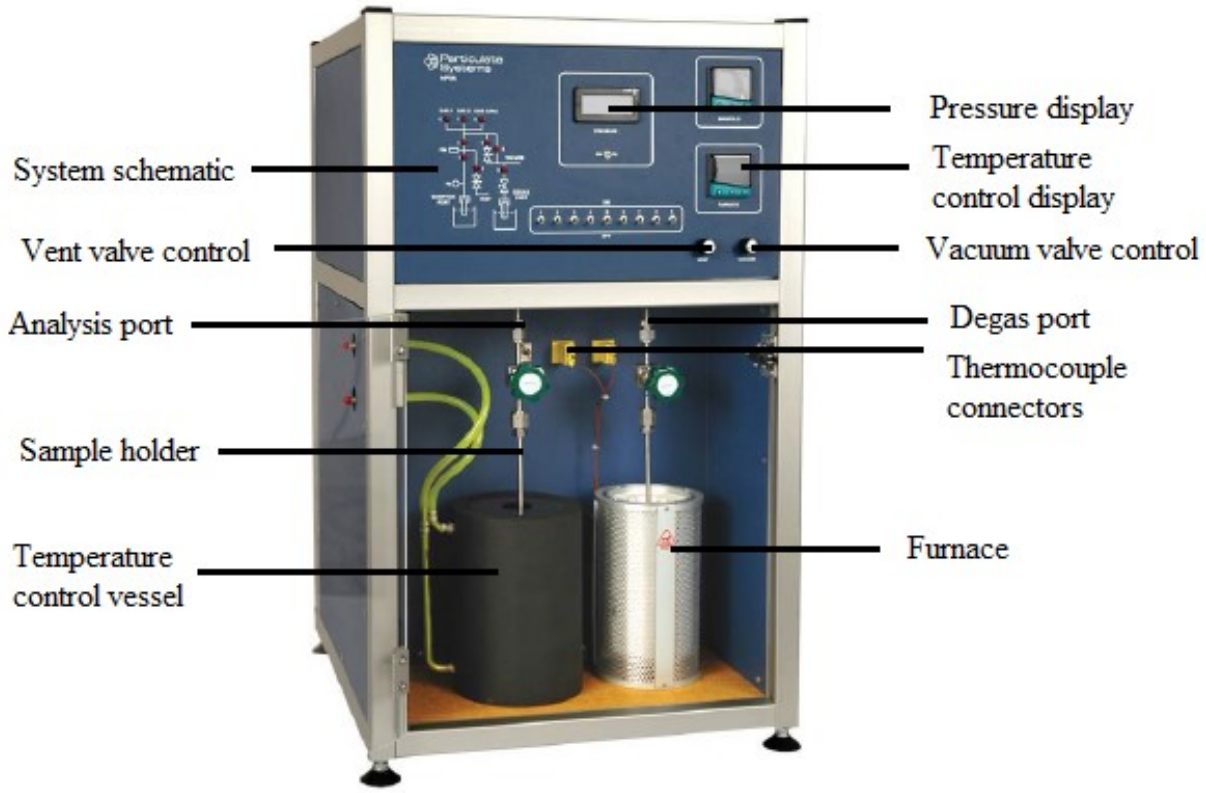


Figure 2- 7: High pressure volumetric analyser (HPVA)

2.6.2. Experimental procedure

2.6.2.1. Before the commencement of experiment

i. The system was manually purged with He gas (Figure 2- 8) to clean the line from any impurities. This step was repeated three times.

ii. Next, the operating conditions such as experiment time, analysis gas port, operating pressure and temperature were pre-defined (Figure 2- 9).

iii. After that, the sample cell was charged with wet silica gel and was placed inside water bath (70 vol% water + 30 vol% antifreeze) and the cell's valve was initially closed.

2.6.2.2. During experiment

i. The cell was pressurised to required pressure through a supply vessel containing CO_2 gas with a purity of 99.99% (supplied by BOC - a member of the Linde Group) and at the same time the desired operating temperature was established through constant temperature bath.

ii. After the operating conditions were achieved, the cell's valve was fully opened.

iii. Subsequently, the experiment was left running for 1200 minutes.

2.6.2.3. After the completion of experiment

i. The pressure was reduced to atmospheric pressure at the same operating temperature for hydrate decomposition.

ii. Then, the system was automatically vented with He gas several times to clean the line for the next experiment.

iii. Subsequently, the cell's valve was fully closed and the sample cell was removed from the HPVA.

iv. Finally, the pressure–time (P-t) curve obtained after completion of the experiment was analysed.

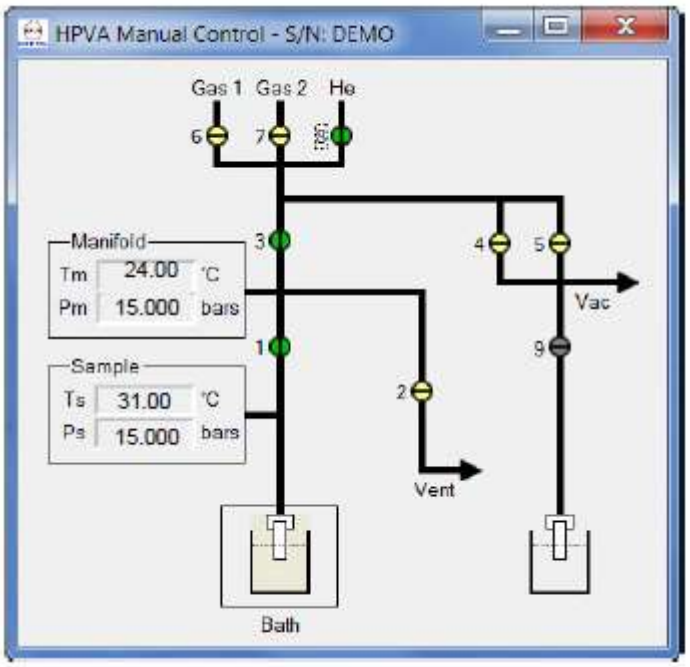


Figure 2- 8: Manual control window during purging process

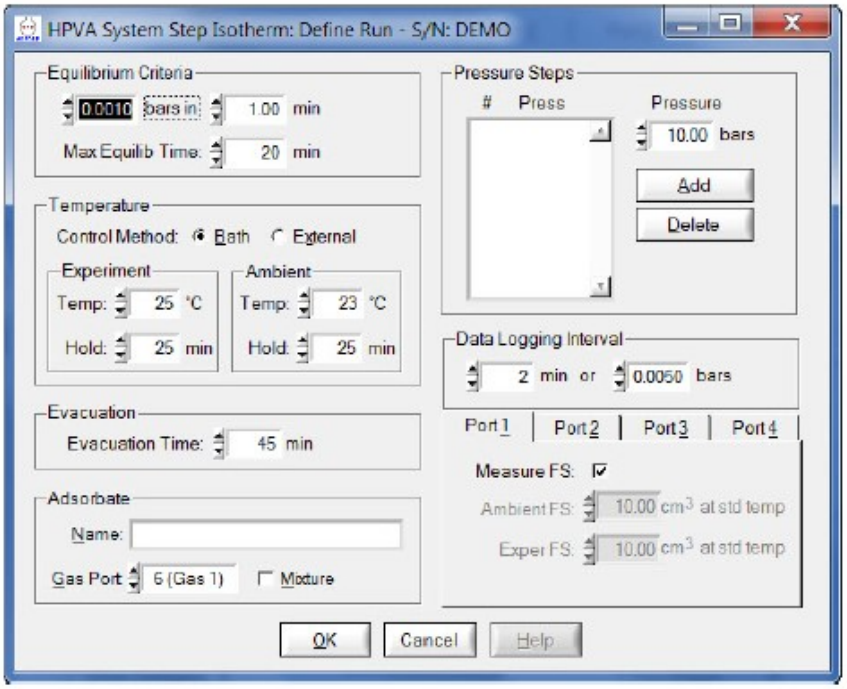


Figure 2- 9: Define run experiment window to insert operating conditions

2.6.3. Calculation of the amount of CO_2 consumed (mol)

The number of moles of gas consumed for hydrate formation is the difference between the number of moles of gas at the start of experiment (t = 0) and the number of moles of gas at time t in the sample cell (S).

Equation 2-6 was used to calculate the number of moles of CO_2 gas consumed, $\Delta n_{\downarrow}$.

$$(\Delta n_{\downarrow})_t = V_S \left(\frac{P}{zRT}\right)_0 - V_S \left(\frac{P}{zRT}\right)_t \qquad (2-6)$$

where the compressibility factor, z, is obtained from REFPROP*, V_S** is the volume of the sample cell, R is the gas constant, P and T are the pressure and temperature of the sample cell.

***NIST standard reference database – National Institute of Standards and Technology**

****Vs obtained in the data sheet was in ccSTP. The conversion of ccSTP to cm^3 by using combined gas law is shown in Appendix 3.**

2.6.4. Calculation of the amount of CO_2 involved in hydrate formation

The amount of CO_2 consumed for each experiment was further analysed to investigate the formation of hydrate by using Henry's Law. If the total mole fraction of CO_2, x_D dissolved in water exceeded the value calculated from Henry's Law, it shows the formation of hydrate in the system.

2.6.4.1. Henry's Law

Equation 2-7 was used to calculate the theoretical value of $x_{D,t}$ by using Henry's Law.

$$x_{D,t}\ (mole\ fraction) = \frac{(\text{Partial pressure of } CO_2)_t}{(KH)_t} \qquad (2-7)$$

where, KH is the value of Henry's constant at operating pressure and temperature respectively (Carrol et al., 1991).

Equation 2-8 was used to calculate the value of $x_{D,e}$ at time t during the experiment.

$$x_{D,e} at\ time\ t\ (mole\ fraction) = \frac{(\text{mol of } CO_2)_t}{(\text{mol of } CO_2 + \text{mol of } H_2O)_t} \quad (2-8)$$

2.6.4.2. Total number of moles of CO_2 consumed to form hydrate

Equation 2-9 was used to calculate the number of moles of CO_2 consumed to form hydrate, $\Delta n_{H,\downarrow}$ (Sun et al., 2014).

$$\left(\Delta n_{H,\downarrow}\right)_t = (n_\downarrow)_0 - (n_\downarrow)_t - n_{D,t} \quad (2-9)$$

where, $(n_\downarrow)_0$ is CO_2 consumed at time t = 0, $(n_\downarrow)_t$ is the CO_2 consumed at time t and $n_{D,t}$ is the CO_2 dissolved in water phase.

Equation 2-10 was used to calculate the number of moles of CO_2 dissolved in water phase, $n_{D,t}$ (Servio et al., 2001).

$$n_{D,t} = \frac{\left[\left(\frac{x_{D,t} \times n_{water}}{1 - x_{D,t}}\right) \times \left(\frac{1}{x_{D,e}} - 1\right) - n_{water}\right]}{\left[1 - \frac{1}{x_{D,e}}\right]} \quad (2-10)$$

2.6.5. Conversion of water to hydrate (mol%)

Equation 2-11 was used to calculate the conversion of water to CO_2 hydrate.

$$Conversion\ of\ water\ to\ hydrate\ (mol\%) = \frac{\Delta n_{H,\downarrow} \times hydrationnumber}{n_{H_2O}} \times 100\% \quad (2-11)$$

where $\Delta n_{H,\downarrow}$ is the number of moles of gas consumed for hydrate formation at the end of the experiment determined from the gas uptake and n_{H_2O} is the total number of moles of water in the system. The hydration number is the number of water molecules per guest molecule.

The hydration number used for pure CO_2 gas system was 5.75 (Babu et al., 2015; Teng et al., 1996) and 7.09 for fuel gas system (Babu et al., 2015).

2.6.6. CO_2 uptake (mmol of CO_2/g of H_2O)

Equation 2-12 was used to calculate the amount of CO_2 uptake with respect to dry silica gel weight.

$$CO_2 uptake(mmol\ of\ CO_2/g\ of\ H_2O) = \frac{\Delta n_{H,\downarrow}}{weight\ of\ H_2O} \times 1000 \qquad (2-12)$$

2.6.7. Rate of hydrate formation (mmol CO_2 per g H_2O per min)

Equation 2-13 was used to calculate the rate of hydrate formation.

$$\left(\frac{\Delta n_{H,\downarrow}}{\Delta t}\right) = \frac{\left(\Delta n_{H,\downarrow}\right)_{t+\Delta t} - \left(\Delta n_{H,\downarrow}\right)_t}{\Delta t}, \Delta t = 30\ min \qquad (2-13)$$

The rate of hydrate formation was reported every 30 minutes because the data was very large; the sampling time for data acquisition of pressure and temperature were taken every 5 s by the HPVA. Thus, the rate for every 30 minutes helps for proper visualisation of the rate change during 1200 minutes.

CHAPTER 3: THE EFFECT OF VARIOUS SAMPLE PREPARATION METHODS

3.1.Introduction

As previously mentioned, mesoporous and microporous silica gels have lower rates of hydrate formation as compared to macroporous silica due to the decreased activity of water inside smaller pore silica gels caused by the partial ordering and bonding of water molecules with hydrophilic surfaces of pores (Park et al., 2013). Thus, an investigation on various sample preparation methods is presented in this chapter where the main aim is to enhance the availability and activity of water inside mesoporous silica gel for hydrate formation. Standard silica gel with a mean particle size of 200-500 μm, mean pore size of 5.14 nm, pore volume of 0.64 cm^3/g and surface area of 499 m^2/g was used. The method with the best performance was then used throughout this work. The formation of hydrate in the HPVA was examined by studying the P-t curves obtained and also the analysis on CO_2 dissolutions in water (Diamond et al., 2003; Servio et al., 2001 and Carrol et al., 1991). Additionally, some control experiments were performed to distinguish between hydrate formation and physical adsorption by using HPVA. Then, the application of promoters in this study was introduced. Finally, the comparison of hydrate formation experiment for three different silicas was presented where the best silica was then used throughout this work.

3.2.Analysis of various sample preparation methods

Four sample preparation methods were investigated in this work namely methods 1, 2, 3 and 4. The full description of each method was described in Chapter 2 (pages 63-66). Hence, Table 3- 1 shows a brief description of each method. Then, the results of equilibrium moisture content and hydrate formation for samples prepared from each method are presented. The confidence interval (CI) calculated was based on a 90% CI level and is presented in the results and discussion throughout this thesis when necessary.

Table 3- 1: Brief description of the type of methods that were investigated

Method	Description
1	Dry silica gel was left at atmospheric condition to naturally adsorb moisture
2	Dry silica gel and water mixture were slowly stirred by using magnetic stirrer
3	Dry silica gel was submerged in excess water
4	Dry silica gel and water mixture were vigorously stirred by using high speed blender

3.2.1. The effect on the amount of equilibrium moisture content

The formation of hydrate is closely related to the amount of water available in the system. The total amount of equilibrium moisture content was determined by subtracting the weight of wet silica gel with the weight of dry silica gel as described in chapter 2. Thus, the calculated amount of water available for each prepared sample is presented in Table 3-2. It was determined that the sample prepared by method 4 had the highest moisture content with the lowest CI: 14.79±0.34 wt%. The employment of vigorous stirring was expected to give this result which is essential for the CO_2 hydrate formation process. Then, it was followed by method 3 (silica was submerged in excess water) (13.83±2.87 wt%), method 2 (the lowest rates of stirring of silica) (13.64±0.51 wt%) and method 1 (silica was left to naturally adsorbed moisture) (13.56±2.45 wt%). The relatively low CI obtained for methods 2 and 4 is explained by the need for stirring during sample preparation to ensure the water is well distributed inside silica gel pores. These also indicated that samples prepared from both methods had high reproducibility as compared to methods 1 and 3. Figure 3- 1 summarises the results shown in Table 3- 2.

Table 3- 2: The equilibrium moisture content in wet silica gel for different types of sample preparation methods

Sample	Exp.	SiG (wet) (g)	SiG (dry) (g)	Equil. moisture content (wt%)	Mean equil. moisture content (wt%)	SD	90% C1 (±)
Method 1	1	0.06	0.05	15.05	13.56	2.11	2.45
	2	0.08	0.07	12.07			
Method 2	1	0.06	0.05	13.33	13.64	0.44	0.51
	2	0.09	0.07	13.95			
Method 3	1	0.05	0.04	16.52	13.83	2.47	2.87
	2	0.11	0.10	11.65			
Method 4	1	0.14	0.12	15.00	14.79	0.29	0.34
	2	0.10	0.08	14.58			

- Method 1 (silica was left to naturally adsorbed moisture), method 2 (the lowest rates of stirring of silica), method 3 (silica was submerged in excess water) and method 4 (the highest rates of stirring of silica)

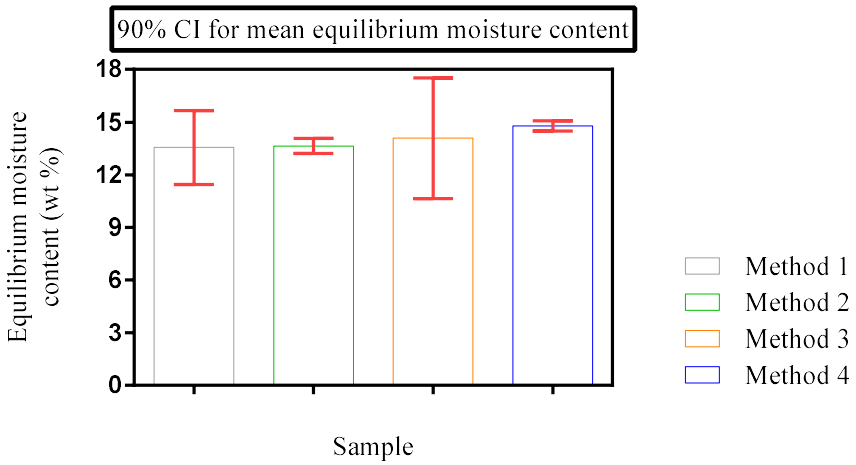


Figure 3- 1: The equilibrium moisture content in wet silica gel for methods 1 – 4 (all methods were referred to Table 3- 1)

3.2.2. Hydrate formation

All prepared samples were used to investigate hydrate formation in the HPVA at 275 K and 35 bar by using pure CO_2 gas (99.99% purity). All experiments were conducted for 1200 minutes to obtain maximum CO_2 uptake. The P-t curves obtained were firstly used to justify the formation of hydrate together with the study of CO_2 dissolution in water according to Henry's Law and then followed by analysis of CO_2 uptake and rate of hydrate formation.

3.2.2.1. Justification on CO_2 hydrate formation

Due to the limitation of the crystallizer in which the formation of hydrate could not be seen directly by the eyes, there was a necessity to justify the formation of hydrate in this work. Thus, two approaches were used to examine the formation of hydrate: analysis of P-t curves and study of CO_2 dissolution in water suggested by Servio et al. (2001). Three sets of experiment were performed for each sample for assessing hydrate; only experiment number 1 from each method is presented here. The analyses on experiments 2 and 3 were not presented because the same trends were observed as in experiment 1 for each sample.

3.2.2.1.1. P-t curve

According to Tang et al. (2013), there must be at least a two-stage pressure drop upon completion of the experiment to ensure the formation of hydrate. The first stage of pressure drop indicates the dissolution of CO_2 in water and the subsequent stages indicate hydrate growth. This trend was observed for all samples during the hydrate formation experiment (Figure 3- 2) where the total pressure drop achieved after 1200 minutes was around 2 bar. For all samples, the complete dissolution of CO_2 in water inside silica gel pores was observed after the pressure dropped approximately to 33.5 bar. This first stage of pressure drop was followed by constant pressure for several minutes before the second stage of pressure drop started which indicated the growth of hydrate. Then, several stages of pressure drop were observed for all samples before it became a plateau. For the sample prepared by the highest rates of stirring (method 4), the pressure became constant approximately after 500 minutes, followed by method 3 (800 minutes), method 1 (900 minutes) and method 2 (1200 minutes). For a clear picture on the hydrate formation mechanism, the explanation of the P-t curve is further discussed in chapter 6.

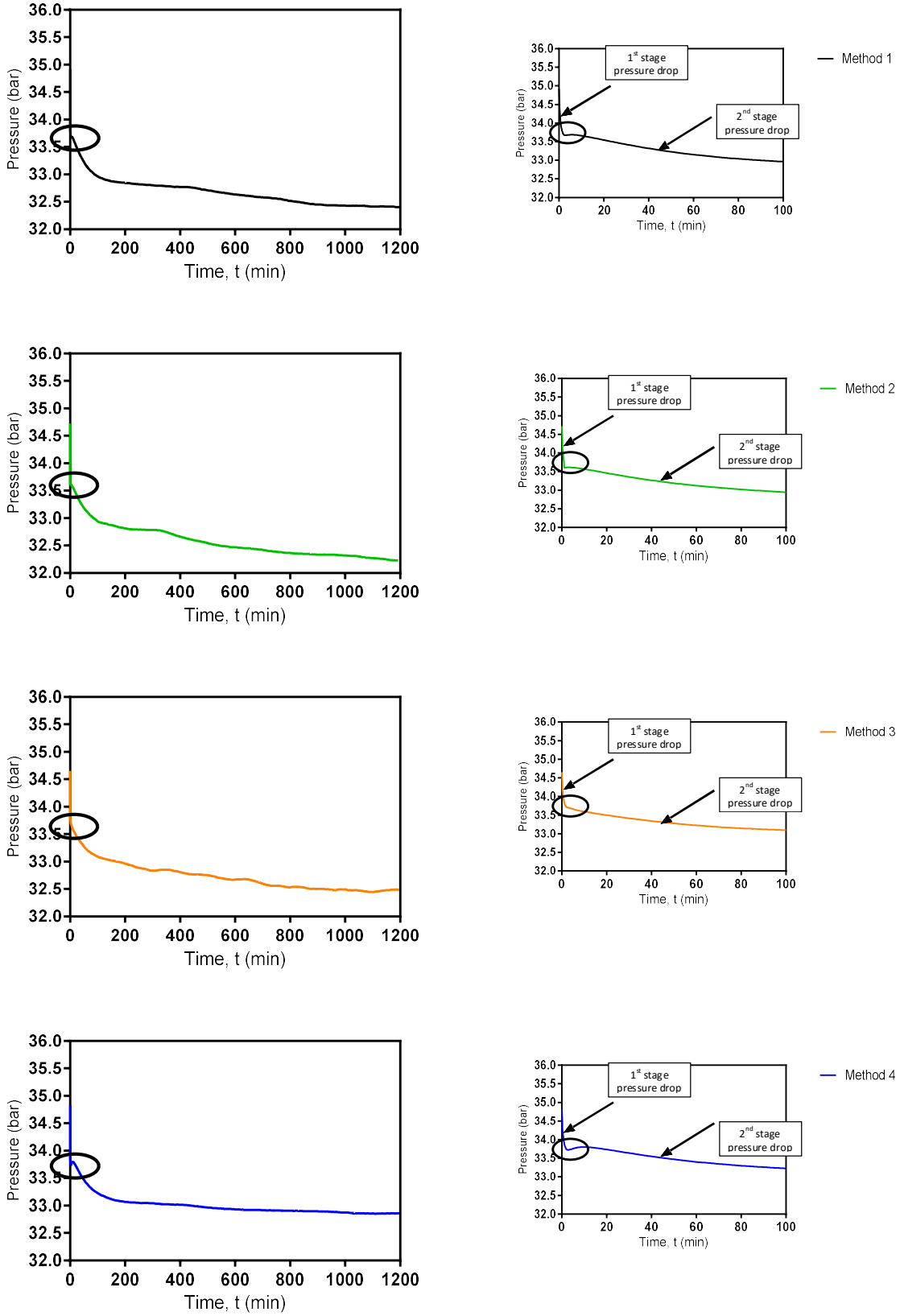


Figure 3- 2: P-t curves that show 2-stage pressure drop in 1200 minutes and the first 100 minutes respectively for methods 1 – 4 (all methods were referred to Table 3- 1)

3.2.2.1.2. CO_2 solubility in water

Since the experiments were conducted in batch mode or isochoric condition, the total number of moles of CO_2 consumed can easily be calculated by using the Ideal Gas Law equation as described in chapter 2. Then, the mole fraction of CO_2 dissolved in water was calculated to be 0.0438 where the value of Henry's constant at 275 K was obtained from Carrol et al. (1991). This value was not considered for the justification of hydrate formation because the value of Henry's constant in their work was calculated at atmospheric pressure which was not the same with the operating pressures employed in this work. However, this value was presented in the figure for the comparison purpose. Thus, the equilibrium mole fraction of CO_2 in water at various operating temperatures and pressures plotted by Servio et al. (2001) was used as a guideline to determine the formation of hydrate in the system. The formation of hydrate was confirmed when the total experimental mole fraction was higher than the equilibrium mole fraction at the experimental conditions (275 K and 35 bar). Based on the data given by Servio et al. (2001), the equilibrium mole fraction was found to be 0.0165 at these experimental conditions.

Figure 3- 3 (a) illustrates the total mole fraction of CO_2 consumed in water for all samples throughout the experiments while Figure 3- 3 (b) illustrates the mole fraction of CO_2 consumed during hydrate growth. The red-dashed line in Figure 3- 3 (a) shows the total CO_2 dissolved in water at the experimental conditions in which further CO_2 consumed after that is known as the growth of hydrate. The highest total mole fraction of CO_2 involved in hydrate formation was observed for the sample prepared using method 4 (the highest rates of stirring of silica) (0.060) followed by methods 2 (the slowest rates of stirring of silica) (0.059), 1 (silica was left to naturally adsorbed moisture) (0.057) and 3 (silica was submerged in excess water) (0.050) as shown in Figure 3- 3 (b). Since the formation of

hydrate was justified, next the study on final water to hydrate conversion, CO_2 uptake and rate of hydrate formation for all samples are presented in the next section.

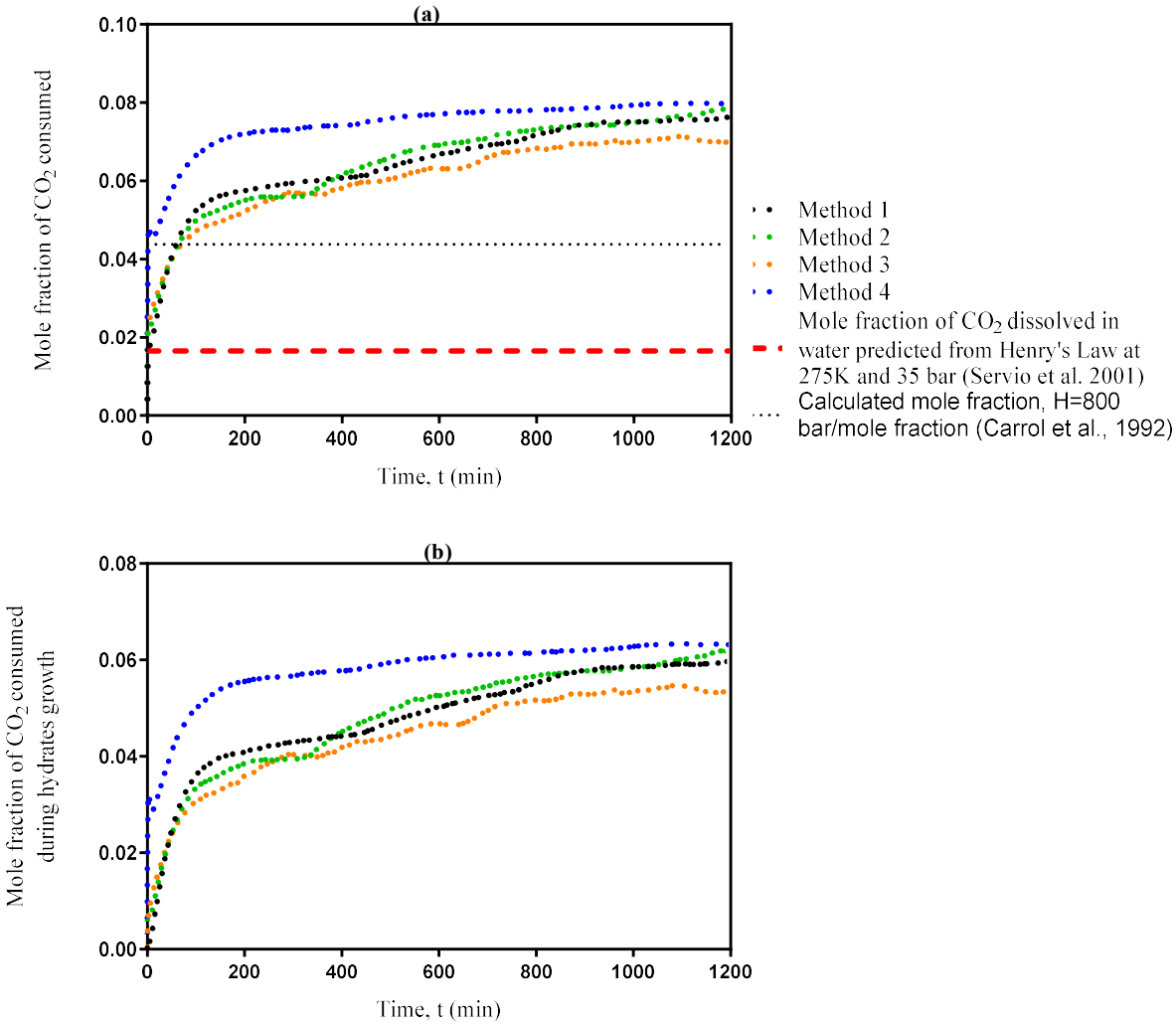


Figure 3- 3: Mole fraction of CO_2 in water inside silica gel pores for methods 1 – 4 at experimental conditions of 275 K and 35 bar in 1200 minutes; (a) total mole fraction of CO_2, (b) mole fraction of CO_2 during hydrate growth (all methods were referred to Table 3- 1)

3.2.2.2. Water conversion to hydrate and CO_2 uptake

Hydrate formation experiments were investigated at 275 K and 35 bar in the HPVA by using various prepared samples with approximately 0.5 g of wet silica. The hydrate formation procedure and formulae used to calculate water conversion to hydrate and CO_2

uptake were explained in chapter 2. The hydration number of 5.75 (Babu et al., 2015) was used to calculate the water conversion to hydrate as 6 water molecules are needed to form CO_2 hydrate ($CO_2.6H_2O$). This study is essential to determine the best sample preparation method which was implemented later in the rest of this work. Table 3- 3 shows the summary of results obtained where the experiments were repeated three times for each sample to analyse the reproducibility of the results.

Table 3- 3: Summary of results for hydrate formation experiments performed at 275 K and 35 bar in 1200 minutes (samples prepared by Methods 1 – 4)

Sample	Exp.	Water conversion to hydrate (mol%)	Mean water conversion to hydrate (mol%) (90% CI)	SD	CO_2 uptake (mmol of CO_2/g of H_2O)	Mean CO_2 uptake (mmol of CO_2/g of H_2O) (90% CI)	SD	CO_2 formed in hydrate (mmol)	Mean CO_2 formed in hydrate (mmol)
Method 1	1	37.8	40.0 ± 4.84	5.1	3.7	3.9 ± 0.47	0.5	0.24	0.26
	2	36.4			3.5			0.23	
	3	45.9			4.4			0.30	
Method 2	1	36.8	40.3± 3.42	3.6	3.6	3.9 ± 0.38	0.4	0.24	0.27
	2	40.1			3.9			0.27	
	3	44.0			4.3			0.29	
Method 3	1	34.8	37.9± 4.46	4.7	3.4	3.7 ± 0.47	0.5	0.24	0.26
	2	43.3			4.2			0.29	
	3	35.6			3.4			0.24	
Method 4	1	40.6	40.5± 2.28	2.4	3.9	3.9 ± 0.19	0.2	0.29	0.29
	2	38.0			3.7			0.28	
	3	42.8			4.1			0.31	

- Method 1 (silica was left to naturally adsorbed moisture), method 2 (the lowest rates of stirring of silica), method 3 (silica was submerged in excess water) and method 4 (the highest rates of stirring of silica)

The sample prepared by the highest rates of stirring (method 4) had the highest water conversion to hydrate with a value of 40.5 ± 2.28 mol% followed by method 2 (40.3 ± 3.42 mol%), method 1 (40.0 ± 4.84 mol%) and method 3 (37.9 ± 4.46 mol%). The amount of gas uptake was directly related to the amount of water conversion to hydrate. Hence, the gas

uptake obtained for methods 1, 2 and 4 were 3.9 mmol of CO_2/g of H_2O, 0.2 mmol of CO_2/g of H_2O higher than method 3. However, method 4 consumed the highest amount of CO_2 molecules with the value of 0.29 mmol followed by methods 2, 1 and 3 with values of 0.27, 0.26 and 0.26 mmol respectively. The CI for samples with stirring process was lower than methods 1 and 3. Additionally, it was observed that the sample with the highest equilibrium moisture content yielded the highest water conversion to hydrate. Figure 3- 4illustrates the water conversion to hydrate and CO_2 uptake for each sample.

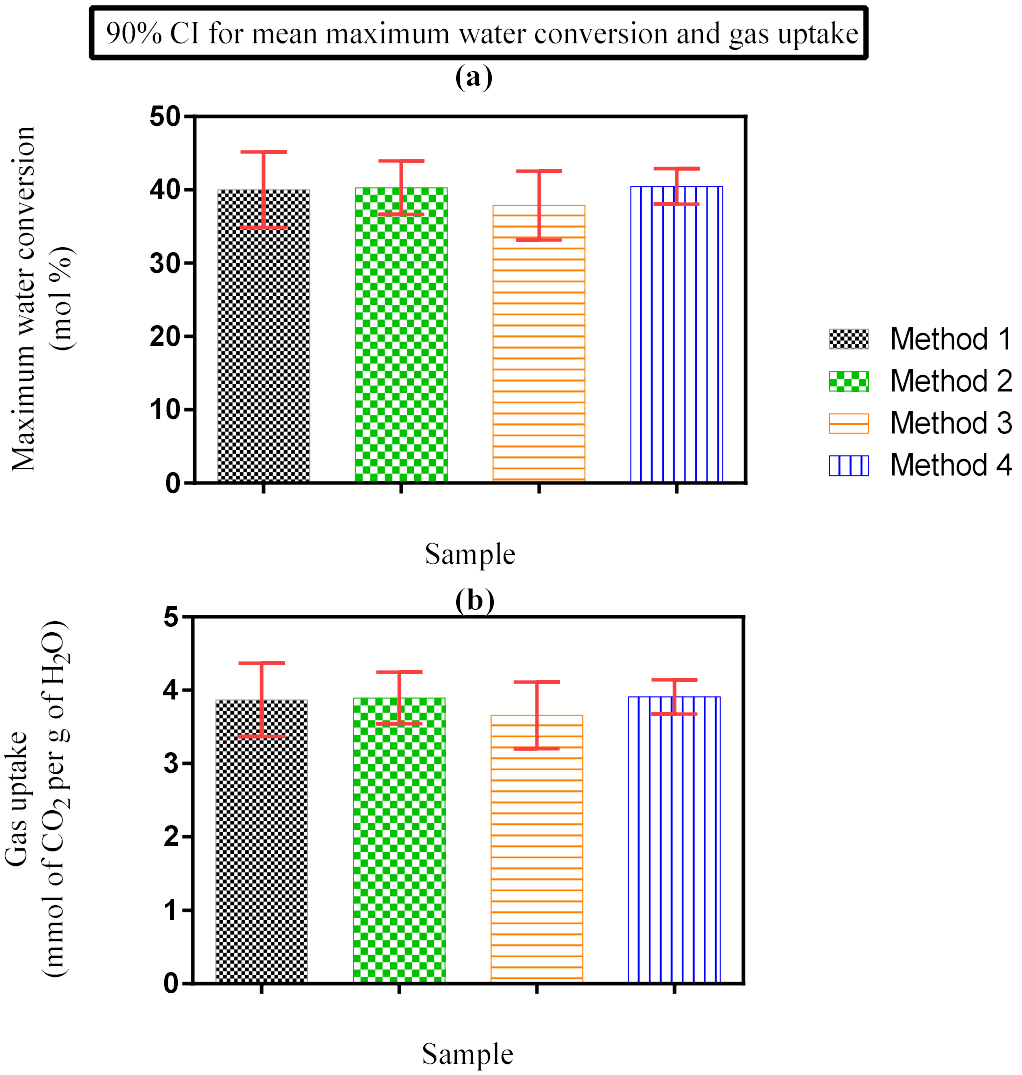


Figure 3- 4: Comparison of (a) water conversion to hydrate and (b) gas uptake for methods 1 - 4 at the operating conditions of 275 K and 35 bar in 1200 minutes (all methods were referred to Table 3- 1)

3.2.2.3. Rate of hydrate formation

Since the data was very large with the sampling time for data acquisition of pressure and temperature taken every 5 s by the HPVA, the average rate of hydrate formation was reported for every 30 min. Figure 3- 5 illustrates the rate of hydrate formation in 1200 min and inset for the first 150 minutes. At 1200 min period, the rate of hydrate formation could not be seen clearly, thus the comparison was done for the first 150 min. The sample prepared by the highest rates of stirring (method 4) demonstrated the fastest kinetics in which the initial rate of hydrate formation was more than 0.05 mmol of CO_2/g of H_2O/min, followed by methods 2, 1 and 3. The slowest initial rate was demonstrated by method 3, almost 40% slower than method 4. The kinetics for all methods were almost the same after 120 minutes of the experiments. Thus, the initial rate of hydrate formation for the samples prepared with stirring (methods 2 and 4) was better than the methods without stirring (methods 1 and 3). Overall, the silica contacted with water from method 4 showed the best results and reproducibility. Thus, method 4 was chosen as the preferred sample preparation method for the rest of this work and also the silica contacted with water from this method was used as a baseline result for comparison purposes.

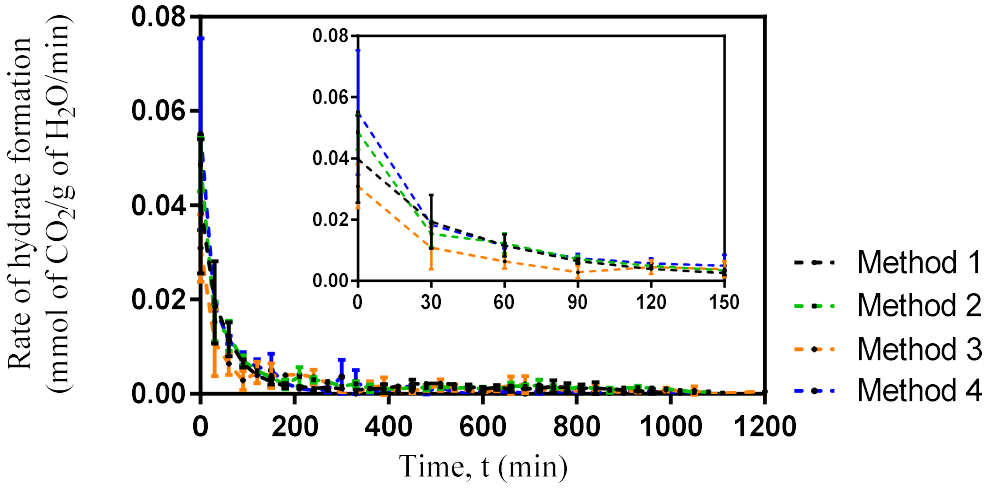


Figure 3- 5: Rate of hydrate formation for 1200 minutes and inset for the first 150 minutes (methods 1 - 4) (all methods were referred to Table 3- 1)

3.3.Control experiments

Some control experiments were performed by using silica contacted with water prepared from method 4 (the highest rates of stirring of silica) at various operating conditions. Initially, the experiments using wet and dry silica gels were performed to distinguish the formation of hydrate and physical adsorption in the HPVA. Then, the experiments at various operating pressures and temperatures were performed to further investigate the formation of hydrate in the HPVA.

3.3.1. CO_2 adsorption profile for dry and wet silica gel

Dry silica gel was prepared by using a degassing unit as described in chapter 2. The sample was dried at 100 ^{o}C for one night before the commencement of the experiment. The experiments on wet and dry silica gels were performed at the same operating pressure (36 bar) and different operating temperatures (275 K and 298 K). Figure 3- 6 illustrates the P-t curves for wet and dry silica gels in 600 minutes. The rapid one-stage pressure drop obtained for dry silica gel at both operating temperatures was expected due to normal physical adsorption. The experiment conducted at 298 K on wet silica gel gave slight one-stage pressure drop and was expected due to the normal solubility of CO_2 in water. Further investigation of mole fraction of CO_2 dissolved in water at this operating temperature is presented in the next section. Two-stage pressure drop was observed for the experiment using wet silica gel executed at 275 K due to the formation of hydrate as previously explained. The nucleation stage started after almost 10 minutes and this is known as the induction time for CO_2 hydrate formation. Next, the hydrate growth stage was seen in which the pressure drop of 1 bar occurred after almost 550 minutes duration. Then, the constant pressure until 600 minutes indicated the end of hydrate formation. Thus, the formation of hydrate in the HPVA was confirmed.

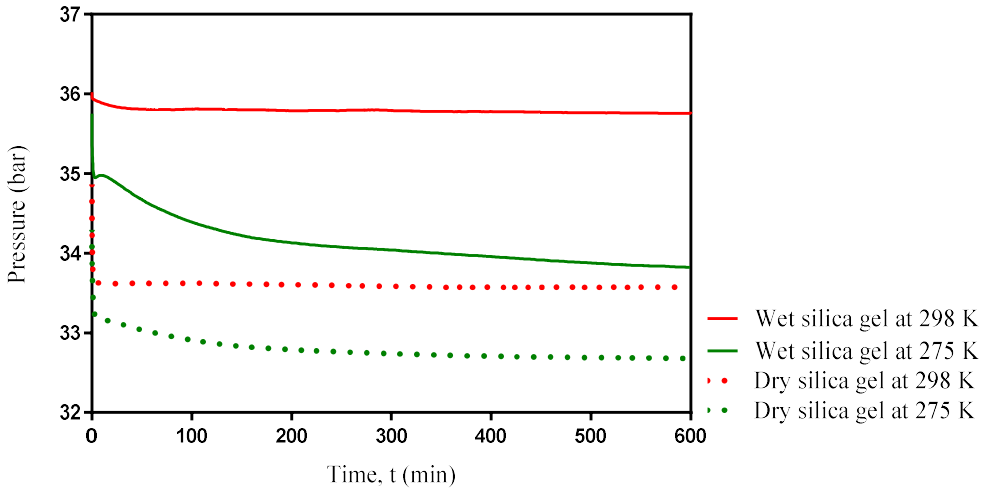


Figure 3- 6: P-t curves for dry and wet silica gels at the operating pressure of 36 bar and temperatures of 275 K and 298 K in 600 minutes

3.3.2. Various operating conditions

More hydrate formation experiments were investigated within and outside of hydrate forming conditions. Table 3- 4 summarises the operating conditions together with their calculated driving force (ΔP) in which the equilibrium pressure at each operating temperature was obtained from the experimental data plotted by Yang et al. (2013).

Table 3- 4: Experimental operating conditions with their respective calculated driving force

Exp.	Operating temperature (K)	Operating pressure (bar)	Equilibrium pressure (bar)	Driving force, ΔP (bar)	Hydrate forming region
1	275	36	17	19	Yes
2	275	30	17	13	Yes
3	275	22	17	5	Yes
4	280	36	30	6	Yes
5	280	26	30	-	No
6	288	36	-	-	No
7	293	36	-	-	No
8	298	36	-	-	No

The study on CO_2 solubility in water at these various operating conditions was performed to justify the formation of hydrate. Then, further study on CO_2 uptake was executed for the experiments that exhibited hydrate formation.

3.3.2.1. CO_2 solubility in water

The analysis of solubility of CO_2 in water was done according to Servio et al. (2001) for experiments executed within hydrate forming conditions and Diamond et al. (2003) for experiments performed outside hydrate forming regions. Based on the data plotted (Appendix 5 – Figure A- 2) by Servio et al. (2001), the solubility of CO_2 in water in the presence of hydrate at 36 bar was 0.0165 mole fraction of CO_2 at 275 K and 0.021 mole fraction of CO_2 at 280 K. The plotted data also showed that at 275 K, the solubility of CO_2 was the same at pressure ranges from 20 to 60 bar. Thus, the value of 0.0165 was also chosen for the operating pressure of 22 and 30 bar, at the operating temperature of 275 K. According to data plotted (Appendix 5 – Figure A- 3) by Diamond et al. (2003), the solubility of CO_2 in water at 280 K and 26 bar was 0.023 mole fraction of CO_2. The value observed at 36 bar was 0.022 mole fraction of CO_2 at 288 K, 0.021 mole fraction of CO_2 at 293 K and 0.018 mol fraction of CO_2 at 298 K. Figure 3- 7 and Figure 3- 8 illustrate the mole fraction of CO_2 dissolved in water at hydrate forming conditions in 600 minutes. It was observed that the total mole fraction of CO_2 soluble in water for experiments 1 (275 K and 36 bar), 2 (275 K and 30 bar), 3 (275 K and 22 bar), and 4 (280 K and 36 bar) was higher than the value provided by Servio et al. (2001).

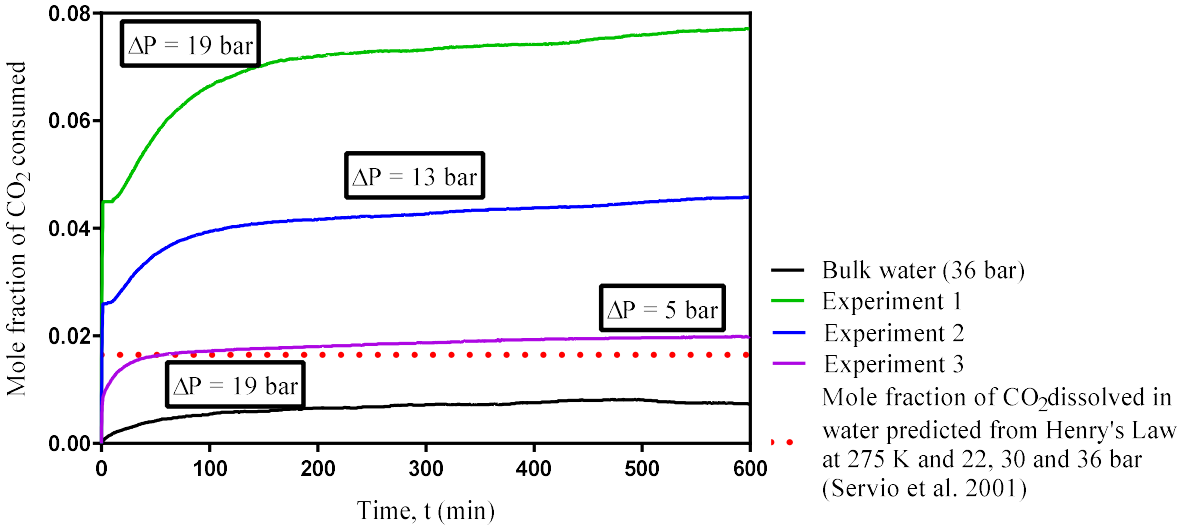


Figure 3- 7: Mole fraction of CO_2 consumed at the operating temperature of 275 K and various driving forces (ΔP) in 600 minutes (all experiments were referred to Table 3- 4)

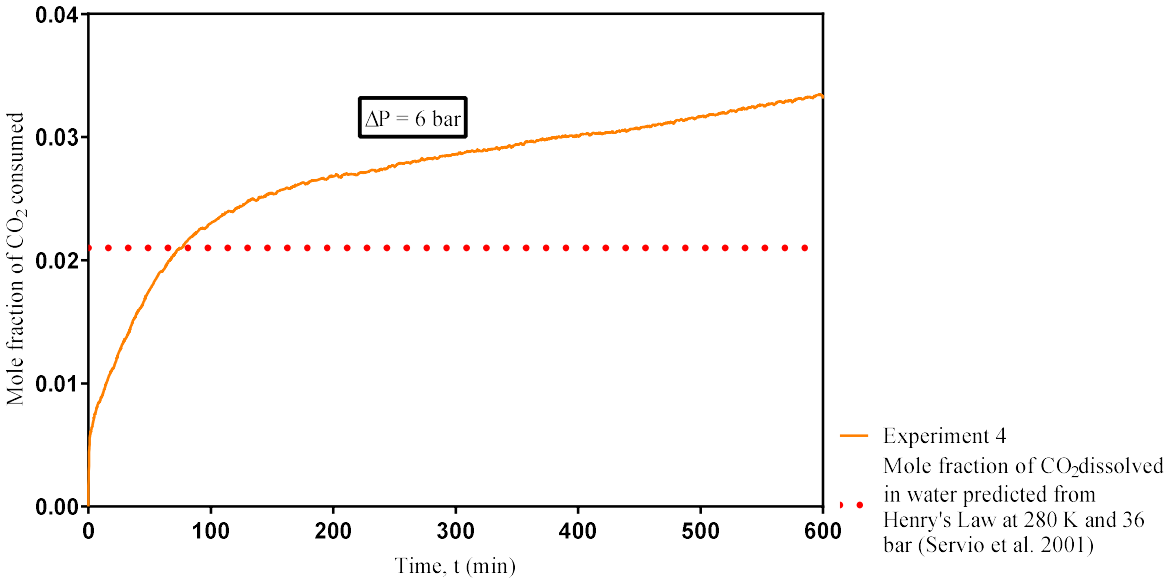


Figure 3- 8: Mole fraction of CO_2 consumed at the operating conditions of 280 K and 36 bar in 600 minutes (all experiments were referred to Table 3- 4)

The CO_2 consumption obtained before it reached the red-dashed line was assumed due to the formation of labile clusters. Hence, further CO_2 consumption observed after that was due to the formation of CO_2 hydrate. The total mole fraction of CO_2 dissolved in water

increased drastically as the driving force increased which also justified the formation of CO_2 hydrate. The highest value observed was from experiment 1 with the driving force of 19 bar, followed by experiment 2 (driving force of 13 bar), experiment 4 (driving force of 6 bar) and experiment 3 (driving force of 5 bar). Even though the driving force for experiments 3 and 4 was almost the same, only minimal hydrate growth was observed for experiment 3 due to the low pressure in the system. This indicates that in hydrate forming regions, hydrate formation is easily enhanced by increasing the pressure rather than lowering the temperature. Thus, the effect of promoter on enhancing hydrate formation at high temperature (IGCC temperature) is reported in the next section. In contrast, the experiment by employing bulk water did not show any hydrate formation at all after 600 minutes such as shown in Figure 3- 7 which explained the importance of a porous medium replacing the stirring process in bulk water system.

Figure 3- 9 illustrates the mole fraction of CO_2 dissolved in water at non-hydrate forming conditions in 600 minutes. It was observed that the total mole fraction of CO_2 soluble in water for experiments 5 (280 K and 26 bar), 7 (293 K and 36 bar) and 8 (298 K and 36 bar) was lower than the equilibrium mole fraction of CO_2 in water presented by Diamond et al. (2003). However, a small amount of CO_2 dissolved in water was observed which was higher than the equilibrium mole fraction of CO_2 for experiment 6 (288 K and 36 bar). This indicated that at 288 K (IGCC condition), CO_2 hydrate formation was possible providing a driving force high enough to shift the system to a hydrate forming region. The application of promoters will be a good option to make it viable.

In summary, in the hydrate forming region, the equilibrium mole fraction of CO_2 in water was reduced as the temperature decreased (Servio et al., 2001). Thus, the highest solubility of CO_2 observed in water at the lowest temperature in this study was due to the existence of CO2 hydrate. In contrast, the solubility of CO_2 in water reduced as the temperature

increased in the non-hydrate forming region. This trend was comparable to the equilibrium mole fraction of CO_2 in water as shown in the literature (Diamond et al., 2003) which explains the non-existence of hydrate at these conditions.

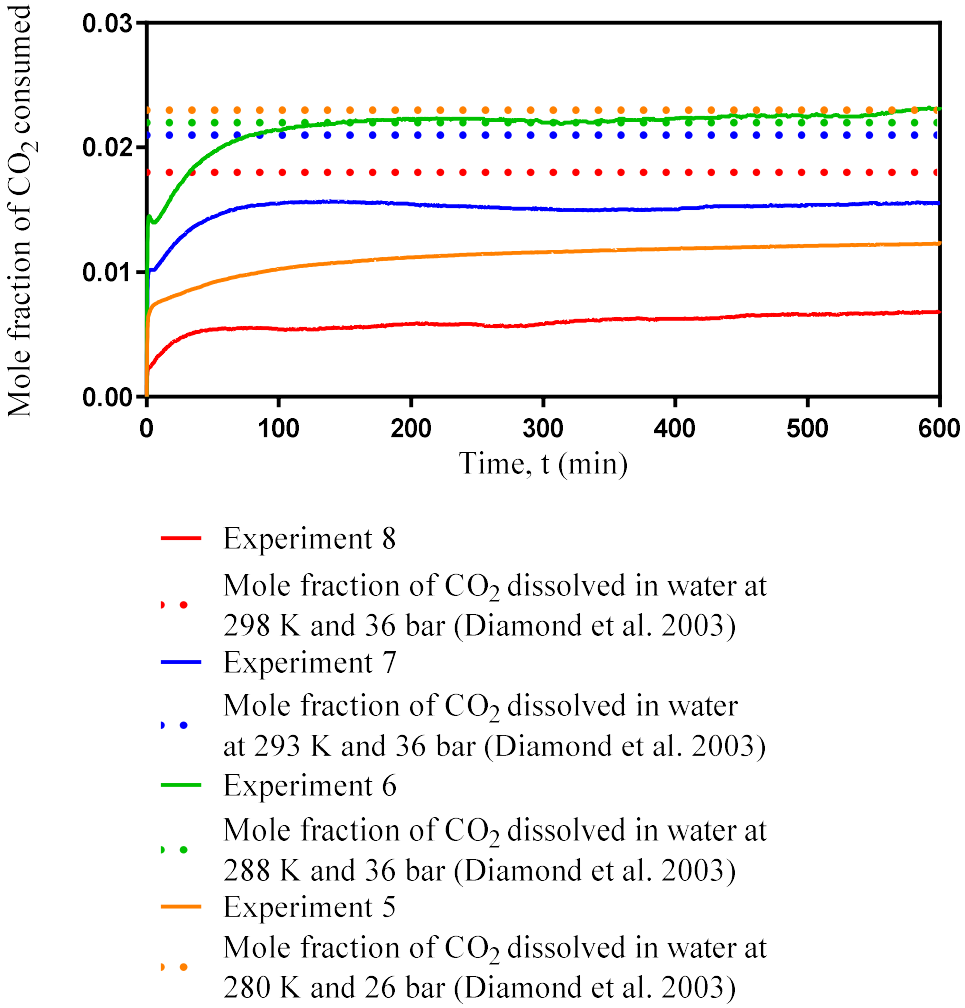


Figure 3- 9: Mole fraction of CO_2 consumed at the non-hydrate forming conditions (experiments 5 – 8) in 600 minutes (all experiments were referred to Table 3- 4)

3.3.2.2. Water conversion to hydrate and gas uptake

The study on CO_2 uptake was performed for experiments 1 - 4 where CO_2 hydrate was previously found to exist at these experimental operating conditions. Due to the high reproducibility of the sample prepared by method 4 (the highest rates of stirring of silica), each experiment was repeated once. The average weight of wet silica gel used was 0.5 g

which led to a total of 0.004 moles of water. All experiments were analysed for a 600-minute period as this was the average time for the hydrate formation to be completed. The conversion of water to hydrate and gas uptake for experiments 1 – 4 with their respective error bars are presented in Figure 3-10.

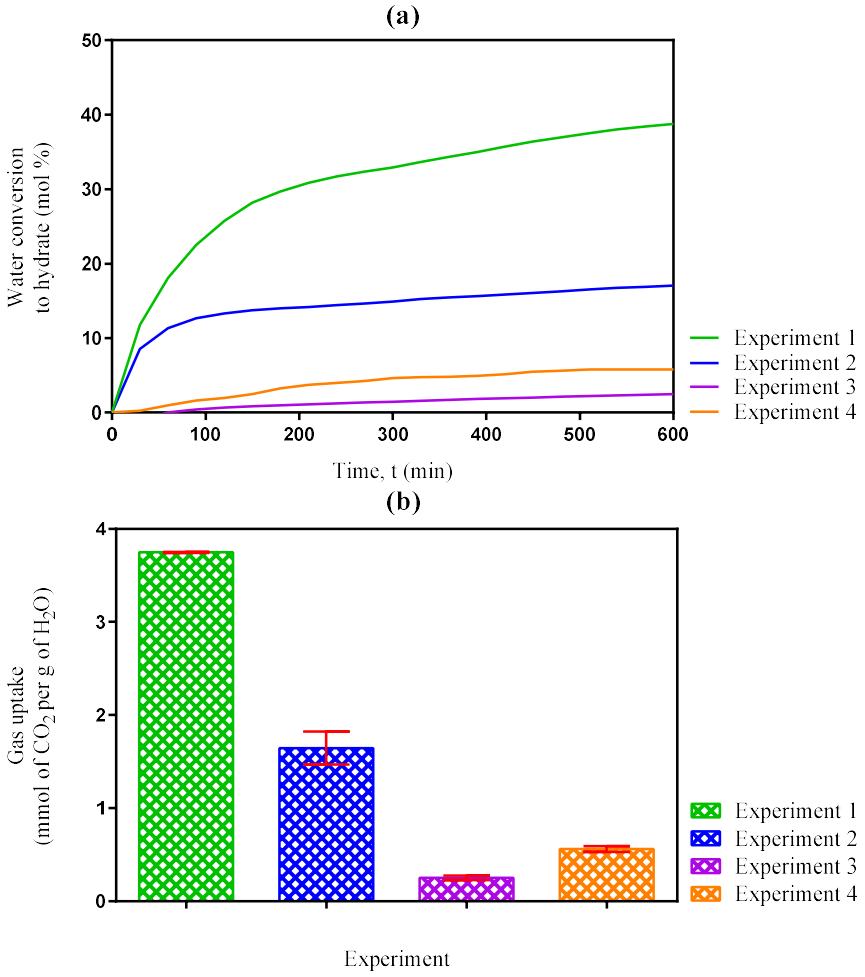


Figure 3- 10: Comparison of (a) water conversion to hydrate and (b) CO_2 uptake at the hydrate forming conditions in 600 minutes (all experiments were referred to Table 3- 4)

The highest driving force experiment (experiment 1 with the driving force of 19 bar) converted the highest water to hydrate with 40 mol% in 600 minutes which was 50% higher than experiment 2. This was followed by experiment 2, almost 16 mol% higher than experiment 3. These three experiments were executed at 275 K with experiment 3 having

the lowest driving force (5 bar). Furthermore, experiment 4 which was performed at higher temperature (280 K) but with ΔP of 6 bar exhibited 50% greater result as compared to experiment 3. This indicated that the increased driving force enhanced the water conversion to hydrate which was also the case for CO_2 uptake.

Table 3- 5: Summary of results for hydrate formation experiments performed at various hydrate forming conditions in 600 minutes (experiments 1 – 4) (all experiments were referred to Table 3- 4)

Exp.	Operating conditions	Driving force, ΔP (bar)	Exp. No.	CO_2 uptake (mmol of CO_2/g of H_2O)	Mean CO_2 uptake (mmol of CO_2/g of H_2O) (90% CI)	SD
1	275 K & 36 bar	19	1 2	3.74 3.75	3.75 ± 0.01	0.01
2	275 K & 30 bar	13	1 2	1.77 1.52	1.65 ± 0.21	0.18
3	275 K & 22 bar	5	1 2	0.23 0.27	0.26 ± 0.02	0.02
4	280 K & 36 bar	6	1 2	0.54 0.58	0.56 ± 0.03	0.03

Table 3- 5 shows that experiment 1 had the highest CO_2 uptake with a value of 3.75 ± 0.01mmol of CO_2 per g of H_2O followed by experiment 2 (1.65 ± 0.18mmol of CO_2 per g of H_2O), experiment 4 (0.56 ± 0.03mmol of CO_2 per g of H_2O) and finally experiment 3 (0.26 ± 0.02mmol of CO_2 per g of H_2O). All experiments had relatively low CI which showed good reproducibility of the experiments at these various operating conditions.

3.3.2.3. Rate of hydrate formation

The average rate of hydrate formation was measured every 30 minutes. Experiment 1 demonstrated the fastest kinetics in which the initial rate of hydrate formation was almost 0.06 mmol of CO_2/g of H_2O/min, followed by experiments 2, 1 and 3. The slowest initial rate shown by experiment 3 was more than 90% slower than experiment 1. The kinetics for experiments 2 - 4 were almost the same after 150 minutes. The initial rate of hydrate

formation for the experiment (experiment 1) with the highest driving force was the fastest compared to other experiments. Figure 3- 11 summarises the results.

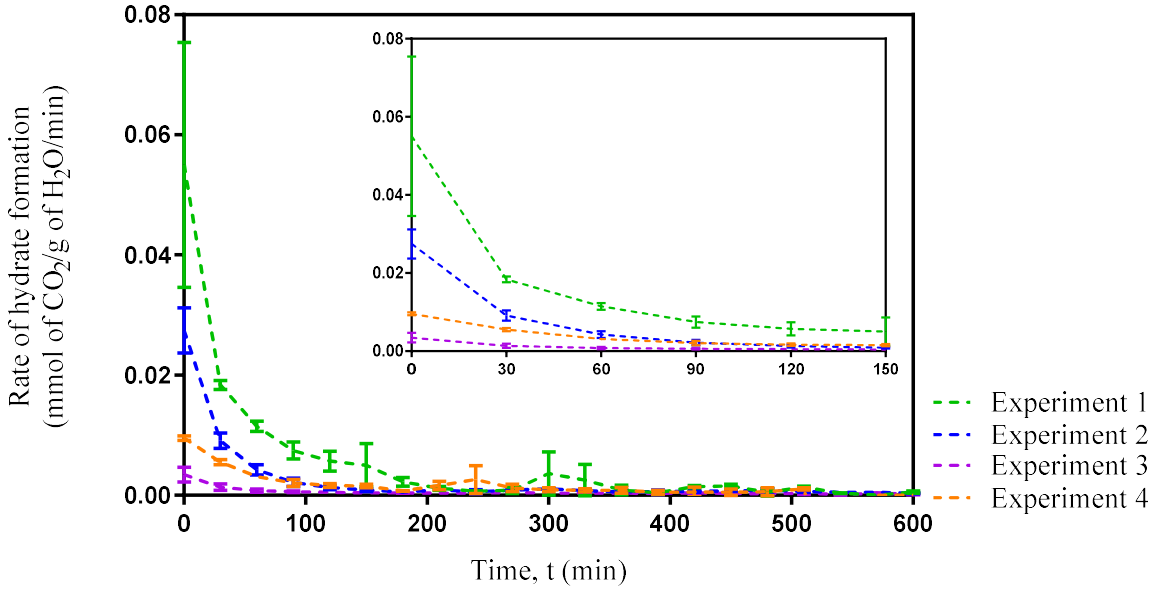


Figure 3- 11: Rate of hydrate formation for 600 minutes and inset for the first 150 minutes (experiments 1 - 4) (all experiments were referred to Table 3- 4)

3.4.Effect of single promoter on gas uptake and hydrate formation kinetics

Three types of promoters were employed in this work with the main purpose to investigate the ability of each promoter contacted with silica gel to enhance hydrate formation at the optimum concentration obtained by Yang et al. (2013) and Li et al. (2011). Table 3- 6 summarises the concentration of promoters and the amount of equilibrium moisture content that was employed. The concentration used for each promoter was 3 mol% for THF, 0.01 mol% for SDS and 0.29 mol% for TBAB. The amount of equilibrium moisture content measured for each prepared sample was 13.87 $\pm$ 0.46 wt% for THF, 13.09 $\pm$ 0.28 wt% for SDS and 8.48 $\pm$ 0.02 mol% for TBAB. In this section, the application of a single promoter contacted with silica gel for hydrate formation in the HPVA is presented. The comparison on water conversion to hydrate, CO_2 uptake and rate of hydrate formation with the baseline

experiment was performed. Consequently, more works on combining promoters at various concentrations and operating conditions are presented in chapter 4 and inevitably the optimum concentration for each combined-promoter is also highlighted.

Table 3- 6: Type of promoters employed in this work based on the optimum concentration obtained by previous researchers

No.	Type of promoter	Promoter	Remark	Concentration of promoter (mol%)	Equil. moisture content (wt%)
1	Oxygenated solvent	THF	Yang et al. (2013)	3.00	13.87 ± 0.46
2	Surfactant	SDS	Yang et al. (2013)	0.01	13.09 ± 0.28
3	Semi-clathrate	TBAB	Li et al. (2011)	0.29	8.48± 0.02

3.4.1. CO_2 solubility in water in the presence of promoter

Two operating temperatures were investigated at the same operating pressure (36 bar) in which the first experiment was conducted at 275 K and the second one was performed at 288 K. The weight of silica gel contact with promoter used inside the HPVA was approximately 0.5 g for each experiment. The experiments were conducted in 600 min and repeated once. The analysis on CO_2 solubility in water in the presence of promoter by using the highest rates of stirring (method 4 sample preparation) at 275 K and 36 bar is shown in Figure 3- 12. The solubility of CO_2 in water increased as compared to baseline when THF or SDS was applied to the system. SDS had the highest solubility in water in which the value observed was more than 0.08 mol fraction of CO_2 with almost 15% increment. This was followed by THF with almost 8% rise. However, TBAB showed an inhibition effect where the mole fraction of CO_2 in water decreased by almost half. Further investigation at 288 K and 36 bar (Figure 3- 13) revealed that THF gave the greatest effect on driving force with the highest mole fraction of CO_2 (0.035 mol fraction of CO_2). SDS also showed an increment by almost 0.01 mole fraction of CO_2 as compared to baseline experiment. The

investigation on TBAB was not performed at this operating condition since it only showed an inhibition effect at the lower temperature.

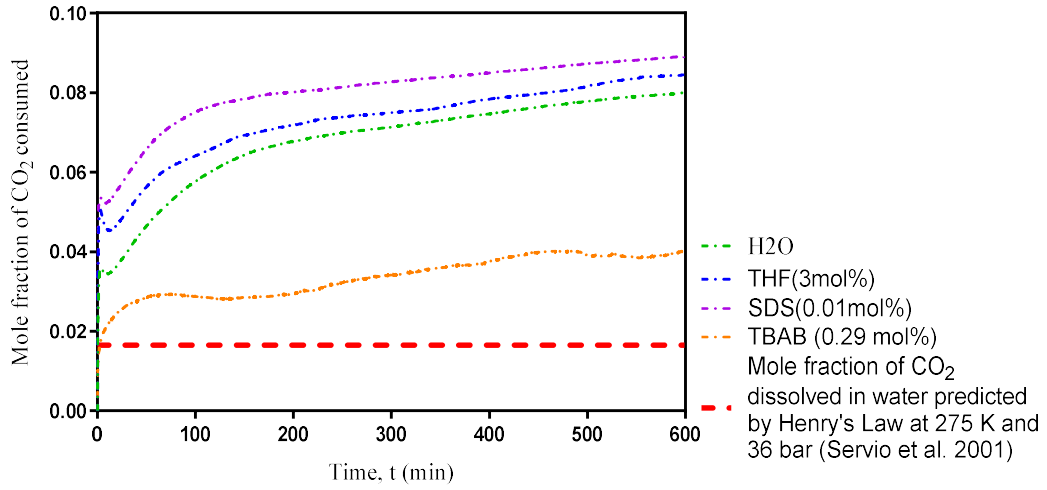


Figure 3- 12: CO_2 solubility in water in the presence of promoter at operating conditions of 275 K and 36 bar in 600 minutes

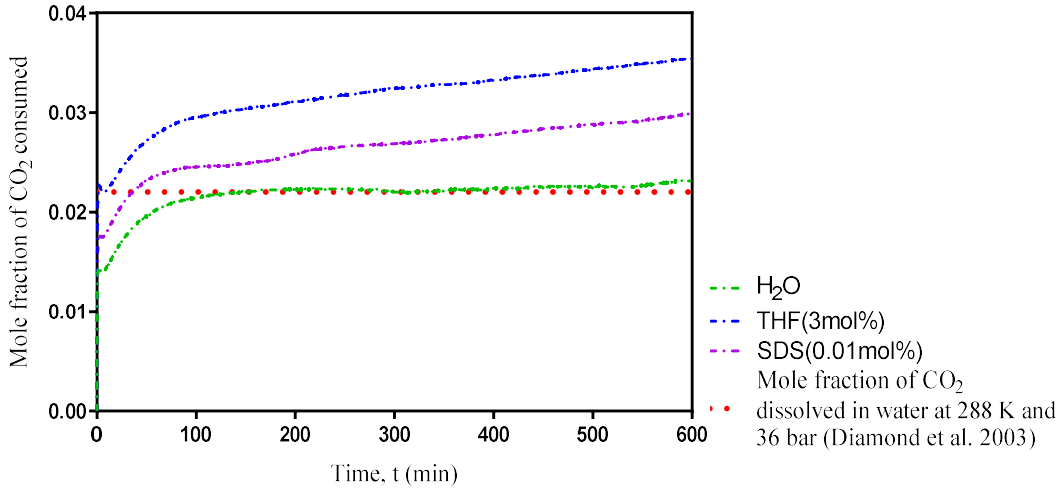


Figure 3- 13: CO_2 solubility in water in the presence of promoter at operating conditions of 288 K and 36 bar in 600 minutes

3.4.2. Water conversion to hydrate and CO_2 uptake

Figure 3-14 (a) and (b) shows water conversion to hydrate at 36 bar and the operating temperatures of 275 K and 288 K respectively. The highest conversion of water to hydrate was observed for the experiment that employed SDS at 275 K which was almost 50 mol%

conversion followed by THF with the conversion of almost 45 mol%. However, TBAB inhibited the formation of hydrate by almost half as compared to baseline experiment.

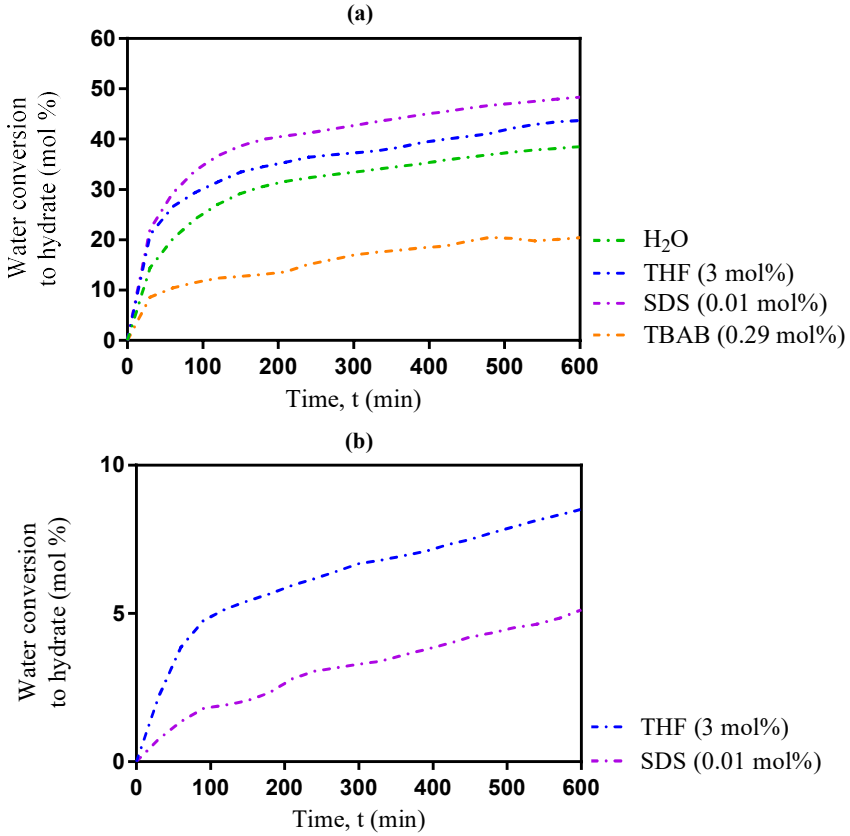


Figure 3- 14: Comparison of water conversion to hydrate by employing promoters in 600 minutes at 36 bar; (a) 275 K and (b) 288 K

An insignificance amount of hydrate was formed at 288 K for the baseline experiment and no experiment was conducted for TBAB due to the inhibition effect at 275 K. However, THF demonstrated the highest water conversion to hydrate at this operating temperature with almost 10 mol% conversion followed by SDS with 5 mol% conversion. Thus, THF was the best promoter at higher hydrate formation temperature as compared to SDS.

Figure 3-15 illustrates the CO_2 uptake of hydrate formation at 36 bar and operating temperatures of 275 K and 288 K with Table 3- 7 summarising all results observed. The CO_2 uptake was the lowest for TBAB which was 50% lower than baseline experiment. The greatest result at 275 K was observed for the experiment that used SDS with the value of

4.68 ± 0.06 mmol of CO_2 per g of H_2O and then followed by THF with the difference of 0.05 mmol of CO_2 per g of H_2O. In contrast, CO_2 uptake for THF was higher than SDS at 288 K by 0.57 mmol of CO_2 per g of H_2O.

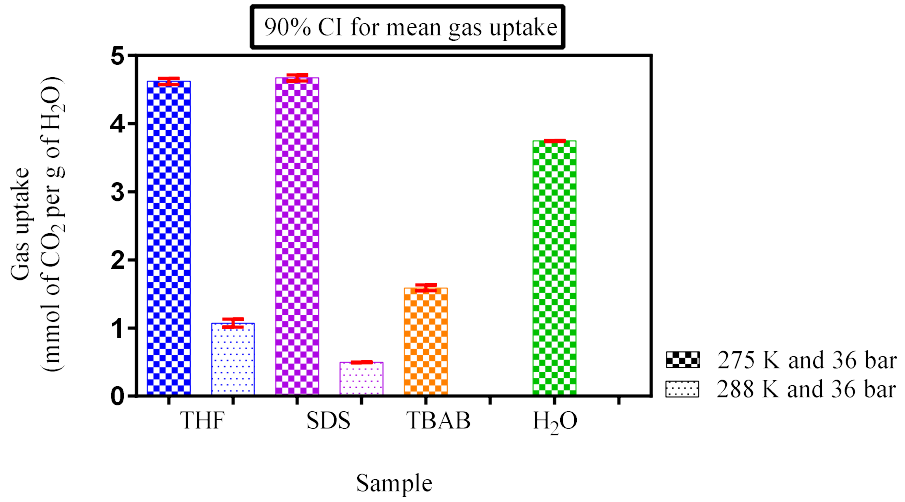


Figure 3- 15: Comparison of CO_2 uptake by employing promoters in 600 minutes at 36 bar and various operating temperatures (275 K & 288 K)

Table 3- 7: Summary of results for hydrate formation experiments performed by employing promoter at 36 bar and various operating temperatures (275 K and 288 K) in 600 minutes

Operating conditions	Promoter	Exp. number	CO_2 uptake (mmol of CO_2/g of H_2O)	Mean CO_2 uptake (mmol of CO_2/g of H_2O) (90% CI)	SD
275 K & 36 bar	H_2O	1	3.74	3.75 ± 0.01	0.01
		2	3.75		
	THF	1	4.66	4.63 ± 0.06	0.05
		2	4.59		
	SDS	1	4.64	4.68 ± 0.06	0.05
		2	4.71		
	TBAB	1	2.15	1.98 ± 0.29	0.25
		2	1.80		
288 K & 36 bar	THF	1	1.03	1.07 ± 0.07	0.06
		2	1.11		
	SDS	1	0.49	0.50 ± 0.01	0.01
		2	0.50		

3.4.3. Rate of hydrate formation

The average rate of hydrate formation was measured every 30 minutes. The fastest initial rate of CO_2 hydrate formation was demonstrated by the experiment that employed SDS at 275 K with a value of 0.07 mmol of CO_2/g of H_2O/min. The slowest rate was observed for TBAB in which it inhibited the rate of hydrate formation by 40% as compared to the baseline experiment. The most significant observation in this study was shown by employing THF at 288 K in which the initial rate of hydrate formation was comparable to the TBAB experiment at 275 K. The application of SDS to the system at 288 K also enhanced hydrate formation but the initial rate of hydrate formation was around 70% slower than THF at this operating temperature. This shows that THF can shift the phase equilibrium of hydrate formation by providing better driving force to the system at high hydrate formation temperature. Figure 3- 16 summarises the results.

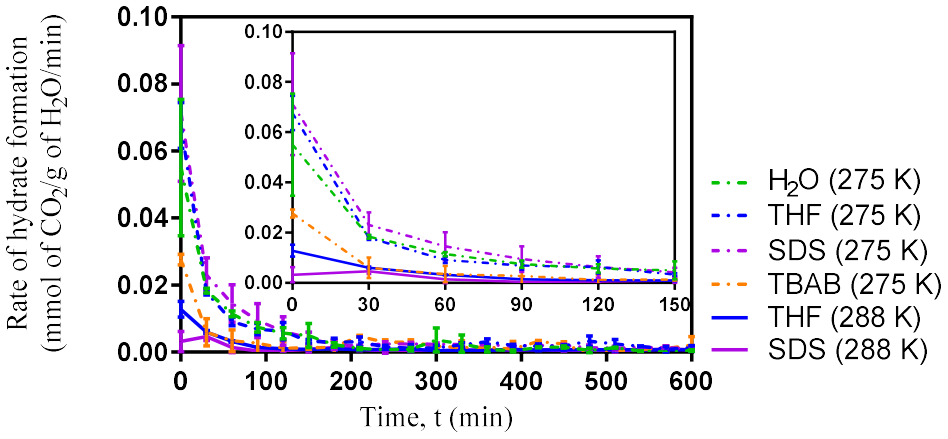


Figure 3- 16: Rate of hydrate formation at 36 bar for 600 minutes and inset for the first 150 minutes (various promoters)

3.5.Hydrate formation comparison between three silicas

Three types of silica namely standard silica gel, zeolite 13X and spherical MCF-17 as described in chapter 2 were used to study the effect of adsorbent characteristics on hydrate formation. Method 4 (the highest rates of stirring) was used to prepare these silicas contacted with water. The equilibrium moisture content of each silica was measured to be

14.8 wt%, 21.3 wt% and 50.8 wt% respectively. The hydrate formation experiments were performed in a pure CO_2 system at 275 K and 35 bar in 1200 minutes. The CO_2 dissolved in water and P-t curve for each silica was presented in Figure 3- 16. As seen in Figure 3-16Figure 3- 16: Comparison of (a) CO_2 dissolved in water and (b) P-t curve for various silicas at the operating conditions of 275 K and 35 bar in 1200 minutes(a), only standard silica gel had the mole fraction of CO_2 dissolved in water exceeded the Henry's Law value. Also, a two-stage pressure drop in the experimental P-t curve was only observed for standard silica (Figure 3- 16Figure 3- 16: Comparison of (a) CO_2 dissolved in water and (b) P-t curve for various silicas at the operating conditions of 275 K and 35 bar in 1200 minutes(b)). These indicate that zeolite 13X and MCF-17 were not suitable for CO_2 hydrate formation due to the smaller particle size (Park et al., 2013) and higher pore volume (Babu et al., 2013) as compared to standard silica gel respectively. Both reasons could lead to the decrease of the activity of water caused by the partial ordering and bonding of water molecules with hydrophilic surfaces of pores. Thus, standard silica gel was selected as the preferable adsorbent in this study.

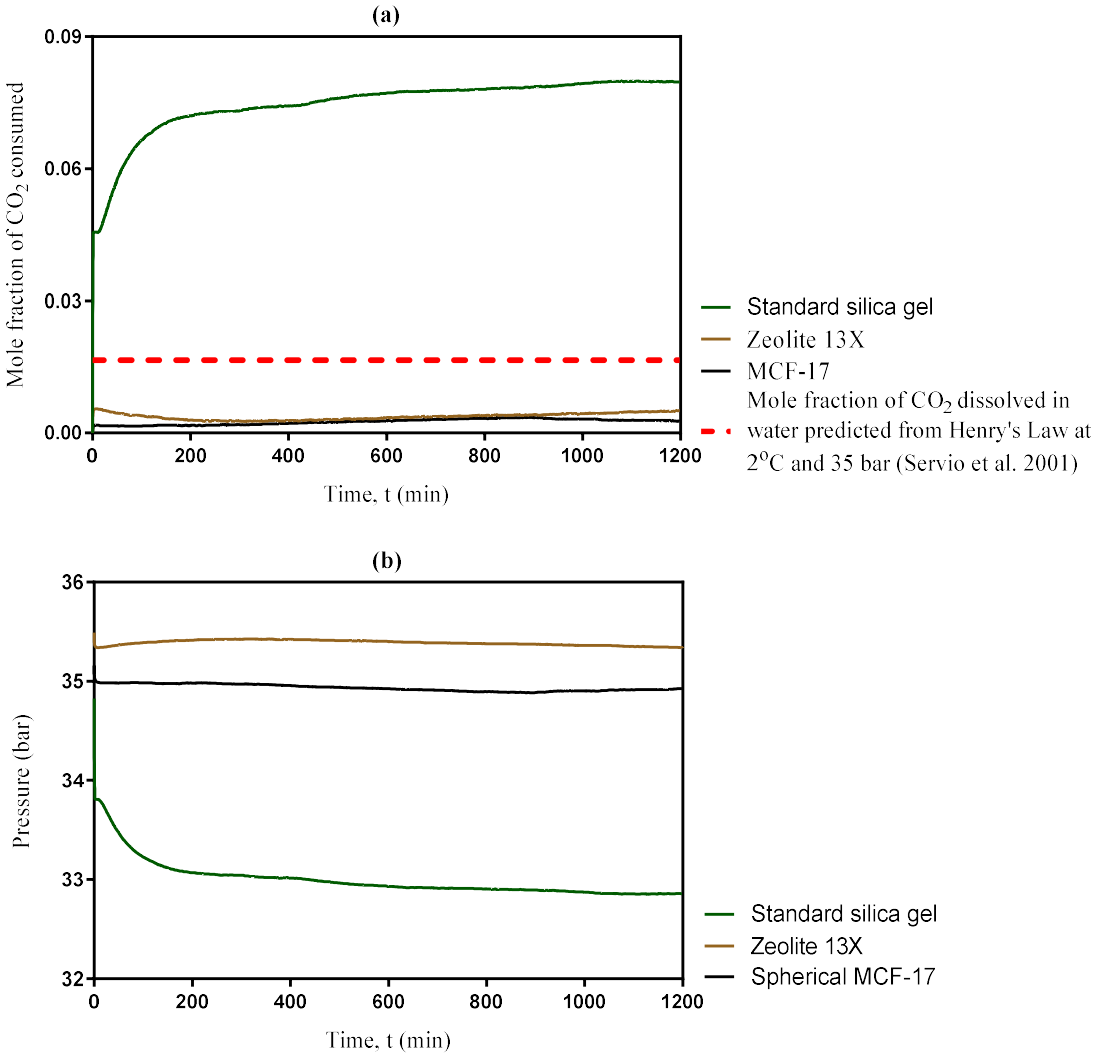


Figure 3- 16: Comparison of (a) CO_2 dissolved in water and (b) P-t curve for various silicas at the operating conditions of 275 K and 35 bar in 1200 minutes

3.6.Summary

i. The initial study on various sample preparation methods led to the selection of the highest rates of stirring (method 4) as the preferable method wherein the mean CO_2 conversion to hydrate was the highest (40.5 ± 2.28 mol%) and the standard deviation calculated was the lowest as compared to other methods (1,2 and 3; brief explanation on these methods was described in Table 3- 2).

ii. Some control experiments that were investigated in the HPVA at various operating conditions justified that hydrate formation only occurred at hydrate forming conditions with the lowest CO_2 uptake of 0.26 ± 0.02 mmol of CO_2 per g of H_2O at 22 bar and 275 K and the highest CO_2 uptake of 3.75 ± 0.01 mmol of CO_2 per g of H_2O at 36 bar and 275 K.

iii. The execution of promoters such as THF (3 mol%) and SDS (0.01 mol%) enhanced hydrate formation wherein the CO_2 hydrate was obtained at 1.07 ± 0.07 and 0.50 ± 0.01 mmol of CO_2 per g of H_2O respectively in non-hydrate forming conditions (288 K and 36 bar). However, TBAB (0.29 mol%) showed an inhibition effect with the CO_2 uptake of almost 2 mmol of CO_2 per g of H_2O lower than the baseline experiment (H_2O only) even though in hydrate forming conditions (275 K and 36 bar).

iv. The study on various silicas led to the selection of standard silica gel (average particle size of 200-500 µm, mean pore size of 5.14 nm, a pore volume of 0.64 cm^3/g and a surface area of 499 m^2/g) as the preferable adsorbent because zeolite 13X and spherical MCF-17 had the mole fraction of CO_2 dissolved in water below the Henry's Law value at 275 K and 36 bar which showed no hydrate formation for both adsorbents.

CHAPTER 4: THE EFFECT OF COMBINING PROMOTERS

4.1.Introduction

The focus in this specific chapter was investigating the optimum concentration of promoters for each combined-promoter in batch FBR with the presence of mesoporous silica. Also, the outcome of combining promoters in mitigating the inhibition effect shown by TBAB on hydrate formation was studied. Then, the optimum combined-promoter achieved was used to investigate the suitability of microporous silica on hydrate formation. Also, the effect of bed height on hydrate formation was studied and reported.

4.2.Various combinations of promoters

Six types of combinations previously mentioned in chapter 1 involved the combination of different categories of promoters such as oxygenated solvent, surfactant, semi-clathrate and hydrophobic former. However, in this particular work, hydrophobic former (CP) was not investigated as several works have been performed by previous researchers by combining CP with THF (oxygenated solvent; Herslund et al., 2013), SDS (surfactant; Ho et al., 2013) and TBAB (semi-clathrate; Li et al., 2011) and due to the lack of focus on pairing between three other promoters. Even though several works have highlighted the synergic effect on the combination of THF and SDS (Silva et al., 2013 and Yang et al., 2013), more investigation on various concentrations were studied in this work to obtain the optimum combined-concentration. Therefore, Table 4- 1 shows the pairing details between THF, SDS and TBAB which were investigated in this work where type 3 (T3) has never been investigated before.

Table 4- 1: Combinations of promoters investigated in this particular study

Type of promoter	Oxygenated solvent (THF)	Surfactant (SDS)	Semi-clathrate (TBAB)
Oxygenated solvent (THF)		Type 1 (T1) THF-SDS	Type 2 (T2) TBAB-THF
Surfactant (SDS)			Type 3 (T3) SDS-TBAB
Semi-clathrate (TBAB)			

4.2.1. Hydrate formation

Initially, the equilibrium moisture content for each prepared sample was measured. Then, the hydrate formation experiments were performed at 275 K and 36 bar for 1200 min. For each experiment, approximately 0.5g of silica gel contacted with combined-promoter namely T1, T2 and T3 were employed inside the HPVA and the experiment was repeated once. The average water conversion to hydrate, CO_2 uptake and rate of hydrate formation were calculated.

4.2.1.1. Type 1 (T1)

Several T1 samples were prepared at different combined-concentrations of THF and SDS. In the previous chapter, 3 mol% of THF was used and 0.01 mol% of SDS. In this chapter, the concentrations of THF were varied from 1 mol% to 7 mol% while for SDS from 0.005 mol% to 0.1 mol% to investigate the optimum concentration for each promoter (Table 4- 2). This led to the production of seven samples namely T1-1 (3 mol% THF & 0.01 mol% SDS), T1-2 (3 mol% THF & 0.02 mol% SDS), T1-3 (3 mol% THF & 0.1 mol% SDS), T1-4 (1 mol% THF & 0.01 mol% SDS), T1-5 (5.6 mol% THF & 0.01 mol% SDS), T1-6 (3 mol% THF & 0.005 mol% SDS) and T1-7 (7 mol% THF & 0.01 mol% SDS).

4.2.1.1.1. Equilibrium moisture content at different combined-concentrations

Table 4- 2 and Figure 4- 1 summarise the equilibrium moisture content for various T1 samples. The equilibrium moisture content inside silica gel pores increased from 13.14 to 14.36 wt% as the concentration of THF was reduced from 7 to 1 mol%. Additionally, the second lowest equilibrium moisture content was obtained at the highest concentration of SDS (0.1 mol%) which showed that the highest concentration of promoters reduced the amount of water present inside silica gel pores. The highest equilibrium moisture content was achieved for T1-4 (14.36 ± 0.69 wt%), followed by T1-6 (13.90 ± 0.26 wt%), T1-1 (13.81 ± 0.14 wt%), T1-2 (13.71± 0.15 wt%), T1-5 (13.28 ± 0.18 wt%), T1-3 (13.17 ± 0.06 wt%) and T1-7 (13.14 ± 0.16 wt%). The CI observed was relatively low for all T1 samples which indicated that this combined-promoter was well distributed inside silica gel pores.

Table 4- 2: The summary of results for equilibrium moisture content at various concentrations of T1 combined-promoter (brief description on each code – page 108)

Sample	Promoter concentration (mol%)		Exp. No.	Equilibrium moisture content (wt%)	Mean equilibrium moisture content (wt%) (90% CI)	SD
	THF	SDS				
T1-1	3.000	0.010	1 2	13.72 13.89	13.81 ± 0.14	0.12
T1-2	3.000	0.020	1 2	13.63 13.82	13.71± 0.15	0.13
T1-3	3.000	0.100	1 2	13.20 13.14	13.17 ± 0.06	0.05
T1-4	1.000	0.010	1 2	13.94 14.78	14.36 ± 0.69	0.59
T1-5	5.600	0.010	1 2	13.40 13.18	13.28 ± 0.18	0.15
T1-6	3.000	0.005	1 2	14.05 13.74	13.90 ± 0.26	0.22
T1-7	7.000	0.010	1 2	13.04 13.24	13.14 ± 0.16	0.14

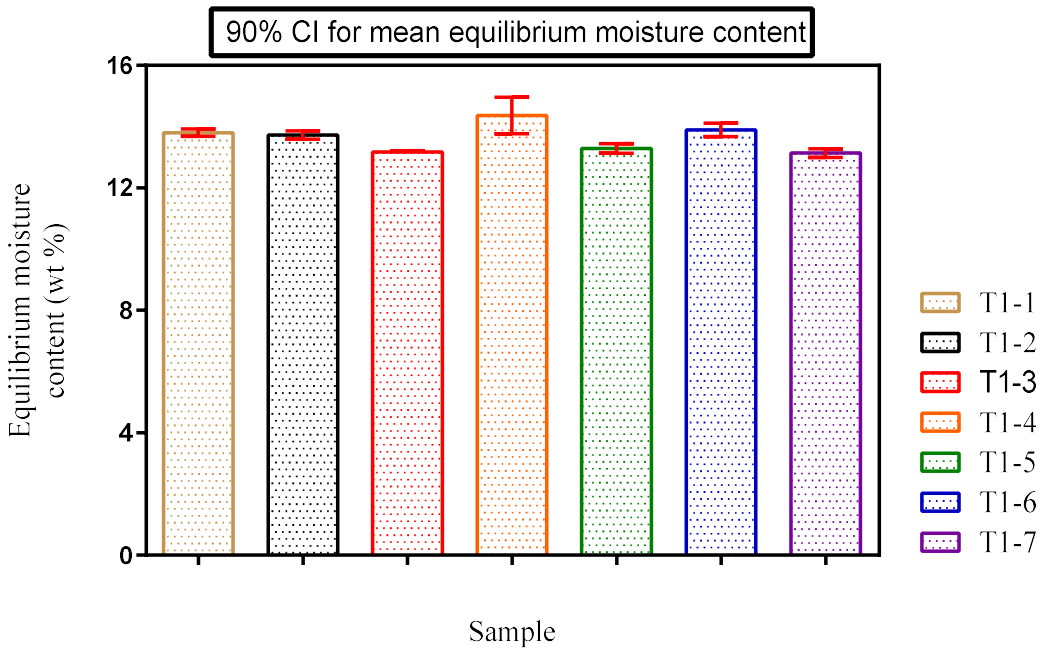


Figure 4- 1: Summary of results for equilibrium moisture content at various T1 samples (brief description on each code – page 108)

4.2.1.1.2. Water conversion to hydrate and CO_2 uptake

The average number of moles of water calculated for each sample was approximately 4 mmol. Then, the CO_2 consumed was used together with the number of moles of water to calculate the water conversion to hydrate and also CO_2 uptake. The results obtained in this section were compared with the baseline experiment and silica contacted with single promoters (3 mol% THF and 0.01 mol% SDS) which were reported in the previous chapter. The CO_2 solubility in water in the presence of hydrate is shown in Figure A- 4 (Appendix 5) wherein all samples demonstrated the formation of hydrate.

Figure 4- 2(a) and (b) illustrates the comparison of water conversion to hydrate and maximum CO_2 uptake between each sample respectively. The highest conversion of water to hydrate was observed for T1-5 which was approximately 65 mol%. It was 25 mol% higher than the baseline experiment and almost 15 mol% higher than silica gel contacted with either THF or SDS. Then, T1-1, T1-7 and T1-2 followed which were approximately 15%

lower than T1-5. T1-4 was slightly higher than the baseline experiment but significantly lower than silica gel contacted with either THF or SDS. However, the lowest water conversion to hydrate obtained by T1-6 and T1-3 which were lower than baseline experiments demonstrated an inhibition effect on hydrate formation at both combined-concentrations.

Table 4- 3 summarises CO_2 uptake obtained in each sample. The highest CO_2 uptake was observed for T1-5 with the value of 5.95 $\pm$ 0.21 mmol of CO_2 per g of H_2O followed by T1-1 (5.68 $\pm$ 0.09 mmol of CO_2 per g of H_2O), T1-7 (5.43 $\pm$ 0.07 mmol of CO_2 per g of H_2O), T1-2 (5.35 $\pm$ 0.08 mmol of CO_2 per g of H_2O), T1-4 (4.84 $\pm$ 0.07 mmol of CO_2 per g of H_2O), T1-6 (4.23 $\pm$ 0.49 mmol of CO_2 per g of H_2O) and finally T1-3 (3.75 $\pm$ 0.31 mmol of CO_2 per g of H_2O). The maximum CO_2 uptake was proportional to the conversion of water to hydrate. Also, the amount of CO_2 uptake decreased as the concentration of SDS increased from 0.01 to 0.1 mol%. However, T1-6 with the lowest concentration of SDS (0.005 mol%) and T1-3 with the highest concentration of SDS (0.100 mol%) attained the two lowest gas uptakes indicating that 0.01 mol% was the optimum concentration for SDS.

At this SDS optimum concentration, the gas uptake decreased as the concentration of THF decreased from 5.6 to 1 mol% of THF. However, the gas uptake of T1-7 which was at 7 mol% concentration of THF was lower than T1-5 with THF concentration of 5.6 mol%. Based on these results, it was concluded that the optimum concentration of THF was achieved at 5.6 mol% and 0.01 mol% SDS as indicated by sample T1-5.

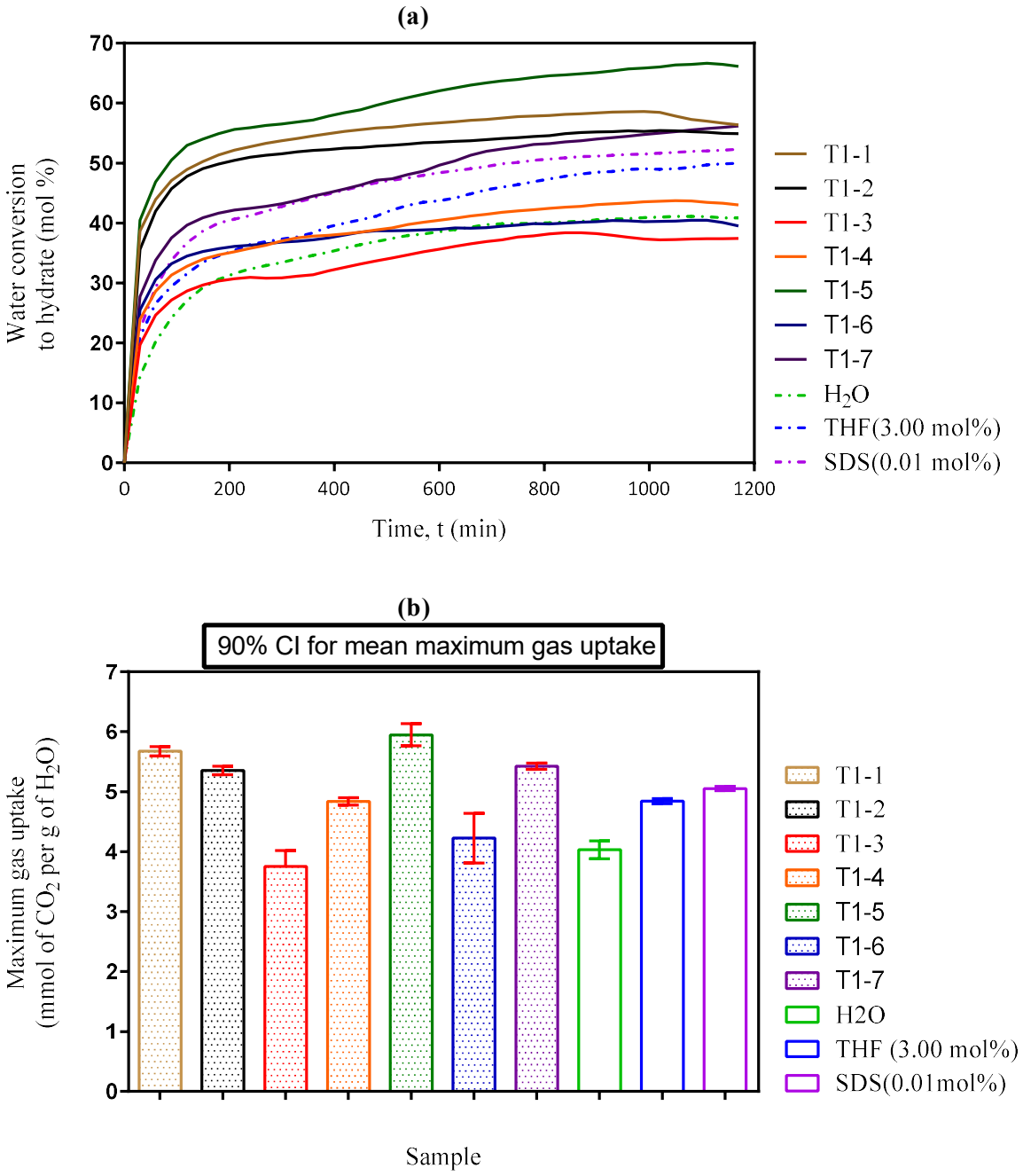


Figure 4- 2: Comparison of (a) water conversion to hydrate and (b) gas uptake for various T1 samples and baseline experiments at the operating conditions of 275 K and 36 bar in 1200 minutes (brief description on each code – page 108)

Table 4- 3: Maximum CO_2 uptake in 1200 minutes at 275 K and 36 bar for various concentrations of T1 combined-promoter and baseline experiments (brief description on each code – page 108)

Sample	Exp. No.	CO_2 uptake (mmol of CO_2/g of H_2O)	Mean CO_2 uptake (mmol of CO_2/g of H_2O) (90% CI)	SD
T1-1	1	5.73	5.68 ± 0.09	0.08
	2	5.62		
T1-2	1	5.30	5.35 ± 0.08	0.07
	2	5.40		
T1-3	1	3.94	3.75 ± 0.31	0.27
	2	3.56		
T1-4	1	4.79	4.84 ± 0.07	0.06
	2	4.88		
T1-5	1	5.82	5.95 ± 0.21	0.18
	2	6.08		
T1-6	1	3.93	4.23 ± 0.49	0.42
	2	4.52		
T1-7	1	5.47	5.43 ± 0.07	0.06
	2	5.39		
H_2O	1	3.93	4.04 ± 0.17	0.15
	2	4.14		
THF*	1	4.81	4.84 ± 0.03	0.04
	2	4.87		
SDS**	1	5.03	5.06 ± 0.03	0.04
	2	5.08		

*THF at 3.00 mol%; **SDS at 0.01 mol%

4.2.1.1.3. Rate of hydrate formation

Generally, the rate of hydrate formation observed in Figure 4- 3 demonstrated that the use of promoters enhanced the formation of hydrate. Even though T1-3 showed an inhibition effect towards CO_2 consumption due to hydrate formation, the initial kinetics exhibited faster kinetics as compared to baseline. The kinetics of T1-1 were the fastest followed by T1-5 and T1-2 in which these three samples had almost the same kinetics and significantly greater than other samples by more than 30%. T1-4, T1-6 and T1-7 followed wherein their initial kinetics at 0.09 mmol of CO_2 per g of H_2O per min were approximately identical.

Finally, T1-3 (0.06 mmol of CO_2 per g of H_2O per min) exhibited the slowest kinetics among all T1 combined-promoters which were also slower than results from a single promoter. Based on these observations, it was concluded that THF at 3 mol% exhibited the fastest kinetics when it was combined with 0.01 mol% SDS, almost 50% greater than a single promoter alone at the same concentration.

In addition, the increased SDS concentration from 0.01 to 0.1 mol% which was combined with 3 mol% THF led to reduced kinetics. However, at the lowest concentration of SDS (0.005 mol%), the kinetics were slower than that observed at 0.01 mol% SDS. Thus, it was confirmed that SDS at 0.01 mol% gave the highest rate of hydrate formation and also CO_2 uptake. Meanwhile, THF at 3 mol% exhibited the fastest kinetics and the highest gas uptake was observed at 5.6 mol%. In conclusion, the rate of hydrate formation was not directly proportional to the maximum CO_2 uptake.

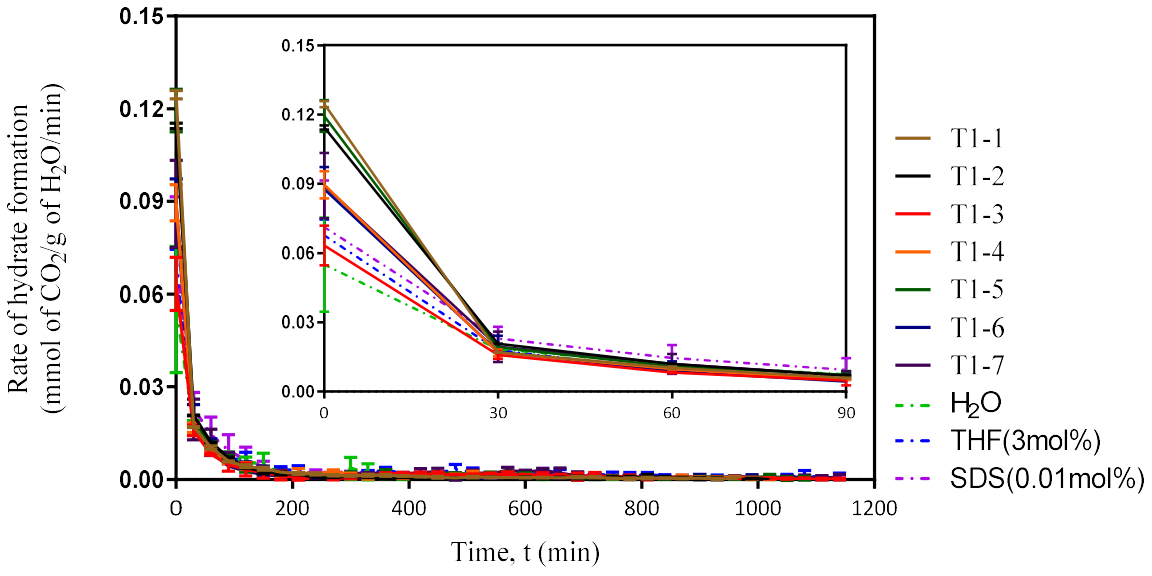


Figure 4- 3: Rate of hydrate formation at 275 K and 36 bar for 1200 minutes and inset for the first 150 minutes (brief description on each code – page xviii (abbreviations))

4.2.1.2. Types 2 (T2) and 3 (T3)

In this study, TBAB was combined with THF and SDS at their optimum concentration respectively which was discovered in the previous section. The first concentration of TBAB used was 0.29 mol% while THF and SDS were 3 mol% and 0.01 mol% respectively. Based on the CO_2 uptake and rate of hydrate formation observed for both samples, the concentration of TBAB was reduced to 0.1 mol% while maintaining the concentration of SDS to further investigate the effect of TBAB concentration on hydrate formation. No additional investigation on the combination of TBAB and THF was performed and the discussion is presented in the next section. The characteristics of these three samples namely, T2-1, T3-1 and T3-2 are described in Table 4- 4.

4.2.1.2.1. Equilibrium moisture content at different combined-concentrations

Table 4- 4 summarises the equilibrium moisture content calculated for all samples at specific concentrations of each combined-promoter and Figure 4- 4 illustrates the results observed with their respective error bars. The presence of THF in T2-1 (3 mol% THF and 0.29 mol% TBAB) sample increased the amount of equilibrium moisture content to 10.25 $\pm$ 0.42 wt% from 8.48 wt% for a single TBAB promoter (0.29 mol%) as previously discovered in chapter 3. However, the addition of SDS significantly reduced the amount of water inside silica gel pores that was available for hydrate formation. The lowest concentration of TBAB in the T3-2 (0.01 mol% SDS and 0.10 mol% TBAB) sample led to an improved moisture content by almost 0.1 wt% as compared to T3-1 (0.01 mol% SDS and 1.00 mol% TBAB). The presence of aqueous THF solution in TBAB could improve the equilibrium moisture content which was not the case for SDS. The CI observed for T2 and T3 samples was a little bit higher than T1 but the results were still considered reproducible.

Table 4- 4: Summary of results for equilibrium moisture content at various concentrations of T2 and T3 combined-promoters (brief description on each code was referred to page 116 (Table 4- 4))

Sample	Promoter concentration (mol%)			Exp. No.	Equilibrium moisture content (wt%)	Mean equilibrium moisture content (wt%) (90% CI)	SD
	TBAB	THF	SDS				
T2-1	0.29	3.00	-	1 2	10.60 10.09	10.25 ± 0.42	0.36
T3-1	0.29	-	0.01	1 2	8.12 8.65	8.38± 0.43	0.37
T3-2	0.10	-	0.01	1 2	8.33 8.58	8.46 ± 0.20	0.17

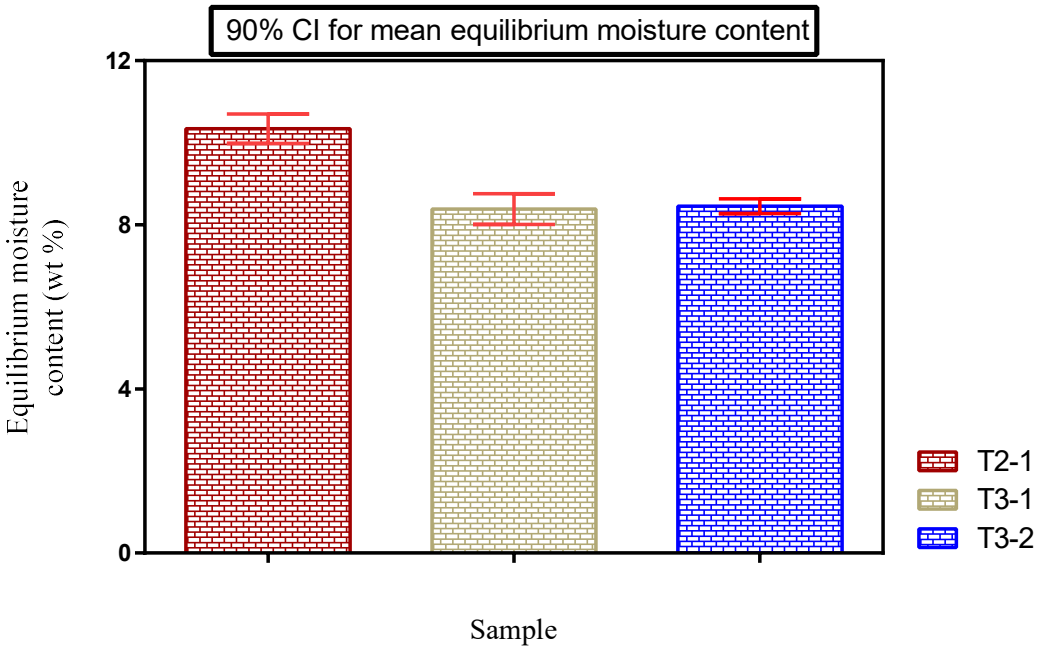


Figure 4- 4: Summary of results for equilibrium moisture content at various T2 and T3 samples (brief description on each code was referred to page 116 (Table 4- 4))

4.2.1.2.2. Water conversion to hydrate and CO_2 uptake

The number of moles of water calculated for T2-1 was around 3 mmol whereas for T3-1 and T3-2 were roughly 2 mmol. This number of moles of water for each sample was necessary to calculate water conversion to hydrate and CO_2 uptake respectively. The results obtained

in this section were compared with the baseline experiment and silica contacted with 0.29 mol% TBAB which were reported in previous chapter. The CO_2 dissolved in water in the presence of hydrate is shown in Figure A- **5** (Appendix 5) where the formation of hydrate was observed for each sample.

Figure 4- **5** (a) illustrates the water conversion to hydrate for each sample. The addition of THF at 3 mol% (T2-1) and SDS at 0.01 mol% (T3-1) did not omit the inhibition effect which was previously demonstrated by TBAB (0.29 mol%) contacted with silica gel alone. The water conversion to hydrate obtained by both samples was 75% and 25% lower as compared to the baseline experiment respectively. However, the water conversion achieved by T3-1 had improved the result achieved by 0.29 mol% TBAB. Hence, it was expected that 3 mol% THF could not enhance the rate of hydrate formation whereas 0.01 mol% SDS could. Therefore, T3-2 was prepared in which the concentration of TBAB was reduced to 0.1 mol% and SDS remained the same. As a result, the total water conversion to hydrate improved drastically which was 50% higher than the baseline experiment (40 mol%).

The same trend was observed for the maximum CO_2 uptake obtained by each sample as illustrated in Figure 4- 5 (b) and summarised in Table 4- 5. The highest CO_2 uptake was achieved by T3-2 with the value of 5.57 ± 0.34 mmol of CO_2 per g of H_2O. This was followed by T3-1 which was almost 50% lower than T3-2 and 50% higher than T2-1. As the concentration of TBAB increased, the water conversion to hydrate and maximum CO_2 uptake were reduced. Also, the inhibition effect for hydrate formation was observed. Thus, the optimum concentration attained by TBAB was 0.1 mol% at 0.01 mol% concentration of SDS.

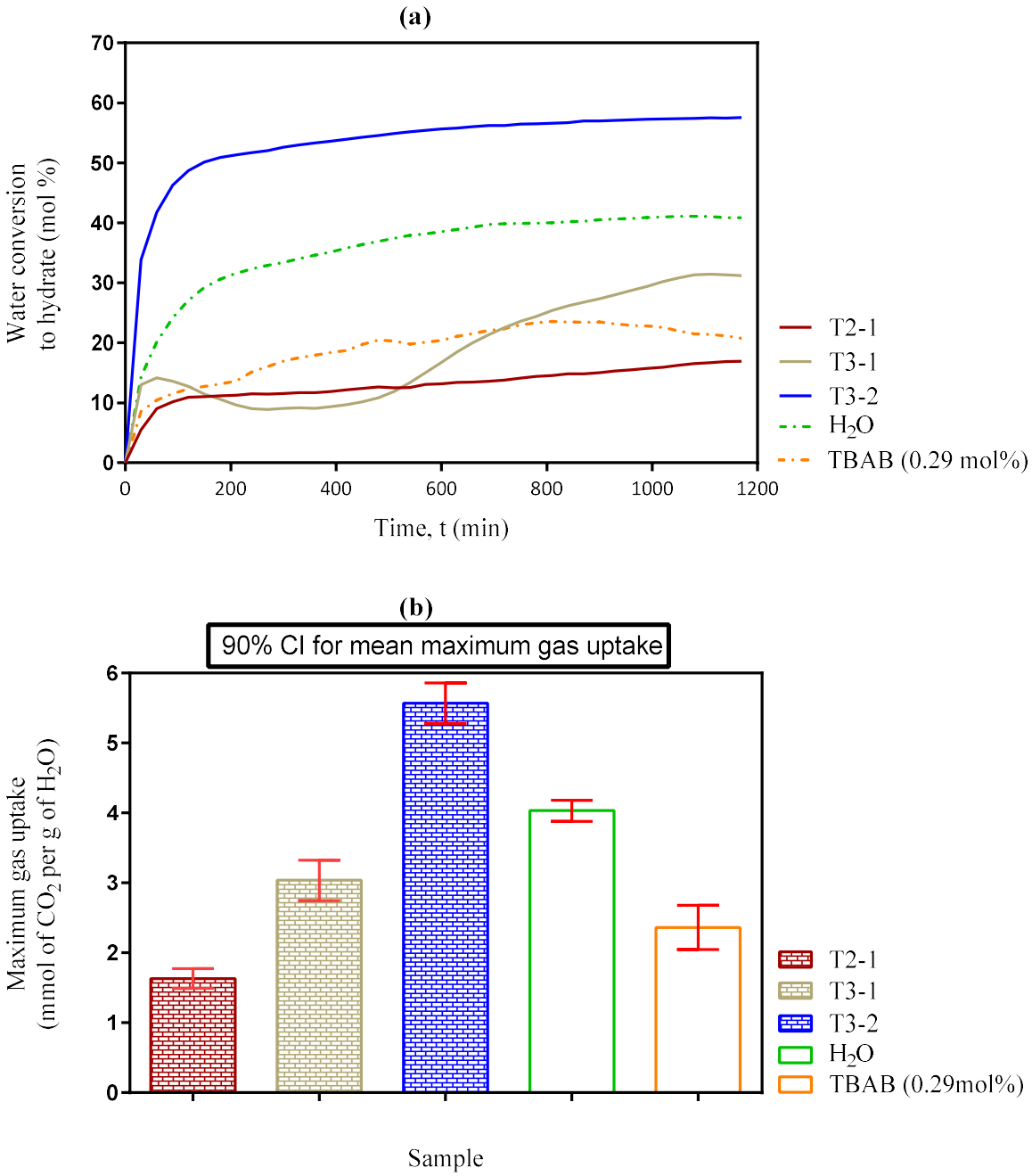


Figure 4- 5: Comparison of (a) water conversion to hydrate and (b) maximum CO_2 uptake for various T2 and T3 samples and baseline experiments at the operating conditions of 275 K and 36 bar in 1200 minutes (brief description on each code was referred to page 116 (Table 4- 4))

Table 4- 5: Maximum CO_2 uptake in 1200 minutes at 275 K and 36 bar for various concentrations of T2 and T3 combined-promoters and baseline experiments (brief description on each code was referred to page 116 (Table 4- 4))

Sample	Exp. No.	CO_2 uptake (mmol of CO_2/g of H_2O)	Mean CO_2 uptake (mmol of CO_2/g of H_2O) (90% CI)	SD
T2-1	1	1.53	1.63 ± 0.16	0.14
	2	1.73		
T3-1	1	2.83	3.03 ± 0.33	0.28
	2	3.23		
T3-2	1	5.36	5.57 ± 0.34	0.29
	2	5.77		
H_2O	1	3.93	4.04 ± 0.17	0.15
	2	4.14		
TBAB***	1	2.59	2.37 ± 0.37	0.32
	2	2.14		

***TBAB at 0.29 mol%

4.2.1.2.3. Rate of hydrate formation

Figure 4- 6 illustrates the rate of hydrate formation for T2 and T3 samples where the highest kinetics were shown by T3-2 (0.01 mol% SDS and 0.10 mol% TBAB). The initial kinetics of T3-1 (0.01 mol% SDS and 0.29 mol% TBAB) at almost 0.045 mmol of CO_2 per g of H_2O per min were more than 50% slower than T3-2. T2-1 (3 mol% THF and 0.29 mol% TBAB) demonstrated the slowest kinetics where no sign of improvement on rate of hydrate formation was seen. Based on this observation, the co-existence of 3 mol% THF and 0.29 mol% TBAB inside silica gel pores was not practical for hydrate formation and the low concentration of TBAB (0.1 mol%) was mandatory for hydrate formation to occur.

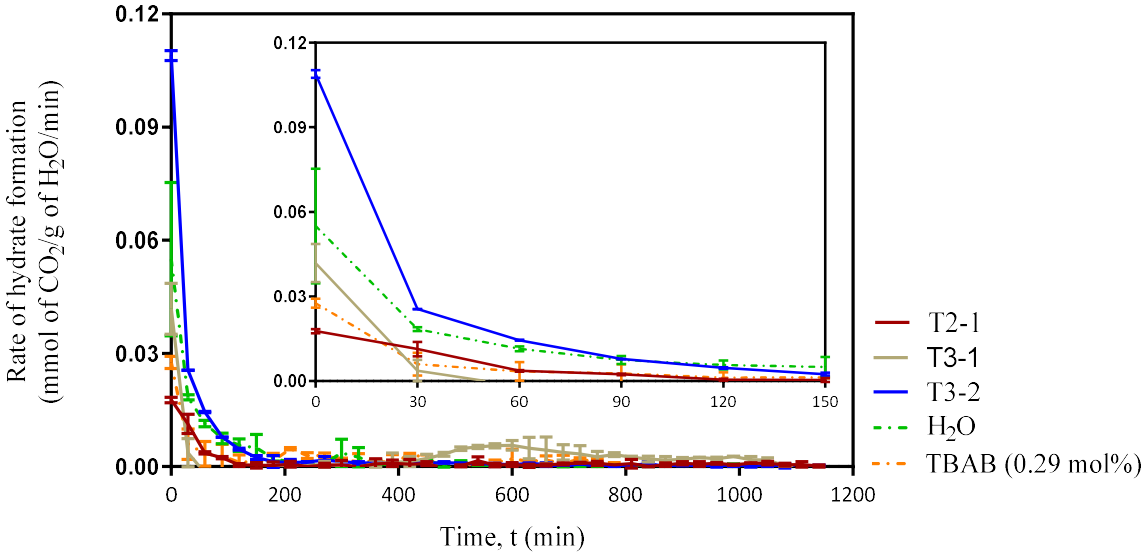


Figure 4- 6: Rate of hydrate formation at 275 K and 36 bar for 1200 minutes and inset for the first 150 minutes (various T2 and T3 concentrations and baseline experiments) (brief description on each code was referred to page 116 (Table 4- 4))

4.2.1.3. T1A (EGME as an alternative to THF)

The results observed for T1, T2 and T3 samples were compared and subsequently, T1-5 (5.60 mol% and 0.01 mol%) showed the best results among all samples. Further investigation was performed to explore an alternative to THF and consequently EGME was selected. EGME was purchased from Acros Organics with 99% purity. The concentration of EGME was varied from 0.01 to 1 mol% while the concentration of SDS was retained at 0.01 mol%. This led to the existence of three new combined-promoters, namely T1A-1 (0.01 mol% EGME & 0.01 mol% SDS), T1A-2 (0.1 mol% EGME & 0.01 mol% SDS) and T1A-3 (1 mol% EGME & 0.01 mol% SDS).

4.2.1.3.1. Equilibrium moisture content at different combined-concentrations

As shown in Table 4- 6, as the concentration of EGME increased from 0.01 to 1 mol%, the equilibrium moisture content proportionally decreased from 12.89 ± 0.48 to 12.06 ± 0.46 wt%. These results were compared with the baseline experiment and obviously the existence of promoters inside silica gel pores reduced the amount of water available for hydrate formation. The same trend was also observed for T1, T2 and T3 combined-promoters in which samples with a high concentration of promoters exhibited low equilibrium moisture content. However, based on previous investigations the amount of water available inside silica gel pores in the presence of promoters did not immediately affect the maximum CO_2 uptake and rate of hydrate formation. Thus, the investigations on various T1A samples were performed to study the optimum concentration of EGME and the results are presented in the next section. Figure 4- 7 summarises the results.

Table 4- 6: Summary of results for equilibrium moisture content at various concentrations of type T1A combined-promoters

Sample	Promoter concentration (mol%)		Exp. No.	Equilibrium moisture content (wt%)	Mean equilibrium moisture content (wt%) (90% CI)	SD
	EGME	SDS				
T1A-1	0.01	0.01	1 2	13.18 12.60	12.89 ± 0.48	0.41
T1A-2	0.10	0.01	1 2	12.81 12.38	12.59± 0.36	0.31
T1A-3	1.00	0.01	1 2	11.78 12.34	12.06 ± 0.46	0.39

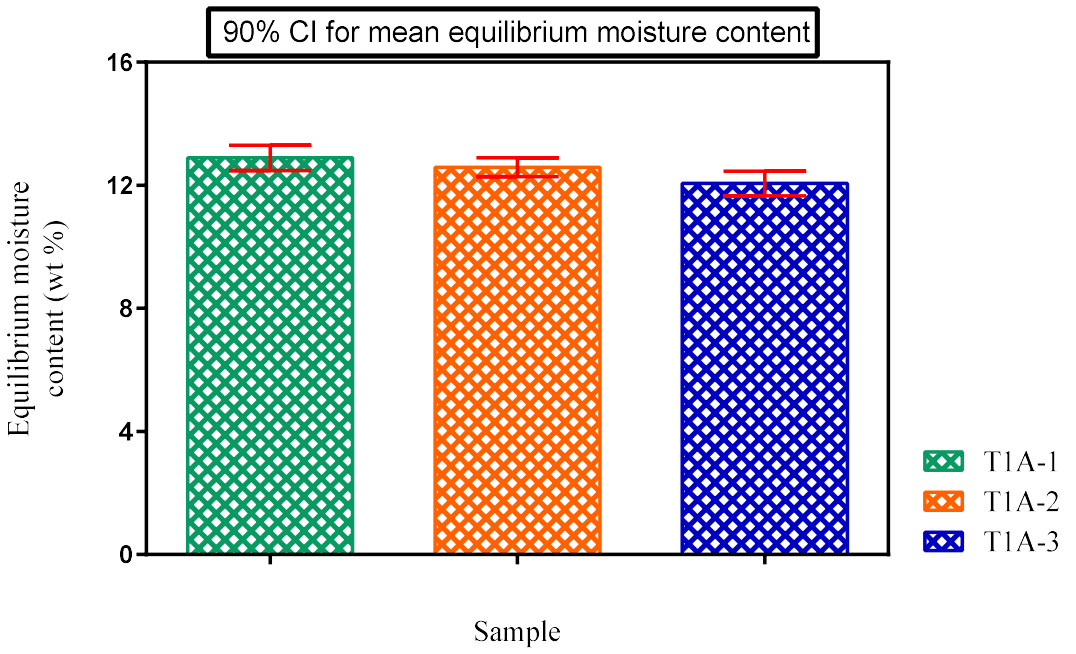


Figure 4- 7: Summary of results for equilibrium moisture content at various T1A samples (brief description of each T1A code was referred to page 121 (Table 4- 6))

4.2.1.3.2. Water conversion to hydrate and CO_2 uptake

The CO_2 solubility in water in the presence of hydrate is shown in Figure A- 6 (Appendix 5) in which the formation of hydrate was observed for all T1A samples. The number of moles of water calculated for all T1A samples was around 3 mmol and was used to calculate the water conversion to hydrate and CO_2 uptake respectively. The results obtained in this section were compared with the baseline experiment.

Figure 4- 8 (a) illustrates that the highest water conversion to hydrate was observed for TA1-2 with the value of more than 55 mol%, followed by T1A-1 (0.01 mol% SDS and 0.01 mol% EGME) which was 5 mol% lower than TA1-2 (0.01 mol% SDS and 0.10 mol% EGME). However, T1A-3 (0.01 mol% SDS and 1.00 mol% EGME) showed an inhibition effect compared to the baseline experiment with only 35 mol% conversion. The same trend was observed for the maximum CO_2 uptake as shown in Figure 4- 8 (b).

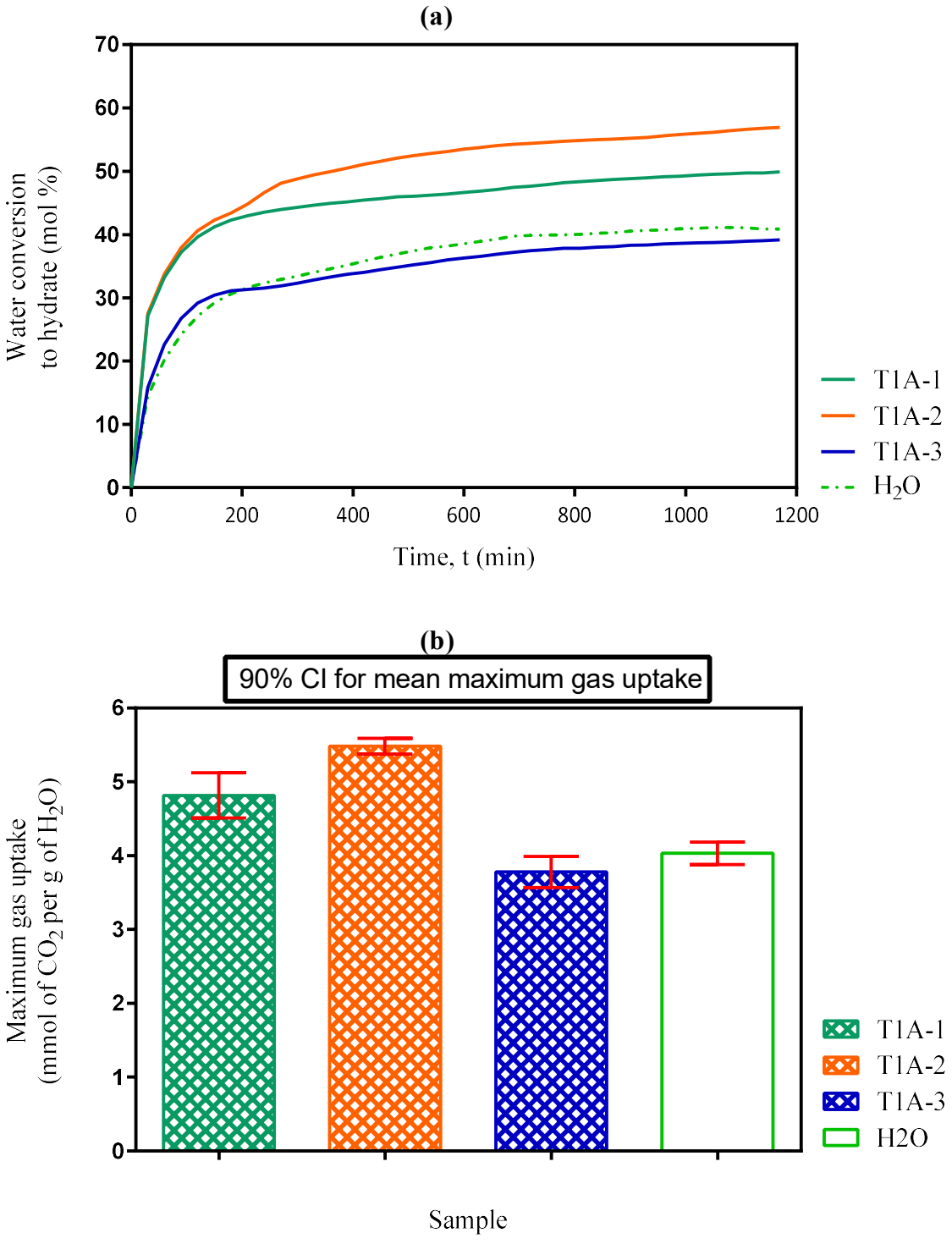


Figure 4- 8: Comparison of (a) water conversion to hydrate and (b) maximum CO_2 uptake for various T1A samples and baseline experiment at the operating conditions of 275 K and 36 bar in 1200 minutes (brief description of each T1A code was referred to page 121 (Table 4- 6))

Table 4- 7 summarises the maximum CO_2 uptake obtained for each sample. The maximum CO_2 uptake was increased from 4.82 ± 0.35 to 5.45 ± 0.12 mmol of CO_2 per g of H_2O as the concentration of EGME increased from 0.01 to 0.1 mol%. However, the value decreased as the concentration reached 1 mol% which indicated that 0.1 mol% was the optimum concentration for EGME.

Table 4- 7: Maximum CO_2 uptake in 1200 minutes at 275 K and 36 bar for various concentrations of T1A combined-promoters and baseline experiment (brief description of each T1A code was referred to page 121 (Table 4- 6))

Sample	Exp. No.	CO_2 uptake (mmol of CO_2/g of H_2O)	Mean CO_2 uptake (mmol of CO_2/g of H_2O) (90% CI)	SD
T1A-1	1	5.03	4.82 ± 0.35	0.30
	2	4.60		
T1A-2	1	5.56	5.45 ± 0.12	0.10
	2	5.41		
T1A-3	1	3.63	3.78 ± 0.24	0.21
	2	3.93		
H_2O	1	3.93	4.04 ± 0.17	0.15
	2	4.14		

4.2.1.3.3. Rate of hydrate formation

Figure 4- 9 illustrates the rate of hydrate formation for all T1A samples. The initial kinetics for T1A-1 (0.01 mol% SDS and 0.01 mol% EGME) and T1A-2 (0.01 mol% SDS and 0.10 mol% EGME) were the same at 0.09 mmol of CO_2 per g of H_2O per min and were faster than the baseline experiment. The kinetics of T1A-3 (0.01 mol% SDS and 1.00 mol% EGME) was almost 50% slower than both samples and also slightly slower than the baseline experiment. The medium concentration of EGME (0.1 mol%) could enhance the rate of hydrate formation and also the maximum CO_2 uptake as shown by T1A-2.

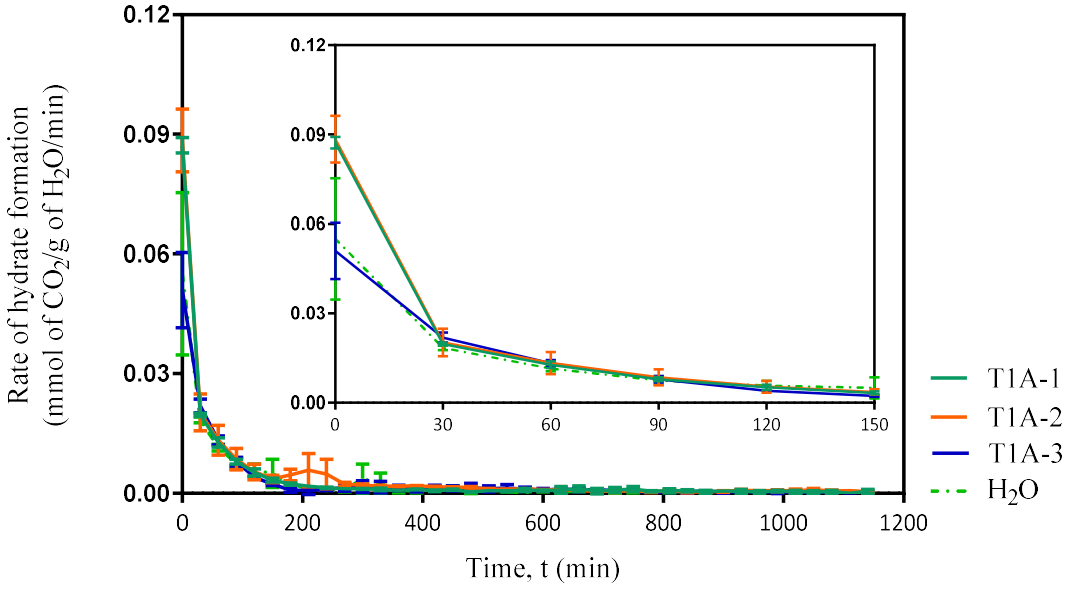


Figure 4- 9: Rate of hydrate formation at 275 K and 36 bar for 1200 minutes and inset for the first 150 minutes (various T1A concentrations and baseline experiment) (brief description of each T1A code was referred to page 121 (Table 4- 6))

4.2.2. Optimum combined-concentrations

The optimum combined-concentrations for hydrate formation for each type of combined-promoter was achieved by T1-5 (5.60 mol% THF and 0.01 mol% SDS), T3-2 (0.01 mol% SDS and 0.10 mol% TBAB) and T1A-2 (0.01 mol% SDS and 1.00 mol% EGME). At 0.01 mol% SDS, all promoters demonstrated improvement for hydrate formation whereas THF at 3 mol% was not compatible with TBAB at 0.29 mol% in which an inhibition effect on hydrate formation was observed. Then, EGME was discovered as an alternative to THF in which it was combined with SDS. Table 4- 8 summarises the results observed for T1-5, T3-2 and T1A-2.

The average number of moles of water for the baseline experiment was 4.2mmol. A combined-promoter inside silica gel pores reduced the amount of water available for hydrate

formation in which T1-5 and T1A-2 were 0.5 and 0.7 mmol lower than baseline respectively. T3-2 had the lowest moisture content and was 1.8 mmol lower than the baseline experiment.

Table 4- 8: The optimum results observed for each type of combined-promoter and baseline experiment at 275 K and 36 bar (brief description on each code (T1-5, T3-2 and T1A-2) – page 108, 116 (Table 4- 4) and 121 (Table 4- 6) respectively)

Sample	Exp. No.	No. of moles of water (mmol)	CO_2 formed in hydrate (mmol)	Mean CO_2 formed in hydrate (mmol)	CO_2 uptake (mmol of CO_2/g of H_2O)	Mean CO_2 uptake (mmol of CO_2/g of H_2O) (90% CI)	SD
T1-5	1	3.70	0.39	0.40	5.82	5.95 ± 0.21	0.18
	2	3.70	0.41		6.08		
T3-2	1	2.40	0.23	0.24	5.36	5.57 ± 0.34	0.29
	2	2.40	0.25		5.77		
T1A-2	1	3.50	0.35	0.35	5.56	5.45 ± 0.12	0.10
	2	3.50	0.34		5.41		
H_2O	1	4.10	0.29	0.31	3.93	4.04 ± 0.17	0.15
	2	4.30	0.32		4.14		

The trend for maximum CO_2 uptake was identical to the kinetics of hydrate formation as shown in Figure 4-10. The highest CO_2 uptake was observed for T1-5 with the value of 5.95 ± 0.21 mmol of CO_2 per g of H_2O and followed by T3-2 which was 0.38 mmol of CO_2 per g of H_2O less than T1-5 as illustrated in Figure 4-10 (a). Even though, the CO_2 uptake of T1A-2 was 0.12 mmol of CO_2 per g of H_2O lower than T3-2, due to its greater moisture content, it consumed a higher amount of CO_2 molecules which was 0.11 mmol higher than T3-2. In addition, the total amount of CO_2 consumed by the baseline experiment was also higher than T3-2 by 0.07 mmol. In contrast, the amount of CO_2 molecules captured by T1-5 was the highest (0.40 mmol) even though the baseline experiment had the highest moisture content. Also, T1A-2 managed to capture 0.04 mmol CO_2 molecules more than the baseline experiment at a lower equilibrium moisture content. Based on the results obtained, T1-5 was the best promoter when employed in a pure CO_2 system.

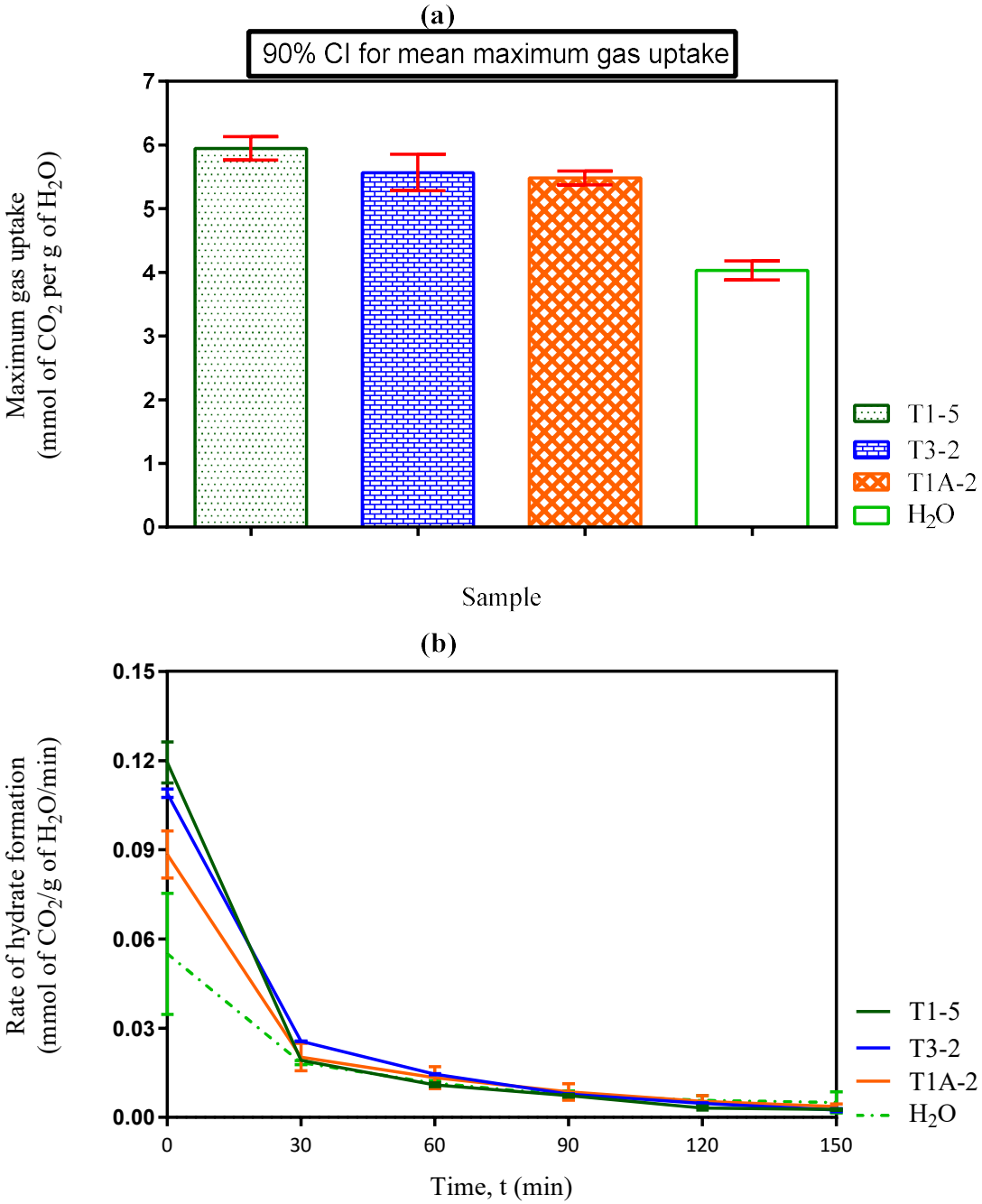


Figure 4- 10: Comparison of (a) maximum CO_2 uptake and (b) rate of hydrate formation for the optimum concentration of each combined-promoter and baseline experiment at the operating conditions of 275 K and 36 bar (brief description on each code (T1-5, T3-2 and T1A-2) – page 108, 116 (Table 4- 4) and 121 (Table 4- 6) respectively)

4.3.Enhancing hydrate formation in microporous silica

As previously discussed in chapter 1, the characteristics of solid adsorbent could affect the formation of hydrate. It mentioned by Adeyemo et al. (2010), larger pores and particle size of silica gel could increase the rate of hydrate formation. As a result, employing microporous silica has not been widely explored by researchers. Recently, Zhong et al. (2015) discovered that the selectivity for hydrate formation was lower for the fixed bed of zeolite 13X as compared to STRs. Hence, in this work the investigation on the implementation of optimum combined-promoter (T1-5; 5.60 mol% THF and 0.01 mol% SDS) and the effect of bed height were performed to further study the feasibility of zeolite 13X for hydrate formation in FBR. The bed height was measured by using a vernier calliper. Powder zeolite 13X with a mean particle size of 2 μm, mean pore size of 1.50 nm, pore volume of 0.31 cm^3/g and surface area of 819 m^2/g was used.

4.3.1. CO_2 solubility in water

Initially, 0.5g or 3 cm bed height of zeolite 13X contacted with water (13X-H_2O_3cm) was used to investigate the formation of hydrate at 275 K and 36 bar inside the HPVA. The study on CO_2 solubility in water showed that no hydrate formation was observed because the total CO_2 consumed after 1200 minutes was below the red-dashed line as illustrated in Figure 4- 11. The same result was observed for zeolite 13X contacted with 5.6 mol% THF and 0.01 mol% SDS (13X-5_3cm) when 0.5g of this sample was employed during the experiment. However, the total CO_2 consumed in 1200 minutes was slightly higher than the previous sample. Subsequently, the use of 0.3g of 13X-5 inside the sample cell and reducing the bed height to 2cm led to the formation of hydrate. The total CO_2 dissolved was above the red-dashed line.

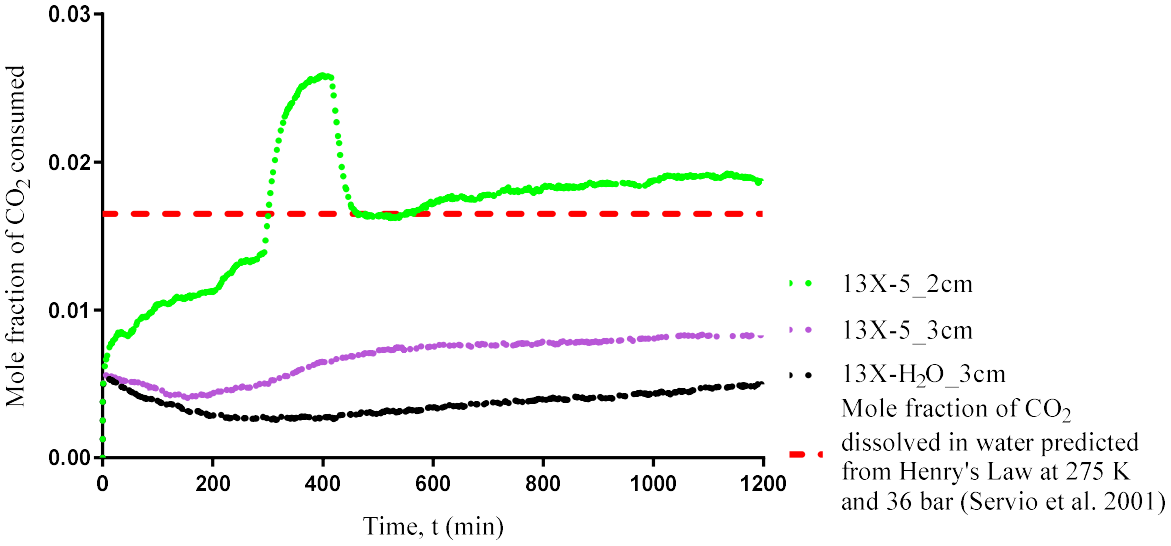


Figure 4- 11: Mole fraction of CO_2 consumed at the operating conditions of 275 K and 36 bar in 1200 minutes (*13X-5 = zeolite contacted with 5.6 mol% THF and 0.01 mol% SDS) (brief description on 13X-5 was referred to page 127)

4.3.2. Water conversion and maximum gas uptake

Performance comparison of microporous and mesoporous silica for CO_2 hydrate formation was performed as illustrated in Figure 4- 12. In this analysis, the best result of mesoporous silica (T1-5_3cm; 5.6 mol% THF and 0.01 mol% SDS) at 275 K and 36 bar was chosen together with baseline experiment (SiG-H_2O_3cm) with both samples weighing 0.5g.

The equilibrium moisture content for 13X-5 at 0.5g was around 20 wt% as illustrated in Figure 4- 12 (a) which was more than 30% higher than the baseline experiment and T1-5. Figure 4- 12 (b) and Table 4- 9 demonstrate that the maximum gas uptake of 13X-5_2cm was the lowest around 0.6 mmol of CO_2 per g of H_2O and was almost 5.5 and 3.5 mmol of CO_2 per g of H_2O lower than T1-5_3cm and baseline experiment respectively. At this bed height, the amount of equilibrium moisture content of 13X-5 was reduced from 5.7 to 3.5 mmol of H_2O which was almost comparable to T1-5 and baseline experiment. However, at this comparable amount of moisture content, mesoporous silica was found to have better CO_2 capture capability where the total CO_2 molecules consumed was 10 times higher than

microporous silica. Figure 4- 12 (c) shows that the highest water conversion to hydrate observed for 13X-5_2cm was almost 10 mol% in the first 400 minutes. However, after 400 minutes, the CO_2 hydrate was found to dissociate before it started to increase again at 600 minutes. This indicated that the CO_2 hydrate formed during the experiment was not stable and also requires future investigation if microporous silica is going to be implemented for CO_2 capture with hydrate formation. In contrast, the CO_2 hydrate formed by implementing mesoporous silica was stable throughout the experiment which is necessary for CO_2 transport and storage purposes.

Table 4- 9: The comparison of gas uptake of 13X-5_2cm, 13X-5_3cm, 13X-H_2O_3cm, T1-5_3cm and baseline experiment at 36 bar and 275 K in 1200 minutes (brief description on 13X-5 and T1-5 was referred to page 127 and 108 respectively)

Sample	Bed height (cm)	Exp. No.	No. of moles of water (mmol)	CO_2 formed in hydrate (mmol)	Mean CO_2 formed in hydrate (mmol)	CO_2 uptake (mmol of CO_2/g of H_2O)	Mean CO_2 uptake (mmol of CO_2/g of H_2O) (90% CI)	SD
13X-5	2	1	3.40	0.03	0.04	0.56	0.58 ± 0.03	0.03
		2	3.50	0.04		0.60		
13X-5	3	1	5.70	-	-	-	-	-
		2	5.70	-		-		
13X-H_2O	3	1	5.90	-	-	-	-	-
		2	5.90	-		-		
T1-5	3	1	3.70	0.39	0.40	5.82	5.95 ± 0.21	0.18
		2	3.70	0.41		6.08		
H_2O	3	1	4.10	0.29	0.31	3.93	4.04 ± 0.17	0.15
		2	4.30	0.32		4.14		

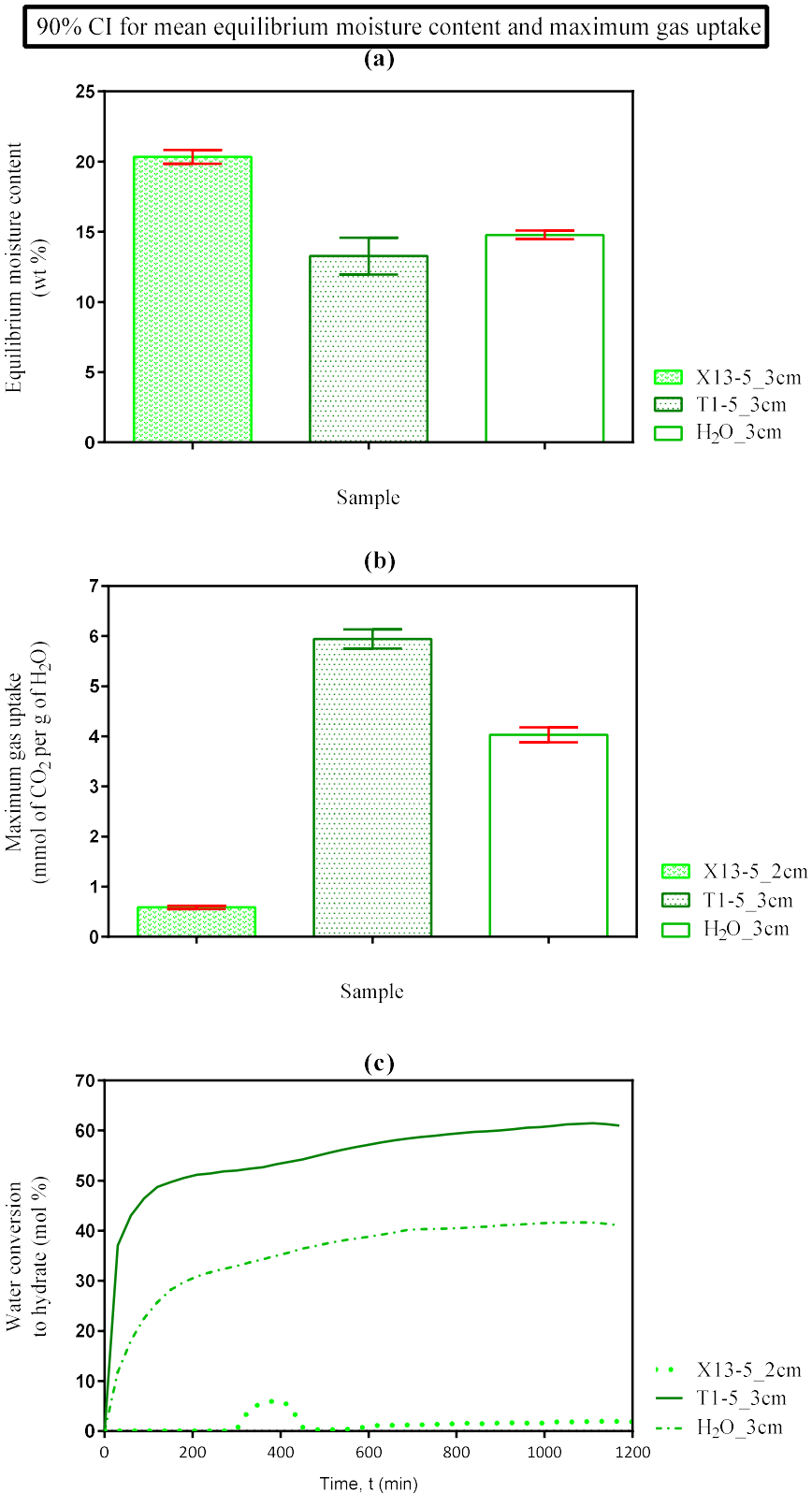


Figure 4- 12: Comparison of (a) equilibrium moisture content at 3cm bed height, (b) maximum gas uptake and (c) water conversion to hydrate for 13X-5_2cm, T1-5_3cm and baseline experiment at 275 K and 36 bar in 1200 minutes (brief description on 13X-5 and T1-5 was referred to page 127 and 108 respectively)

4.3.3. Rate of hydrate formation

Generally, Figure 4- 13 illustrates that the kinetics of mesoporous silica was extensively higher than microporous silica. The initial kinetics of 13X-5_2cm was really slow wherein it indicated that the induction time for hydrate growth was longer than T1-5_3cm and the baseline experiment.

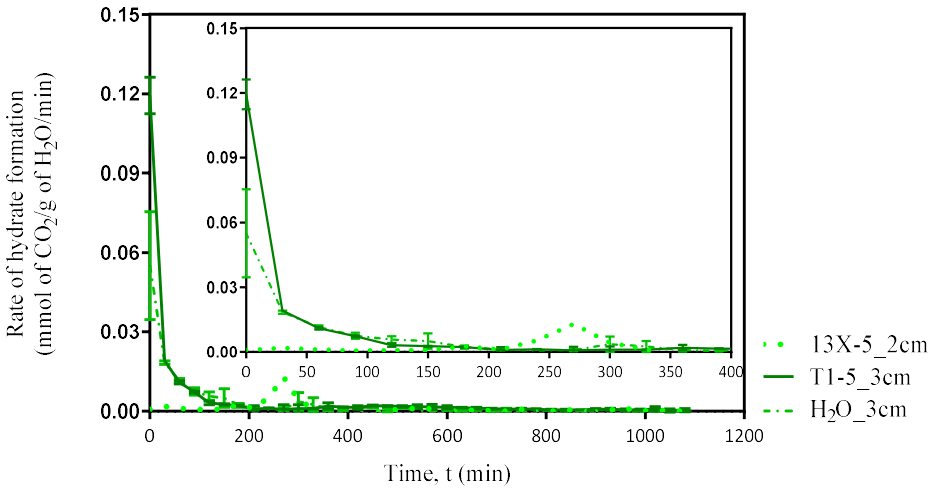


Figure 4- 13: Rate of hydrate formation at 275 K and 36 bar for 1200 minutes and inset for the first 400 minutes (13X-5_2cm, T1-5_3cm and baseline experiment) (brief description on 13X-5 and T1-5 was referred to page 127 and 108 respectively)

Generally, the effect of employing a combined-promoter inside zeolite pores did not really enhance hydrate formation and is considered a disadvantage of employing microporous silica for CO_2 capture with hydrate formation. Only when the bed height was reduced from 3 to 2cm, then the rate of hydrate formation was improved. In conclusion, the effect of bed height on hydrate formation was more significant as compared to the implementation of combined-promoter.

4.4.Summary

i. The combination of promoters at certain concentrations was not compatible with an inhibition effect on hydrate formation as observed for the combination of THF at 3 mol% and TBAB at 0.29 mol%. The CO_2 uptake was reduced by 2.41 mmol of CO_2 per g of H_2O as compared to the baseline experiment (H_2O; 4.04 mmol of CO_2 per g of H_2O).

ii. The inhibition effect by TBAB at 0.29 mol% was improved when the concentration was reduced to 0.1 mol% and combined with 0.01 mol% SDS (designated type T3-2) wherein the gas uptake was increased from 2 (TBAB at 0.29 mol% only) to 5.6 mmol of CO_2 per g of H_2O (designated type T3-2).

iii. SDS at 0.01 mol% improved hydrate formation when combined with any type of promoter (THF, TBAB and EGME). The optimum results were obtained by combined-promoters designated type T1-5 at the concentrations of 5.6 mol% THF and 0.01 mol% SDS where the water conversion to hydrate was almost 70 mol% and the maximum gas uptake was 5.95 mmol of CO_2 per g of H_2O.

iv. EGME was an alternative to THF where the optimum CO_2 uptake (5.45 mmol of CO_2 per g of H_2O) was achieved at a concentration of 0.1 mol% when combined with 0.01mol% SDS (designated type T1A-2).

v. The total CO_2 molecules involved in hydrate formation was dependant on the amount of moisture content available inside silica gel pores and also the type of combined-promoter used in which the highest value was observed at 0.40 mmol by employing combined-promoter designated type T1-5 (5.6 mol% THF and 0.01 mol% SDS).

vi. Bed height influenced hydrate formation whereby reducing the bed height of zeolite 13X from 3 to 2cm led to the formation of hydrate with the CO_2 uptake of 0.58 mmol of CO_2 per g of H_2O.

vii. The discovery of two new combined-promoters (designated types T3-2 and T1A-2) in this work will provide more options for the HBGS research field.

CHAPTER 5: IGCC PLANT CONDITIONS

5.1.Introduction

Generally, the operating conditions of the IGCC are in the range of 283-290 K and 20-70 bar (fuel gas mixture) and are outside the hydrate forming conditions. The minimum pressure required for CO_2 hydrate to form at 283 K is 30 bar (pure CO_2) as discovered by Servio et al. (2001) or equivalent to 75 bar for the case of fuel gas mixture. Nevertheless, the initial investigation on implementation of promoters in chapter 3 directed attention to the hydrate in non-hydrate forming conditions. Therefore, the focus of the study in this specific chapter was to obtain optimum hydrate formation in the IGCC operating conditions. Furthermore, several experimental parameters previously investigated and described were used with the highest rates of stirring (method 4 sample preparation) and T1-5 sample (5.60 mol% THF and 0.01 mol% SDS) providing the optimum effect on hydrate formation. Also, the influence of bed height on hydrate formation was highlighted.

Hence, additional experimental parameters were investigated and reported in this chapter which indicated that hydrate formation is possible in IGCC conditions. The experimental parameters that were studied include hydrate formation driving force, various non-hydrate forming conditions especially in the IGCC conditions with the employment of fuel gas mixture, regeneration capability and the significance of reducing bed height in the IGCC conditions.

5.2.Various driving forces in hydrate forming region

A study was performed to investigate the effect of driving force on hydrate formation. Various operating pressures (36, 30 and 22 bar) in pure CO_2 gas were investigated at 275 K by employing silica contacted with different combined-promoters. T1-5 and T3-2 (0.01 mol% SDS and 0.10 mol% TBAB) were the preferred combined-promoters due to their great CO_2

uptake achieved at 275 K and 36 bar (ΔP = 19 bar) in chapter 4. Then, some additional experiments at 30 bar (ΔP = 13 bar) and 22 bar (ΔP = 5 bar) for T1-5 and T3-2 were performed. In each experiment, approximately 0.5 g wet silica was used and the investigations were performed in the HPVA for 1200 minutes. Then, the results were compared with the baseline experiment at various driving forces which were previously presented in chapter 3.

5.2.1. Water conversion and maximum gas uptake

The comparison of hydrate formation at various driving forces is illustrated in Figure 5- 1 and Figure 5- 2. Figure 5- 1 (a) and (b) shows that T3-2 had the highest water conversion to hydrate and CO_2 uptake respectively at 275 K and 30 bar followed by T1-5 and the baseline experiment. However, T1-5 demonstrated the best results at 275 K and 22 bar as shown in Figure 5- 2 (a) and (b) with T3-2 and baseline experiment obtaining almost identical results.

Table 5- 1 summarises the gas uptake obtained by each sample at various operating pressures. In general, the gas uptake for all samples increased as the driving force (ΔP) increased from 5 to 19 bar with T1-5 demonstrating the best result at all driving forces except at ΔP = 5 bar. Even though the gas uptake of T3-2 was the highest at this driving force which was almost 0.5 mmol of CO_2 per g of H_2O higher than T1-5, the total CO_2 molecules captured by T1-5 was the highest (0.17 mmol) which was 0.03 mmol higher than T3-2. This was expected due to the higher amount of available water molecules attained by T1-5, 1.3 mmol higher than T3-2.

In contrast, the total CO_2 molecules captured by the baseline experiment was lower than T1-5 at all driving forces even though the amount of water molecules available for hydrate formation was higher than T1-5 by almost 0.5 mmol. However, the CO_2 molecules captured by the baseline experiment was higher than T3-2 at all driving forces except at ΔP = 13 bar.

In addition, at this medium driving force, T3-2 exhibited the closest result to T1-5. The results showed that high operating pressure enhanced the formation of hydrate due to the greater driving force (ΔP). Also, different samples had diverse effects on hydrate formation at different driving forces.

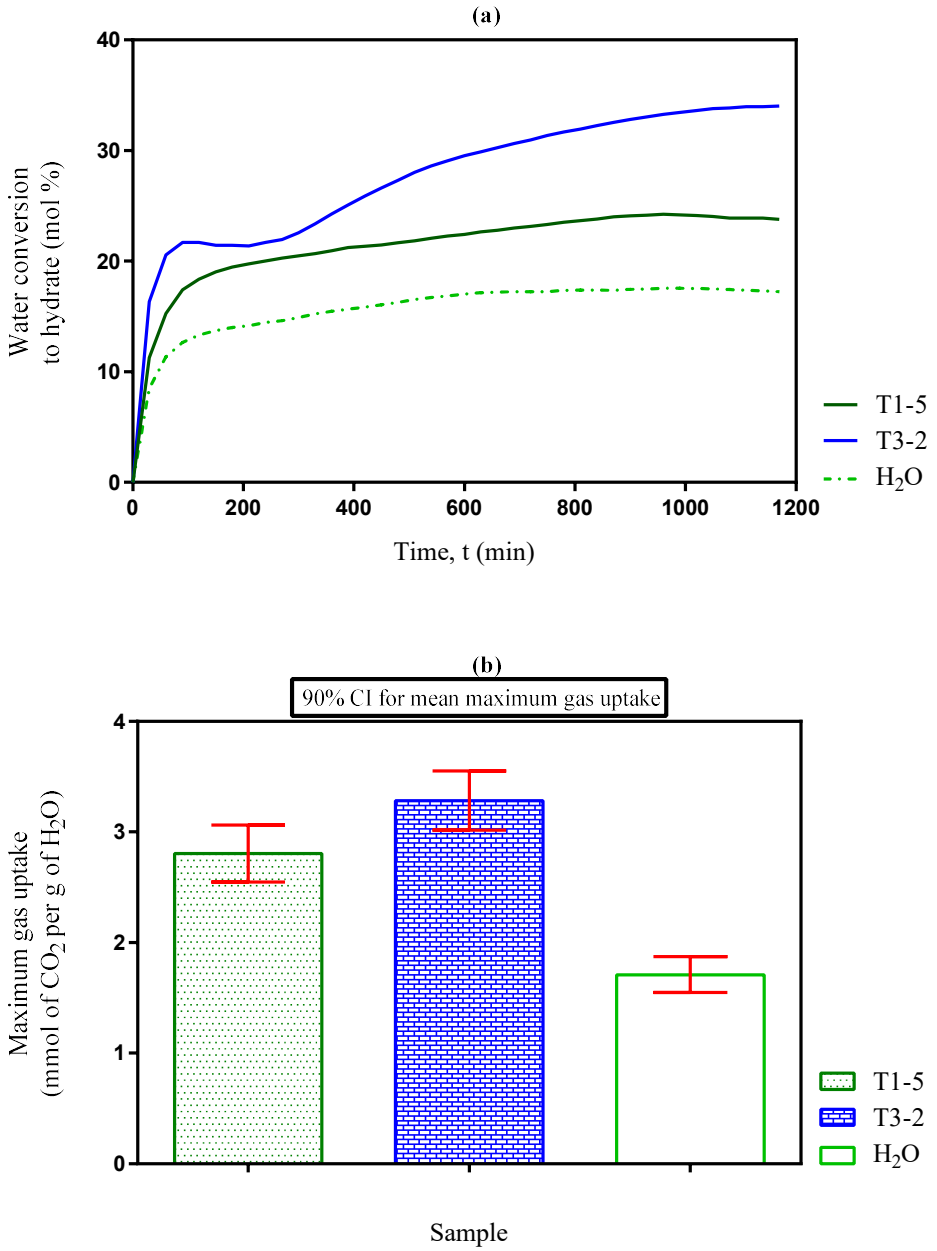


Figure 5- 1: Comparison of (a) water conversion to hydrate and (b) gas uptake for T1-5, T3-2 and baseline experiment at 275 K and 30 bar in 1200 minutes (brief description on each sample code was referred to page 108 and 116 (Table 4- 4) respectively)

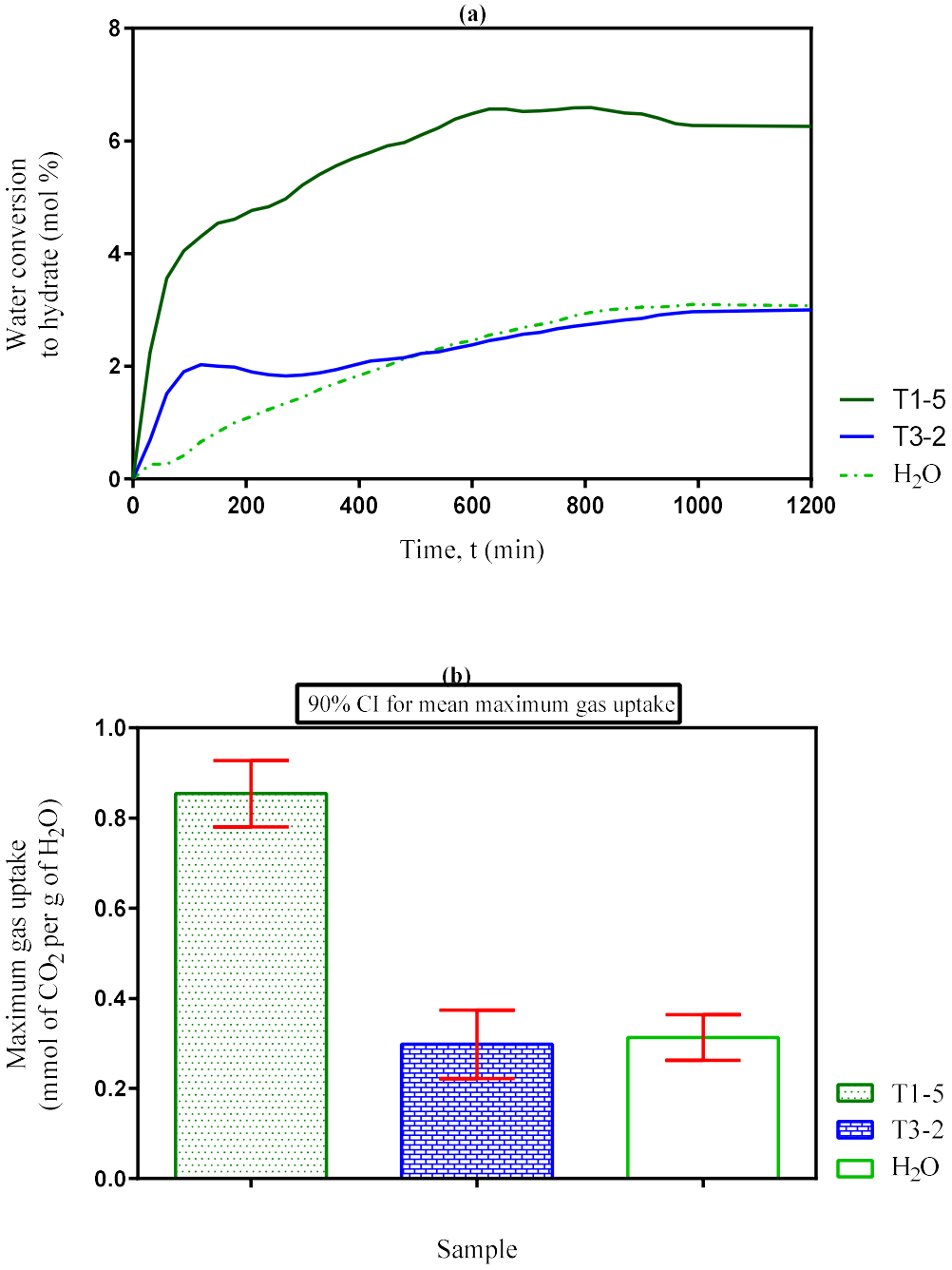


Figure 5- 2: Comparison of (a) water conversion to hydrate and (b) gas uptake for T1-5, T3-2 and baseline experiment at 275 K and 22 bar in 1200 minutes (brief description on each sample code was referred to page 108 and 116 (Table 4- 4) respectively)

Table 5- 1: Comparison of gas uptake for T1-5, T3-2 and baseline experiment at 275 K and the operating pressures of 36, 30 and 22 bar in 1200 minutes (brief description on each sample code was referred to page 108 and 116 (Table 4- 4) respectively)

Operating conditions	Sample	Exp. No.	No. of moles of water (mmol)	CO_2 formed in hydrate (mmol)	Mean CO_2 formed in hydrate (mmol)	CO_2 uptake (mmol of CO_2/g of H_2O)	Mean CO_2 uptake (mmol of CO_2/g of H_2O) (90% CI)	SD
275 K & 36 bar	T1-5	1	3.70	0.39	0.40	5.82	5.95 ± 0.21	0.18
		2	3.70	0.41		6.08		
	T3-2	1	2.40	0.23	0.24	5.36	5.57 ± 0.34	0.29
		2	2.40	0.25		5.77		
	SiG-H_2O	1	4.10	0.29	0.31	3.93	4.04 ± 0.17	0.15
		2	4.30	0.32		4.14		
275 K & 30 bar	T1-5	1	3.70	0.15	0.17	2.62	2.81 ± 0.30	0.26
		2	3.70	0.18		2.99		
	T3-2	1	2.40	0.13	0.14	3.09	3.28 ± 0.31	0.27
		2	2.40	0.15		3.47		
	SiG-H_2O	1	4.20	0.14	0.13	1.82	1.71 ± 0.19	0.16
		2	4.10	0.12		1.60		
275 K & 22 bar	T1-5	1	3.70	0.05	0.05	0.91	0.86 ± 0.09	0.08
		2	3.70	0.04		0.80		
	T3-2	1	2.40	0.01	0.01	0.35	0.30 ± 0.09	0.08
		2	2.40	0.01		0.24		
	SiG-H_2O	1	4.10	0.02	0.03	0.28	0.32 ± 0.06	0.05
		2	4.20	0.03		0.35		

5.2.2. Rate of hydrate formation

Figure 5- 3 illustrates that the initial rate of hydrate formation of T3-2 at 275 K and 30 bar was the fastest which was 13% greater than T5-1 and almost 70% faster than the baseline experiment. However, the initial rate of hydrate formation at 275 K and 22 bar as shown in Figure 5- 4 was the fastest for T1-5 with the value of 0.012 mmol of CO_2 per g of H_2O per min followed by T3-2 (0.005 mmol of CO_2 per g of H_2O per min) and baseline experiment (0.004 mmol of CO_2 per g of H_2O per min). T1-5 was the best option for hydrate formation at low driving force.

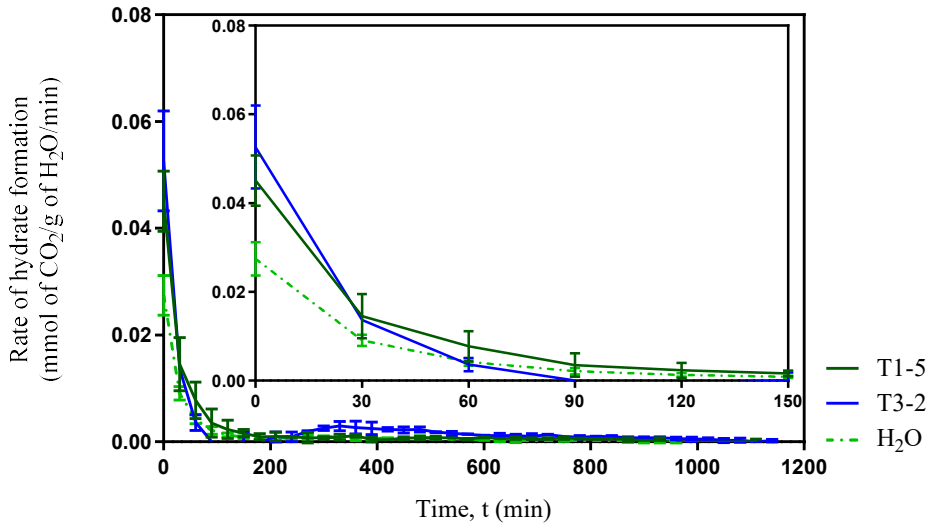


Figure 5- 3: Rate of hydrate formation at 275 K and 30 bar for 1200 minutes and inset for the first 150 minutes (T1-5, T3-2 and baseline experiment) (brief description on each sample code was referred to page 108 and 116 (Table 4- 4) respectively)

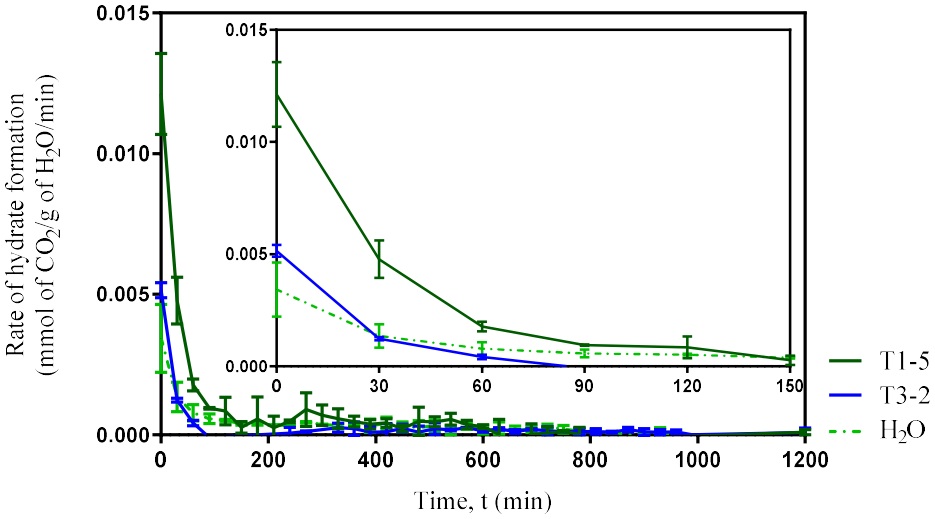


Figure 5- 4: Rate of hydrate formation at 275 K and 22 bar for 1200 minutes and inset for the first 150 minutes (T1-5, T3-2 and baseline experiment) (brief description on each sample code was referred to page 108 and 116 (Table 4- 4) respectively)

5.3.Enhanced hydrate formation in non-hydrate forming region

As previously discovered in chapter 3, the use of promoters could enhance hydrate formation in which the baseline experiment did not show any hydrate formation at 288 K and 36 bar. Thus, in this particular section, the investigation of hydrate formation in non-

hydrate forming region was performed at 36 bar and various operating temperatures (288 and 293 K) by employing pure CO_2 gas and several combined-promoters. Yang et al. (2013) plotted the phase equilibrium of hydrate formation in pure CO_2 gas system and showed that at 36 bar, the equilibrium temperature was 280 K. In this study, the operating temperature of 288 K led to the driving force of $\Delta T = 8$ K and for 293 K, $\Delta T = 13$ K. Unlike ΔP, the highest value of ΔT was equivalent to the lowest driving force available for the system because the operating conditions will be shifted to the right hand side of phase equilibrium, also known as the non-hydrate forming region. This study was then used as a basis for the investigation of hydrate formation at IGCC plant operating conditions in which fuel gas mixture was employed at the operating temperature of 280 K and operating pressures of 58 (P_{CO2} = 23 bar) and 70 bar (P_{CO2} = 28 bar) respectively.

5.3.1. Pure CO_2 gas investigation

The initial investigation in this non-hydrate region by employing THF and SDS showed hydrate formation at the operating conditions of 288 K and 36 bar in chapter 3. Hence, further investigation was performed by employing combined-promoters (T1-5; 5.60 mol% THF and 0.01 mol% SDS, T3-2; 0.01 mol% SDS and 0.10 mol% TBAB and T1A-2; 0.01 mol% SDS and 0.10 mol% EGME) at the same operating conditions. Then, T1-5 and T3-2 were employed for the investigation at 293 K and 36 bar. All experiments were conducted for 1200 minutes and 0.5 g of silica contacted with combined-promoter was used for each experiment.

5.3.1.1. Water conversion and maximum gas uptake

Figure 5- 5 (a) illustrates the conversion of water to hydrate at 288 K and 36 bar wherein T3-2 was found to show the best result with around 10 mol% conversion. This was followed

by T1-5 and THF with both having a conversion around 9 mol%, followed by T1A-2 and SDS with around 6 mol% for both conversions. Figure 5- 5 (b) and Table 5- 2 show that the highest gas uptake was observed for T1-5 with the value of 1.25 mmol of CO_2 per g of H_2O followed by THF (1.15 mmol of CO_2 per g of H_2O), T3-2 (1.00 mmol of CO_2 per g of H_2O), T1A-2 (0.68 mmol of CO_2 per g of H_2O) and SDS (0.66 mmol of CO_2 per g of H_2O).

The results showed that by adding THF, TBAB and EGME to SDS, the water conversion to hydrate and maximum gas uptake was increased accordingly. Significant improvement was observed when 5.6 mol% THF was added to 0.01 mol% SDS with almost double gas uptake obtained as compared to SDS (0.01 mol%) alone. In addition, the gas uptake for 3 mol% THF alone was almost comparable to T1-5 which showed that THF was a very good promoter for hydrate formation at high temperature. The same trend was observed for T3-2 in which 0.10 mol% TBAB was added to 0.01 mol% SDS. However, 0.1 mol% EGME only showed a minimal effect on hydrate formation when it was added to 0.01 mol% SDS.

Based on the results obtained at these operating conditions, T1-5 and T3-2 were further investigated at 293 K and 36 bar. Figure 5- 6 (a) also demonstrates that T3-2 had the greatest water conversion to hydrate with a conversion around 6 mol% at 293 K and 36 bar. This was followed by T1-5 being almost 70% lower than T3-2. However, the maximum gas uptake for T1-5 was 0.03 mmol of CO_2 per g of H_2O higher than T3-2 as presented in Figure 5- 6 (b) and Table 5- 2. The same trend was observed at both operating temperatures due to high equilibrium moisture content in T1-5 which was 50% higher than T3-2. Thus, T3-2 demonstrated the highest water conversion to hydrate due to lower water presence inside silica gel pores as compared to T1-5. As a result, fewer CO_2 molecules were consumed in hydrate formation at 288 K for T3-2 which was 0.02 mmol less than T1-5. Moreover, the slightly high error bar for T3-2 observed at these operating conditions was due to the regeneration experiment performed by reusing the same sample. However, other

regeneration experiments demonstrated quite high regeneration values as shown in Table 5-2. Finally, the CO_2 molecules captured at 293 K were comparable for both samples which showed that THF and TBAB demonstrated the same effect at this operating temperature.

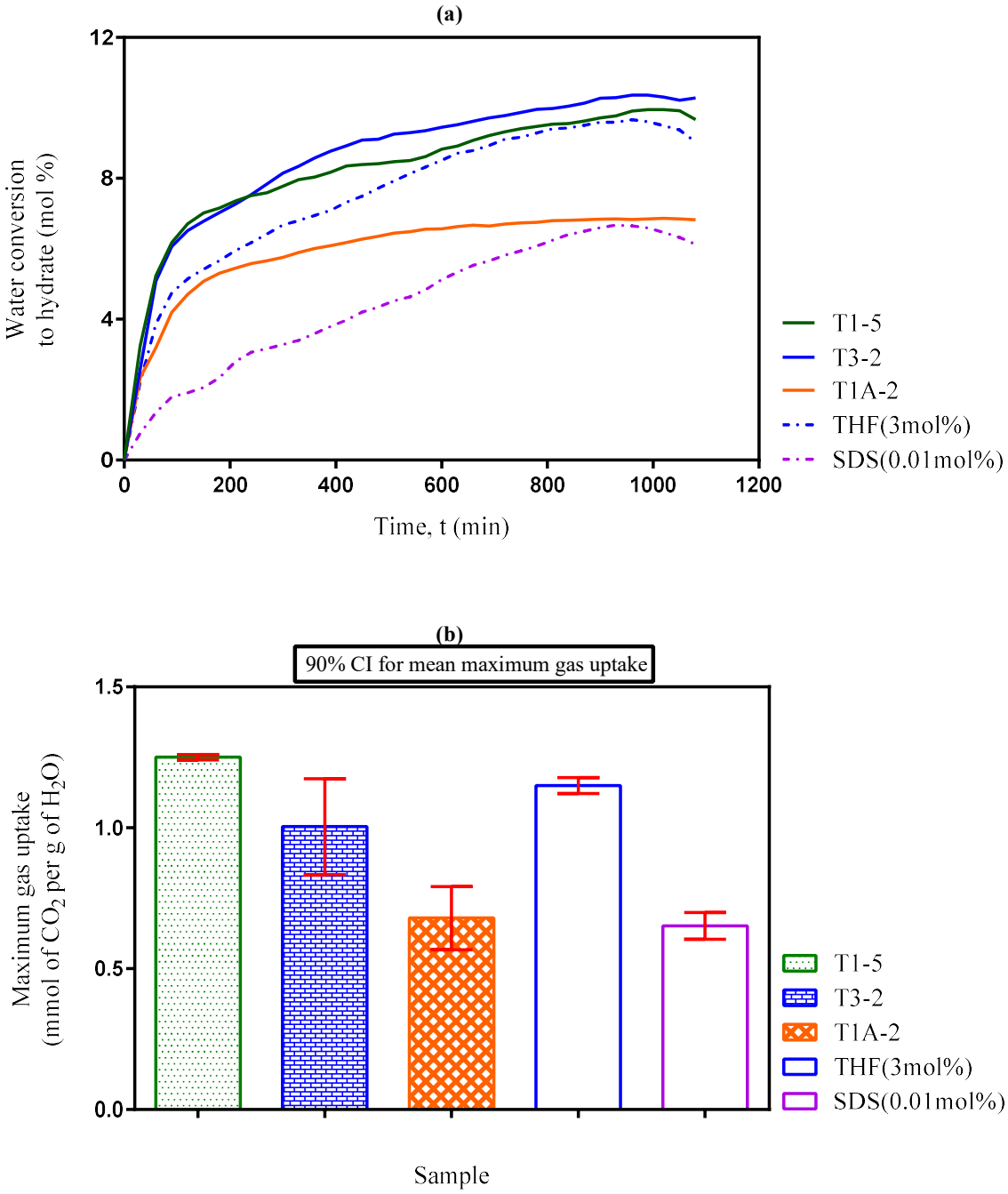


Figure 5- 5: The comparison of (a) water conversion to hydrate and (b) gas uptake for T1-5, T3-2, T1-A and baseline experiments at 288 K and 36 bar in 1200 minutes (brief description on each sample code was referred to page 108, 116 (Table 4- 4) and 121 (Table 4- 6) respectively)

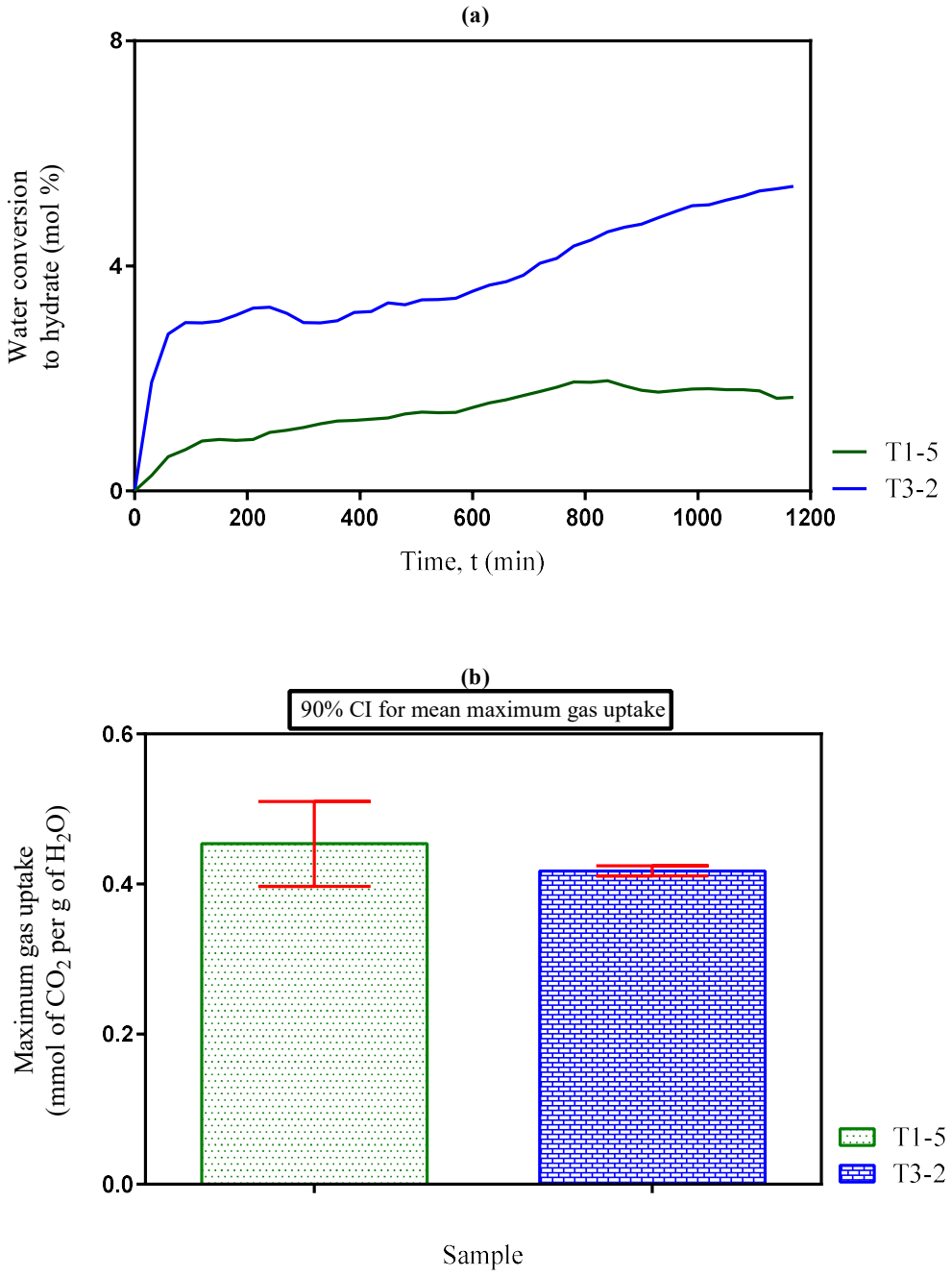


Figure 5- 6: The comparison of (a) water conversion to hydrate and (b) gas uptake for T1-5 and T3-2 at 293 K and 36 bar in 1200 minutes (brief description on each sample code was referred to page 108 and 116 (Table 4- 4) respectively)

Table 5- 2: The comparison of gas uptake at 36 bar and operating temperatures of 288 K & 293 K in 1200 minutes (brief description on each sample code (T1-5, T3-2, T1A-2) was referred to page 108, 116 (Table 4- 4) and 121 (Table 4- 6) respectively)

Operating conditions	Sample	Exp. No.	No. of moles of water (mmol)	CO_2 formed in hydrate (mmol)	Mean CO_2 formed in hydrate (mmol)	CO_2 uptake (mmol of CO_2/g of H_2O)	Mean CO_2 uptake (mmol of CO_2/g of H_2O) (90% CI)	SD
288 K & 36 bar	T1-5	1	3.70	0.07	0.07	1.26	1.25 ± 0.01	0.01
		2 [r]	3.70	0.07		1.24		
	T3-2	1	2.40	0.05	0.05	1.12	1.00 ± 0.20	0.17
		2[r]	2.40	0.04		0.88		
	T1A-2	1	3.50	0.05	0.05	0.76	0.68 ± 0.13	0.11
		2 [r]	3.50	0.04		0.60		
	SiG-THF	1	3.50	0.06	0.07	1.17	1.15 ± 0.03	0.03
		2	3.50	0.07		1.13		
	SiG-SDS	1	3.70	0.04	0.04	0.62	0.66 ± 0.06	0.05
		2	3.60	0.04		0.69		
293 K & 36 bar	T1-5	1	3.70	0.02	0.02	0.41	0.45 ± 0.07	0.06
		2 [r]	3.70	0.02		0.49		
	T3-2	1	2.40	0.02	0.03	0.41	0.42 ± 0.01	0.01
		2	2.30	0.03		0.42		

[r] regeneration experiment

5.3.1.2. Rate of hydrate formation

Figure 5- 7 illustrates the rate of hydrate formation at 288 K and 36 bar where the addition of 5.6 mol% THF to form T1-5 significantly increased the initial kinetics of silica contacted with single SDS (0.01 mol%) from 0.005 to 0.015 mmol of CO_2 per g of H_2O per min. Moreover, the addition of 0.1 mol% TBAB and 0.1 mol% EGME in 0.01 mol% SDS also doubled the initial rate of hydrate formation for single SDS as illustrated by T3-2 and T1A-2 respectively. These indicated that the combination of other promoters with SDS enhanced the kinetics of hydrate formation known as a synergic effect which is discussed later in chapter 6. The initial kinetics of the sample that employed THF alone were faster than T3-2 and T1A-2 and slightly slower than T1-5 which showed that THF was the best promoter to

be combined with SDS for enhancing hydrate formation. However, at 293 K and 36 bar, T1-5 and T3-2 demonstrated almost comparable rates of hydrate formation as illustrated in Figure 5- 8. This indicated that at high temperature, TBAB was the best alternative to THF to be employed together with SDS.

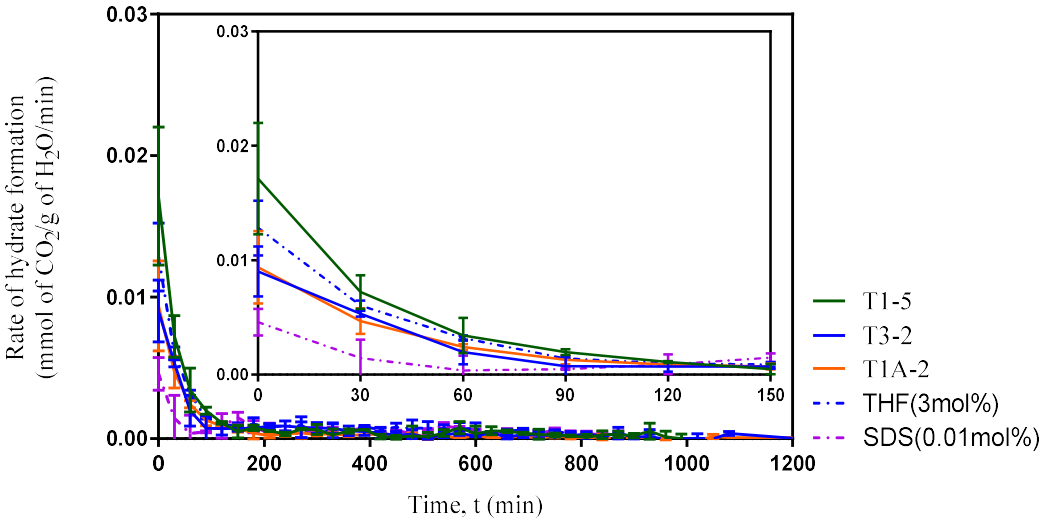


Figure 5- 7: Rate of hydrate formation at 288 K and 36 bar for 1200 minutes and inset for the first 150 minutes (T1-5, T3-2, T1A-2 and baseline experiments) (brief description on each sample code was referred to page 108, 116 (Table 4- 4) and 121 (Table 4- 6) respectively)

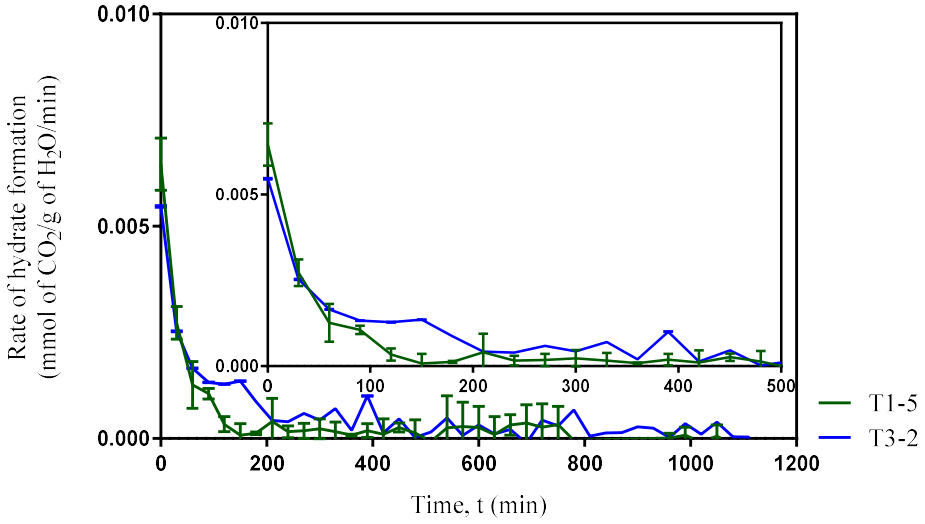


Figure 5- 8: Rate of hydrate formation at 293 K and 36 bar for 1200 minutes and inset for the first 500 minutes (T1-5 and T3-2) (brief description on each sample code was referred to page 108 and 116 (Table 4- 4) respectively)

5.3.2. IGCC operating conditions and the effect of bed height on hydrate formation

This particular section was solely focused on hydrate formation in the IGCC conditions wherein fuel gas mixture was employed as an adsorbate. Fuel gas mixture with the composition of 40% CO_2 and 60% H_2 was purchased from BOC. The range of operating pressure in the IGCC is between 20-70 bar which means the partial pressure of CO_2 (P_{CO2}) is between 8-28 bar. The operation temperature is between 283-290 K. A previous study showed that for a pure CO_2 system, minimal hydrate formation was observed at 293 K and 36 bar by employing T1-5 (5.60 mol% THF and 0.01 mol% SDS) and T3-2 (0.01 mol% SDS and 0.10 mol% TBAB). In addition, hydrate formation was also observed at 22 bar but at 275 K. Thus, the initial operating conditions selected for the study in this section was 283 K and 58 bar which led to the partial pressure of CO_2 of 23 bar. Long experiments at 2cm bed height of T1-5 at these operating conditions showed minimal hydrate formation. The measurement of bed height was previously explained in chapter 4. Further investigation was performed at higher driving force (283 K and 70 bar) where the partial pressure of CO_2 was 28 bar. The results obtained for the effect of bed height on hydrate formation are reported.

5.3.2.1. CO_2 solubility in water

The CO_2-H_2 solubility in water has not yet been reported in the literature. Since, the mole fraction of H_2 gas dissolved in water is too small at the IGCC operating pressures (Table A-6 - Appendix 6), the mole fraction of CO_2 dissolved in water at the partial pressure of CO_2 in fuel gas mixture was assumed to be the same as in pure CO_2 gas in the presence of hydrate. The interpolated mole fraction of H_2 dissolved in water at the IGCC conditions (T = 283 K) was found to be 0.0005 at 58 bar (P_{H_2} = 35 bar and P_{CO2} = 23 bar) and 0.0006 at 70 bar (P_{H_2}P = 42 bar and P_{CO_2}P = 28 bar) respectively (Table A- 7- Appendix 6). These values

are too small compared to the mole fraction of CO_2 dissolved in water at 283 K in pure CO_2 gas with the value of 0.0175 at P_{CO_2}P = 23 bar and 0.0185 at P_{CO_2}P = 28 bar respectively. The initial investigation at 283 K and 58 bar by employing 0.5g or 3cm bed height of T1-5 and T3-2 did not show any hydrate formation in 1200 minutes as illustrated in Figure 5- 9. Then, the bed height of T1-5 was reduced to 2cm but the CO_2 dissolved in water just slightly increased to around 0.014 mole fraction of CO_2 with no hydrate observed in 1200 minutes. Subsequently, minimal formation of hydrate was observed after 2500 min at these conditions when the long experiment was conducted.

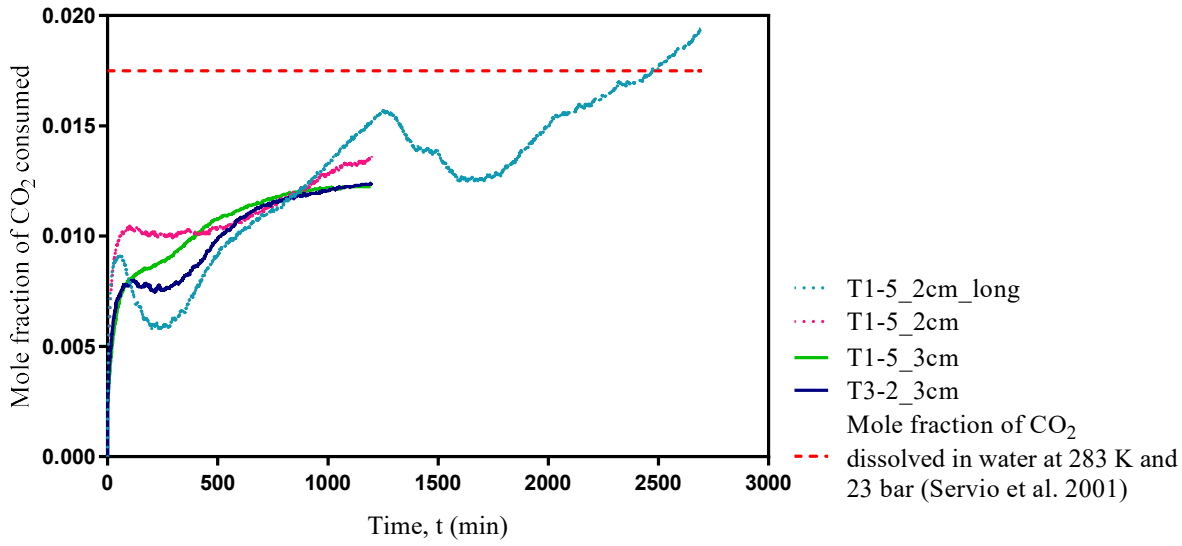


Figure 5- 9: CO_2 solubility in water for T1-5_2cm, T1-5_3cm and T3-2_3cm at the operating conditions of 283 K and 58 bar by employing fuel gas mixture (brief description on each sample code was referred to page 108 and 116 (Table 4- 4) respectively)

The driving force was then increased which led to the operating pressure of 70 bar at 283 K wherein various bed heights were used to investigate the formation of hydrate in these operating conditions. No formation of hydrate was observed for T3-2_3cm as shown in Figure 5- 10. Subsequently, the bed height of T3-2 was reduced to 2cm and T1-5 was also investigated at 2cm bed height. As a result, T3-2_2cm and T1-5_2cm did attain formation of

hydrate in 1200 minutes in which the final mole fraction of CO_2 in water was above the red-dashed line.

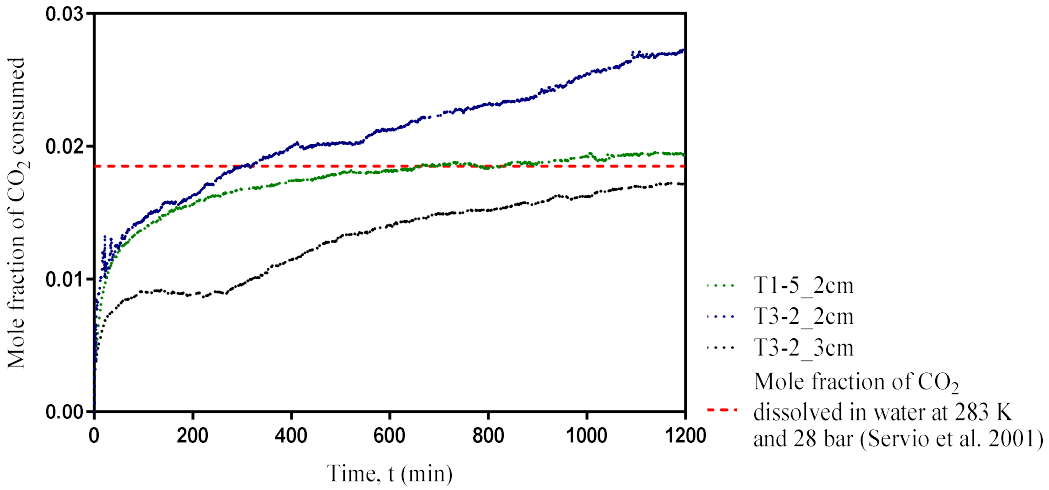


Figure 5- 10: CO_2 solubility in water for T1-5_2cm, T3-2_2cm and T3-2_3cm at the operating conditions of 283 K and 70 bar by employing fuel gas mixture (brief description on each sample code was referred to page 108 and 116 (Table 4- 4) respectively)

5.3.2.2.Water conversion and maximum gas uptake

Table 5- 3 summarises the CO_2 dissolved in water and gas uptake for experiments that were conducted at 283 K and various IGCC operating pressures (58 and 70 bar) and sample bed heights. There was no hydrate growth observed for T1-5 (5.60 mol% THF and 0.01 mol% SDS) and T3-2 (0.01 mol% SDS and 0.10 mol% TBAB) at 58 bar for the experiment conducted at 3 cm bed height in 1200 minutes. Then the bed height was reduced from 3 to 2cm for both samples. As the bed height of T1-5 decreased from 3 to 2 cm, the amount of water available for hydrate also decreased from 3.9 to 2.3 mmol. The same result was also observed for T3-2 where the amount of water was reduced from 2.4 to 1.4 mmol. Consequently, the formation of hydrate was observed at both operating pressures when the sample bed height was reduced to 2 cm. However, the formation of hydrate was slow at 58 bar because no formation of hydrate was observed for T1-5 in 1200 minutes as compared to 70 bar in which the hydrate at 58 bar started to form after 2500 minutes duration.

The maximum water conversion to hydrate observed in Figure 5- 11 (a) showed that the highest conversion at the operating conditions of 283 K and 70 bar was obtained by T3-2 with a value around 20 mol%, followed by T1-5 (around 14 mol%). Also, the value for T1-5 at 58 bar (long experiment) was almost the same as at 70 bar (1200 minutes). Additionally, the highest gas uptake was observed for T3-2 at 70 bar with the value of 1.55 mmol of CO_2 per g of H_2O which was almost 0.44 mmol of CO_2 per g of H_2O higher than T1-5 as shown in Figure 5- 11 (b). Then, the gas uptake of T1-5 at 283 K and 58 bar for the long experiment was 1.09 mmol of CO_2 per g of H_2O. In conclusion, T3-2 demonstrated the best results when applied in the IGCC conditions in which the ratio of CO_2 molecules consumed per amount of water was higher by 0.008 mmol CO_2 per mmol of H_2O than T1-5.

Table 5- 3: Comparison of gas uptake at various IGCC operating conditions and bed heights of T1-5 and T3-2 (brief description on each sample code was referred to page 108 and 116 (Table 4- 4) respectively)

Sample	T1-5					T3-2				
Operating conditions	283 K & 58 bar		283 K & 58 bar		283 K & 70 bar	283 K & 58 bar		283 K & 70 bar		283 K & 70 bar
Bed height (cm)	3		2		2	3		3		2
Experiment	1	2	1	2[1]	1	1	2	1	2	1
No. of moles of water (mmol)	3.9	3.8	2.3	2.3	2.3	2.4	2.4	2.4	2.4	1.4
CO_2 formed in hydrate (mmol)	-	-	-	0.045	0.046	-	-	-	-	0.039
Ratio of CO_2 consumed per amount of water (mmol CO_2 per mmol of H_2O)	-	-	-	0.019	0.020	-	-	-	-	0.028
CO_2 uptake (mmol of CO_2/g of H_2O)	-	-	-	1.087	1.111	-	-	-	-	1.548

[1] **long experiment**

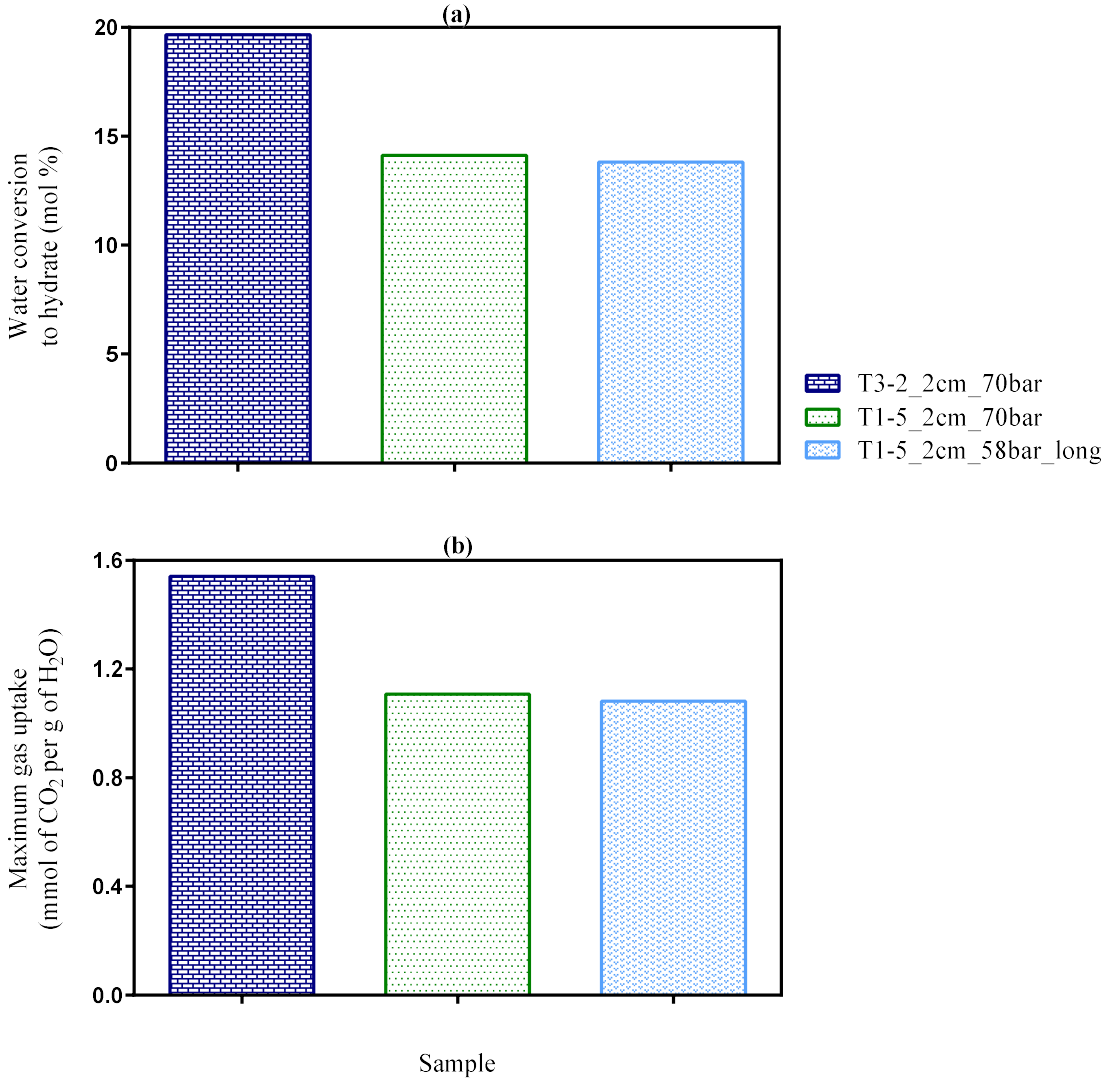


Figure 5- 11: Comparison of (a) water conversion to hydrate and (b) gas uptake for T1-5_2cm and T3-2_2cm at 283 K and various IGCC operating pressures (brief description on each sample code was referred to page 108 and 116 (Table 4- 4) respectively)

5.4.Long experiments

In general, hydrate formation is known to be a slow process since it involves several stages namely dissociation, nucleation and hydrate growth stages. Normally, studies have been performed between 600 to 1200 minutes by previous researchers because hydrate growth started to slow down between these periods. The highest water conversion to hydrate

reported by the literature and this work was around 60 mol%. Thus, some investigations in this work examined a period of more than 1200 minutes to further explore the growth of hydrate. Some experiments were performed by employing various samples in a pure gas system at different driving forces and also one experiment in a fuel gas system. The results for gas consumed are reported and compared with the experiment performed at 1200 minutes.

5.4.1. CO_2 solubility in water

Figure 5- 12 illustrates the solubility of CO_2 in water for several long experiments in pure CO_2 gas and fuel gas systems. In this investigation, the bed height of 3cm was employed unless otherwise stated. Generally, the trend of CO_2 solubility in water was increased for all experiments as the time increased. Only experiments that employed zeolite 13X did not show any improvement after 1200 minutes. Additionally, X13-5 did not show any hydrate formation at all after 2500 minutes. However, the hydrate formation was observed for X13-5 after the bed height was reduced from 3 to 2 cm with no further hydrate growth observed after 400 minutes.

Additionally, the most significant result was observed for T1-5 at 2cm bed height wherein the formation of hydrate occurred after 2500 minutes duration at 283 K and 58 bar in fuel gas mixture system. Moreover, the growth of hydrate was expected to continue because the mole fraction of CO_2 dissolved in water did not plateau within this period. However, for all long experiments in batch FBR, the trend of solubility of CO_2 in water was not consistently increased due to a series of numerous equilibrium states (Kobayashi et al., 2007). In conclusion, the solubility of CO_2 in water for both pure CO_2 and fuel gas systems for the long experiment was slightly improved by employing mesoporous silica gel, which was not the case for microporous silica gel.

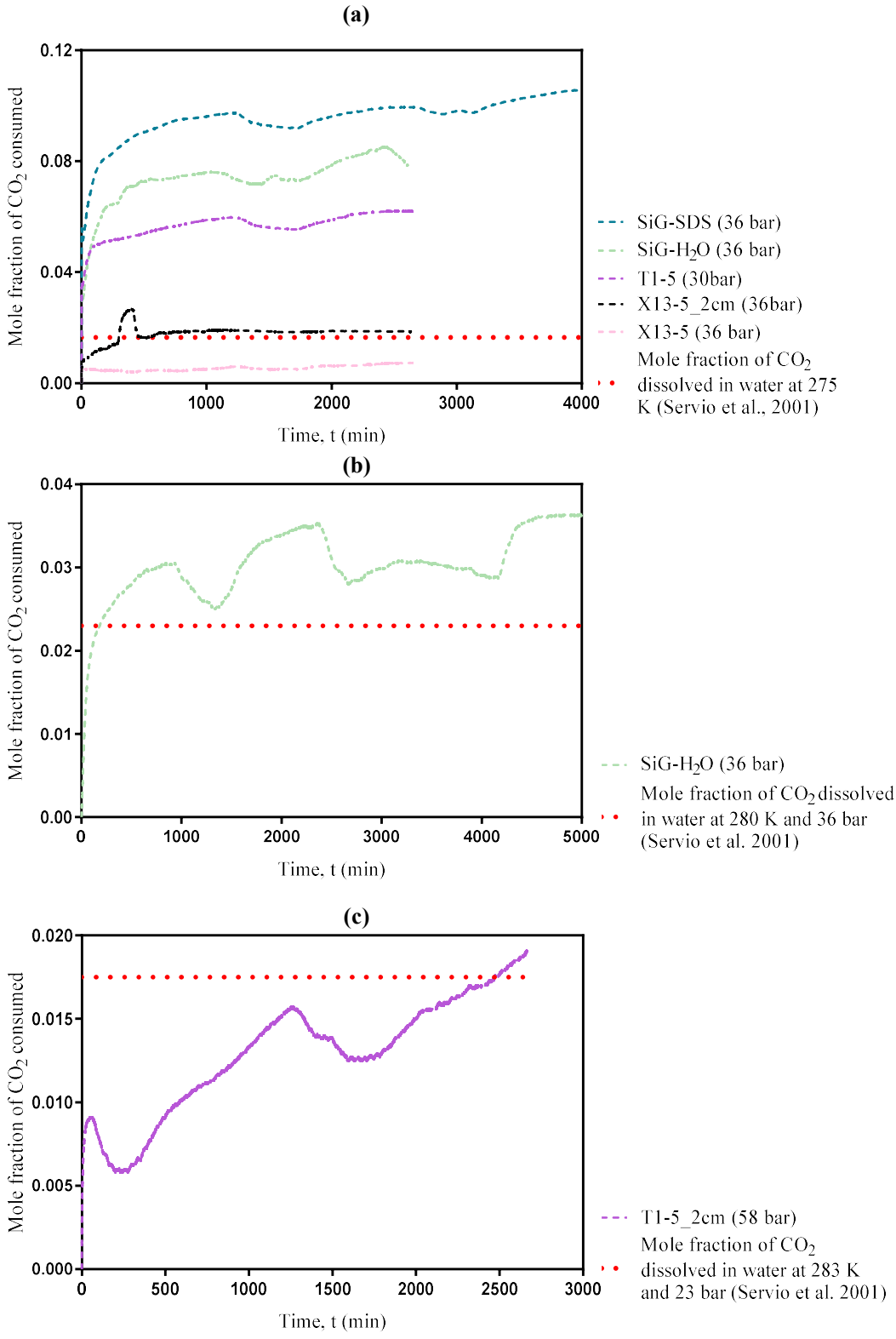


Figure 5- 12: CO_2 solubility in water for long experiments; (a) pure CO_2 gas system at 275 K and various driving forces, (b) pure CO_2 gas system at 280 K and 36 bar and (c) fuel gas system at 283 K and 28 bar (brief description on each sample code (T1-5 and 13X-5) was referred to page 108 and 128 respectively)

5.4.2. Water conversion to hydrate

Figure 5- 13 illustrates that as the duration of experiment went on, the total water conversion to hydrate increased where only zeolite 13X did not show significant increment. The maximum increment was observed for T1-5 in fuel gas mixture at 283 K and 58 bar with the increment of 13.82 mol% where hydrate growth could not be observed if the experiment was only performed in 1200 minutes as shown in Table 5- 4. This was followed by silica contacted with SDS at the operating conditions of 275 K and 36 bar with the value of 58.63 mol% after 4000 minutes, increment of 6.62 mol%. Moreover, the experiment by employing silica contacted with water showed a comparable increment which was around 3.50 mol% at the operating temperatures of 275 and 280 K respectively. T1-5 also showed an increment in pure CO_2 and fuel gas mixture with the value of 2.00 and 1.61 mol% respectively. In conclusion, the water conversion to hydrate was slightly improved as the duration of the experiment increased.

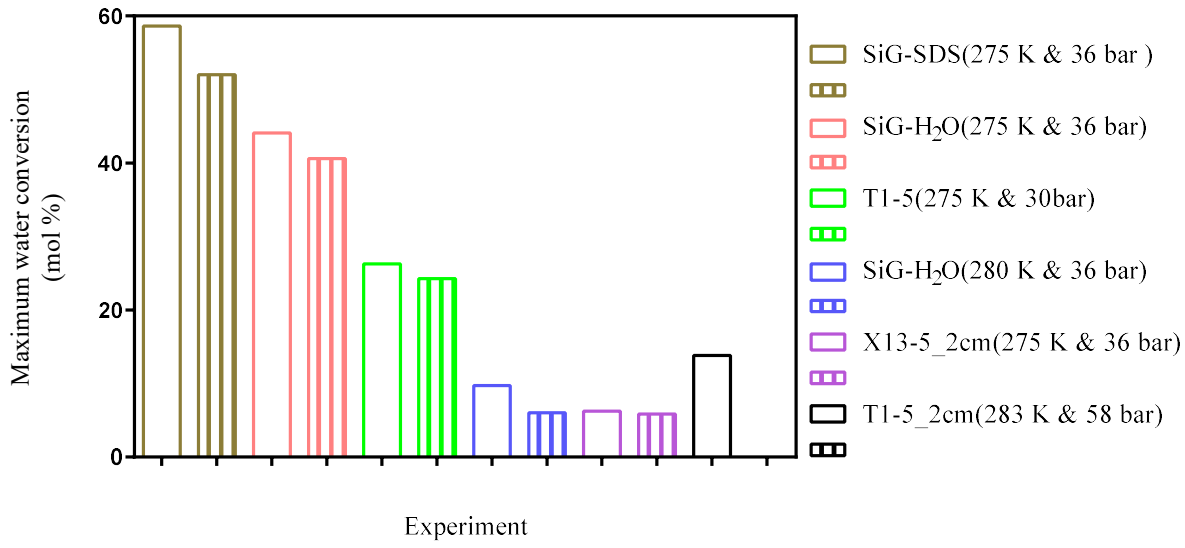


Figure 5- 13: Comparison of water conversion to hydrate at various experimental conditions; non-filled box indicates long experiments and filled-box indicates short experiments (brief description on each sample code (T1-5 and 13X-5) was referred to page 108 and 128 respectively)

Table 5- 4: Comparison of water conversion to hydrate for long and short experiments at various experimental conditions (brief description on each sample code (T1-5 and 13X-5) was referred to page 108 and 128 respectively)

Sample	Gas system	Experiment conditions	Experiment duration (min)	Water conversion to hydrate (mol%)	Increment (mol%)
SiG-SDS	Pure CO_2	275 K & 36 bar	4000 1200	58.63 52.01	6.62
SiG-H_2O	Pure CO_2	275 K & 36 bar	2500 1200	44.10 40.63	3.47
T1-5	Pure CO_2	275 K & 30 bar	2600 1200	26.26 24.26	2.00
SiG-H_2O	Pure CO_2	280 K & 36 bar	5000 600	9.73 6.01	3.72
X13-5_2cm	Pure CO_2	275 K & 36 bar	2600 1200	6.25 5.82	0.43
T1-5_2cm	Fuel gas mixture	283 K & 58 bar	2600 1200	13.82 -	13.82

5.5.Comparison with previous works

Generally, most of the literature has investigated CO_2 hydrate formation from fuel gas mixture in non-IGCC operating conditions whereas most experiments performed in this work particularly in this chapter used the IGCC conditions. Therefore, some additional experiments in fuel gas system at the operating conditions identical to the one investigated by previous researchers were reported in this section. Silica contacted with single promoter THF or TBAB were used in the non-IGCC conditions in order to make the operating conditions comparable to the literature.

The obvious difference was that some studies (Babu et al., 2014; Adeyemo et al., 2010) used macroporous silica in FBR whereas this work examined mesoporous silica. Also, some studies used semi-batch system (Babu et al., 2014; Park et al., 2013; Adeyemo et al., 2010) whereas this work examined the batch system. All experiments in the non-IGCC conditions were performed just once due to the high reproducibility and low error bar illustrated in the previous experiments. The comparison was performed for the IGCC conditions. Finally, the

comparisons between pure CO2 gas (this work) and fuel gas systems (literature) in the non-IGCC conditions were conducted to highlight the effect of H_2 molecules in the presence in fuel gas mixture system on hydrate formation.

5.5.1. Experiments on fuel gas mixture in the non-IGCC operating conditions

Initially, an experiment was performed at 275 K and 58 bar by employing T1-5 (5.60 mol% THF and 0.01 mol% SDS) at 3cm bed height but no hydrate formation was observed. The experiment was then repeated for a second time and still the same result was observed which indicated that the ratio of CO_2 molecules with the amount of water present in fuel gas system affected the formation of hydrate in this work. Hence, the bed height was reduced to 1.5cm which was comparable to Babu et al. (2014) where approximately 0.2g of silica contacted with promoter was used.

The investigation at 276 K and 60 bar by employing 0.29 mol% TBAB was performed and the gas uptake observed was 1.144 mmol of CO_2 per g of H_2O, which was comparable to Babu et al. (2014). Then, THF (3 mol%) was employed at the same operating conditions and the gas uptake obtained was 0.763 mmol of CO_2 per g of H_2O (in 1200 minutes) which was more than 50% higher than Adeyemo et al. (2010) in which THF (1 mol%) was contacted with silica gel at 274 K and 50 bar in a semi-batch FBR. This was expected due to higher driving force (ΔP) employed in this work. Then, the gas uptake reached 1.328 mmol of CO_2 per g of H_2O for the long experiment (5900 minutes) in this work with the same operating conditions. Also, in this work the gas uptake for 0.29 mol% TBAB was 38% higher than THF (3 mol%) at 276 K and 60 bar during 1200 minutes.

Subsequently, further experiments were performed at higher temperature and pressure, 286 K and 80 bar respectively, and the gas uptake obtained was 1.660 mmol of CO_2 per g of H_2O which was 42% more than Park et al. (2013) wherein THF (5.6 mol%) was employed

in semi-batch STR at 287 K and 80 bar. This result showed that THF is suitable for the IGCC operating temperature as shown by T1-5 and T3-2 (0.01 mol% SDS and 0.10 mol% TBAB) in the previous section. However, the only study obtaining a higher result compared to this work at comparable experimental conditions was Adeyemo et al. (2010). The 1.8 mmol of CO_2 per g of H_2O gas uptake achieved was almost 20% higher than this work in which silica gel was contacted with H_2O at 275 K and 80 bar. This was expected due to the semi-batch system employed in the literature. The results discussed in this section are summarised in Table 5- 5 and illustrated in Figure 5- 14.

Table 5- 5: CO_2 uptake for silica contacted with promoters at various non-IGCC operating conditions by employing fuel gas mixture in this work (brief description on T1-5 sample code was referred to page 108)

Sample	Experiment conditions	Bed height (cm)	Experiment duration (min)	CO_2 uptake (mmol of CO_2 per g of H_2O)
T1-5	275 K & 58 bar	3.0	1200	-
SiG-TBAB	276 K & 60 bar	1.5	1200	1.144
SiG-THF	276 K & 60 bar	1.5	1200	0.763
SiG-THF	276 K & 60 bar	1.5	5900	1.328
SiG-H_2O	275 K & 80 bar	1.5	1200	1.535
SiG-THF	286 K & 80 bar	1.5	1200	1.660

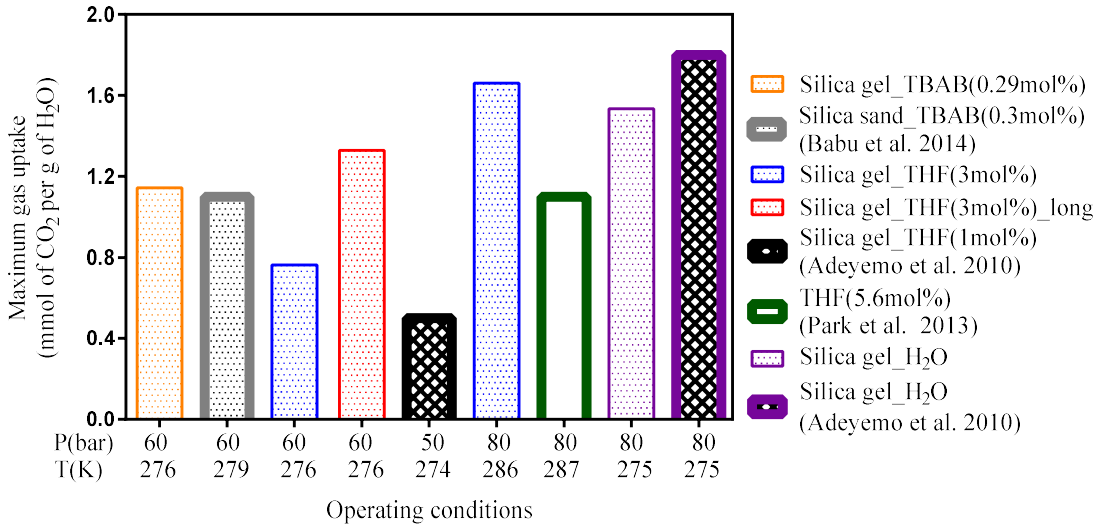


Figure 5- 14: CO_2 uptake at various non-IGCC operating conditions by employing fuel gas mixture (thick border – literature results; dotted – batch FBR, crossed – semi-batch FBR, unfilled – semi-batch STR)

5.5.2. Experiments on fuel gas mixture for the IGCC operating conditions

A comparison was performed between results achieved in this work with previous works for the IGCC conditions as shown in Figure 5- 15. The main reason was to highlight that the formation of hydrate achieved in this work by employing mesoporous silica in batch FBR at the IGCC conditions is feasible. Also, the advantage of employing horizontal batch FBR by Zheng et al. (2016) as compared to vertical configuration in this work is highlighted. Generally, the results obtained in this work by employing fuel gas mixture were lower than the one reported by Zheng et al. (2016) at the same bed height as this work (2 cm). However, the results achieved in this work were higher than Babu et al. (2016).

The highest result was recently achieved by Zheng et al. (2016) with a gas uptake of 2.4 mmol of CO_2 per g of H_2O by employing 5.56 mol% THF and silica sand (macroporous silica) in batch FBR at 283 K and 60 bar wherein they discovered that the gas uptake of horizontal orientation was 1.5 times greater than the vertical. This was followed by results achieved in this work by employing T3-2 (0.01 mol% SDS and 0.10 mol% TBAB) and T1-5 (5.60 mol% THF and 0.01 mol% SDS). The best result was observed for T3-2 at 283 K and 70 bar wherein the gas uptake obtained was 1.548 mmol of CO_2 per g of H_2O which was approximately 40% higher than T1-5. Also, the lower gas uptake obtained by T1-5 at 283 K and 58 bar (long experiment) with the difference of 0.461 mmol of CO_2 per g of H_2O as compared to T3-2 at 283 K and 70 bar was due to the difference in driving force. Finally, these were followed by Babu et al. (2016) with the gas uptake of 0.8 mmol of CO_2 per g of H_2O in the presence of 5.56 mol% THF in batch STR for the IGCC operating conditions (283 K and 60 bar).

The low results obtained in this work as compared to Zheng et al. (2016) in fuel gas mixture for the IGCC conditions were expected due to the employment of mesoporous silica which shifted the hydrate phase equilibria to the inhibition region (Park et al., 2013). Also, their

horizontal batch FBR meant a larger cross sectional area was available as compared to the vertical configuration. In contrast, the low results obtained in batch STR by Babu et al. (2016) as compared to batch FBR in this work was expected due to the large amount of contact area available inside the porous medium as compared to bulk solution. Also, the ΔP employed in this work was 10 bar higher than Babu et al. (2016).

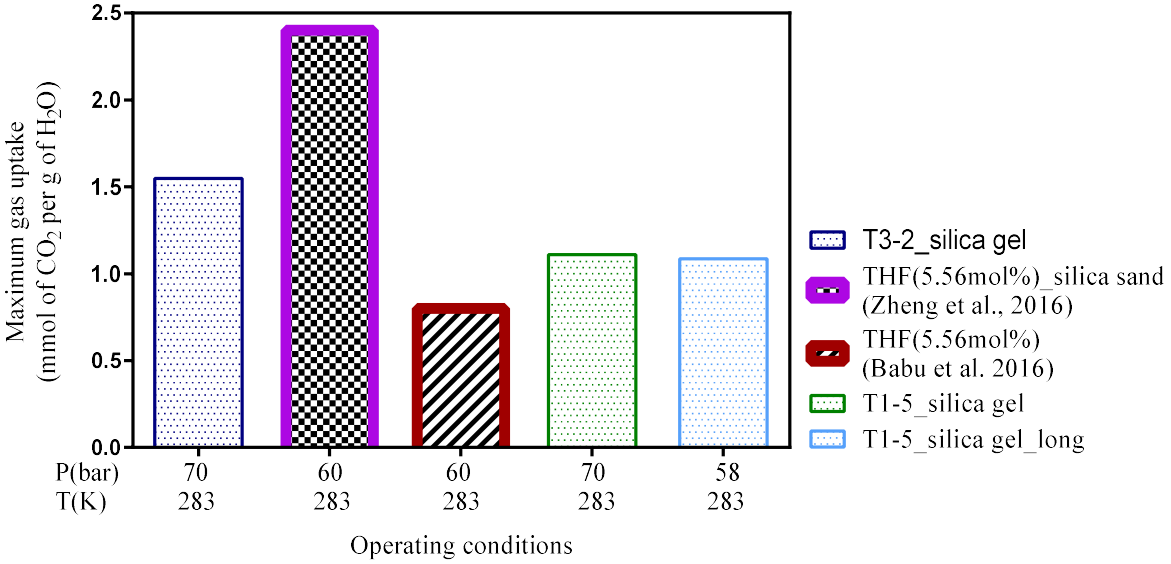


Figure 5- 15: CO_2 uptake at various IGCC operating conditions by employing fuel gas mixture (thick border – literature results; dotted – vertical batch FBR, grid – horizontal batch FBR, slanted – batch STR)

5.5.3. Comparison between pure CO_2 gas and fuel gas mixture systems

Generally, most of the results that employed pure CO_2 gas (at 36 bar) as an adsorbate in this work demonstrated greater gas uptake as compared to the fuel gas mixture used in the literature as illustrated in Figure 5- 16. This comparison is necessary so that the factors that affected hydrate formation can be highlighted. The bed height (silica gel) used for each experiment that employed pure CO_2 gas as an adsorbate in this work was 3cm whereas some of the past studies used 1.5cm bed height of silica sand (Babu et al., 2014; Babu(c) et al., 2014). As previously discussed, low bed height can enhance

hydrate formation. Also, it was noted that the use of combined-promoters, high driving force and low pore size silica in this work also affected the formation of hydrate.

The highest gas uptake obtained in this work was shown by T1-5 in which silica gel was contacted with 0.01 mol% SDS mixed with 5.6 mol% THF which was comparable to T3-2 where silica gel was contacted with SDS (0.01 mol%) mixed with TBAB (0.1 mol%) at 275 K and 36 bar. The gas uptake obtained for both samples was around 5 mmol of CO_2 per g of H_2O. Meanwhile, the best CO_2 uptake obtained in the literature was reported by Babu(c) et al. (2014) with a value of around 4 mmol of CO_2 per g of H_2O. They used propane as a promoter in batch FBR (100 nm pore size silica sand) with the presence of fuel gas mixture at 274 K and 60 bar (P_{CO2} = 24 bar). This result was comparable to T1A-2 (0.01 mol% SDS and 0.10 mol% EGME) combined-promoter used in this work at 275 K and P_{CO2} = 36 bar. Even though the driving force (ΔP) used by them was lower than this work, but the shorter bed height and macroporous silica contacted with propane were expected to give this relatively great result. Therefore, the result achieved by Babu(c) et al. (2014) is considered a great achievement for the implementation of batch FBR in fuel gas mixture. Yet, the operating temperature of 274 K was far below the IGCC operating temperature.

As for the application of a single promoter in this work, the 3 mol% THF gas uptake at 275 K and P_{CO2} = 36 bar was almost 0.75 mmol of CO_2 per g of H_2O higher than reported by Babu et al. (2014) in which 5.53 mol% THF was employed in batch FBR consisting of silica sand at 279 K and P_{CO2} = 24 bar. Their lower driving forces (ΔP and ΔT) were expected even though the bed height used was lower than this work. However, 1 mmol of CO_2 per g of H_2O gas uptake obtained by 0.29 mol% TBAB at 275 K and P_{CO2} = 36 bar in this work was comparable to 0.3 mol% TBAB in batch FBR consisting of silica sand at 276 K and P_{CO2} = 24 bar reported by Babu et al. (2014). Even though

their driving force was lower than this work, the shorter bed height (macroporous silica) employed was expected to give this result.

For the silica contacted with water at 275 K and P_{CO2} = 36 bar, the gas uptake achieved in this work was approximately 1.5 mmol of CO_2 per g of H_2O higher than the one reported by Babu et al. (2013) in semi-batch FBR at the 5cm bed height of silica sand. Since, the operating conditions were the same, it was expected that the presence of H_2 molecules in fuel gas mixture affected the hydrate formation obtained by Babu et al. (2013). Also, the lower results observed in some past studies employing fuel gas mixture were due to the lower CO_2 partial pressure used, between 24 to 32 bar, which resulted in a lack of driving force. Thus, the factors affecting hydrate formation are a bit complicated. A detailed explanation of each factor affecting hydrate formation is presented in chapter 6.

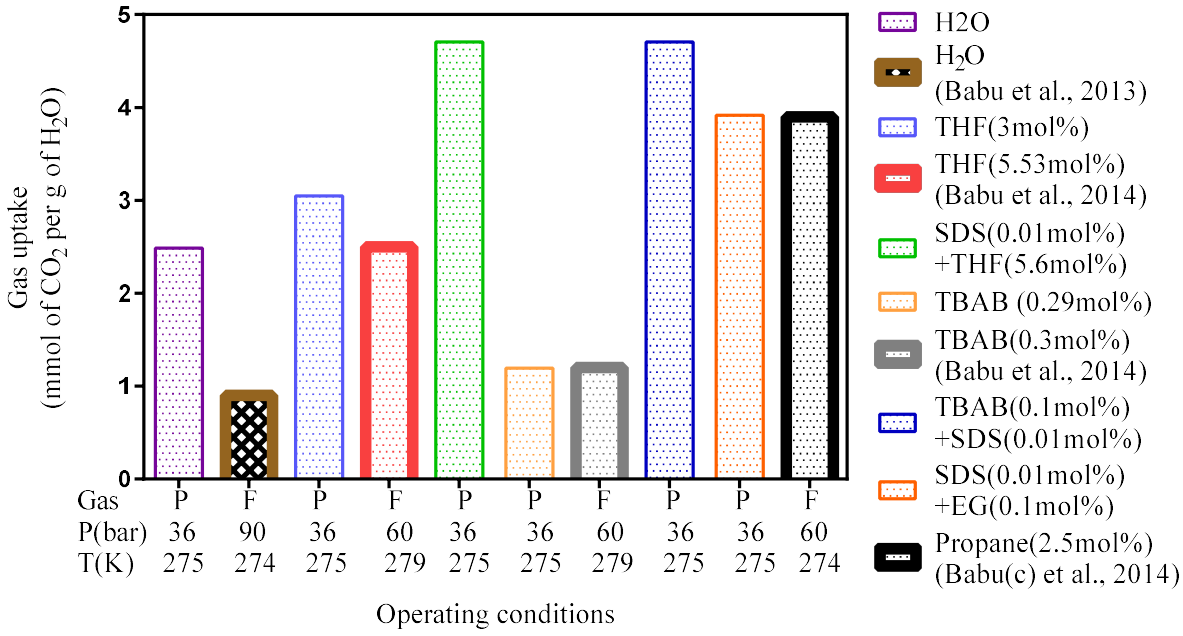


Figure 5- 16: Comparison of gas uptake between pure CO_2 gas and fuel gas mixture systems after 120 min by employing silica in non-IGCC conditions (thick border – literature results; dotted – batch FBR, crossed – semi-batch FBR; P-pure CO_2 gas, F-fuel gas mixture)

5.6.Summary

i. Overall, the gas uptake for all samples in hydrate forming conditions increased as the driving force (ΔP) of the pure CO_2 system increased. Combined-promoters designated type T1-5 (5.60 mol% THF and 0.01 mol% SDS) demonstrated the best result with the value of CO_2 uptake increasing from 0.86 ± 0.09 to 5.95 ± 0.21 mmol of CO_2 per g of H_2O as ΔP increased from 5 to 19 bar at constant temperature (275 K). In contrast, the gas uptake was reduced from 5.95 ± 0.21 to 0.45 ± 0.07 mmol of CO_2 per g of H_2O as ΔT increased from -5 to 13 K at constant pressure (36 bar).

ii. In general, the amount of available water inside silica gel pores determined the total number of CO_2 molecules captured through hydrate formation. Combined-promoters designated type T3-2 (0.01 mol% SDS and 0.10 mol% TBAB) captured the fewest CO_2 molecules at all driving forces due to the lowest amount of available moisture content. However, T3-2 achieved an optimum result at the CO_2 partial pressure of 30 bar (identical to the IGCC operating pressure of 70 bar) where the total number of CO_2 molecules captured was 0.01 mmol higher than the baseline experiment (0.13 mmol) due to synergic effect.

iii. The study on non-hydrate forming region by employing pure CO_2 gas led to the selection of 283 K and 58 and 70 bar as the operating conditions in the IGCC by employing fuel gas mixture wherein combined-promoters designated types T1-5 and T3-2 were chosen as an adsorbent.

iv. By reducing the bed height of T1-5 from 3 to 2 cm, the formation of hydrate was achievable with minimal gas uptake (1.09 mmol of CO_2 per g of H_2O) observed after 2500 minutes at 58 bar and 283 K using fuel gas mixture. A comparable amount of CO_2 uptake (1.11 mmol of CO_2 per g of H_2O) by T1-5 was observed

at 70 bar after 1200 minutes due to a higher driving force applied. The same trend was observed for T3-2, however the gas uptake was 0.44 mmol of CO_2 per g of H_2O higher than T1-5 at 70 bar and 283 K which indicated that T3-2 was the most suitable combined-promoter to be employed in the IGCC conditions.

v. The total water conversion to hydrate for all samples at various operating conditions increased as the duration of the experiment increased with only zeolite 13X not showing any significant increment. The most significant result was observed for T1-5 (2cm bed height) at 283 K and 58 bar where no formation of hydrate was observed in the first 1200 minutes, however 13.82 mol% of water conversion to hydrate was obtained in 2600 minutes.

vi. The experiments employing fuel gas mixture in batch FBR demonstrated that the lower CO_2 uptake (1.55 mmol of CO_2 per g of H_2O) obtained in this work as compared to Zheng et al. (2016) (2.40 mmol of CO_2 per g of H_2O) in the IGCC conditions was expected due to the decreased activity of water in the presence of H_2 molecules when silica with small pore sizes was employed (Park et al., 2013) and also due to the vertical batch FBR.

vii. Also, the lower CO_2 uptake (1.66 mmol of CO_2 per g of H_2O) obtained in batch FBR system in this work as compared to semi-batch FBR obtained by Adeyemo et al. (2010) (1.80 mmol of CO_2 per g of H_2O) by employing silica gel contacted with water was expected due to the decreased driving force given that the existence of H_2 molecules compete with CO_2 molecules in batch FBR. Additionally, the use of macroporous silica gel by Adeyemo et al. (2010) shifted the hydrate phase equilibrium to the hydrate forming region.

CHAPTER 6: DISCUSSION OF RESULTS

6.1.Introduction

First, the reason method 4 (the highest rates of stirring) sample preparation was selected in this work is discussed. Then, the mechanism of hydrate formation in batch FBR in this work is described in detail by referring to the experiment of T3-2 (0.01 mol% SDS and 0.10 mol% TBAB) at 283 K and 70 bar in chapter 5. Subsequently, various factors (reported in chapters 3-5) that affected hydrate formation in this work such as the use of combined-promoters (chapters 4 and 5), variation in driving force (chapters 3 and 5), impact of employing mesoporous silica in batch FBR especially in fuel gas mixture (chapter 5), bed height roles (chapter 5) and the amount of equilibrium moisture content available inside silica pores are explained (chapters 3-5).

6.2.Vigorous stirring increased the amount of equilibrium moisture content inside silica gel pores as well as gas uptake with minimum error bars

The effect of a sample preparation method is firstly discussed in this chapter to show that the vigorous stirring in method 4 slightly enhanced hydrate formation due to the increased equilibrium moisture content (as shown in chapter 3; Table 3- 2) as compared to other methods (methods 1-3; Table 3- 1). Also, method 4 was selected given the minimum error bars (Figure 3- 4) and enormous reproducibility of hydrate formation when all samples prepared by this method were employed in CO_2 gas (as shown in Tables 3- 3, 3- 7, 4- 8 and 5- 1).

The amount of water available inside silica pores is vital for the formation of CO_2 hydrate in batch FBR. Previously, Babu et al. (2013) and Adeyemo et al. (2010) used a magnetic stirrer and Park et al. (2013) used ultrasonic wave during sample preparation with the same

intention - to aid dispersion of water inside silica pores. However, the sample prepared by method 4 with vigorous stirring using a high speed blender in this work had the highest equilibrium moisture content with the lowest CI which was 14.79 ± 0.34 wt%. As for methods 1-3 in this work, the amount of equilibrium moisture content was almost identical which was around 13.68 wt% but the CI for method 2 (gentle stirring by magnetic stirrer) was the lowest among those three with the value of ±0.51 wt%. Both methods 1 and 3 without stirring demonstrated quite high CI values, ±2.45 and ±2.87 wt% respectively (these results were reported in Table 3- 2).

Studying total water conversion to hydrate further showed the significance of vigorous stirring as summarized in Table 3- 3. The sample prepared by the highest rates of stirring (method 4) had the highest water conversion to hydrate, 40.5 ± 2.28 mol%, followed by method 2 (40.3 ± 3.42 mol%), method 1 (40.0 ± 4.84 mol%) and method 3 (37.9 ± 4.46 mol%). The same trend for CI was observed in water conversion to hydrate as shown by equilibrium moisture content. Also, the total number of CO_2 molecules consumed was the highest for the sample prepared by method 4: 0.29 mmol which was almost 0.03 mmol higher than the other samples.

The results observed in this work agreed with the one obtained by Wang et al. (2008) wherein the formation of methane hydrate for the sample (mixture of silica and water) stirred at the highest speed attained the highest gas uptake. Additionally, Rajnauth et al. (2012) mentioned that gas hydrate has a high gas to solid ratio where 1 ft^3 of hydrate contains 150-180 ft^3 of gas per ft^3 of water. Since the sample prepared by method 4 had the highest moisture content, this is the main explanation for the highest CO_2 uptake attained. Furthermore, the implementation of method 4 for the preparation of silica contacted with combined-promoter in this work showed fairly high regeneration results (T3-2; 0.01 mol% SDS and 0.10 mol% TBAB) with CI value of ± 0.34 mmol of CO_2 per g of H_2O as shown

in Table 4- 5. High regeneration and repeatability (Table 5- 1) were similar to past studies with consistent results using silica sand and PU foam (Babu et al., 2014; Babu(c) et al., 2014; Mekala et al., 2014). Hence, the results observed explain the advantages of the vigorous stirring process during sample preparation as the amount of water that gets occluded inside silica gel pores (Babu et al., 2015) is overcome and beneficial for the utilisation of water in hydrate formation.

The vigorous stirring of the silica mixture with water employed by several researchers (Dawson et al., 2014; Wang et al., 2008) and this work is useful because water droplets are surrounded by a network of silica which prevents coalescence of the droplets (Wang et al., 2008) thus increasing the amount of water inside silica pores. Wang et al. (2008) mentioned that the higher the mixing speed, the lower the average particle size which increased the gas-water interfacial surface area for hydrate formation due to the presence of dispersed water phase. Moreover, Yuan et al. (2013) stated that a small contact angle was observed when the liquid spread on the surface, while a large contact angle was observed when the liquid beads (compact liquid droplet) exist on the surface. This contact angle is closely related to the spreadability or wettability (Zisman, 1964) in which a small contact angle ($< 90^{o}$) indicates that wetting of the surface is favourable thus increasing the interaction between CO_2 gas-water with porous medium and as a result, enhancing hydrate formation. Yuan et al. (2013) added that small droplets and bubbles are spherical, which gives a minimum surface area for a fixed volume and increases the surface tension of water. Thus, the use of vigorous stirring which dispersed water molecules is expected to reduce the surface tension of water inside silica pores.

6.3.Hydrate formation mechanism in the HPVA

The mechanism of CO_2 hydrate formation in the HPVA (or batch FBR) in this work is discussed by referring to the P-t curve (Figure 6- 1) for the experiment that employed T3-2 (0.01 mol% SDS and 0.10 mol% TBAB) at 283 K and 70 bar in chapter 5. In general, the P-t curve for all experiments that exhibited hydrate formation either in pure CO_2 (Figure 3- 2) or fuel gas mixture systems showed a similar trend. Thus, the P-t curve for the best result attained in the IGCC conditions was preferred and presented in detail.

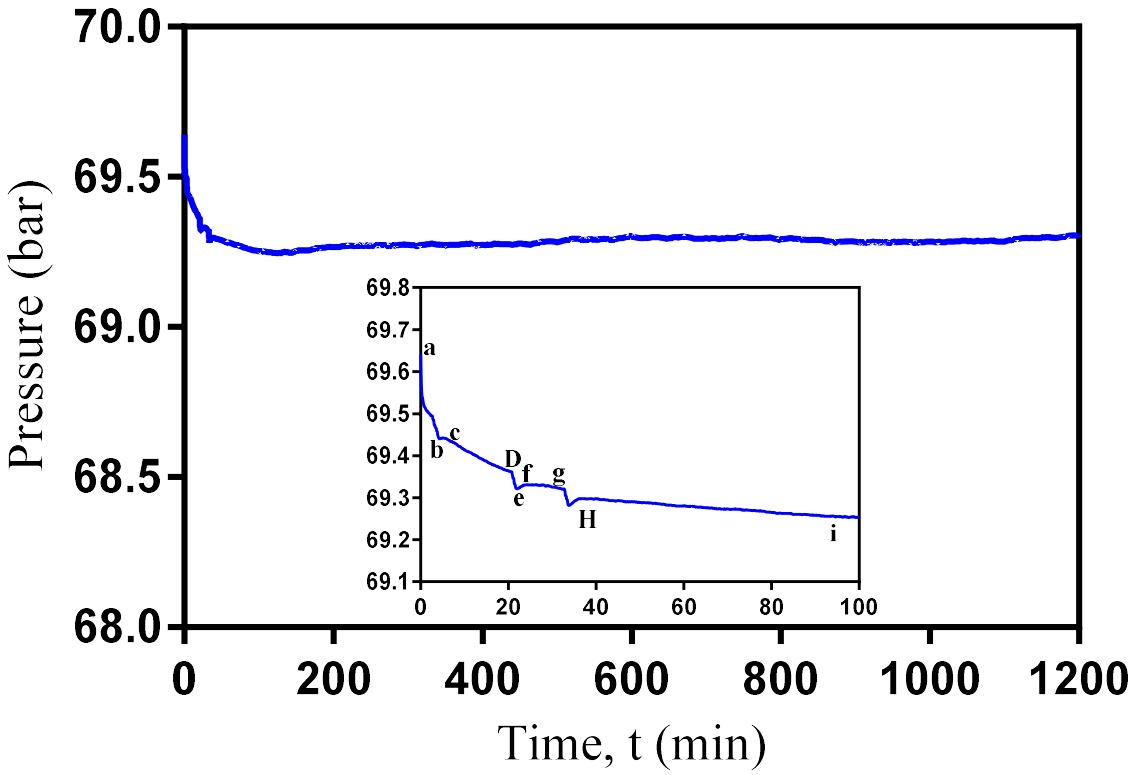


Figure 6- 1: P-t curve for T3-2 at 283 K and 70 bar in fuel gas mixture system after 1200 minutes inside batch FBR (insert is the P-t curve for the first 100 minutes; points D & H are the process repetition of point b-c and e-g respectively) (brief description on T3-2 code was referred to page 116 (Table 4- 4))

As seen in Figure 6- 1, the first 100 minutes showed several stages of pressure drop in which Tang et al. (2013) mentioned that there must be at least a two-stage pressure drop to demonstrate the formation of hydrate. Additionally, the first stage of pressure drop indicates

the dissolution of CO_2 in water and the subsequent stages indicate hydrate growth. In this work, point **a-c** is considered the first stage of pressure drop. Initially, point **a-b** indicates that the dissolution of CO_2 in water happened around 5 minutes in which Sloan et al. (2008) stated that upon dissolution of gas in water, labile clusters form immediately. Concurrently, labile clusters started to agglomerate by sharing faces, thus increasing disorder which explained no pressure drop from point **b-c**. This process continued until the size of the cluster agglomerate reached a critical value at point **c** wherein Sloan et al. (2008) said this was the point where primary nucleation happens. Also, Tang et al. (2013) described the time from point **a-c** as an induction time for hydrate formation. Moreover, the fast induction time observed in this work which was less than 10 minutes by employing FBR agreed with the one reported in the literature (Zheng et al., 2016; Babu et al., 2014 & 2013; Linga et al., 2007).

Then, the second stage of pressure drop was observed immediately after point **c** and this significant pressure drop is known as the hydrate growth stage. After that, the same process as seen from point **b-c** is repeated at point **D** where the pressure became constant in a period of less than 1 minute before hydrate growth continued until point **e**. Next, from point **e-f** the sudden increase in pressure was observed and according to Kobayashi et al. (2007) is due to the batch system keeping itself in thermodynamic equilibrium which also means the system was urged to move to a new equilibrium state. Thus, it is expected that from point **f-g** enough driving force was available for hydrate growth to slightly occur. Then, the repetition of process **e-g** was seen at point **H**. Kobayashi et al. (2007) said this transient hydrate forming process was observed as a series of numerous equilibrium states which slightly differed from the previous state due to a quasi-static and irreversible change in state. Consequently, these explained the significant two-stage pressure drop observed in the initial

stage (the first 20 minutes) before being followed by several small pressure drops (until 100 minutes) until no more drop in pressure was observed in batch FBR as indicated by point **i**.

6.4.Various factors that affected hydrate formation

Babu et al. (2015) discussed several factors that considerably affect the rate of hydrate formation such as type of promoters employed, operating pressure and temperature which provide driving force to the system, gas (adsorbate) used and reactor configuration. They also reviewed the effect of adsorbent's pore size employed in FBR which was previously reported by Adeyemo et al. (2010) and bed height influence on CO_2 uptake discovered by Babu et al. (2014). These factors together with the effect of various equilibrium moisture contents available in the system that were investigated in this work are discussed.

6.4.1. Synergic effect of combined-promoters

Three well-known promoters were studied in this work namely SDS, TBAB and THF due to their capability to promote hydrate formation (as shown in Table 3- 7). Each promoter was extensively investigated by previous researchers where SDS (Kumar et al., 2013; Lim et al., 2013; Silva et al., 2013; Tang et al., 2013) can avoid the development of obstructing hydrate film whilst TBAB (Babu et al., 2014; Kim et al., 2011; Li et al., 2010; Shimada et al., 2005) and THF (Babu et al., 2014; Park et al., 2013; Silva et al., 2013; Tang et al., 2013; Yang et al., 2013; Adeyemo et al., 2010; Lee et al., 2010) can form semi-clathrate and sII hydrates respectively. Both types of hydrate are said to entrap more CO_2 molecules in the small cage of sII hydrate and semi-clathrate hydrate cavities correspondingly (Yang et al., 2015). Moreover, several researchers (Torre et al., 2015; Ricaurte et al., 2014; Silva et al., 2013; Yang et al., 2013) have investigated the effect of combining SDS and THF on CO_2 hydrate formation and they discovered that the synergic effect improves hydrate formation. Recently,

Yang et al. (2015) reported the synergic effect of THF and TBAB combined-promoter by performing a study on the hydrate phase equilibrium. However, the synergic effect of combining SDS and TBAB has not yet been reported in the literature. Thus, this section will explain the synergic effect of combined-promoters used in this work (T1 – SDS+THF, T2 – THF+TBAB and T3 – SDS+TBAB) in which an overall effect on hydrate formation was greater than the sum of individual effects of any of the promoters (Biology-online). Also, the role of EGME in promoting hydrate formation when combined with SDS (T1A) as an alternative to THF which is known to be harmful and difficult to handle (Torre et al., 2015) is highlighted. As mentioned in chapter 1, SDS was found to inhibit the formation of hydrate without stirring or the presence of porous medium (Ho et al. 2013; Lim et al., 2013). Consequently, the investigations performed in this work by employing FBR filled with silica gel contacted with combined-promoters especially in the presence of SDS encountered this issue (as shown in Tables 4- 3, 4- 5, 4- 7, 4- 9 and 5- 2).

6.4.1.1. Thermodynamically shifted hydrate phase equilibrium in the IGCC conditions

One of the most important findings in this work was the ability of combined-promoters to shift the hydrate phase equilibrium to a higher operating temperature. No proper experiment on phase equilibrium investigation was performed in this work (Tables 5- 2 and 5- 3). However, the final experimental pressure of this isochoric system was used as a guideline to determine the equilibrium pressure at the experimental temperature since most of the experimental pressures plateaued after hydrate growth at 1200 minutes (Appendix 8 – Figure A- 13). This observation is considered reliable because Yang et al. (2015) and Joshi et al. (2013) used almost the same method to determine the hydrate phase equilibrium in

their work. Figure 6- 2 and Figure 6- 3 demonstrate the hydrate phase equilibrium for pure CO_2 (refer to Table 5- 2) and fuel gas systems (refer to Table 5- 3) respectively.

As described earlier, the use of solid adsorbent for hydrate formation will lead to the use of FBR whilst STR is required for a bulk system. Previously, some works on the application of FBR by using pure CO_2 gas were performed by Yang et al. (2015 & 2013), Mekala et al. (2014) and Kumar et al. (2013). Kumar et al. (2013) and Mekala et al. (2014) investigated FBR in which 0.25mm silica gel and 0.46mm silica sand (particle sizes) were employed respectively with no improvement in hydrate phase equilibrium compared to bulk water (Carrol, 2009) as shown in Figure 6- 2.

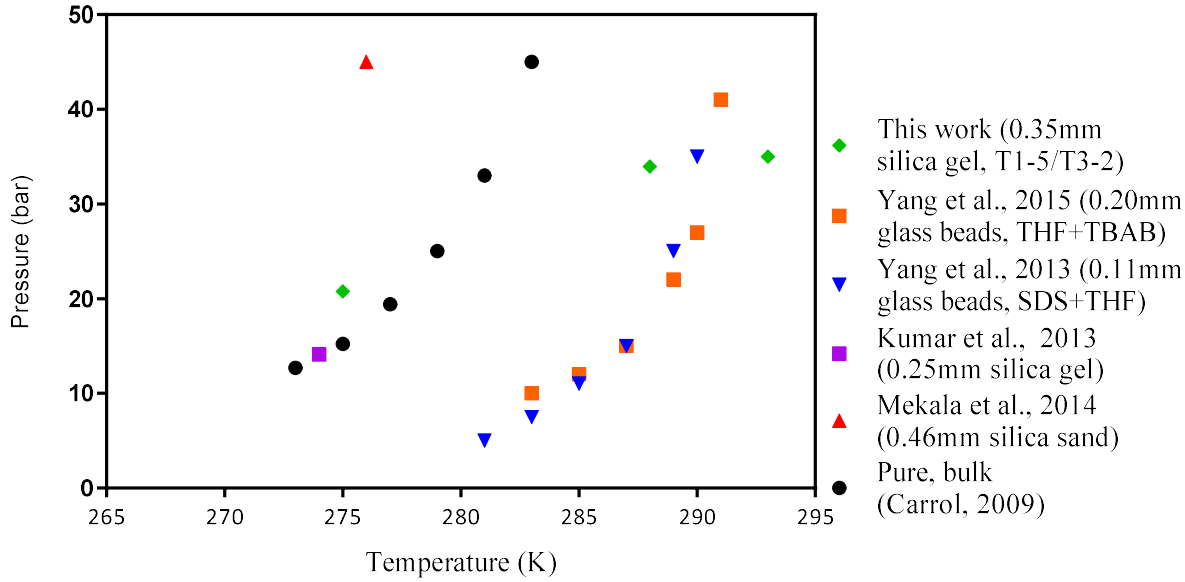


Figure 6- 2: Hydrate phase equilibrium of pure CO_2 gas (comparison with the literature)

However, Yang et al. (2015 & 2013) managed to prove that the application of combined-promoters at optimum concentrations (3 mol% THF & 0.01 mol% SDS) & (5 mol% THF & 5 mol% TBAB) inside glass bead pores shifted the phase equilibrium to a higher temperature region (290 and 291 K respectively). In addition, Yang et al. (2015) also discovered that both THF and TBAB showed the same role in thermodynamically shifting

the phase equilibrium to a higher temperature region. At the same concentration of TBAB (5 mol%), the temperature increased from 286 to 291 K at the operating pressure of 35 bar as the concentration of THF increased from 0-5 mol%. Also, at the same concentration of THF (5 mol%) and 35 bar, the temperature was observed to increase from 289 to 291 K as the concentration of TBAB increased from 0-5 mol%.

Moreover, Joshi et al. (2013) reported that the addition of SDS did not mitigate the phase equilibrium of the CO_2-TBAB-H_2O system while Yang et al. (2015) mentioned that SDS is known as a kinetic additive which can change the kinetic properties and has no influence on the hydrate phase equilibrium (Kumar et al., 2015). Thus, the presence of 5.6 mol% THF & 0.1 mol% TBAB in T1-5 (5.60 mol% THF and 0.01 mol% SDS) and T3-2 (0.01 mol% SDS and 0.10 mol% TBAB) combined-promoters respectively inside silica gel in this work (as shown in Table 5- 2) promoted the phase equilibrium to 293 K and not the existence of 0.01 mol% SDS.

As for fuel gas system, some researchers employed the FBR (Park et al., 2013) and STR (Park et al., 2013; Kim et al., 2011; Kumar et al.,2006). Park et al. (2013) found that the phase equilibrium was shifted to the higher temperature region as the particle size of silica gel increased from 6 to 100 nm as illustrated in Figure 1- 24 (chapter 1). However, they concluded that the use of silica gel in FBR shifted the hydrate phase equilibrium to the inhibition region of bulk water (STR) due to the presence of geometrical constraints (capillary effect). Figure 6- 3 shows that the use of promoters in the STR such as 3 mol% TBAB (Kim et al., 2011) and 5.6 mol% THF (Park et al., 2013) promoted the phase equilibrium to the IGCC conditions with the need for stirring during hydrate formation.

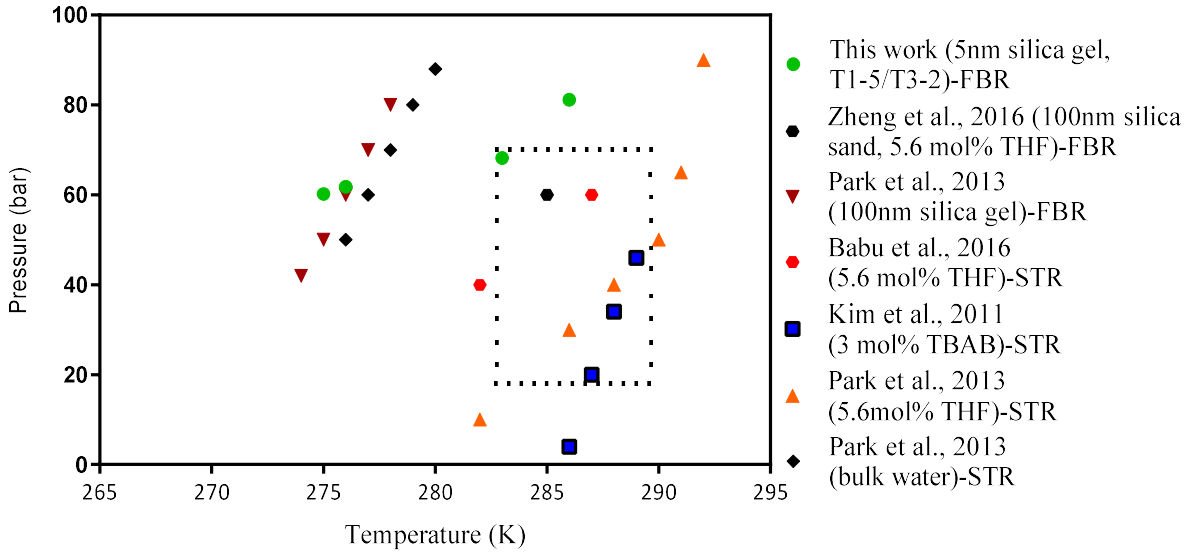


Figure 6- 3: Hydrate phase equilibrium of fuel gas (comparison with the literature); black-dotted region represents the IGCC operating conditions

Zhang et al. (2014) performed phase equilibrium measurements for the THF-SDS-CO_2-N_2-H_2O system at a fixed SDS concentration of 1000 ppm and various concentrations of THF in the presence of glass beads and the phase equilibrium shifted to a higher temperature (293 K at 90 bar) as the concentration of THF increased from 0-5 mol%. This indicated that the presence of THF can greatly increase the driving force of the system which also means mitigating the hydrate formation condition (Tang et al., 2013).

In addition, Babu(b) et al. (2014) investigated the formation of hydrate in the system of $TBANO_3$- CO_2-H_2-H_2O where $TBANO_3$ is also known as one type of semi-clathrate hydrate such as TBAB. They discovered that by introducing $TBANO_3$ in a fuel gas mixture system, the heat of dissociation increased significantly and also this semi-clathrate hydrate is said to be more stable than hydrate formed from the fuel gas mixture. Consequently, these contribute in shifting the hydrate phase equilibrium to the higher temperature region wherein this effect is expected if $TBANO_3$ is substituted by TBAB in that system.

Recently, Babu et al. (2016) managed to observe CO_2 hydrate formation in fuel gas mixture at the operating temperature of 279-287 K and operating pressure of 40-60 bar by employing 5.56 mol% THF in batch STR. Then, Zheng et al. (2016) managed to observe CO_2 hydrate formation at 285 K and 60 bar by employing 5.56 mol% THF contacted with silica sand inside batch FBR which demonstrates the continued interest in improving hydrate formation with FBR to make it instantly feasible in the IGCC operating conditions. Hence, the application of T3-2 (0.01 mol% SDS and 0.10 mol% TBAB) and T1-5 (5.60 mol% THF and 0.01 mol% SDS) combined-promoters in the FBR in this work (as shown in Table 5- 3) which thermodynamically shifted the hydrate phase equilibrium of fuel gas mixture to the IGCC conditions in the presence of silica gel was expected due to the thermodynamic effect of TBAB and THF respectively.

6.4.1.2. Improvement in hydrate formation and kinetics

In this section, only the results from the pure CO_2 system (as shown in Tables 3- 7, 4- 3, 4- 5, 4- 7, 4- 9 and 5- 2) were analysed because all combined-promoters investigated in this work were tested in this system whereas for fuel gas mixture system (Table 5- 3), the top two optimum combined-promoters (T1-5 & T3-2) were studied. The initial experiments employing a single promoter in pure CO_2 gas system at 275 K and 36 bar for 600 minutes in this work (Table 3- 7) showed the highest conversion of water to hydrate for SDS (0.01 mol%) which was almost 50 mol% conversion. This was followed by THF (3 mol%) with the conversion of almost 45 mol%, only 5 mol% more than the baseline experiment. Sowjanya et al. (2014) mentioned that a simple criterion for a guest molecule to encase in a vacant cage demands that the ratio for molecular diameter to vacant cage diameter should be in the range 0.76-1.00 (Appendix 9 – Table A- 8) Thus, this slight increase was due to CO_2 molecules (guest molecule) in double hydrates (CO_2-THF hydrates) competing with THF

molecules because most of the CO_2 molecules will occupy large cages of sI hydrate structures with only a small amount occupying smaller cages of sI and sII hydrate structures which was not the case for SDS (only CO_2 hydrate presence).

As for SDS, Kumar et al. (2015) explained the effect of SDS on lowering the contact angle (the gas-liquid interface meets a solid surface) which created a film-like interface along the reactor wall and porous medium. This film is believed to be the preferred location for nucleation and initiation of hydrate growth. According to Yuan et al. (2013), small contact angles ($< 90^o$) correspond to high wettability, while large contact angles ($> 90^o$) correspond to low wettability. Thus, the formation of hydrate is expected to fully utilise the space and surface available inside the reactor which increased the consumption of water and CO_2 molecules. This explained the higher water conversion attained by SDS as compared to THF. The results obtained agreed with the trends obtained by Kumar et al. (2013) and Park et al. (2013). Kumar et al. (2013) managed to slightly improve the system of silica gel-water-CO_2 from 51 to 54 mol% with the addition of 0.02 mol% SDS while Park et al. (2013) reported that by adding 5.6 mol% THF to the system of CO_2-H_2-water, the amount of hydrate formed slightly increased by 5%. In contrast, THF demonstrated the highest water conversion to hydrate at 288 K and 36 bar with more than 20 mol% conversion followed by SDS with 15 mol% conversion. The highest value obtained by THF as compared to SDS justifies the thermodynamic ability of THF to enhance the driving force of hydrate formation at the higher experimental temperature.

Next, the use of T1-1 (brief description of T1 code was referred to page 108) combined-promoter managed to improve the result to approximately 60 mol% and also significantly enhanced the kinetics (as shown in Table 4- 3). Further increasing the THF concentration to 5.6 mol% (T1-5) considerably increased the water conversion to hydrate to around 65 mol% in 600 minutes. The results obtained by SDS-THF (T1) combined-promoter in this work

showed the same trends as Torre et al. (2015) and Yang et al. (2013). Torre et al. (2015) reported that the CO_2 consumed during hydrate formation was almost doubled when THF was employed in the system of SDS-water-CO_2. Moreover, the kinetics of hydrate formation increased drastically with the addition of SDS in the system consisting of glass beads-water-THF-CO_2 as reported by Yang et al. (2013). The presence of THF hydrate (THF:17H_2O - Sloan et al., 2008) enhanced the cage occupancies in the hydrate lattice (Park et al., 2013) by forming sII hydrate which allowed some CO_2 molecules to occupy the small cavities available (Tang et al., 2013). Also, the existence of THF was expected to dramatically decrease the hydrate phase equilibrium pressure (Yang et al., 2013) which resulted in an increased driving force (ΔP) of hydrate formation.

Additionally, the co-existence of SDS in FBR sped up the hydrate growth rate by forming micelles (Kumar et al., 2013) which facilitated gas molecule solubilisation (Tang et al., 2013) or enhanced gas-water interactions which reduced the induction time of hydrate nucleation (Kumar et al., 2015). SDS also avoided the development of obstructing hydrate film (Kumar et al., 2013) which not only enhanced the mass transfer but also changed the morphology of hydrate formation (Kumar et al., 2015). Yang et al. (2013) concluded that the combination of SDS+THF can efficiently promote hydrate formation and allow a full water-to-hydrate conversion, apart from the moderate conditions for the hydrate formation reaction. Thus, these explained the synergic effect of several T1 combined-promoters observed in this work wherein CO_2 uptake, water-to-hydrate conversion and the kinetics improved significantly (Table 4- 3).

For other types of promoters, Babu et al. (2014) investigated the performance of employing 0.3 mol% TBAB in FBR containing silica sand in fuel gas mixture and the gas uptake attained was 1.2 mmol of CO_2/g of H_2O at the operating conditions of 279 K and 60 bar (P_{CO2} = 24 bar). Moreover, they managed to obtain gas uptake of 2.5 mmol of CO_2/g of H_2O

when 5.53 mol% THF was employed at the same operating conditions. However, the result obtained in this work by employing combined-promoter, T2-1 (0.29 mol% TBAB and 3 mol% THF) in FBR that contained pure CO_2 gas at 275 K and 36 bar (Table 4- 5) showed the hydrate inhibition process in which the gas uptake obtained was 60% less than silica contacted with water (baseline experiment). In addition, the use of TBAB alone at 0.29 mol% (Table 3- 7) also inhibited the formation of hydrate by almost half as compared to the baseline experiment. Both CO_2 uptake for T2-1 and TBAB alone after 1200 minutes (1.6 & 2.0 mmol of CO_2/g of H_2O respectively) were higher than TBAB alone attained by Babu et al. (2014) due to the higher driving force employed in pure CO_2 gas system (P_{CO2} = 36 bar) in this work.

T2-1 inhibited hydrate formation (Table 4- 5) given that the formation of pure TBAB hydrate lack gas-filled cavities (Yang et al., 2015; Li et al., 2009). Babu(b) et al. (2014) mentioned that one possible reason for the low gas uptake in the presence of semi-clathrate hydrate is due to its ability to readily form semi-clathrate hydrate with water at hydrate forming conditions in which TBA^+ occupies the large cages leaving the small cages empty/partially empty with gas molecules. Moreover, the formation process and hydrate species are said to be very complex in the THF-TBAB-CO_2 system due the ability of both promoters to separately participate in hydrate formation and the hydrate species are very different (Yang et al., 2015).

As for T3-1 (0.01 mol% SDS and 0.29 mol% TBAB) combined-promoter, the gas uptake obtained (Table 4- 5) was almost double the T2-1 (3 mol% THF and 0.29 mol% TBAB) which was expected due to the presence of SDS but still 25% lower than the baseline experiment. However, by reducing the concentration of TBAB from 0.29 mol% (T3-1) to 0.1 mol% (T3-2) at the same SDS concentration (0.01 mol%), the gas uptake increased tremendously to 5.57 mmol of CO_2 per g of H_2O (Table 4- 5) which was approximately 40%

higher than the baseline experiment. This was expected because more CO_2 molecules could participate in hydrate formation due to the reduced TBAB hydrate formation which also meant diminishing lack of the gas-filled cavities problem. Thus, more investigations need to be performed on T2 combined-promoter at lower TBAB concentrations to understand the formation of hydrate especially in THF-TBAB-CO_2-H_2 for implementation in the IGCC.

THF is known to have several drawbacks such as high volatility (readily shifts to the vapour phase) and lowers the selectivity towards CO_2 uptake in the hydrate phase compared to the unpromoted system (Herslund et al., 2014). Zare et al. (2015) discovered that the addition of a small amount (0.01 mol%) of EGME to ionic liquids enhanced the formation of methane hydrate while it inhibited the process at the concentration of 0.1 mol%. Since EGME (flash point = 317 K) has almost comparable properties with THF (flash point = 259 K) such as high miscibility in water with higher flash point, it was used in this work to study the effect on CO_2 hydrate formation. Several concentrations of EGME were combined with 0.01 mol% SDS (Table 4- 7) and 0.1 mol% EGME (T1A-2) was found to be the optimum concentration in which the conversion of water to hydrate was almost 60 mol% and CO_2 uptake was 5.45 mmol of CO_2 per g of H_2O after 1200 minutes. With only 0.5 mmol of CO_2 per g of H_2O deviation from T1-5 (5.60 mol% THF and 0.01 mol% SDS) as shown in Table 4- 8, EGME can be a good alternative to THF when being combined with SDS and should be further investigated extensively in future work. Dhondge et al. (2011) studied the volumetric and viscometric of aqueous binary mixtures of EGME at 275 K and they observed a negative excess molar volume in the water rich region which was expected due to iceberg formation or hydrophobic interactions in the mixture. They concluded that EGME molecules act as structure maker solutes when dissolved in water. Moreover, Pandhurnekar et al. (2013) performed the same studies and they observed the same observation at 278 and 288 K at minimal concentration of EGME and as the concentration increased, this observation

diminished. They concluded that at minimum concentration of EGME in the water rich region, the formation of stable stoichiometric hydrate was observed. Thus, the formation of hydrate in this work at low concentration of EGME was expected. Furthermore, future studies on the morphology of CO_2 hydrate formation in the presence of EGME need to be performed to fully understand the mechanism of hydrate formation in this condition.

6.4.1.3. Optimum concentration of each combined-promoter

Generally, the rate of hydrate formation observed in this work (chapter 4; Tables 4- 3 and 4-7) increased as the concentration of promoters increased until a certain level. Then, it reduced significantly when the concentration of the promoter exceeded the optimum level. Initially, various concentrations of T1 combined-promoter (Table 4- 3) were investigated in a pure CO_2 gas system in which concentrations of SDS varied from 0.005-0.1 mol% while the concentration of THF varied from 1-7 mol%. The optimum concentrations of SDS and THF were 0.01 mol% and 5.6 mol% respectively. At the highest concentration of SDS (0.1 mol%, T1-3), hydrate formation was inhibited where the CO_2 uptake was about 0.3 mmol of CO_2 per g of H_2O lower than the baseline experiment. Furthermore, at the highest concentration of THF (7 mol%, T1-7), the CO_2 uptake started to reduce when compared to the optimum concentration of THF (5.6 mol%, T1-5) with 0.5 mmol of CO_2 per g of H_2O deviation.

Tang et al. (2013) studied the influence of SDS and THF on CO_2 hydrate formation and they reported that as SDS concentration increases, split and loss fraction increase initially and then decrease slightly, resulting in decreased CO_2 hydrate formation. They also mentioned that the variations of split and loss fraction and hydrate formation depend on the concentration of THF added. Lee et al. (2010) studied CO_2 hydrate formation in fuel gas mixture in the presence of various concentrations of THF (0.5-3 mol%); as the concentration

of THF increased, the hydrate phase equilibrium was promoted to the lower pressure and higher temperature regions. However, they found that at the highest THF concentration, the CO_2 uptake obtained was not the greatest with 1 mol% THF providing the optimum result. The hydrate formation rate was believed to decrease with the addition of THF above the optimum concentration due to the pre-occupation of cavities by THF which resulted in fewer available cavities that could be occupied by CO_2 gas. They also mentioned that the lower hydrate formation observed at the lowest THF concentration was probably due to the limited large cages available for hydrate which resulted in the relatively small amount of small cages for the occupancy of CO_2.

Sowjanya et al. (2014) investigated the formation kinetics and phase stability of double hydrates of THF and CO_2 and they said the resultant hydrate structure was sII and the bulky THF molecules occupied the large cages leaving small cages vacant for CO_2 molecules. Therefore, the reduction in gas uptake obtained in this work above the optimum concentration of SDS and THF respectively were expected due to the difficulty of CO_2 hydrate to form with the massive amount of both molecules (SDS and THF) present in the system. Also, the lower CO_2 uptake obtained at the lowest concentrations of SDS and THF compared to the respective optimum concentrations was expected due to the lower synergic effect provided to the system at these concentrations.

Then, at THF concentration of 3 mol%, T2-1 combined-promoter was studied with the addition of 0.29 mol% TBAB (Table 4- 5) and hydrate formation was inhibited where the CO_2 uptake was 2.4 mmol of CO_2 per g of H_2O lower than the baseline experiment. Next, T3-1 combined-promoter was investigated wherein TBAB concentration remained the same at 0.29 mol% and was combined with 0.01 mol% SDS (Table 4- 5). The CO_2 uptake was double that of T2-1 but still 1 mmol of CO_2 per g of H_2O lower than the baseline experiment. Consequently, the TBAB concentration was reduced to 0.1 mol% and combined

with 0.01 mol% SDS (Table 4- 5) and it significantly promoted hydrate formation with gas uptake of 1.6 mmol of CO_2 per g of H_2O greater than the baseline experiment. Scondo et al. (2011) studied the effect of TBAB on hydrate formation from simulated flue gas and they discovered that too much TBAB will lead to the formation of pure TBAB hydrate with no CO_2 hydrate formation. Kim et al. (2011) investigated the formation of CO_2 hydrate from fuel gas mixture at various TBAB concentrations (0.5, 1.0, 3.0 and 6.0 mol% TBAB) and they found 1.0 mol% was the optimum concentration for hydrate formation in STR (batch mode). They said the decreased hydrate formation with increasing amount of TBAB above 1.0 mol% was probably due to the decreased relative amounts of water which resulted in decreased host molecules and/or insufficient CO_2 dissolution. Also, as previously mentioned the presence of porous medium in FBR shifted the hydrate phase equilibrium to the non-favourable hydrate region (Park et al., 2013). Thus, these might explain the inhibition effect observed when 0.29 mol% TBAB was employed in FBR (this work; Table 3- 7).

Next, EGME was studied as an alternative to THF (combined with 0.01 mol% SDS; Table 4- 7) and at a concentration of 0.01 mol% (T1A-1), the formation of hydrate was slightly promoted to 4.82 mmol of CO_2 per g of H_2O while it inhibited the process (3.78 mmol of CO_2 per g of H_2O) at the concentration of 1 mol% (T1A-3). However, with a 0.1 mol% concentration of EGME, the highest CO_2 uptake for type A1 combined-promoter was obtained at 5.45 mmol of CO_2 per g of H_2O. The presence of 0.01 mol% SDS in each combined-promoter was found to provide the required synergic effect to give a maximum effect on hydrate formation in this work (Table 4- 8). At this SDS concentration, the optimum concentration of other promoters when combined with SDS was 5.6 mol% for THF and 0.1 mol% for both TBAB and EG. Hence, it can be concluded that even though the hydrate phase equilibrium was mitigated to the favourable region of hydrate with the

presence of combined-promoter, it can significantly reduce the CO_2 uptake if the concentration of the promoter used was too low or too high.

6.4.2. Improving driving force

Babu et al. (2015) stated that an increase in the driving force generally increases the rate of hydrate formation. There were four factors that affected the driving force for hydrate formation in this work: variation in operating pressure (ΔP; Tables 3- 5, 5- 1, 5- 2 and 5- 3) or temperature (ΔT; Table 3- 5 and 3- 7), the implementation of combined-promoters (Tables 4- 3, 4- 5 and 4- 7), ratio of CO_2 to water molecules in batch FBR (section 3.5 – page 103, Tables 3- 3, 4- 9) and pore size of silica gel used (Table 4- 9). As for the first factor, it was reported in chapters 3 and 5 that the CO_2 uptake increased as the initial operating pressure increased (ΔP) at the same operating temperature (Tables 3- 5 and 5- 1). In contrast, CO_2 uptake decreased as the temperature increased (ΔT) at the same operating pressure (Tables 3- 5, 3- 7 and 5- 3) which indicated decreasing driving force. Babu et al. (2016) observed random induction times (2 min to about 6 h) for an experiment conducted at 287 K and 60 bar in fuel gas mixture and described this as a stochastic state which caused a decrease in average gas uptake.

For ΔP, the baseline experiment (silica gel contacted with water) in pure CO_2 showed that the CO_2 uptake improved tremendously from 0.32 to 4.04 mmol of CO_2 per g of H_2O as the initial operating pressure increased from 22 to 36 bar at 275 K. The same trend was observed in fuel gas mixture system and also when combined-promoter was employed to both pure CO_2 and fuel gas mixture systems. As for ΔT, the CO_2 uptake for T1-5 (5.6 mol% THF & 0.01 mol% SDS) was found to increase from 0.45 to 5.95 mmol of CO_2 per g of H_2O as the operating temperature decreased from 293 to 275 K at 36 bar.

The study on hydrate phase equilibria showed that when one of the operating conditions (temperature or pressure) remained constant, ΔP and ΔT increased as the initial operating pressure or temperature increased respectively. For example, at 275 K (equilibrium pressure = 17 bar), ΔP was calculated to be 19 and 5 bar when the initial operating pressure was 36 and 22 bar respectively. Additionally, at 36 bar (equilibrium temperature = 280 K), ΔT was calculated to be (-5 K) and 13 K when the operating temperature was 275 and 293 K respectively. Hence, based on the CO_2 uptake obtained, the increased ΔP and reduced ΔT signified the increased driving force which also enhanced hydrate formation which Babu et al. (2016) described as the pressure driving force or subcooling (the magnitude of the difference between the experimental and equilibrium pressure or temperature).

These also explained the hydrate phase equilibria promoting the lower pressure and high temperature regions when the thermodynamic promoters were introduced (as shown in Tables 4- 3, 4- 5 and 4- 7) which is the second factor that affects driving force. Thus, this was the reason CO_2 uptake was almost 2 mmol of CO_2 per g of H_2O higher than the baseline experiment when T1-5 and T3-2 (0.1 mol% TBAB & 0.01 mol% SDS) combined-promoters were employed in FBR (Tables 4- 3 and 4- 5). The effect of promoters in mitigating hydrate phase equilibria to the hydrate forming region was explained earlier in which THF and TBAB are known as thermodynamic promoters due to their ability to form sII and semi-clathrate hydrates respectively which attracted more CO_2 molecules to get involved in hydrate formation.

In addition, Gayet et al. (2005) discovered that with the presence of SDS in bulk water, hydrate grow as a porous structure on the reactor wall and liquid migrates from the bulk phase to the porous structure due to the capillary forces. So, vast hydrate formation on the reactor walls and porous medium were expected providing extra driving force with the involvement of more CO_2 molecules that enhanced the conversion of water to hydrate in this

work. So, for the third factor, the ratio of CO_2 to water molecules was expected to affect the driving force of hydrate formation in batch FBR (Tables 3- 3 and 4- 9) wherein Babu et al. (2015) said an increase in CO_2 content can be associated with an increase in driving force. Kobayashi et al. (2007) said a batch system is assumed to instantaneously keep itself in thermodynamic equilibrium and Mori et al. (2008) mentioned that the change in the gas-phase composition in batch mode is inevitably accompanied by a change in the guest-molecule composition in the hydrate instantaneously formed. These can be associated with the decrease in driving force in batch mode upon hydrate growth wherein in a pure CO_2 system in this work, this effect was only observed when the initial operating pressure was below 30 bar. At high initial operating pressure (36 bar), a massive ratio of CO_2 to water molecules was expected to provide extra driving force which explained the high CO_2 uptake obtained.

As for fuel gas mixture system, the presence of H_2 molecules compete with CO_2 molecules to interact with water molecules in batch FBR reducing the driving force which caused the low CO_2 uptake attained in this work as compared to a pure CO_2 system. Also, the lower CO_2 uptake obtained by zeolite 13X as compared to silica gel in this work (section 3.5 – page 103 and Table 4- 9) was expected due to the massive amount of water molecules present inside this microporous silica which also reduced the ratio of CO_2 to water molecules. However, this problem was resolved by reducing the bed height of silica inside this batch FBR (Table 4- 9). Thus, the ratio of CO_2 molecules available for hydrate formation compared to water molecules increased which also caused an increase in driving force.

As for the last factor, Adeyemo et al. (2010) reported that silica with higher pore size exhibited higher CO_2 uptake and also the best driving force for hydrate formation. This was another reason for lower CO_2 uptake obtained by zeolite 13 X (Table 2- 1 shows pore size)

as compared to silica gel in this work (Table 4- 9 shows CO_2 uptake). The effect of pore size on hydrate formation is further discussed in next section.

6.4.3. Mesoporous silica and batch FBR concurrently reduced hydrate formation in fuel gas mixture

Two types of adsorbate namely pure CO_2 gas and fuel gas mixture (40% CO_2 and 60% H_2) were investigated in this work regarding the formation of CO_2 hydrate in batch FBR by employing mesoporous silica gel (Tables 3- 7, 4- 3, 4- 5, 4- 7, 4- 9 and 5- 2). As for pure CO_2 gas system in FBR, Kumar et al. (2013) managed to slightly improve the system of silica gel-water-CO_2 in semi-batch mode from 51 to 54 mol% at the operating conditions of 274 K and 36 bar with the addition of 0.02 mol% SDS. Then, Mekala et al. (2014) managed to obtain higher hydrate conversion (59 mol%) as compared to Kumar et al. (2013) by employing silica sand-water-CO_2 at 276 K and 60 bar in batch mode. Even though they did not use a promoter, macroporous silica and high driving force were expected to result in this high hydrate conversion.

The highest hydrate conversion for pure CO_2 gas in FBR was achieved in this work with almost 70 mol% conversion by employing T1-5 (5.6 mol% THF & 0.01 mol% SDS) combined-promoter at 275 K and 36 bar (Table 4- 3). It was expected that at high operating pressure ($P_{CO2} \geq 36$ bar) and low operating temperature ($T \approx 275$ K), the driving force (ΔP) of more than 19 bar ($P_{eq} = 17$ bar) in batch mode (isochoric condition) was enough to give the same effect as in semi-batch mode (isobaric condition). This was expected due to massive CO_2 molecules present in the system fully contacting with water during hydrate growth. Thus, it was concluded that in pure CO_2 gas system, FBR in semi-batch mode did not really have an advantage as compared to batch mode.

The experiments with fuel gas mixture by employing mesoporous silica in batch FBR demonstrated quite significant observations in this work (Table 5- 3). The highest CO_2 uptake was approximately 1.548 mmol of CO_2 per g of H_2O at 283K and 70 bar by employing T3-2 (0.01 mol% SDS and 0.10 mol% TBAB) combined-promoter. Then, by employing T1-5 at the same operating conditions, the CO_2 uptake was approximately 1.111 mmol of CO_2 per g of H_2O. However, Babu(c) et al. (2014) managed to achieve massive gas uptake around 4 mmol of CO_2 per g of H_2O in batch FBR (100 nm pore size silica sand) with the presence of fuel gas mixture (60 bar) + 2.5 mol% propane + water. Yet, the operating temperature used (274 K) was far below the IGCC operating temperature. Their gas uptake was more than two times higher than the best result obtained in this work and was due to the combination of macroporous silica with propane which will be explained later.

Meanwhile, Babu et al. (2014) managed to obtain 1.1 mmol of CO_2 per g of H_2O CO_2 uptake by employing 0.3 mol% TBAB as promoter in batch FBR configuration where silica sand was also employed at 279 K and 60 bar. Even though this result was comparable to single TBAB (0.29 mol%) applied in this work (Table 5- 5), the higher ΔT by 3 K (T = 276 K, P = 60 bar) in this work is believed to omit the greater effect of macroporous silica employed by them. Consequently, the gas uptake was enhanced by around 0.4 mmol of CO_2 per g of H_2O when the combined-promoter (T3-2) was employed in this work wherein 0.01 mol% SDS provided a synergic effect with 0.1 mol% TBAB inside mesoporous silica gel pores (Table 5- 3).

Next, Zheng et al. (2016) managed to improve the gas uptake to 2.4 mmol of CO_2 per g of H_2O by employing 5.56 mol% THF in horizontal batch FBR with the presence of silica sand at 283 K and 60 bar. They discovered that the gas uptake of horizontal configuration was 1.5 times better than the vertical due to the larger cross sectional area available. Also, the

massive effect of large pore size silica on hydrate formation was expected to contribute to this high gas uptake and will be discussed in the next section. Additionally, the gas uptake obtained by Adeyemo et al. (2010) in semi-batch STR was almost 0.3 mmol of CO_2 per g of H_2O higher than this work (Table 5- 5) with the use of silica gel contacted with water at 275 K and 80 bar respectively. Thus, in a fuel gas system, the use of mesoporous silica inside vertical batch FBR was suboptimal as compared to macroporous silica inside horizontal batch FBR. Also, the use of macroporous silica gel inside semi-batch FBR was observed to surpass mesoporous silica gel inside batch FBR in this work.

Subsequently, the observed results are discussed in detail. As reported earlier in chapter 5, some CO_2 uptake of hydrate formation in pure CO_2 gas was higher than fuel gas mixture at almost comparable driving force. The most significance result observed was no CO_2 hydrate formed at 58 bar (P_{CO_2}= 23 bar; Table 5- 3) in fuel gas mixture as compared to pure CO_2 gas (P_{CO_2} = 22 bar; Table 3- 5) at the same operating temperature (275 K) and experimental conditions. Also, the result obtained by Babu et al. (2013) in fuel gas mixture at comparable operating conditions (275 K and P_{CO_2} = 36 bar) was 75% lower than pure CO_2 gas obtained in this work (Table 3- 5) when silica was contacted with water. Thus, the effect of H_2 molecules in fuel gas mixture was then reviewed to further understand the lower results obtained as compared to pure CO_2 in this work (Figure 5- 16).

The equilibrium pressure of H_2 hydrate in pure H_2-water system is approximately 5000-7000 bar (Figure 1- 17) at the temperature range of 274-280 K which served as the basis for CO_2 separation from H_2 in the IGCC. Though, some researchers have shown that in the presence of thermodynamic promoters, the H_2 hydrate phase equilibrium is tremendously mitigated to the lower pressure region and higher temperature region. Hashimoto et al. (2006) reported that the equilibrium pressure shifted within the range of 10-110 bar wherein the equilibrium temperature was between 277-283 K with the addition of 5.6 mol% THF and 286-288 K in

the presence of 3.6 mol% TBAB (Appendix 7 – Figure A- 12). This pressure range of 10-110 bar for pure H_2 gas is equivalent to P_{H_2} of 16-176 bar in fuel gas mixture which shows the possibility of H_2 molecules to participate in cage occupancy during CO_2 hydrate formation in the IGCC operating conditions.

Furthermore, Li et al. (2010) investigated the hydrate nucleation and growth kinetics of the simulated fuel gas mixture in the presence of TBAB in semi-batch mode. They discovered that when the driving force (ΔP) was more than 25 bar, H_2 prefers to go into the hydrate phase as compared to CO_2. Nevertheless, they also reported that the temperature has little effect on hydrate formation. Additionally, Veluswamy et al. (2014) managed to show the formation of H_2 hydrate in STR (batch mode) from pure H_2 gas system in the presence of THF or TBAB at 279 K and 120 bar. At these operating conditions, the P_{eq} for the system with THF was found to be 30 bar and for TBAB was approximately 10 bar. This 30 and 10 bar equilibrium pressure in pure H_2 was equivalent to P_{H_2} of 48 and 16 bar respectively in fuel gas mixture which theoretically also shows the possibility of H_2 molecules competing with CO_2 molecules around that operating temperature. Another reason for the lower results observed in the fuel gas mixture as compared to pure CO_2 in this work was expected due to the tiny amount of solubility of H_2 gas in water (Appendix 6 – Table A- 6 & Table A- 7) that reduced the availability of water for CO_2 hydrate to form in this batch system. Kim et al. (2011) said the decrease in hydrate formation in fuel gas mixture was probably due to the decreased relative amounts of water upon TBAB-CO_2-H_2 hydrate formation resulting in lower host molecules and/or insufficient CO_2 dissolution.

As for the effect of batch system on hydrate formation, some researchers explained the possible reasons for the reduced production of hydrate in this isochoric system. Kobayashi et al. (2007) said a thermodynamic system composed of the contents of the batch system is assumed to be subjected to a quasi-static, irreversible change in state, instantaneously

keeping itself in thermodynamic equilibrium. Moreover, Mori et al. (2008) mentioned that the change in the gas-phase composition in batch mode was inevitably accompanied by a change in the guest-molecule composition in the hydrate instantaneously formed. Both explanations from Mori et al. (2008) and Kobayashi et al. (2007)can be related to the decreased driving force in batch mode upon hydrate growth. Recently, Yang et al. (2015) investigated the effects on CO_2 hydrate phase equilibrium by employing glass beads in the presence of combined-promoter (THF and TBAB) in batch mode. They expected the effects of different additive concentrations on hydrate phase equilibrium curves would be weakened due to decreases in CO_2 gas when the pressure decreases in batch mode, which causes the production of hydrate to decrease. Thus, it was expected that the presence of H_2 molecules which compete with CO_2 molecules for cage occupancy in fuel gas mixture (Lee et al. 2010; Li et al., 2010; Linga et al., 2007) in batch mode would reduce the driving force in the system. This caused the low CO_2 uptake attained in this work as compared to Adeyemo et al. (2010) with the same experimental conditions (Figure 5- 14). The use of macroporous silica in semi-batch FBR can be the best system for hydrate formation in fuel gas mixture and will be considered in future work with the implementation of a combined-promoter.

6.4.4. Effect of silica pore size on hydrate formation

As previously mentioned in chapter 1, silica with higher pore size exhibited higher CO_2 uptake (Adeyemo et al., 2010) and also the best driving force for hydrate formation (Figure 1- 24). In addition, Kumar et al. (2013) showed that the water conversion to hydrate by employing silica gel with large surface area (0.13-0.25 mm particle size) was almost 50% higher than the silica gel with low surface area (0.04-0.06 mm particle size) with a comparable pore size. Recently, Zheng et al. (2016) managed to achieve gas uptake of 2.3 mmol of CO_2 per g of H_2O by employing 5.56 mol% THF and 100 nm silica sand at 283 K

and 60 bar. The combination of high pore size silica and horizontal orientation resulted in this high gas uptake. However, Babu(c) et al. (2014) managed to achieve massive gas uptake (4 mmol of CO_2 per g of H_2O) even though they employed batch FBR in vertical orientation wherein 100 nm pore size silica sand (1.5 cm bed height) was used in the presence of fuel gas mixture (60 bar) + 2.5 mol% propane + water at 274 K (non-IGCC operating temperature). This value was more than two times higher than this work (Figure 5- 16) at comparable operating conditions where 5 nm silica gel was contacted with 3 mol% THF. They mentioned that this massive gas uptake in batch mode was due to hydrate nucleation occurring in the interstitial large pore space between the silica sand particles. Then, drastic hydrate growth occurred in the hydrate formation region especially in the gas phase above the silica sand bed due to the ability of propane to draw water dispersed in silica sand to the gas phase region. Yet, the use of propane was not considered in this work because this flammable liquid is 1.5 times heavier than air which is highly dangerous in case of leakage (Clough, 2014).

Both silica gel and zeolite 13X used in this work were contacted with 0.01 mol% SDS and 5.6 mol% THF (T1-5 and 13X-5 combined-promoters respectively) and investigated in pure CO_2 gas at 275 K and 36 bar (Table 4- 9). Initially, no hydrate was observed at 3 cm bed height of X13-5 due to the massive amount of moisture content (5.7 mmol of H_2O) with respect to the amount of CO_2 molecules present in FBR. Then, at a comparable amount of equilibrium moisture content (around 3.6 mmol of H_2O), 13X-5 (2 cm bed height) was observed but the CO_2 uptake obtained was 10 times lower than T1-5 (3 cm bed height). These results were theoretically comparable to Adeyemo et al. (2010) where at a comparable pore volume, they reported that silica with smaller pore size and higher surface area exhibited three times lower gas uptake. Mu et al. (2008) reported that the properties of the porous medium such as pore size, porosity and connection of pores would affect the gas

diffusion rates. Furthermore, Park et al. (2013) mentioned that the capillary effect due to the presence of geometrical constraints caused the equilibrium lines to shift to the inhibition region which reduced the driving force of hydrate formation. They added that this effect was more significant at smaller pore sizes due to the decrease of the activity of water caused by the partial ordering and bonding of water molecules with hydrophilic surfaces of pores.

Thus, the results observed for 13X-5 in this work can be explained by the disadvantage of employing microporous silica for CO_2 capture through hydrate formation. However, this effect was reduced by decreasing the amount of zeolite 13X inside FBR or in other words decreasing the bed height from 3 to 2 cm during hydrate formation (Table 4- 9). The effect of bed height is discussed in the next section.

6.4.5. Bed height roles in enhancing hydrate formation

In this work, reducing the bed height of silica inside batch FBR enhanced the hydrate formation (Tables 4- 9 and 5- 3). The investigation employing zeolite 13X (13X-5) in pure CO_2 showed no hydrate formation after 1200 min when the bed height was 3cm but the CO_2 uptake due to hydrate formation increased significantly when the bed height was reduced to 2cm. For fuel gas mixture, the formation of hydrate was observed at 283 K and 70 bar after the bed height of silica gel (T3-2; 0.01 mol% SDS and 0.10 mol% TBAB & T1-5; 5.60 mol% THF and 0.01 mol% SDS) was reduced from 3 to 2cm too (Table 5- 3). As previously discussed, the driving force of hydrate formation was enhanced by reducing the bed height of silica inside FBR due to the improvement in the ratio of CO_2 to water molecules which ensures more CO_2 molecules are available to interact with water molecules.

Massoudi et al. (1974) reported that the surface tension of water decreases as the pressure inside the CO_2-water system increases. Furthermore, they added that the drop in surface tension with pressure was somewhat larger at the lower temperature. Additionally, Zheng et

al. (2016) observed the increased CO_2 uptake in batch FBR as the bed volume reduced which was due to higher contact area to the ratio of gas phase and bed volume. They also added that a higher contact area to volume ratio provided a better heat transfer efficiency since more contact area was available per unit bed volume for heat exchange. Moreover, McCallum et al. (2005) observed a reduction in overpressure for the accumulation of hydrate at shorter bed volume (big size pressure vessel) as compared to higher bed volume (small size pressure vessel) at equivalent operating conditions. They said this may be attributed to the increase in contact area and gas concentration. Hence, the increased CO_2 to water molecules at shorter bed height in this work is believed to decrease the surface tension of liquid water or lowering the contact angle which increased the interaction between CO_2 gas-water with porous medium and as a result, enhanced hydrate formation.

6.4.6. Equilibrium moisture content affected total CO_2 consumed

The amount of equilibrium moisture content inside silica pores was affected by three factors in this work namely sample preparation method (Table 3- 2), concentration of combined-promoter used (Tables 4- 2, 4- 4 and 4- 6) and also the bed height of silica employed inside FBR (Tables 4- 9 and 5- 3). The first factor was previously discussed in the early part of this chapter in which the vigorous stirring process (method 4) was reported to give the highest moisture content inside silica pores which resulted in the highest CO_2 consumption. The second factor is quite straightforward in which the combined-promoter with the lowest combined-concentrations was found to have the highest equilibrium moisture content due to the increase in the ratio of water to combined-promoter molecules. The comparison between optimum combined-promoters (T1-5, T3-2 and T1A-2; brief description on each code was referred to page 108, 116 (Table 4- 4) and 121 (Table 4- 6) respectively) showed that the

total CO_2 consumption was directly proportional to the amount of equilibrium moisture content present in silica gel pores (Table 4- 8 and Appendix 4 – Table A- 5).

T1-5 combined-promoter with the highest moisture content (13.28 wt% or 3.7 mmol of H_2O) consumed the highest amount of CO_2 molecules (0.40 mmol) as compared to T3-2 (8.46 wt% or 2.4 mmol of H_2O) and T1A-2 (12.59 wt% or 3.5 mmol of H_2O) with the total CO_2 consumption of 0.24 and 0.35 mmol respectively. The slightly higher total CO_2 uptake observed for T3-2 (5.57 mmol of CO_2 per g of H_2O) as compared to T1A-2 (5.45 mmol of CO_2 per g of H_2O) was due to the lower moisture content for T3-2 combined-promoter. Thus, it was assumed that T1-5 and T1A-2 had higher equilibrium moisture content than T3-2 due to the high immiscibility of THF and EGME in water respectively as compared to TBAB. Since the THF molecule structure (C_4H_8O) is shorter than the EGME ($C_4H_{10}O_2$), this was the expected reason for T1-5 attaining higher equilibrium moisture content as compared to T1A-2 (0.01 mol% SDS and 0.10 mol% EGME) due to lower competition between THF and water molecules inside silica pores.

In contrast, for the same type of combined-promoter (Tables 4- 2, 4- 4 and 4- 6), the total CO_2 molecules formed in hydrate was not directly proportional to the amount of equilibrium moisture content available inside silica gel pores. For example, for T1 combined-promoters, T1-4 (brief description on T1-4 and T1-5 codes was referred to page 108) with the highest equilibrium moisture content (14.36 wt% or 4.0 mmol of H_2O) consumed less CO_2 as compared to T1-5 (13.28 wt% or 3.7 mmol of H_2O) with the difference around 0.05 mmol of CO_2. One of the reasons might be due to the effect of combined-promoter concentrations for hydrate formation as previously discussed in which the optimum concentrations for gas uptake was highest. Also, the total CO_2 consumed for each T1 combined-promoter was proportional to the respective gas uptake. The same trend was observed for other types of combined-promoters which indicated that the effect of equilibrium moisture content on the

total consumption of CO_2 was only significant when comparing different types of combined-promoters. Thus, for the same type of combined-promoter, the high ratio of water to combined-promoter molecules does not guarantee high consumption of CO_2 molecules. Conversely, at different bed heights of the same combined-promoter (Tables 4- 9 and 5- 3), the total CO_2 consumed was highly dependent on the amount of moisture content available inside silica pores. The most significance result was observed for zeolite 13X-5. With a high amount of equilibrium moisture content (5.7 mmol of H_2O), 13X-5 (3cm bed height) was not found to form hydrate whereas at 2cm bed height hydrate formation was observed (Table 4- 9). The reduced bed height meant reduced equilibrium moisture content to 3.4 mmol of H_2O (this value was similar to T1-5 and baseline experiment) indicating that high moisture content did not guarantee enormous hydrate formation. Moreover, by reducing bed height, the ratio of CO_2 molecules available for hydrate formation in batch FBR as compared to water molecules increased meaning increased driving force for hydrate formation.

Additionally, at a comparable amount of moisture content, mesoporous silica was found to have better CO_2 capture capability, 10 times higher than microporous silica (Table 4- 9). Hence, this result justified the finding obtained by Adeyemo et al. (2010) in which larger pores and particle size of silica were said to enhance the formation of hydrate. Park et al. (2013) mentioned that the capillary effect due to the presence of geometrical constraints caused the equilibrium lines to be shifted to the inhibition region and this effect was more significant at smaller pore sizes due to the decreased activity of water caused by the partial ordering and bonding of water molecules with hydrophilic surfaces of pores. The small pore size of zeolite 13X is expected to result in a high possibility of water molecules interacting with each other to give the same effect as in bulk water which reduces the advantage of using silica by omitting the stirring process.

Recently, Zheng et al. (2016) reported that low water saturation (50%) inside silica sand pores utilised more water for hydrate formation as compared to high saturation (100%). The CO_2 uptake at low water saturation was 25% higher than the high saturation at the same operating conditions. Zheng et al. (2016) and Babu et al. (2014 & 2013) reported the importance of interstitial spaces related to the kinetics of hydrate formation due to its low resistance for the diffusion of gases into the inter-particle spaces wherein liquid saturation in the bed was said to affect this interstitial spaces. Zheng et al. (2016) mentioned that for 100% saturation, the interstitial spaces between silica sand particles are fully occupied by water which means diffusion of gas molecules into the water is required for hydrate nucleation as well as hydrate growth. In contrast, gas molecules are said to readily be available in the interstitial spaces of 50% saturation, resulting in a larger contact area with water which ensures more chances for CO_2 molecules to interact with water.

In this work, the water saturation of X13-5 was calculated to be higher than T1-5 with values of 54% and 24% respectively (Table 4- 9 and Appendix 10). Li et al. (2013) stated that zeolite has strong moisture adsorption behaviour wherein the moisture content of zeolite is normally over 20% of its own weight. Thus, this higher water saturation as compared to T1-5 might be another reason for low CO_2 consumed observed for X13-5 at the same bed height and operating conditions.

6.5.Summary of the factors improving hydrate formation

Figure 6- 4 shows the factors that improved the formation of CO_2 hydrate in FBR (silica bed) by comparing pure CO_2 gas and fuel gas mixture systems. The importance of each factor that affected the formation of hydrate in both systems was ranked based on the results obtained in this work and some past studies (Zheng et al., 2016; Babu et al., 2014; Babu(c) et al., 2014; Adeyemo et al., 2010). There were three important factors that affected the

formation of hydrate in pure CO_2 gas system. The most important factor was the type of solid adsorbent used wherein mesoporous silica showed massive CO_2 uptake as shown in Table 4- 9 (4.04 mmol of CO_2 per g of H_2O) as compared to microporous silica (zeolite 13X; 0.58 mmol of CO_2 per g of H_2O). Next, the type of combined-promoter used was important in which combined-promoters designated type T1-5 (5.60 mol% THF and 0.01 mol% SDS) showed the greatest gas uptake (5.95 mmol of CO_2 per g of H_2O) out of all promoters that were investigated in this work (Table 4- 8). The final one was the driving force employed wherein pure CO_2 gas at 275 K and 36 bar demonstrated higher CO_2 uptake (baseline experiment; 4.04 mmol of CO_2 per g of H_2O) than fuel gas mixture system at 275 K and 80 bar (P_{CO2} = 32 bar) in non-IGCC conditions (baseline experiment; 1.54 mmol of CO_2 per g of H_2O) as shown in Figures 5- 14 and 5- 16. Also, 1.5 mmol of CO_2 per g of H_2O higher CO_2 uptake obtained in batch FBR (this work; Table 5- 1) as compared to semi-batch FBR (Babu et al., 2013) in pure CO_2 showed an insignificant effect of semi-batch mode when high driving force was employed.

Meanwhile, the factors that affected the formation of hydrate in fuel gas mixture were a bit complicated. The used of macroporous silica (Zheng et al., 2016; Babu(c) et al., 2014) was found to have greater CO_2 uptake than mesoporous silica in this work designated by T3-2 (0.01 mol% SDS and 0.10 mol% TBAB; 1.55 mmol of CO_2 per g of H_2O) as shown in Table 5- 3 wherein Babu(c) et al. (2014) demonstrated the highest CO_2 uptake in fuel gas mixture to date with the value of 4 mmol of CO_2 per g of H_2O in the presence of propane. Then, the use of semi-batch FBR for silica contacted with water by Adeyemo et al. (2010) was also found to have higher CO_2 uptake as compared to batch FBR in this work (Table 5- 5). The 1.8 mmol of CO_2 per g of H_2O gas uptake achieved was almost 20% higher than this work in which for both experiments silica gel was contacted with H_2O at 275 K and 80 bar. The use of high driving force also showed high gas uptake in all works indicating the CO_2

uptake in non-IGCC conditions was relatively higher than the IGCC conditions (Figures 5-14 and 5- 15).

As for the investigation in IGCC conditions (283 K and 58 bar) performed in this work (Table 5- 3), the used of 2cm silica gel bed height (T1-5; 1.09 mmol of CO_2 per g of H_2O) led to the formation of hydrate which was not the case for 3cm bed height. Moreover, combined-promoters designated type T3-2 was found to show higher gas uptake (1.55 mmol of CO_2 per g of H_2O) than T1-5 (1.11 mmol of CO_2 per g of H_2O) especially at the highest initial operating pressure (70 bar). Therefore, the use of combined-promoter contacts with macroporous silica in semi-batch FBR can further enhance CO_2 capture through hydrate formation in the IGCC which can be considered for future investigations.



Figure 6- 4: Factors that improved CO_2 capture through formation of hydrate

CHAPTER 7: CONCLUSIONS AND RECOMMENDATIONS FOR FUTURE WORK

7.1.Conclusions

The main focus of this study was to show that CO_2 capture through hydrate formation by employing mesoporous silica inside batch FBR was feasible in the IGCC conditions. Initially, the study on various sample preparation methods led to the selection of method 4 sample preparation (the highest rates of stirring) to be implemented in this work. Next, the investigation on several promoters in a pure CO_2 system led to T1-5 (5.60 mol% THF and 0.01 mol% SDS) and T3-2 (0.01 mol% SDS and 0.10 mol% TBAB) combined-promoters being employed in fuel gas mixture system due to their synergic effect on hydrate formation. Also, the study at various operating conditions by employing combined-promoters in pure CO_2 led to the selection of IGCC operating conditions of 283 K and 58 and 70 bar to be investigated in a fuel gas mixture system. Consequently, the findings obtained in this work were compared together with possible future works to further enhance CO_2 capture by HBGS technique.

7.1.1. Vigorous stirring during sample preparation enhanced hydrate formation

i) Method 4 sample preparation with the use of vigorous stirring was chosen in this work due to the highest equilibrium moisture content (14.79 ± 0.34 wt%) obtainedwhich led to the greatest water conversion to hydrate (40.5 mol%) in 1200 minutes. The high mixing speed (37,000 rpm) which resulted in the presence of dispersed water phase increased the gas-water interfacial surface area for hydrate formation.

ii) The repeatability of equilibrium moisture content and gas uptake attained for the sample prepared by the highest rates of stirring (method 4) was the greatest with the CIs of ±0.34 wt% and± 0.19 mmol of CO_2 per g of H_2O respectively because the amount of water occluded inside silica gel pores was not an issue or in other words vigorous stirring increased the spreadability.

iii) The execution of method 4 in preparing silica gel contacted with SDS (0.01 mol%) and THF (3 mol%) enhanced hydrate formation wherein the gas uptake obtained at 275 K and 36 bar after 600 minutes was higher than the baseline experiment (3.75 ± 0.01 mmol of CO_2 per g of H_2O) with the values of 4.68 ± 0.06 and 4.63 ± 0.06 mmol of CO_2 per g of H_2O respectively. However, silica gel contacted with TBAB (0.29 mol%) showed an inhibition effect on hydrate formation with the gas uptake of 1.98 ± 0.29 mmol of CO_2 per g of H_2O. Additionally, by employing silica gel contacted with THF and SDS, CO_2 hydrate was possible in non-hydrate forming conditions (288 K and 36 bar) with a gas uptake of 1.07 ± 0.07 and 0.50 ± 0.01 mmol of CO_2 per g of H_2O respectively.

7.1.2. Synergic effect of combined-promoters

i) SDS at 0.01 mol% improved hydrate formation when combined with any type of promoter with the optimum results obtained by T1-5 when SDS was combined with 5.6 mol% THF. The water conversion to hydrate for T1-5 was almost 70 mol%, the maximum gas uptake was 5.95 mmol of CO_2 per g of H_2O and the total CO_2 molecules consumed was 0.40 mmol. The synergic effect of T1-5 was obtained from SDS which avoided the development of obstructing hydrate film whilst THF formed sII hydrate which attracted more CO_2 molecules for occupancy in small cages.

ii) The inhibition effect demonstrated by silica gel contacted with TBAB at 0.29 mol% was improved when it was combined with 0.01 mol% SDS in which the CO_2 uptake obtained by this T3-1 sample was enhanced by 0.66 mmol of CO_2 per g of H_2O. Furthermore, when the concentration of TBAB was reduced to 0.1 mol% and combined with 0.01 mol% SDS, the CO_2 uptake of this T3-2 sample was improved tremendously to 5.57 $\pm$ 0.34 mmol of CO_2 per g of H_2O which was 38% greater than the baseline experiment. The role of TBAB in T3-2 combined-promoter provided more cavities for the occupancy of CO_2 molecules by forming semi-clathrate hydrate.

iii) However, the combination of TBAB (0.29 mol%) and THF (3 mol%) further inhibited hydrate formation in which this T2-1 sample had 31% lower gas uptake than the TBAB (0.29 mol%) alone due to the co-existence of TBAB semi-clathrate and THF hydrate. Moreover, the ability of TBAB to readily form semi-clathrate hydrate in hydrate forming conditions caused TBA^+ to occupy the large cage leaving the small cages empty/partially empty which reduced the formation of CO_2 hydrate to 0.29 mol% of TBAB.

iv) EGME was an alternative to THF where the optimum result was achieved at the concentration of 0.1 mol% when combined with 0.01mol% SDS. The gas uptake of this T1A-2 sample was 5.45 $\pm$ 0.12 mmol of CO_2 per g of H_2O which was just 9% lower than T1-5 and the total CO_2 molecules consumed was only 0.05 mmol lower. The role of EGME to provide this synergic effect was expected due to the ability of EGME molecules to act as structure maker solutes when dissolved in water.

7.1.3. Other factors that affected hydrate formation

i) Even though the hydrate phase equilibrium mitigated the hydrate forming region with the presence of combined-promoters, it significantly reduced CO_2 uptake if the concentration of the promoter used was too much below or above their respective optimum concentration. For example, combined-promoters designated type T1; the optimum CO_2 uptake was obtained for T1- 5 (5.95 mmol of CO_2 per g of H_2O) when the concentration of THF was at 5.6 mol% and SDS at 0.01 mol%. The CO_2 uptake was reduced to 4.23 mmol of CO_2 per g of H_2O when the concentrations of THF and SDS were reduced to 3 and 0.005 mol% respectively (T1- 6). When the concentration of THF was increased to 7 mol% and SDS was maintained at 0.01 mol% (T1- 7), the CO_2 was 5.43 mmol of CO_2 per g of H_2O. Also, by increasing the concentration of SDS to 0.02 mol% and reducing THF's concentration to 3 mol% (T1- 2), the CO_2 uptake was decreased by 5.35 mmol of CO_2 per g of H_2O.

ii) Hydrate phase equilibrium was improved when ΔP increased (ΔP = 19; operating temperature was shifted from 275 to 293 K). Moreover, the CO_2 uptake by employing microporous silica (zeolite 13X) was 0.58 mmol of CO_2 per g of H_2O which was almost 10 times lesser than combined-promoters designated type T1-5 (mesoporous silica) due to the capillary effect in zeolite 13X which decreased the activity of water such as exhibited in bulk water. Also, as the amount of water increased from 2.40 to 3.70 mmol, the total amount of CO_2 molecules consumed also increased from 0.24 to 0.40 mmol shown by combined-promoters designated types T3-2 (0.01 mol% SDS and 0.10 mol% TBAB) and T1-5 respectively. These four factors provide enough driving force which is important

in batch FBR so that further hydrate growth can be achieved even in new equilibrium state.

iii) The study on bed height influence on hydrate formation demonstrated that by reducing the bed height of zeolite 13X-5 from 3 to 2cm, the formation of hydrate was achievable where the gas uptake of 0.58 $\pm$ 0.03 mmol of CO_2 per g of H_2O was observed. This was expected due to the higher contact area to the ratio of gas phase and bed volume which provided a better heat transfer efficiency.

7.1.4. The feasibility of CO2 capture through hydrate formation in the IGCC conditions

i) The bed height of silica gel contacted with combined-promoter employed in batch FBR affected the formation of hydrate in the IGCC conditions (283 K and 50 or 70 bar). The gas uptake of T3-2 (0.01 mol% SDS and 0.10 mol% TBAB) was found to be 0.44 mmol of CO_2 per g of H_2O higher than T1-5 at 283 K and 70 bar in 1200 minutes when the bed height was reduced from 3 to 2cm which also indicated that T3-2 was the most suitable combined-promoter to be employed in the IGCC conditions.

ii) The results compared with the literature demonstrated that 55% greater gas uptake (2.4 mmol of CO_2 per g of H_2O) obtained by Zheng et al. (2016) at the IGCC conditions was expected due to the employment of macroporous silica inside horizontal batch FBR in their work. Also, the use of macroporous silica contacted with water inside semi-batch FBR by Adeyemo et al. (2010) resulted in 20% higher gas uptake as compared to this work (1.54 mmol of CO_2 per g of H_2O) in the non-IGCC conditions (275 K and 80 bar). However, the results obtained in this work (T3-2; 1.54 mmol of CO_2 per g of H_2O and T1- 5; 1.11 mmol of CO_2 per g of H_2O) were

almost two times greater than Babu et al. (2016) in the IGCC conditions where their employment of batch STR was found to have disadvantages as compared to batch FBR in this work.

7.2.Recommendations for future work

Several improvements can be considered to improve hydrate formation in the IGCC conditions by considering several factors that were discussed in this work. Hence, the study on the selectivity of CO_2 molecules towards hydrate formation in fuel gas mixture by gas chromatography (GC) analysis and the improvement of reactor configuration by employing macroporous or mesoporous silicas (silica sand or gel) with combined-promoters are suggested.

7.2.1. GC analysis on the selectivity of CO_2 hydrate from fuel gas mixture

The gas selectivity experiment by using the HPVA is being proposed to collect remaining gases from fuel gas mixture which is not involved in hydrate formation. Initially, the water bath temperature will be set at hydrate forming temperature. Then, the system will be manually pressurised to the manifold pressure (PM). Next, the valve of PM will be closed and at the same time, fuel gas mixture will be expanded to the sample pressure (PS). After that, the valve of PS will be closed, and sample cell will be pressurised to hydrate forming pressure. The system will be left for 1200 minutes, and the valve of sample cell will be closed when equilibrium has been achieved. The remaining gases will be collected by opening the valve that is being connected to the gas sampling bag. Then, these gases will be analysed by using the GC to study the selectivity of CO_2 towards hydrate formation in the IGCC operating conditions. The schematic diagram of proposed HPVA modification is presented in Appendix 11 (Figure A- 54).

The proposed experimental method for GC analysis is previously employed by Belandria et al. (2011). The GC will be equipped with thermal conductivity detection (TCD) device and PORAPAK-Q packed column (length = 2 m, outer diameter = 1/8 in., 80/100 mesh). The TCD device will be preliminary calibrated for CO_2 and H_2, and N_2 will be used as the carrier gas. The composition of the gas phase under a given equilibrium condition will be determined from the peak area ratio of the unknown sample and the coefficients of the corresponding calibration equation for each compound.

7.2.2. FBR configurations involving macroporous/mesoporous silicas for HBGS improvement in the IGCC

Macroporous silica or silica sand (Zheng et al., 2016) and mesoporous silica or silica gel (this work) managed to show hydrate formation in IGCC conditions. However, Zheng et al. (2016) obtained the highest CO_2 uptake in the IGCC conditions to date (2.4 mmol of CO_2 per g of H_2O) due to the employment of macroporous silica inside horizontal batch FBR. Also, the use of semi-batch FBR by Adeyemo et al. (2010) resulted in the highest CO_2 uptake for the employment of silica contacts with water in fuel gas mixture in the non-IGCC conditions. Thus, two types of reactor configurations are being proposed for changing the process from batch to continuous with the employment of macroporous silica contacts with new combined-promoters (T3-2; 0.01 mol% SDS and 0.10 mol% TBAB or T1A-2; 0.01 mol% SDS and 0.10 mol% EGME). T3-2 is being chosen because of the highest gas uptake observed in this work in the IGCC conditions. As for T1A-2, EGME was a good substitute for THF in which the gas uptake attained in pure CO_2 gas was almost comparable to T1-5 (5.60 mol% THF and 0.01 mol% SDS). The first configuration is quite direct where vertical batch FBR is being converted to semi-batch horizontal FBR. The second one involves dual-batch horizontal FBRs which enables a continuous operation similar to how pressure swing

adsorption would operate (Babu(b) et al., 2013; Grande, 2012). The proposed reactor configurations are presented in Appendix 11 (Figure A- 65 and Figure A- 76).

The four steps' concept of the "Skarstrom cycle" is modified for the continuous hydrates formation in dual-batch horizontal reactor and shown in Figure A- 7 & Table A- 8: Hydrate formation, depressurization, hydrate decomposition and pressurization. In this cycle, in the hydrate formation step, fuel gas mixture is fed to FBR 1 at the IGCC pressure. The porous medium (macroporous silica contacted with combined-promoter) is selective to CO_2, making the exiting stream (after valve V7) richer in H_2. When the porous medium packed in FBR 1 is saturated and cannot form more CO_2 hydrate, flue gas mixture is directed to FBR 2. In order to release part of the CO_2 hydrate formed in FBR 1, the flow direction is reversed and the total pressure (fuel gas mixture) of FBR 1 is reduced by venting to atmosphere (opening valve V3) wherein this step is called as depressurization. In the depressurization step, CO_2 is dissociated from the porous medium and released and at the end of this step, the gas phase inside FBR 1 is rich in CO_2. To additionally remove CO_2 from FBR 1, a hydrate decomposition step is used. The enriched fuel gas mixture is recycled from FBR 2 which is flowing by the pressure differential between both FBRs. After the porous medium is ready to form more CO_2 hydrate, the overall pressure of the system should be restored. That is done in the pressurization step using the feed stream. After all these steps were finished, a complete cycle was completed. It is important to notice that although the horizontal FBR operation is in batch mode, the feed stream is being employed so the process can be viewed as continuous. However, the exit is discontinuous and a tank is required to be coupled for a continuous discharge.

REFERENCES

Aaron, D., Tsouric, C. (2005). "Separation of CO_2 from flue gas: A review", Separation Science & Technology Vol 40, p.p. 321-348.

Adeosun, A., Abu-Zahra, M.R.M. (2013). "Evaluation of amine-blend solvent systems for CO_2 post-combustion capture applications", Energy Procedia Vol 37, p.p. 211-218.

Adeyemo, A., Kumar, R., Linga, P., Ripmeester., J., Englezos, P. (2010), "Capture of CO_2 from flue or fuel gas mixtures by clathrate crystallization in a silica gel column", International Journal of Greenhouse Gas Control Vol 4, p.p. 478-485.

Alphen, K.V., Noothout, P.M., Hekkert, M.P., Turkenberg, W.C. (2010). "Evaluating the development of carbon capture and storage technologies in the United States", Renewable and Sustainable Energy Reviews Vol 14, p.p. 971-986.

Angus MacNeil's committee, (2016). "Future of carbon capture and storage in the UK". House of Commons Energy and Climate Change Committee-Second Report of Session 2015-16, UK: London.

Arletti, R., Gigli, L., Renzo, D.F.., Quartieri, S. (2016). "Evidence for the formation of stable CO_2 hydrates in zeolite Na-Y: Structural characterization by synchrotron X-ray powder diffraction", Microporous and Mesoporous Materials Vol 228, p.p. 248-255.

Atsonios, K., Panopoulos, K.D., Doukelis, A., Koumanakos, A., Kakaras, E. (2013). "Cryogenic method for H_2 and CH_4 recovery from a rich CO_2 stream in pre-combustion carbon capture and storage schemes", Energy Vol 53, p.p. 106-113.

Babu, P., Ong, H.W.N., Linga, P. (2016), "A systematic kinetic study to evaluate the effect of tetrahydrofuran on the clathrate process for pre-combustion capture of carbon dioxide", Energy Vol 94, p.p. 431-442.

Babu, P., Linga, P., Kumar, R., Englezos, P., (2015), “A review of the hydrate based gas separation (HBGS) process for carbon dioxide pre-combustion capture”, Energy Vol 85, p.p. 261-279.

Babu, P., Ho, C.Y., Kumar, R., Linga, P. (2014), “Enhanced kinetics for the clathrate process in a fixed bed reactor in the presence of liquid promoters for pre-combustion carbon dioxide capture”, Energy Vol 70, p.p. 664-673.

Babu(b), P., Yao, M., Datta, S., Kumar, R., Linga, P. (2014), “Thermodynamic and kinetic verification of tetra-n-butyl ammonium nitrate ($TBANO_3$) as a promoter for the clathrate process applicable to precombustion carbon dioxide capture”, Environmental Science Technology Vol 48(6), p.p. 3550-3558.

Babu(c), P., Kumar, R., Linga, P. (2014), “Unusual behaviour of propane as a co-guest during hydrate formation in silica sand: Potential application to seawater desalination and carbon dioxide capture”, Chemical Engineering Science Vol 117, p.p. 342-351.

Babu, P., Kumar, R., Linga, P. (2013), “Pre-combustion capture of CO_2 in a fixed bed reactor using the Clathrate hydrate process”, Energy Vol 50, p.p. 364-373.

Babu(b), P., Kumar, R., Linga, P. (2013), “A new porous material to enhance the kinetics of clathrate process: Application to precombustion carbon dioxide capture”, Environmental Science Technology Vol 47, p.p. 13191-13198.

Babu(c), P., Kumar, R., Linga, P. (2013), “Medium pressure hydrate based gas separation (HBGS) process for pre-combustion capture of carbon dioxide employing a novel fixed bed reactor”, International Journal Greenhouse Gas Control Vol 17(0), p.p. 206-214.

Belandria, V., Eslamimanesh, A., Mohammadi, A. H. (2011), “Study of gas hydrate formation in the carbon dioxide + hydrogen + water systems”, Industrial & Engineering Chemistry Research Vol 50, p.p. 6455-6459.

Biello, D. (2013). “400 ppm: Carbon Dioxide in the Atmosphere Reaches Prehistoric Levels”, Scientific American, http://blogs.scientificamerican.com/observations/2013/05/09

Biology online. “Biology-online dictionary”, Life Science Reference, http://www.biology-online.org/dictionary

Caitlyn, K. (2014). “Climate change: Atmospheric Carbon Dioxide”, National Centers for Environmental Information, https://www.climate.gov/news-features/understanding-climate/climate-change-atmospheric-carbon-dioxide

Carroll, J. (Second Edition) (2009). “Natural gas hydrates (a guide for engineers)”, Elsevier Inc. USA: Burlington.

Carrol, J., Slupsky, J., Mather, E. (1991), “The solubility of CO_2 in water at low pressure”, Journal of Physic and Chemistry Vol 20, No. 6.

Changyu, S., Wenzhi, LI., Xin, Y., Fengguang, LI., Qing, Y., Liang, MU., Jun, C., Bei, L., Guangjin, C. (2011), “Progress in research of gas hydrate”, Chinese Journal of Chemical Engineering Vol 19(1), p.p. 151-162.

Chatti, I., Delahaye, A., Fournaison, L., Petitet, J.P. (2005), “Benefits and drawbacks of Clathrate hydrates: a review of their areas of interest”, Energy Conversion & Management Vol 46, p.p. 1333-1343.

Clough, S.R. (2014), “Propane”, Haley & Aldrich, Inc. USA: Bedford, NH.

Currier, R., I., Deppe, G., Lee, A., Tam, S.S. (2006), “CO_2 capture by formation of hydrates: Economical analysis and new promoter process”, Fifth Annual Conference on Carbon Capture & Sequestration, USA:Virginia.

D’Alessandro, D.M., Smit, B., Long, J.R. (2010), “Carbon dioxide capture: Prospects for new materials”, Angewandte Chemie International Edition Vol 49, p.p. 6058-6082.

Davidson, D.W. (1973), “Water: A comprehensive treatise”, Plenum Press, USA:New York Vol 2, p.p. 129-154

Dawson, R., Stevens, L.A., Williams, O.S.A., Wang, W., Carter, B.O., Sutton, S., Drage, T.C., Blanc, F., Adams, D.J., Cooper, A.I. (2014), "Dry bases: carbon dioxide capture using alkaline dry water", Energy & Environmental Science Vol 7, p.p. 1786-1791.

Demirbas, A. (First Edition) (2010). "Methane gas hydrate", Springer-Verlag London Limited. Turkey: Trabzon.

Dhondge, S.S., Pandhurnekar, C.P., Sheikh, S., Deshmukh, D.W. (2011), "Volumetric and viscometric study of aqueous binary mixtures of some glycol ethers at T = (275.15 and 283.15) K", J. Chem. Thermodynamics Vol 43, p.p. 1961-1968.

Diamond, L.W., Akinfiev, N.N. (2003), "Solubility of CO_2 in water from -1.5 to 100 ^oC and from 0.1 to 100 MPa: evaluation of literature data and thermodynamic modelling", Fluid Phase Equilibria Vol 208, p.p. 265-290.

Dyadin, Y.A., Larionov E.G., Manakov, A.Y., Zhurko, F.V, Aladko, E.Y., Mikina, T.V., Komarov, V.Y. (1999), "Clathrate hydrates of hydrogen and neon", Mendelev Commun Vol 9(5), p.p. 209-210.

Elwell, I.C., Grant, W.S. (2006), "Technology options for capturing CO_2", Power Vol 150, p.p. 60-65.

EPA. "Ecology Dictionary", U.S. Environmental Protection Agency, http://www.ecologydictionary.org/

Fan, S., Wang, Y., Lang, X. (2011), "CO_2 capture in form of clathrate hydrate-problem and practice", Proceedings of the 7th International Conference on Gas Hydrates (ICGH 2011), Scotland:Edinburgh.

Gayet, P., Dicharry, C., Marion, G., Graciaa, A., Lachaise, J., Nesterov, A. (2005), "Experimental determination of methane hydrate dissociation curve up to 55 MPa by using a small amount of surfactant as hydrate promoter", Chemical Engineering Science Vol 60, p.p. 5751-5758.

Grande, C.A. (2012), “Advances in pressure swing adsorption for gas separation”, ISRN Chemical Engineering Science Vol 2012, p.p. 1-13.

Global CCS Institute, (2013). “Large scale CCS demonstration projects”, Global CCS Institute, http://www.globalccsinstitute.com/data/status-ccs-project-database

Han, Y., Lee, S.S., Ying, J.Y. (2007), “Spherical siliceous mesocellular foam particles for high-speed size exclusion chromatography”, Chemistry of Materials Vol 19, p.p. 2292-2298.

Hashimoto, S., Murayama, S., Sugahara, T., Sato, H., Ohgaki, K. (2006), “Thermodynamic and Raman spectroscopic studies on H_2+tetrahydrofuran+water and H_2+tetra-n-butyl ammonium bromide+water mixtures containing gas hydrates”, Chemical Engineering Science Vol 61, p.p. 7884-7888.

Helmenstine, A.M. (2014). “Surfactant definition”, About Education, http://chemistry.about.com/od/chemistryglossary/g/surfactant.htm

Herslund, P.J., Thomsen, K., Abildskov, J., Solms, N.V. (2014), “Modelling of tetrahydrofuran promoted gas hydrate systems for carbon dioxide capture processes”, Fluid Phase Equilibria Vol 375, p.p. 45-65.

Herslund, P.J., Thomsen, K., Abildskov, J., Solms, N.V., Galfre, A., Brantuas, P., Kwaterski, M., Herri, J.M. (2013), “Thermodynamic promotion of carbon-dioxide-clathrate hydrate formation by tetrahydrofuran, cyclopentane and their mixtures”, International Journal of Greenhouse Gas Control Vol 17, p.p. 397-410.

Ho, L.C., Babu, P., Kumar, R., Linga, P. (2013), “HBGS process for carbon dioxide capture employing an unstirred reactor with cyclopentane”, Energy Vol 63, p.p. 252-259.

Hu, Y. (2011). “CO_2 capture from oxy-fuel combustion power plants”, Licentiate Thesis, KTH Royal Institute of Technology. Sweden: Stockholm.

IEA (2015). “Key trends in CO_2 emissions, excerpt from: CO_2 emissions from fuel combustion”. OECD/IEA 2015, France: Paris.

IEA Clean Coal Centre (2014). “Developments in oxyfuel combustion of coal”. No 10/01 August 2014, United Kingdom : London.

IEA (2013). “CO_2 emissions from fuel combustion highlights”. OECD/IEA 2013, France: Paris.

IEA (2012). “A policy strategy for carbon capture and storage”. OECD/IEA 2012, France: Paris.

IEA Clean Coal Centre (2011). “Pre-combustion capture of CO_2 in IGCC plants”. No 11/14, United Kingdom : London.

IEA (2008). “Energy technology perspectives”. OECD/IEA Publications 9, France: Paris.

IEA (2006). “Energy technology essentials”. OECD/IEA 2006, ETE01.

IEAGHG (2015/06). “Integrated CCS project at Saskpower's Boundary Dam Power Station”. August 2015, UK: Cheltenham.

ISO 9277 (2010). “Determination of the specific surface area of solids by gas adsorption – BET method”. September 2010, Switzerland.

Joshi, A., Sangwai, J.S., Das, K., Sami, N.A. (2013), “Experimental investigations on the phase equilibrium of semiclathrate hydrates of carbon dioxide in TBAB with small amount of surfactant”, International Journal of Energy and Environmental Engineering Vol 1, p.p. 4-11.

Kang, SP., Lee, J., Seo, Y. (2013), “Pre-combustion capture of CO_2 by gas Hydrate formation in silica gel pore structure”, Chemical Engineering Journal Vol 218, p.p. 126-132.

Kim, S.M., Lee, J.D., Lee, H.J., Lee, E.K., Kim, Y. (2011), “Gas hydrate formation method to capture the carbon dioxide for pre-combustion process in IGCC plant”, International Journal of Hydrogen Energy Vol 36, p.p. 1115-1121.

Kobayashi, T., Mori, Y.H. (2007), “Thermodynamic simulations of hydrate formation from gas mixtures in batch operations”, Energy Conversion & Management Vol 48, p.p. 242-250.

Kumar, A., Bhattacharjee, G., Kulkarni, B.D, Kumar, R. (2015), “Role of surfactants in promoting gas hydrate formation”, Ind. Eng. Chem. Res. Vol 54, p.p. 12217-12232.

Kumar, A., Sakpal, T., Linga, P., Kumar, R. (2013), “Influence of contact medium and surfactants on carbon dioxide Clathrate hydrate kinetics”, Fuel Vol 105, p.p. 664-671.

Kumar, R., Wu, H.J., Englezos, P. (2006), “Incipient Hydrate phase equilibrium for gas mixtures containing hydrogen, carbon dioxide and propane”, Fluid Phase Equilibria Vol 244, p.p. 167-171.

Kunze, C., Spliethoff, H. (2012). “Assessment of oxy-fuel, pre- and post-combustion-based carbon capture for future IGCC plants”, Applied Energy Vol 94, p.p. 109-116.

Lee, H.J., Lee, J.D., Linga, P., Englezos, P., Kim, Y.S., Lee, M.S., Kim, Y.D. (2010), “Gas hydrate formation process for pre-combustion capture of CO_2”, Energy Vol 35, p.p. 2729-2733.

Li, X.S., Xu, C.G., Chen, Z.Y., Cai, J. (2012), ”Synergic effect of cyclopentane and tetra-n-butyl ammonium bromide on hydrate-based carbon dioxide separation from fuel gas mixture by measurements of gas uptake and X-ray diffraction patterns”, International Journal of Hydrogen Energy Vol 37, p.p. 720-727.

Li, Y., Yi, H., Tang, X., Li, F., Yuan, Q. (2013), ”Adsorption separation of CO_2/CH_4 gas mixture on the commercial zeolites at atmospheric pressure”, Chemical Engineering Journal Vol 229, p.p. 50-56.

Li, X.S., Xu, C.G., Chen, Z.Y., Wu, H.J. (2011), “Hydrate-based pre-combustion carbon dioxide capture process in the system with tetra-n-butyl ammonium bromide solution in the presence of cyclopentane”, Energy Vol 36, p.p. 1394-1403.

Li, X.S., Xia, Z.M., Chen, Z.Y., Yan, K.F., Li, G., Wu, H.J. (2010), “Gas hydrate formation process for capture of carbon dioxide from fuel gas mixture”, Industrial & Engineering Chemistry Research Vol 49 p.p. 11614-11619.

Li, X.S., Lu, Z., Chen, Z.Y., Yan, K.F., Wu, H.J., Li, G. (2009), "Experimental research on hydrate-based CO_2 separation from flue gases (CO_2+N_2)", Modern Chem. Ind. Vol 29 p.p. 37-40.

Lim, Y.A., Babu, P., Kumar, R., J., Englezos, P. (2013), "Morphology of carbon-dioxide-hydrogen-cyclopentane hydrates with or without sodium dodecyl sulfate", Crystal Growth & Design Vol 13(5) p.p. 2047-2059.

Linga, P., Haligva, C., Nam, S.C. (2009), "Gas Hydrate formation in a variable volume bed of silica sand particles", Energy Fuels Vol 23, p.p. 5496-5507.

Linga, P., Kumar, R., Englezos, P. (2007), "Gas Hydrate formation from hydrogen/carbon dioxide and nitrogen/carbon dioxide gas mixtures", Chemical Engineering Science Vol 62, p.p. 4268-4276.

Lo, C., Zhang, J.S., Somasundaran, P., Lu, S., Couzis, A., Lee, J.W. (2008), "Adsorption of surfactants on two different hydrates", Langmuir Vol 24(22), p.p. 12723-12726.

Massoudi, R., King, Jr.A.D. (1974), "Effect of pressure on the surface tension of water: Adsorption of low molecular weight gases on water at 25^o", The Journal of Physical Chemistry Vol 78, No. 22.

McCallum Layton Stats Calculator, https://www.mccallum-layton.co.uk/tools/statistic-calculators/confidence-interval-for-mean-calculator/

McCallum, S.D., Riestenberg, D.E., Zatsepina, O.Y., Phelps, T.J. (2005), "Effect of pressure vessel size on the formation of gas hydrates", Journal of Petroleum Science & Engineering Vol 56, p.p. 54-64.

Mekala, P., Busch, M., Mech, D., Patel, R.S. (2014), "Effect of silica sand size on the formation kinetics of CO_2 hydrate in porous media in the presence of pure water and seawater relevant for CO_2 sequestration", Journal of Petroleum Science & Engineering Vol 122, p.p. 1-9.

Metz, B., Davidson, O., Coninck, H.D., Loos, M., Meyer, L. (2005), "IPCC special report on carbon dioxide capture and storage", Intergovernmental Panel on Climate Change, USA:New York.

Mori, Y.H., Komae, N. (2008), "A note on the evaluation of the guest-gas uptake into a clathrate hydrate being formed in a semi-batch or batch type reactor", Energy Conversion & Management Vol 49, p.p. 1056-1062.

Mu, D., Liu, Z.S., Huang, C., Djilali, N. (2008), "Determination of the effective diffusion coefficient in porous media including Knudsen effects", Microfluid Nanofluid Vol 4, p.p. 257-260.

NOAA (2015), "Global Analysis – September 2015_2015 year-to-date temperature versus previous years", National Centers for Environmental Information (NCEI), https://www.ncdc.noaa.gov/sotc/global/2015/9/supplemental/page-2

Pandhurnekar, C.P., Parwate, D.V., Dhondge, S.S. (2013), "Investigations of volumetric, acoustic and optical properties of aqueous binary mixtures of different glycol ethers at temperatures 278.15 K and 288.15 K", Journal of Molecular Liquids Vol 183, p.p. 94-101.

Park, S., Lee, S., Lee, Y., Lee, Y., Seo, Y. (2013), "Hydrate-based pre-combustion capture of carbon dioxide in the presence of a thermodynamic promoter and porous silica gels", International Journal of Greenhouse Gas Control Vol 14, p.p. 193-199.

Park(b), S., Lee, S., Lee, Y., Lee, Y., Seo, Y. (2013), "CO_2 capture from simulated fuel gas mixtures using semiclathrate hydrates formed by quaternary ammonium salts", Environmental Science & Technology Vol 47, p.p. 7571-7577.

Rackley, S.A. (First Edition) (2010), "Carbon capture and storage", Elsevier Inc. USA: Burlington.

Rajnauth, J., Barrufet, M., Falcone, G., (2012), “Hydrate formation: Considering the effects of pressure, temperature, composition and water”, Energy Science & Technology Vol 4, p.p. 60-67.

Ricaurte, M., Dicharry, C., Renaud, X., Torre, J.P. (2014), “Combination of surfactants and organic compounds for boosting CO_2 separation from natural gas by clathrate hydrate formation”, Fuel Vol 122, p.p. 206-217.

Schell, J., Casas, N., Marx, D., Blom, R., Mazzoti, M. (2013). “Comparison of commercial and new adsorbent materials for pre-combustion CO_2 capture by pressure swing adsorption”, Energy Procedia Vol 37, p.p. 167-174.

Scholes, C.A., Anderson, C.J., Stevens, G.W., Kentish, S.E., (2013). “Membrane gas separation-physical solvent absorption combined plant simulations for pre-combustion capture”, Energy Procedia Vol 37, p.p. 1039-1049.

Scondo, A., Sinquin, A. (2011), “Effect of additives on CO_2 capture from simulated flue gas by hydrates formation in emulsion”, Proceedings of the 7th International Conference on Gas Hydrates (ICGH 2011), Scotland:Edinburgh.

Servio, P., Englezos, P. (2001). “Effect of temperature and pressure on the solubility of carbon dioxide in water in the presence of gas hydrate”, Fluid Phase Equilibria Vol 190, p.p. 127-134.

Shimada, W., Ebinuma, T., Oyama, H., Kamata, Y., Narita, H. (2005). “Free-growth forms and growth kinetics of tetra-n-butyl ammonium bromide semi-clathrate hydrate crystals”, Journal of Crystal Growth Vol 274, p.p. 246-250.

Silva, C.F., Pessoa, F.L.P., Uller, A.M.C. (2013). “Storage capacity of carbon dioxide hydrates in the presence of Sodium Dodecyl Sulfate (SDS) and Tetrahydrofuran (THF)”, Chemical Engineering Science Vol 96, p.p. 118-123.

Skarstrom, C. W. (1960), "Method and apparatus for fractionating gaseous mixtures by adsorption", US Patent, No: 2944627.

Sloan, D. (2011). Natural gas hydrates in flow assurance. USA: Burlington.

Sloan, E.D., Koh, C.A. (Third Edition) (2008), "Clathrate hydrates of natural gases", Taylor & Francis Group USA: Boca Raton.

Sowjanya, Y., Prasad, S.R.P. (2014), "Formation kinetics & phase stability of double hydrates of C_4H_8O and CO_2/CH_4: A comparison with pure system", Journal of Natural Gas Science and Engineering Vol 18. p.p. 58-63.

Stevens, L., Williams, K., Han, W.Y., Drage, T., Snape, C.E., Wood, J., Wang, J. (2013). "Preparation and CO_2 adsorption of diamine modified montmorillonite via exfoliation grafting route", Chemical Engineering Journal Vol 215-216, p.p. 699-708.

Sun, D., Sun, Englezos, P. (2014), "Storage of CO_2 in a partially water saturated porous medium at gas hydrate formation conditions", International Journal of Greenhouse Gas Control Vol 25. p.p. 1-8.

Tam, S.S., Stanton, M.E., Ghose, S., Deppe, G., Spencer, D.F., Currier, R.P., Young, J.S., Anderson, G.K., Le, L.A., Devlin, D.J. (2013), "A high pressure carbon dioxide separation process for IGCC plants", National Energy Technology Laboratory (NETL), U.S., https://www.netl.doe.gov/publications/proceedings/01/carbon_seq/1b4.pdf

Tang, J., Zeng, D., Wang, C., Chen, Y., He, L., Cai, N. (2013), "Study on the influence of SDS and THF on hydrate-based gas separation performance", Chemical Engineering Research and Design Vol 91, p.p. 1777-1782.

Tang, H., Yamasaki, A., Shindo, Y. (1996), "The fate of liquid CO_2 disposed of in the ocean", Energy Vol 21, p.p. 765-774.

Torre, J.P, Haillot, D., Rigal, S. (2015), “1,3 Dioxolane versus tetrahydrofuran as promoters for CO_2-hydrate formation: Thermodynamic properties, and kinetics in presence of sodium dodecyl sulfate ”, Chemical Engineering Science Vol 126, p.p. 688-697.

Veluswamy, H.P, Chin, W.I., Linga, P. (2014), “Clathrate hydrates for hydrogen storage: The impact of tetrahydrofuran, tetra-n-butylammonium bromide and cyclopentane as promoters on the microscopic kinetcics”, International Journal of Hydrogen Energy Vol 39, p.p. 16234-16243.

Wang, W., Bray, C.L., Adams, D.J., Cooper, A.I., (2008), “Methane storage in dry water gas hydrates”, JACS Communications Vol 130, p.p. 11608-11609.

Xiaoya, Z., Jianwei, D.U., Deqing, L., Shuanshi, F., Cuiping, T. (2009), “Influence of A-type zeolite on methane hydrate formation”, Chinese Journal of Chemical Engineering Vol 17, p.p. 854-859.

Yang, H., Xu, Z., Fan M., Gupta, R., Slimane, R.B., Bland, A.E., Wright, I. (2008), “Progress in carbon dioxide separation and capture: A review”, Journal of Environmental Sciences Vol 20, p.p. 14-27.

Yang, M.W., Chen, N.C., Huang C.H., Shen, Y.T., Yang, H.S., Chou, C.T. (2014), “Temperature swing adsorption process for CO_2 capture using polyaniline solid sorbent”, Energy Procedia Vol 63, p.p. 2351-2358.

Yang, M., Jing, W., Wang, P., Jiang, L., Song, Y. (2015), “Effects of additive mixture (THF+TBAB) on CO_2 hydrate phase equilibrium”, Fluid Phase Equilibria Vol 401, p.p. 27-33.

Yang, M., Song, Y., Liu, W., Zhao, J., Ruan, X., Jiang, L., Li, Q. (2013), “Effects of additive mixtures (THF/SDS) on carbon dioxide hydrate formation and dissociation in porous media”, Chemical Engineering Science Vol 90, p.p. 69-76.

Young, C.L. (1981), “Solubility data series – hydrogen and deuterium in water”, International Union of Pure & Applied Chemistry Vol 5/6, p.p. 303-313.

Yuan, Y., Lee, T.R. (2013), “Contact angle and wetting properties”, Surface Science Technique doi: 10.1007/ 978-3-642-34243-1_1.

Zare, M., Haghtalab, A., Ahmadi, A.N., Nazari, K., Mehdizadeh, A. (2015), “Effects of imidazolium based ionic liquids and ethylene glycol monoethyl ether solutions on the kinetic of methane hydrate formation”, Journal of Molecular Liquids Vol 204, p.p. 236-242.

Zhang, Y., Yang, M., Song, Y., Jiang, L., Li, Y., Cheng, C. (2014), “Hydrate phase equilibrium measurements for (THF+SDS+CO_2+N_2) aqueous solution systems in porous media”, Fluid Phase Equilibria Vol 370, p.p. 12-18.

Zheng, J., Lee, Y.K., Babu, P., Zhang, P., Linga, P. (2016), “Impact of fixed bed reactor orientation, liquid saturation, bed volume and temperature on the clathrate hydrate process for pre-combustion capture”, Journal of Natural Gas Science and Engineering doi: 10.1016/ j.jngse.2016.03.100.

Zhong, D.L., Li, Z., Lu, Y.Y., Wang, J.L., Yan, J., Qing, S.L. (2015), “Investigation of CO_2 capture from a CO_2 + CH_4 gas mixture by gas hydrate formation in the fixed bed of a molecular sieve”, Industrial & Engineering Chemistry Research Dec. 21, 2015.

Zisman, W.A. (1964), “Relation of the equilibrium contact angle to liquid and solid constitution”, Advances in Chemistry Vol 43, p.p. 1-5, doi: 10.1021/ba-1964-0043.ch001.

APPENDIX

Appendix 1. BET sample calculation

Firstly, a linear graph from equation 2-1 in chapter 2 (page 59) was plotted wherein;

$$y = \frac{p/p_0}{(1-p/p_0)n_a}, \quad x = \frac{p}{p_0}, \quad m = \frac{C-1}{CV_m} \; and \quad y - intercept = \frac{1}{CV_m}$$

Table A- 1: The calculated experimental values to plot $\frac{p/p_0}{(1-p/p_0)V_a}$ vs $\frac{p}{p_0}$

$\frac{p}{p_0}$	$\frac{p/p_0}{(1-p/p_0)V_a}$	$\frac{p}{p_0}$	$\frac{p/p_0}{(1-p/p_0)V_a}$	$\frac{p}{p_0}$	$\frac{p/p_0}{(1-p/p_0)V_a}$
0.052024	0.000558	0.131129	0.001262	0.255172	0.002318
0.055899	0.000594	0.156031	0.001477	0.280459	0.002531
0.059069	0.000623	0.180914	0.00169	0.306261	0.002749
0.083086	0.00084	0.205746	0.001902	0.332464	0.002973
0.106392	0.001046	0.230351	0.002109	0.357422	0.00319

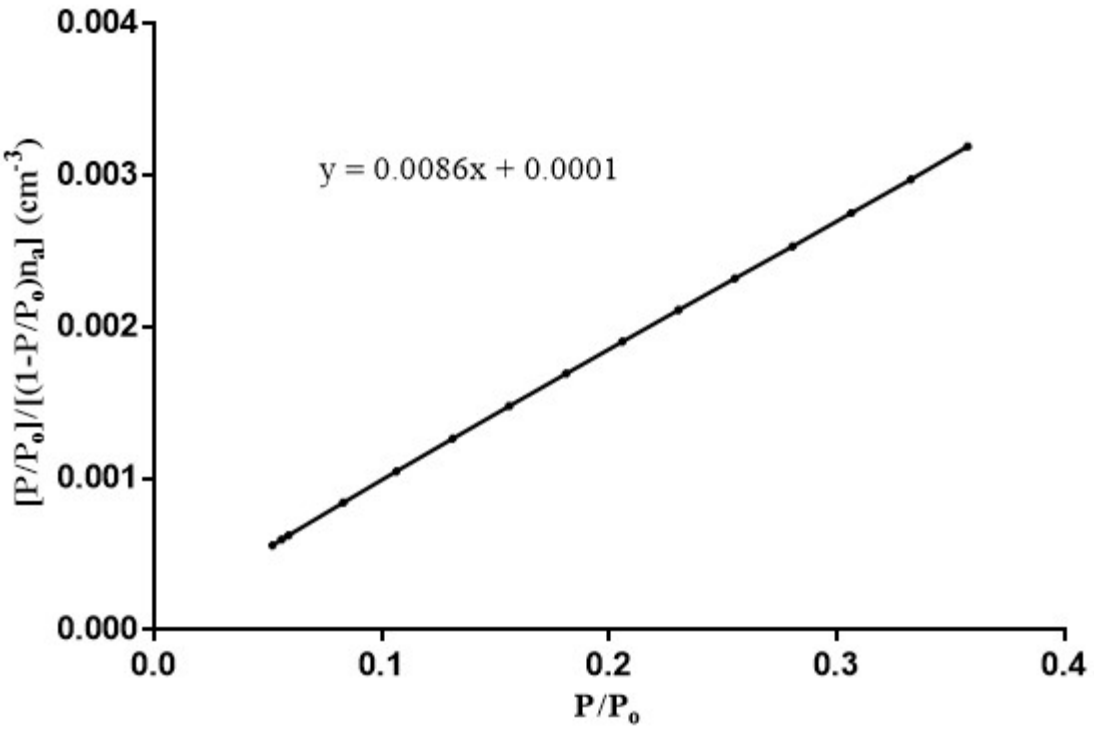


Figure A- 1: Plot of $\frac{p/p_0}{(1-p/p_0)n_a}$ vs $\frac{p}{p_0}$ for BET calculation

From the graph;

$$\mathbf{y} - \text{intercept} = \frac{1}{\mathrm{Cn_m}} = 0.0001\ \mathrm{gcm^{-3}}$$

$$\textbf{slope } (\mathbf{m}) = \frac{\mathbf{C-1}}{\mathbf{Cn_m}} = \frac{\mathbf{C-1}}{\mathbf{0.0001}} = \mathbf{0.0086};\ \mathbf{C = 87}$$

$$\frac{1}{\mathrm{Cn_m}} = \frac{1}{87\mathrm{n_m}}0.0001;\ \mathrm{n_m} = 114.9425\ \mathrm{cm^3g^{-1}}$$

$$\text{No. of } \mathrm{N_2}\text{molecules} = \frac{114.9425}{1000\ \times\ 22.4}\mathrm{dm^3}\ \times 6.02\ \times\ 10^{23} = 30.8908\ \times\ 10^{20}\ \text{molecules}$$

$$\text{Contact area of one } \mathrm{N_2}\text{molecule} = 16.2\ \times\ 10^{-20}\ m^2\mathrm{g^{-1}}$$

$$\text{The total area } (\mathrm{S_{BET}}) = 30.8908\ \times\ 10^{20}\ \times\ 16.2\ \times\ 10^{-20}\ m^2\mathrm{g^{-1}} = 499\ \ m^2\mathrm{g^{-1}}$$

$$\text{Pore volume } (\mathrm{V_{tot}}) = N_2 adsorption\ at\ 0.99\ \frac{P}{P_o} = 0.64\ cm^3\mathrm{g^{-1}}$$

$$\text{Pore size } (\mathrm{D}) = \frac{4\mathrm{V_{tot}}}{\mathrm{S_{BET}}} = \frac{4 \times 0.64\ cm^3\mathrm{g^{-1}}}{499\ cm^2\mathrm{g^{-1}} \times 1000000} = 5.14\ nm$$

Appendix 2. Promoter concentration

Equation 2-2 in chapter 2 was used to calculate the amount of promoter needed.

Sample calculation for 0.29 mol% TBAB:

Let assume, $m_{H_2O} = 47.5\ g\ ; n_{H_2O} = 2.6389$ moles

So, $\frac{n_{TBAB}}{n_{TBAB}+n_{H_2O}} = 0.0029$; $n_{TBAB} = 0.0077$; $m_{TBAB} = 2.4705$ ($Mr_{TBAB} = 321.9\ g/mol$)

Then let assume, $m_{TBAB} = x \& m_{H_2O} = y$; the ratio of $\frac{x}{y} = 0.05201$

So in 47.5 g of solution, $x + y = 47.5$; $0.0520y + y = 47.5$; $y = 45.1517$ & $x = 2.3483$

Table A- 2: The amount of each promoter used to prepare each combined-promoter (brief description of each code (T1, T2, T3 and T1A) was referred to page 108, 116 (Table 4- 4) and 121 (Table 4- 6) respectively)

No.	Type of combined -promoter	Concentration and mass of promoter								Mass of water (g)
		THF		SDS		TBAB		EGME		
		mol %	g	mol %	g	mol%	g	mol%	g	
1	T1-1	3.000	5.229	0.010	0.076	-	-	-	-	89.695
2	T1-2	3.000	5.229	0.020	0.152	-	-	-	-	89.619
3	T1-3	3.000	5.229	0.100	0.760	-	-	-	-	89.021
4	T1-4	1.000	1.845	0.010	0.076	-	-	-	-	93.079
5	T1-5	5.600	9.110	0.010	0.076	-	-	-	-	85.814
6	T1-6	3.000	5.229	0.005	0.038	-	-	-	-	89.733
7	T1-7	7.000	10.992	0.010	0.076	-	-	-	-	83.932
8	T2-1	3.000	5.229	-	-	0.290	2.349	-	-	87.422
9	T3-1	-	-	0.010	0.076	0.290	2.349	-	-	92.576
10	T3-2	-	-	0.010	0.076	0.100	0.835	-	-	94.089
11	T1A-1	-	-	0.010	0.076	-	-	0.010	0.024	94.900
12	T1A-2	-	-	0.010	0.076	-	-	0.100	0.237	94.687
13	T1A-3	-	-	0.010	0.076	-	-	1.000	2.287	92.638

Appendix 3. Combined gas law

To convert the unit of CO_2 volume that involved in hydrates formation from ccSTP to cm^3.

$$\frac{P_1V_1}{T_1} = \frac{P_2V_2}{T_2} \qquad (A-1)$$

Let assume; P_2, V_2 andT_2 are at the STP (P_2 = 1 bar, T_2 = 273 K and V_2 in ccSTP)

P_1, V_1 and T_1 are at the operating conditions (P_1 = 36 bar, T_2 = 275 K and V_2 in cm^3)

Appendix 4. Summary of calculated data

Table A- 3: The summary of equilibrium moisture content (wt%) for method 1, 2, 3 and 4 (baseline experiment)

Sample	Exp.	SiG (wet) (g)	SiG (dry) (g)	Moisture content (g)	Equilibrium moisture content (wt%)	Mean equilibrium moisture content (wt%)	SD
Method 1	1	0.056	0.047	0.008	15.054	13.561	2.111
	2	0.075	0.066	0.009	12.069		
Method 2	1	0.060	0.052	0.008	13.333	13.643	0.439
	2	0.086	0.074	0.012	13.953		
Method 3	1	0.045	0.038	0.007	16.520	13.833	2.475
	2	0.110	0.097	0.013	11.647		
Method 4	1	0.140	0.119	0.021	15.000	14.792	0.295
	2	0.096	0.082	0.014	14.583		

- Method 1 (silica was left to naturally adsorbed moisture), method 2 (the lowest rates of stirring of silica), method 3 (silica was submerged in excess water) and method 4 (the highest rates of stirring of silica)

Table A- 4: The summary of equilibrium moisture content (wt%) for T1, T2, T3, T1A and baseline experiments (brief description of each code was referred to page 108, 116 (Table 4- 4) and 121 (Table 4- 6) respectively)

Sample	Exp.	SiG (wet) (g)	SiG (dry) (g)	Moisture content (g)	Equilibrium moisture content (wt%)	Mean equilibrium moisture content (wt%)	SD
THF*	1	0.039	0.034	0.005	13.590	13.871	0.398
	2	0.107	0.092	0.015	14.153		
SDS**	1	0.044	0.039	0.006	13.258	13.086	0.244
	2	0.130	0.113	0.017	12.913		
TBAB***	1	0.038	0.035	0.003	8.466	8.479	0.019
	2	0.047	0.043	0.004	8.493		
T1-1	1	0.048	0.041	0.007	13.721	13.808	0.122
	2	0.102	0.088	0.014	13.894		
T1-2	1	0.131	0.113	0.018	13.629	13.722	0.131
	2	0.127	0.110	0.018	13.815		
T1-3	1	0.091	0.079	0.012	13.201	13.169	0.046
	2	0.108	0.094	0.014	13.136		
T1-4	1	0.103	0.089	0.014	13.940	14.357	0.590
	2	0.111	0.095	0.016	14.775		
T1-5	1	0.092	0.080	0.012	13.399	13.290	0.154
	2	0.127	0.110	0.017	13.181		
T1-6	1	0.134	0.115	0.019	14.051	13.897	0.218
	2	0.090	0.077	0.012	13.743		
T1-7	1	0.097	0.085	0.013	13.039	13.138	0.140
	2	0.083	0.072	0.011	13.237		
T2-1	1	0.108	0.096	0.011	10.595	10.342	0.358
	2	0.101	0.091	0.010	10.089		
T3-1	1	0.091	0.084	0.007	8.123	8.384	0.370
	2	0.096	0.088	0.008	8.646		
T3-2	1	0.104	0.096	0.009	8.333	8.456	0.174
	2	0.105	0.096	0.009	8.580		
T1A-1	1	0.100	0.087	0.013	13.178	12.888	0.410
	2	0.102	0.089	0.013	12.598		
T1A-2	1	0.101	0.088	0.013	12.810	12.593	0.308
	2	0.110	0.096	0.014	12.375		
T1A-3	1	0.103	0.091	0.012	11.782	12.060	0.394
	2	0.139	0.122	0.017	12.339		

*THF at 3.00 mol%; **SDS at 0.01 mol% and ***TBAB at 0.29 mol%

Table A- 5: The summary of hydrates formation results for T1, T2, T3, T1A and baseline experiments (brief description of each code was referred to page 108, 116 (Table 4- 4) and 121 (Table 4- 6) respectively)

Sample	Exp. No.	No. of moles of water (mmol)	CO_2 formed in hydrates (mmol)	Mean CO_2 formed in hydrates (mmol)	CO_2 uptake (mmol of CO_2/g of H_2O)	Mean CO_2 uptake (mmol of CO_2/g of H_2O) (90% CI)	SD
T1-1	1	3.80	0.39	0.39	5.73	5.68 ± 0.09	0.08
	2	3.80	0.39		5.62		
T1-2	1	3.80	0.36	0.37	5.30	5.35 ± 0.08	0.07
	2	3.80	0.37		5.40		
T1-3	1	3.70	0.26	0.25	3.94	3.75 ± 0.31	0.27
	2	3.70	0.24		3.56		
T1-4	1	4.00	0.35	0.35	4.79	4.84 ± 0.07	0.06
	2	4.00	0.35		4.88		
T1-5	**1**	**3.70**	**0.39**	**0.40**	**5.82**	**5.95 ± 0.21**	**0.18**
	2	**3.70**	**0.41**		**6.08**		
T1-6	1	3.90	0.28	0.30	3.93	4.23 ± 0.49	0.42
	2	3.90	0.31		4.52		
T1-7	1	3.60	0.36	0.36	5.47	5.43 ± 0.07	0.06
	2	3.60	0.35		5.39		
T2-1	1	2.90	0.08	0.09	1.53	1.63 ± 0.16	0.14
	2	2.90	0.09		1.73		
T3-1	1	2.30	0.12	0.13	2.83	3.03 ± 0.33	0.28
	2	2.30	0.14		3.23		
T3-2	**1**	**2.40**	**0.23**	**0.24**	**5.36**	**5.57 ± 0.34**	**0.29**
	2	**2.40**	**0.25**		**5.77**		
T1A-1	1	3.60	0.32	0.31	5.03	4.82 ± 0.35	0.30
	2	3.60	0.30		4.60		
T1A-2	**1**	**3.50**	**0.35**	**0.35**	**5.56**	**5.45 ± 0.12**	**0.10**
	2	**3.50**	**0.34**		**5.41**		
T1A-3	1	3.40	0.24	0.23	3.63	3.78 ± 0.24	0.21
	2	3.40	0.22		3.93		
H_2O	1	4.10	0.29	0.31	3.93	4.04 ± 0.17	0.15
	2	4.30	0.32		4.14		
THF*	1	3.90	0.34	0.34	4.81	4.84 ± 0.03	0.04
	2	3.90	0.34		4.87		
SDS**	1	3.70	0.33	0.34	5.03	5.06 ± 0.03	0.04
	2	3.60	0.34		5.08		
TBAB***	1	2.40	0.11	0.10	2.59	2.37 ± 0.37	0.32
	2	2.40	0.09		2.14		

*THF at 3.00 mol%; **SDS at 0.01 mol% and ***TBAB at 0.29 mol%
Bold column indicated the optimum conditions for each type of combine promoters

Appendix 5. Solubility of CO_2 in H_2O

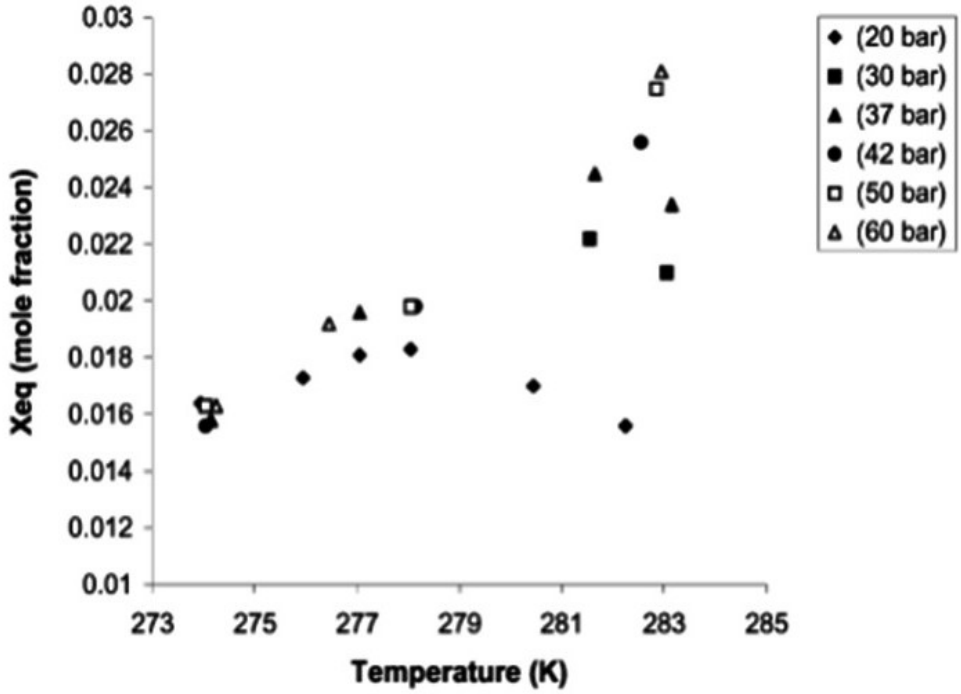


Figure A- 2: Plot of the equilibrium mole fraction of CO_2 in water vs. temperature at given pressures (Servio et al., 2001)

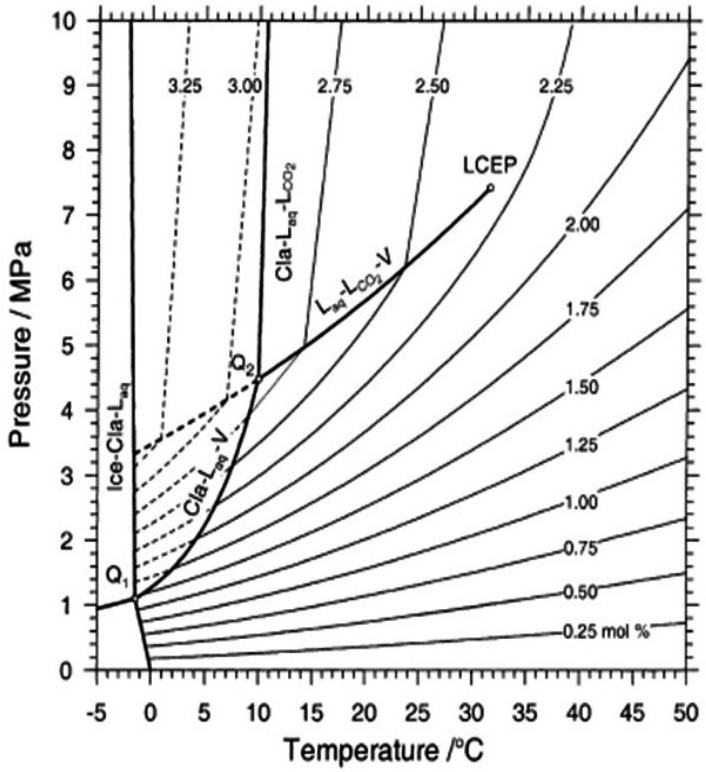


Figure A- 3: P-T diagram showing solubility of CO_2 in water (Diamond et al., 2003)

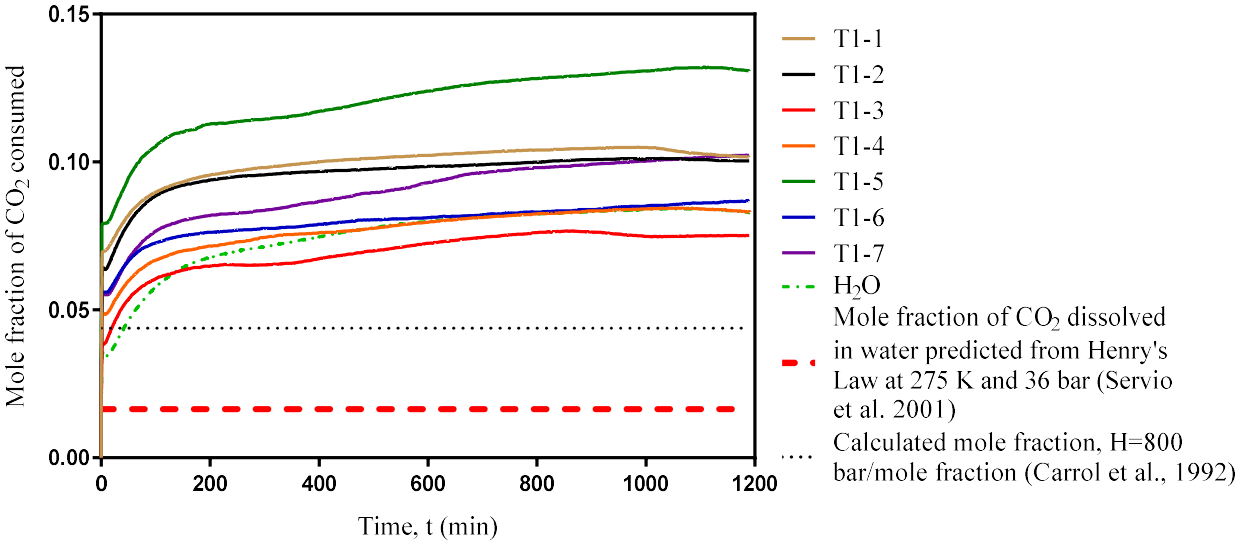


Figure A- 4: CO_2 solubility in water for type 1 combined-promoters at the operating conditions of 275 K and 36 bar by employing pure CO_2 gas

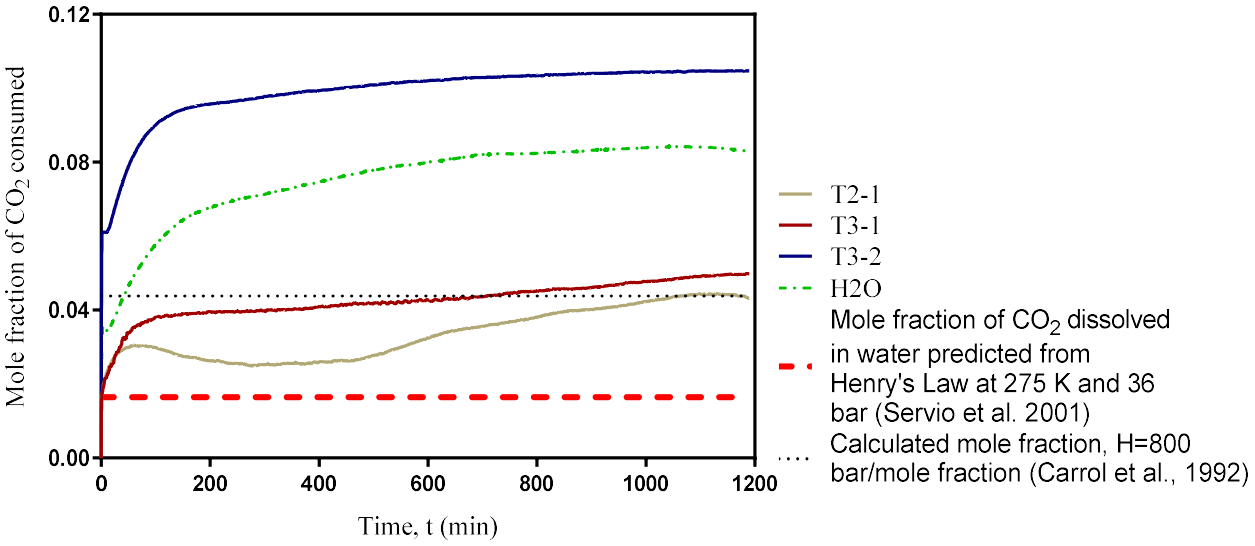


Figure A- 5: CO_2 solubility in water for type 2 & 3 combined-promoters at the operating conditions of 275 K and 36 bar by employing pure CO_2 gas

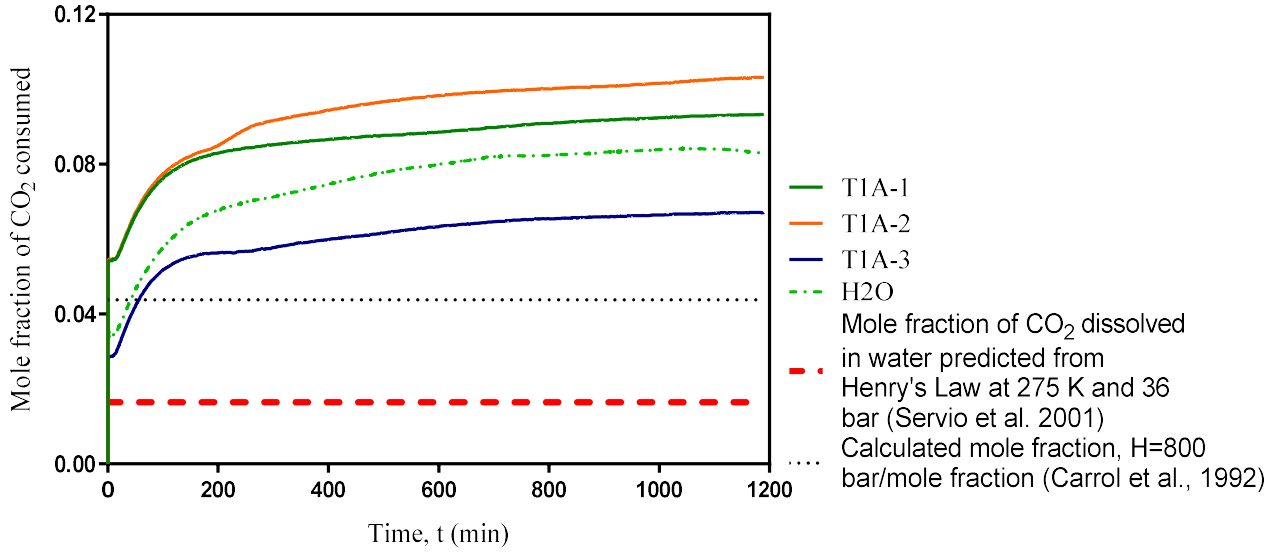


Figure A- 6: CO_2 solubility in water for type 1A combined-promoters at the operating conditions of 275 K and 36 bar by employing pure CO_2 gas

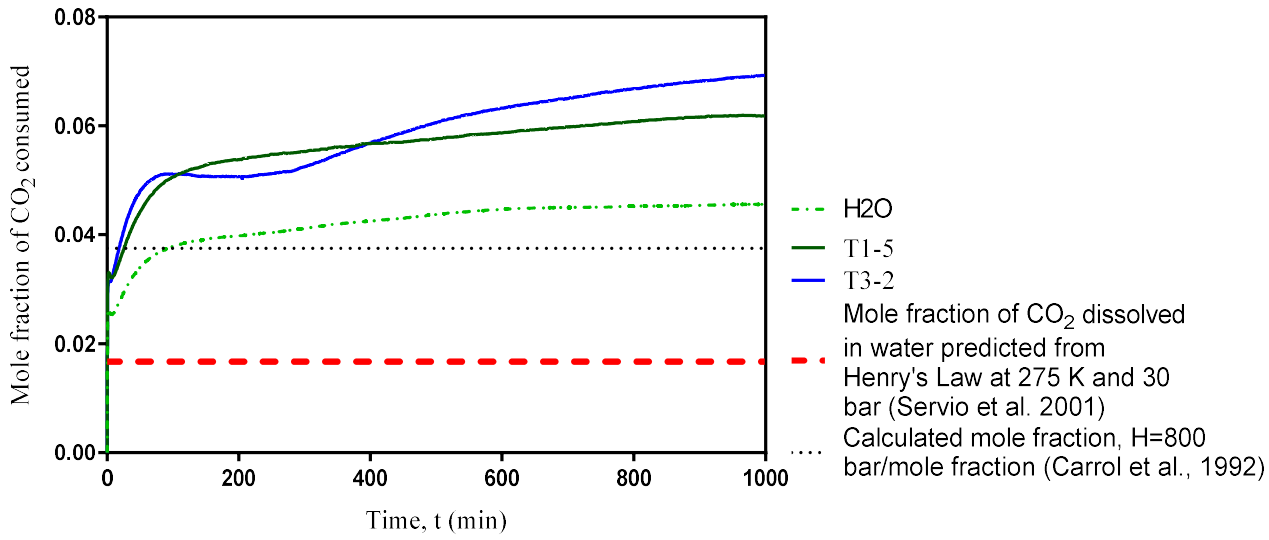


Figure A- 7: CO_2 solubility in water for T1-5 & T3-2 combined-promoters at the operating conditions of 275 K and 30 bar by employing pure CO_2 gas (brief description of each code was referred to page 108 and 116 (Table 4- 4) respectively)

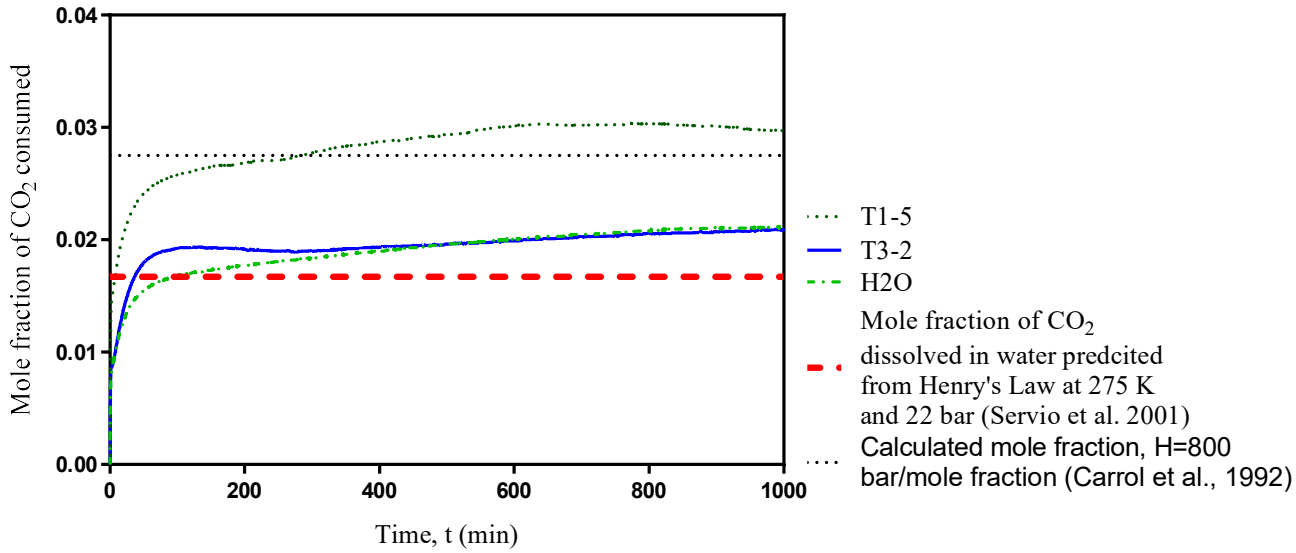


Figure A- 8: CO_2 solubility in water for T1-5 & T3-2 combined-promoters at the operating conditions of 275 K and 22 bar by employing pure CO_2 gas (brief description of each code was referred to page 108 and 116 (Table 4- 4) respectively)

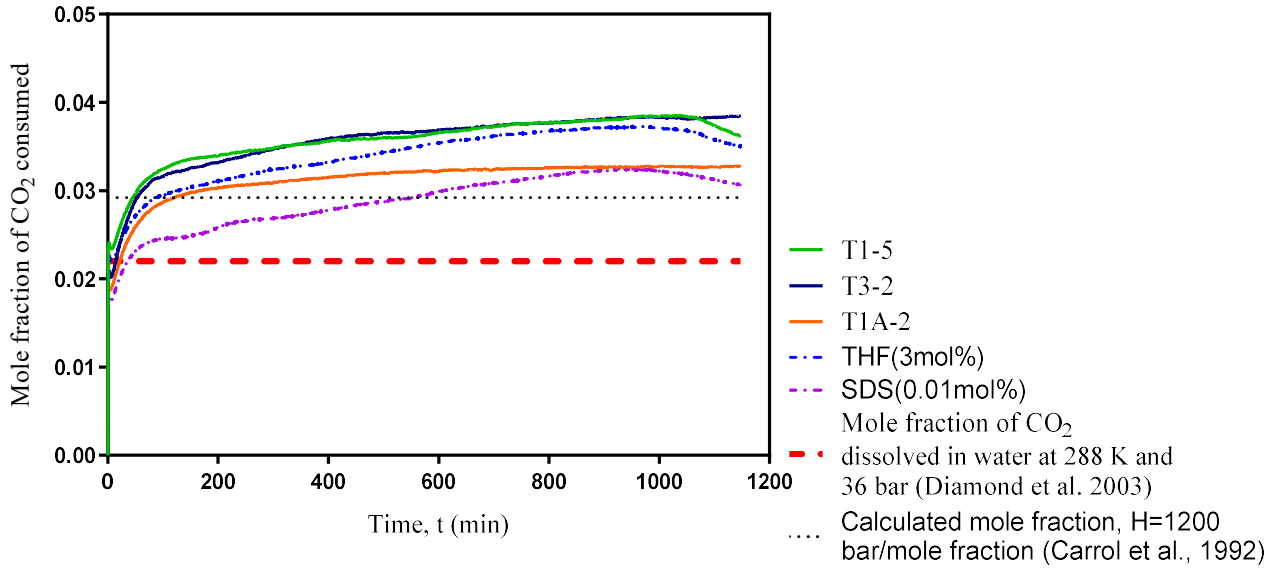


Figure A- 9: CO_2 solubility in water for T1-5, T3-2 & T1A-2 combined-promoters at the operating conditions of 288 K and 36 bar by employing pure CO_2 gas (brief description of each code was referred to page 108, 116 (Table 4- 4) and 121 (Table 4- 6) respectively)

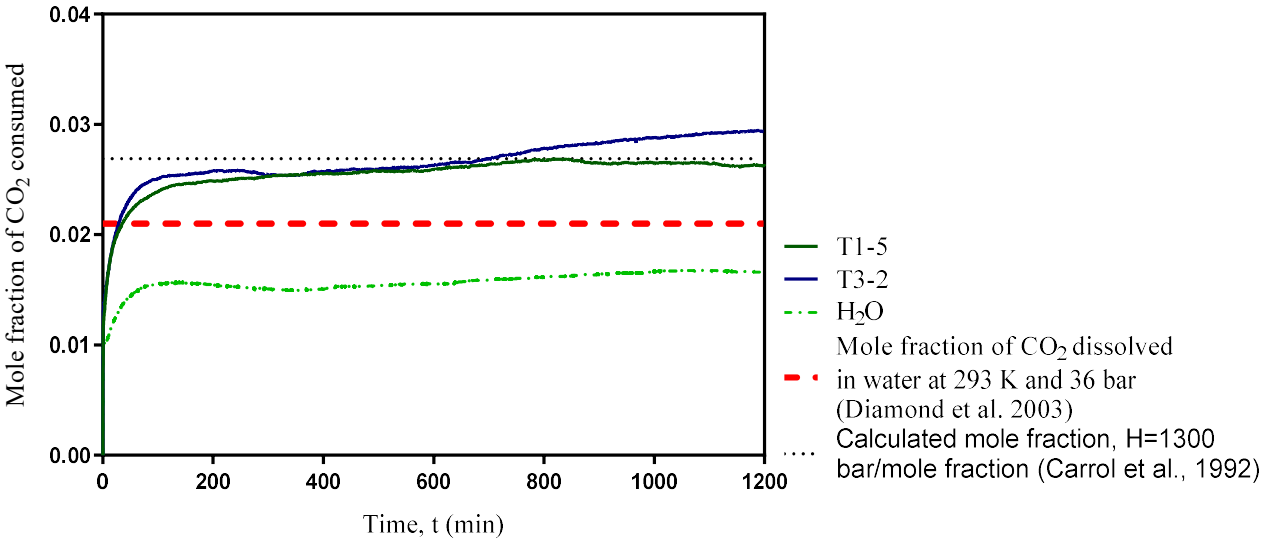


Figure A- 10: CO_2 solubility in water for T1-5 & T3-2 combined-promoters at the operating conditions of 293 K and 36 bar by employing pure CO_2 gas (brief description of each code was referred to page 108 and 116 (Table 4- 4) respectively)

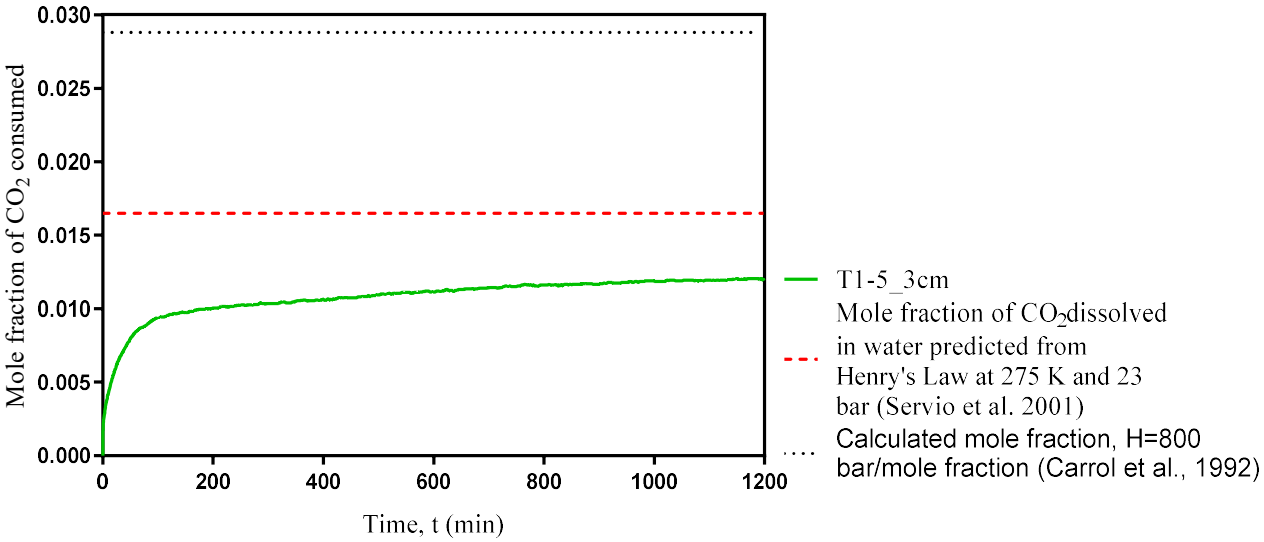


Figure A- 11: CO_2 solubility in water for T1-5_3cm at the operating conditions of 275 K and 58 bar (P_{CO2}=23 bar) by employing fuel gas mixture (brief description of T1-5 code was referred to page 108)

Appendix 6. Solubility of H_2 in H_2O

Table A- 6: Experimental values of the solubility of H_2 gas in water at different partial pressures (Young, 1981)

EXPERIMENTAL VALUES:		Mole fraction of hydrogen in liquid, x_{H2}	T/K	P/bar	Mole fraction of hydrogen in liquid, x_{H2}
T/K	P/bar				
273.15	25.33	0.000383	298.15	25.33	0.000311
	50.66	0.000768		50.66	0.000619
	101.33	0.001520		101.33	0.001233
	202.65	0.002983		202.65	0.002417
	405.30	0.005690		405.30	0.004673
	607.95	0.008239		607.95	0.006799
	810.60	0.010619		810.60	0.008825
	1013.25	0.012700		1013.25	0.010745

Table A- 7: Interpolated values of the solubility of H_2 gas in water at the IGCC and non-IGCC conditions

Temperature (K)	IGCC pressure (bar)	P_{H2} (bar)	Mole fraction of H_2 in water	Remark
276	60	36	0.000533	Non-IGCC
283	58	35	0.000490	IGCC
	70	42	0.000588	
286	80	48	0.000656	Non-IGCC

Appendix 7. Hydrate phase equilibrium for H_2+THF and H_2+TBAB

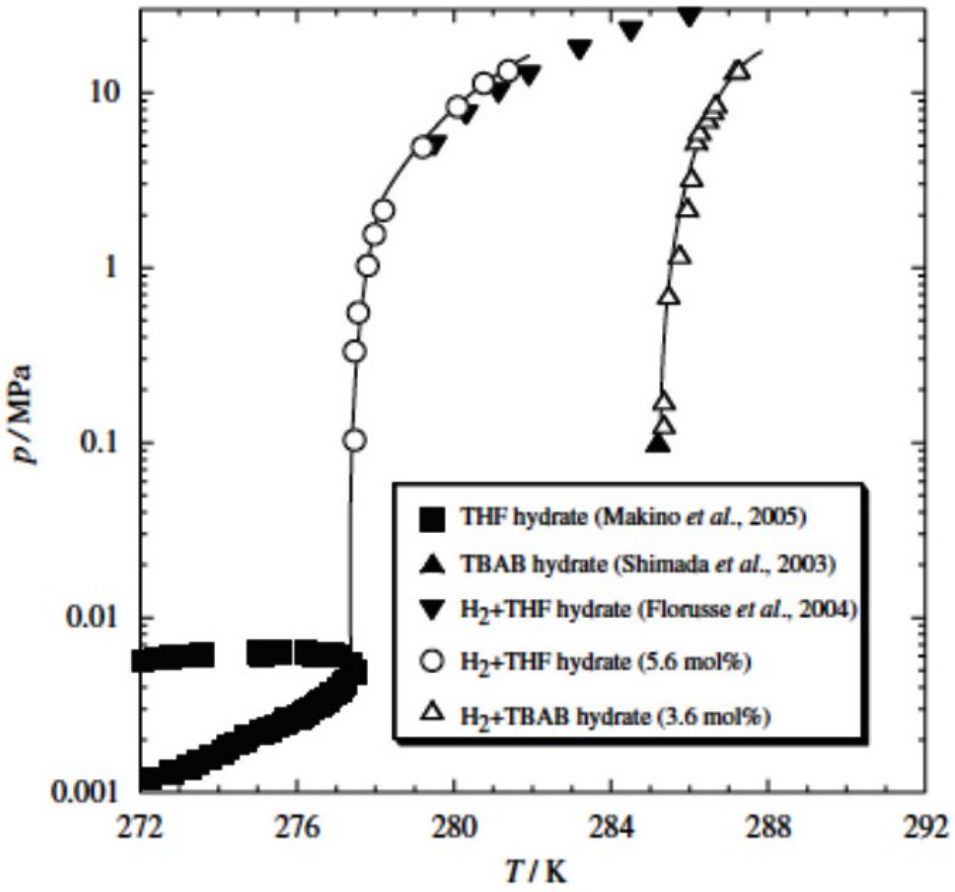


Figure A- 12: Hydrate phase equilibrium for H_2+THF and H_2+TBAB (Hashimoto et al., 2006)

Appendix 8. Hydrate phase equlibrium in this work

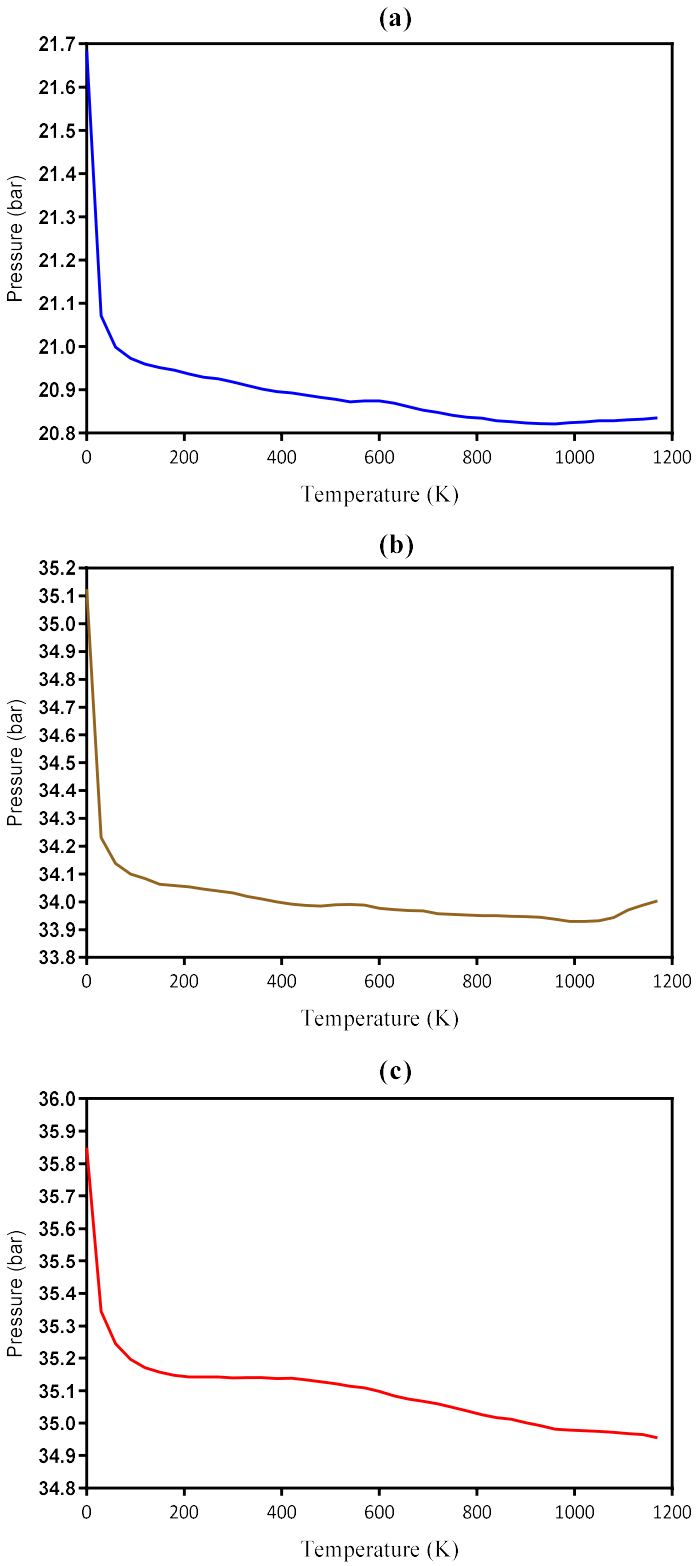


Figure A- 13: Some of pressure profiles used to determine hydrates phase equilibria in this work; (a) 275 K & 22 bar, (b) 288 K & 35 bar, (c) 293 K & 36 bar

Appendix 9. Effect of THF on hydrates cage occupancy

Table A- 8: Ratio of molecular diameter to cage diameter for the guest molecules of sI and sII hydrates (Sowjanya et al., 2014)

Guest molecule	Structure I		Structure II	
	5^{12} (7.90 Å)	$5^{12}6^2$ (8.66 Å)	5^{12} (7.82 Å)	$5^{12}6^4$ (9.46 Å)
CO_2 (5.12 Å)	1.004	0.874	1.020	0.769
CH_4 (4.36 Å)	0.855	0.744	0.868	0.655
THF (6.30 Å)	1.235	1.075	1.255	0.946

Ratio of molecular diameter to cage diameter for the guest molecules of sI and sII clathrates. Diameters of the cages and guest molecules are shown in parentheses. The ratio is calculated by substracting the diameter (2.80 Å) of water molecules from the cage diameter.

Appendix 10. Water saturation inside silica pores

$\text{Pore volume}_{\text{silica gel}} = 0.64\ {}^{\text{cm}^3}/_{\text{g}}$ &$\text{Equilibrium moisture}_{\text{silica gel}} = 13.3\ \text{wt\%}$

$\text{Pore volume}_{\text{zeolite 13X}} = 0.48\ {}^{\text{cm}^3}/_{\text{g}}$ &$\text{Equilibrium moisture}_{\text{zeolite 13X}} = 20.4\ \text{wt\%}$

$\text{Mass}_{\text{silica gel}} = 0.5\text{g};\ \text{Mass}_{H_2O}$ inside silica gel $= 0.133 * 0.5 = 0.067\text{g}$

$\text{Mass}_{\text{zeolite 13}} = 0.5\text{g};\ \text{Mass}_{H_2O}$ inside zeolite $13\text{X} = 0.204 * 0.5 = 0.102\text{g}$

$\text{Dry mass}_{\text{silica gel}} = 0.5\text{g} - 0.067\text{g} = 0.433\text{g};\ \text{Dry mass}_{\text{zeolite 13}} = 0.5\text{g} - 0.102\text{g} = 0.398\text{g}$

Volume_{H_2O} inside silica gel $\approx 0.067\text{cm}^3;\ \text{Volume}_{H_2O}$ inside zeolite $13\text{X} \approx 0.102\text{cm}^3$

$$\text{Water saturation}_{\text{silica gel}} = \frac{0.067}{0.433} * \frac{1}{0.64} * 100\% = 24\%$$

$$\text{Water saturation}_{\text{zeolite 13X}} = \frac{0.102}{0.398} * \frac{1}{0.48} * 100\% = 54\%$$

Appendix 11. Changing the process from batch to continuous process

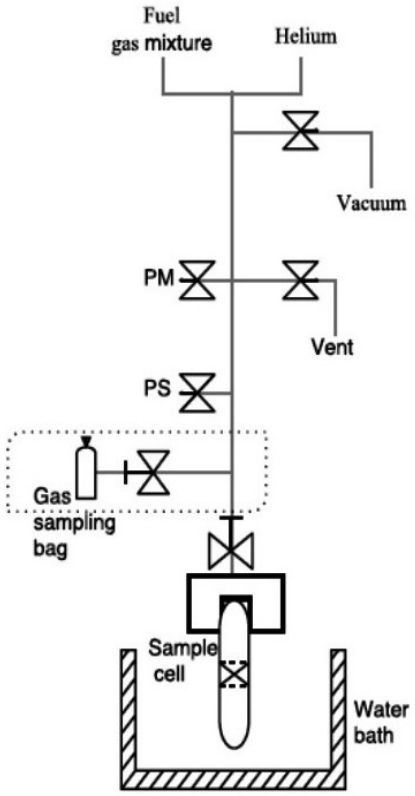


Figure A- 54: Schematic diagram of modified HPVA (dotted region)

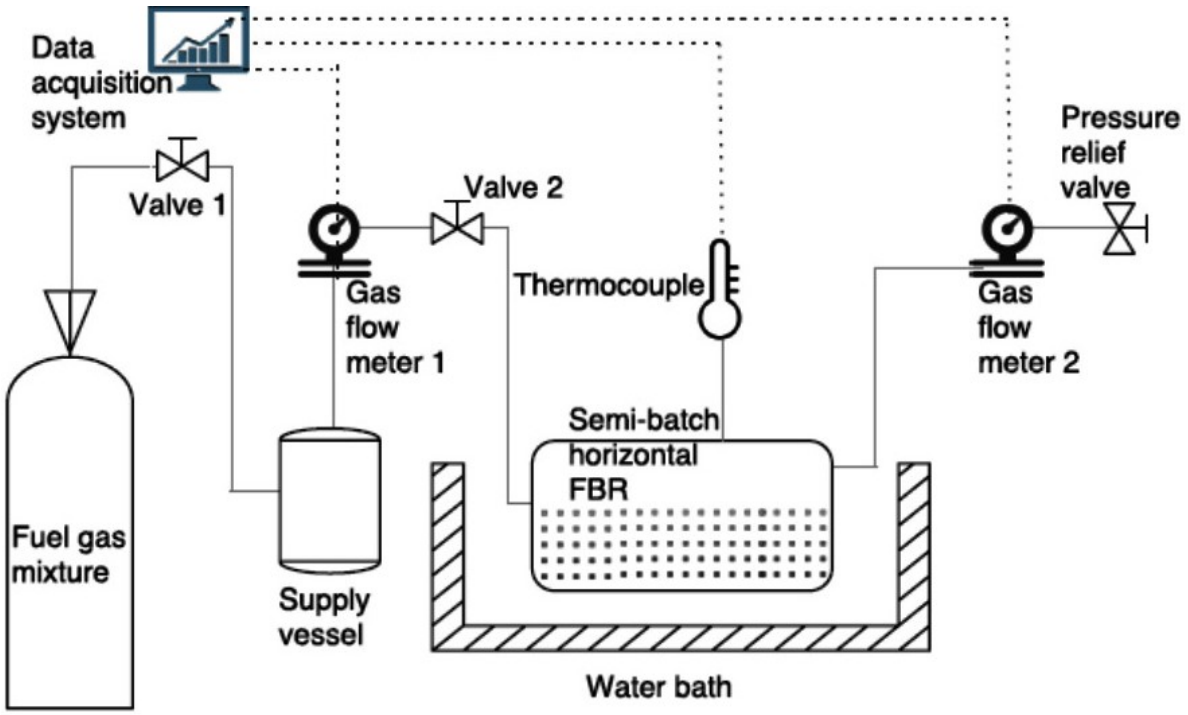


Figure A- 65: Schematic diagram of semi-batch horizontal FBR

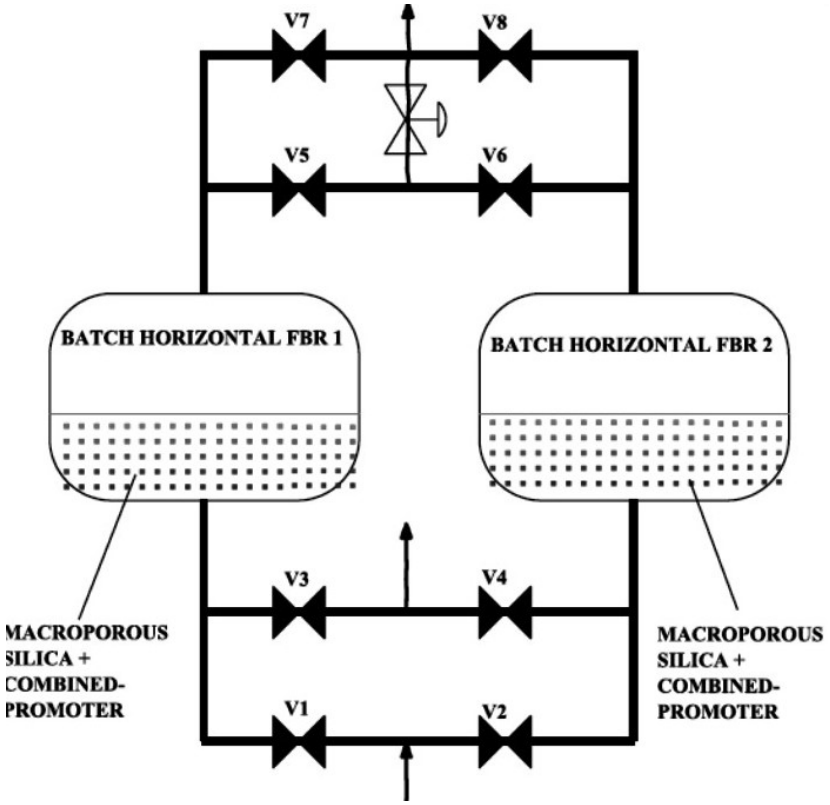


Figure A- 76: Schematic design of dual-batch horizontal FBRs and valve sequencing for four steps in the cycle

Table A- 9: Valve sequencing for four steps in the cycle

FBR 1	Hydrate formation	Depressurization	Hydrate decomposition	Pressurization
	V1, V7	V3	V5, V3	V1
FBR 2	Hydrate decomposition	Pressurization	Hydrate formation	Depressurization
	V6, V4	V2	V2, V8	V4